Synthesis and Studies of Annelated Quinolizinium Derivatives as Versatile Constructs for Fluorescent Probes and Ligands for Triple-Helical and Abasic DNA Structures

DISSERTATION

zur Erlangung des naturwissenschaftlichen Doktorgrades

vorgelegt von

Anton Granzhan

geb. am 14. Oktober 1979 in Rubishne (Ukraine)

eingereicht beim Fachbereich 8 (Chemie–Biologie)

der Universität Siegen

Siegen 2006

urn:nbn:de:hbz:467-2403

Eingereicht am: 14. Juni 2006

beim Fachbereich 8 (Chemie–Biologie)

1. Gutachter: Univ.-Prof. Dr. Heiko Ihmels

2. Gutachter: Univ.-Prof. Dr. Michael Schmittel

der Dissertation

1. Prüfer: Univ.-Prof. Dr. Heiko Ihmels

2. Prüfer: Univ.-Prof. Dr. Michael Schmittel

3. Prüfer: Univ.-Prof. Dr. Alf Mews

des öffentlichen Promotionskolloquiums

Tag des öffentlichen Promotionskolloquiums: 18. August 2006

Doktorurkunde ausgehändigt am: ----------

Le hasard ne favorise que les esprits prepares.

Louis Pasteur

Моїм батькам присвячую

ACKNOWLEDGEMENTS

I am first and foremost thankful to Professor Dr. Heiko Ihmels for giving me an opportunity to work in his group in the stimulating atmosphere of motivation and creativity, and especially for giving generous support to all my ideas. I would like to particularly acknowledge his rapid corrections of this work and other manuscripts.

I am immensely indebted to Dr. Yuri Slominskii and Dr. Julia Bricks (Institute of Organic Chemistry, NAS Ukraine) who first introduced me to Organic Chemistry and, in particular, to the field of organic dyes, and provided me with a plenty of skills, all of which proved to be essential for the realization of this work.

My many warm thanks are due to Dr. Katja Lamber (EMBL-Hamburg) for her cordial support, especially during the “hard times”, and many helpful discussions.

I wish to express my gratitude to the following folks at the University of Siegen:

- Daniela Otto, who has been working side by side with me, for her ready help with the gel electrophoresis, for the proof-reading of this work, and especially for tolerating my awful German during all these years;
- Dr. Thomas Paululat and Christoph Reimer (a.k.a. Barnie) for running an excellent NMR service and help with some advanced NMR experiments;
- Dr. Jutta Arden-Jakob for the help with MPLC purification of the conjugates;
- Prof. Dr. Hans-Jörg Deiseroth and his co-worker Holger Mikus (Institute of Inorganic Chemistry), as well as Dr. Jan Willem Bats (University of Frankfurt) for the cooperation in the X-ray structural analysis and many useful discussions.

I also would like to acknowledge Dr. Giampietro Viola and Anita Faccio (University of Padova) for a favorable welcome in their workgroup during my stay in Italy, and a fruitful cooperation.

Last but not least, I would like to thank the undergraduate students, namely Anna Bergen, Katharina Jäger, Jan P. Meyer, Katya Mikhlina and Norman Schlosser, whom I had a pleasure to supervise and who contributed partly to this work. It remains for me to hope that I could impart most of my skills to them.

LIST OF PUBLICATIONS

K. Faulhaber, A. Granzhan, H. Ihmels, G. Viola, *Pure Appl. Chem*., accepted for publication.
Detection of Biomacromolecules with Fluorescent Light-Up Probes

A. Granzhan, H. Ihmels, *ChemBioChem* **2006**, 7, 1031–1033.
Selective Stabilization of Triple-Helical DNA by Diazoniapolycyclic Intercalators

A. Granzhan, J. W. Bats, H. Ihmels, *Synthesis* **2006**, 1549–1555.
*Synthesis and Spectroscopic Properties of 4a,14a-Diazoniaanthra[1,2-*a*]anthracene and 13a,16a-Diazoniahexaphene Derived from 1,7-Dimethylnaphthalene*

A. Granzhan, H. Ihmels, *Org. Lett.* **2005**, *7*, 5119–5122.
N-*Aryl-9-amino-substituted Acridizinium Derivatives as Fluorescent "Light-up" Probes for DNA and Protein Detection*

A. Granzhan, H. Ihmels, K. Mikhlina, H.-J. Deiseroth, H. Mikus, *Eur. J. Org. Chem.* **2005**, 4098–4108.
Synthesis of Substituted Diazoniapentaphene Salts by an Unexpected Rearrangement–Cyclodehydration Sequence

A. Granzhan, A. Penzkofer, G. Hauska, *J. Photochem. Photobiol, A* **2004**, *165*, 75–89.
Photodegradation of Bacteriochlorophyll c *in Intact Cells and Extracts from* Chlorobium tepidum

I. L. Valyukh, A. Slobodyanyuk, V. B. Kovalska, A. Granzhan, Y. L. Slominskii, S. M. Yarmoluk, *J. Phys. Studies* **2002**, *6*, 236–242 (in Ukrainian).
Spectral Properties of Symmetrical Trimethine Cyanines with α,γ-Substituted Polymethine Chain in the Presence of Nucleic Acids

CONTENTS

GENERAL REMARKS

The chemical compounds, which are often referred to in the text, are labeled with boldfaced Arabic numerals. Appendix A of this work contains a structure chart summarizing the labeling of chemical structures. In the Summary, that precedes this work, the numbering of chemical structures differs from the one in the main text. In this case, boldfaced Roman numerals are used for numbering of the structures.

Reference citations are labeled with superscript Arabic numerals, and the literature references are collected at the end of this work. Footnotes in tables are labeled with superscript letters in square brackets.

In the Experimental Part and in the Appendix A, the keys in square brackets represent references to the corresponding laboratory notebooks:

[AG-I-01] the Roman numeral refers to the notebook number, the Arabic one to the page number;

[MK-I-01] refers to the laboratory notebook of Katya Mikhlina, recorded by her during the *Schwerpunktfachpraktikum (Organische Chemie)*.

For the sake of conciseness and legibility, the conventional term “extinction coefficient” was used throughout this work for the IUPAC-recommended name “molar decadic absorption coefficient”; the trivial name “acridizinium” was used for the benzo[*b*]quinolizinium ion.[a] For the five- and six-ring membered polycyclic salts (Chapter 2), however, the replacement “azonia” nomenclature was used.[b]

In accordance with the current chemical literature, the DNA structures were abbreviated: [poly(dAdT)]$_2$ for [poly(dA–dT) : poly(dT–dA)], [poly(dGdC)]$_2$ for [poly(dG–dC) : poly(dC–dG)], and poly(dA)–[poly(dT)]$_2$ for the triple helix [poly(dT) : poly(dA) × poly(dT)].

[a] C. K. Bradsher, L. E. Beavers, *J. Am. Chem. Soc*. **1955**, *77*, 4812–4813.

[b] IUPAC Recommendations **1993**, Rule RC-82.3.

List of Abbreviations

Reagents and Solvents

AcOEt	Ethyl acetate
DMF	*N*,*N*-Dimethylformamide
DMSO	Dimethyl sulfoxide
EDTA	Ethylenediaminetetraacetic acid
EtOH	Ethanol
Et_2O	Diethyl ether
MeOH	Methanol
MeCN	Acetonitrile
MSA	Methanesulfonic acid
NMM	*N*-Methylmorpholine
NMP	*N*-Methyl-2-pyrrolidone
PPA	Polyphosphoric acid
SDS	Sodium dodecyl sulfate
TFA	Trifluoroacetic acid
THF	Tetrahydrofuran

DNA Structures

AP	apurinic / apyrimidinic
bp	base pair
bt	base triplet
ct DNA	calf thymus DNA
ds DNA	double-stranded (duplex) DNA
ODN	oligodeoxyribonucleotide
$[poly(dAdT)]_2$	$[poly(dA–dT)_n : poly(dT–dA)_n]$; $n \approx 8800$
$poly(dA)–[poly(dT)]_2$	$[poly(dT)_n \times poly(dA)_n : poly(dT)_n]$; $n \approx 300$
$[poly(dGdC)]_2$	$[poly(dG–dC)_n : poly(dC–dG)_n]$; $n \approx 900$
st DNA	salmon testes DNA

Proteins

BSA	albumin from bovine serum
CEA	albumin from chicken egg white
HSA	albumin from human serum

Physical Variables and their Units

A	absorbance
$\hat{A}$	normalized change of absorption
c	molar concentration / M
d	density / g mL^{-1}
E_T^N	normalized solvent polarity function
I_F	intensity of fluorescence emission
I_L	irradiance / W cm^{-2}
$J = \int I_F(\lambda)\,d\lambda$	fluorescence emission integral / nm
${}^nJ$	NMR coupling constant of the *n*th order / Hz
K	affinity constant / M^{-1}
n	binding site size
n_D	refractive index
$r = c_L / c_{DNA}$	ligand-to-DNA ratio
T	optical transmittance
T_m	DNA melting temperature / °C
ΔT_m	ligand-induced shift of the DNA melting temperature / °C
δ	NMR chemical shift / ppm
ε	extinction coefficient / $cm^{-1}\,M^{-1}$
η	dynamic viscosity / cP
λ	wavelength / nm
$\tilde{\nu}$	wavenumber / cm^{-1}
Φ_F	quantum yield of fluorescence

SUMMARY

In the present Thesis, various annelated derivatives of the quinolizinium ion, *i.e.* polycyclic compounds with a bridgehead quaternary nitrogen atom, were synthesized and investigated as fluorescent probes for the detection of biomacromolecules and as ligands for triple-helical DNA and abasic DNA structures.

Fluorescent Probes for the Detection of Biomacromolecules

9-Substituted derivatives of the acridizinium (benzo[*b*]quinolizinium) cation **I–III** were synthesized, in particular the amino derivatives **II–III** were prepared by a novel nucleophilic substitution reaction of the 9-bromoacridizinium bromide with selected aliphatic and aromatic amines. The photophysical properties of these compounds were investigated by absorption and steady-state fluorescence spectroscopy.

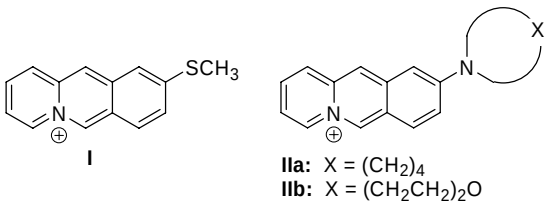

I

IIa: X = $(CH_2)_4$
IIb: X = $(CH_2CH_2)_2O$

IIIa: R = 4-NMe_2 **IIIe:** R = 4-F
IIIb: R = 4-OMe **IIIf:** R = 4-Br
IIIc: R = 4-Me **IIIg:** R = 4-Cl
IIId: R = H **IIIh:** R = 3-Cl

Derivatives **I** and **II** have an intense intrinsic fluorescence (Φ_F = 0.2–0.6), while the *N*-aryl-substituted compounds **III** are virtually non-fluorescent in liquid solutions ($\Phi_F \leq 0.01$). In contrast, the fluorescence of the derivatives of the latter type with halogen substituents in the phenyl ring (R = F, Cl, Br) increases drastically in viscous media, *e.g.* in glycerol solutions, and upon interaction with double-stranded DNA and selected proteins in aqueous solutions. In particular, in the case when R = 3-Cl (**IIIh**), binding to DNA results in a 50-fold increase of fluorescence, whereas the interaction with albumins in the presence of the anionic surfactant (sodium dodecyl sulfate) results in a 20-fold fluorescence enhancement. For comparison, the emission intensity of ethidium bromide, *i.e.* one of the commonly used DNA stains, increases only by a factor of up to 10 in the presence of DNA. The binding of several representative derivatives to double-stranded DNA was also studied by the spectrophotometric titrations and linear dichroism spectroscopy; the results give evidence that the prevailing binding mode is intercalation, and the binding constants lie in the range of (0.5−5.0) × 10^5 M^{-1} (bp).

The mechanism of the excited-state deactivation of *N*-aryl-9-aminoacridizinium derivatives **III** was investigated by the steady-state fluorescence spectroscopy in media of varied viscosity. The excited-state deactivation is due to two non-radiative processes: (i) torsional relaxation by rotation about the N–aryl bond (Scheme S1, path a) and (ii) electron-transfer process from the phenyl ring to the photo-excited acridizinium cation (Scheme S1, path b). Notably, the latter pathway is only significant in the case of electron-donor substituents in the phenyl ring (R = OMe, NMe_2). The binding of derivatives **IIIe–h** to the biomacromolecules is supposed to hinder the torsional-relaxation deactivation pathway, leading to the fluorescence enhancement.

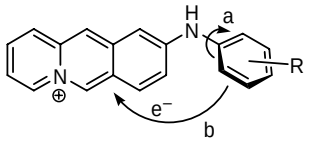

Scheme S1. Excited-state deactivations pathways of *N*-aryl-9-aminoacridizinium derivatives.

Conclusion I: 9-Donor-substituted acridizinium derivatives represent a versatile construct for the development of fluorescent probes. Especially promising are the substituted N-*aryl-9-aminoacridizinium salts, the fluorescence of which is susceptible to the microviscosity of the medium.*

Triplex-DNA Binders

A series of unsubstituted (**IVa–c**) and methyl-substituted (**Va–b**) diazoniapenthaphenes, as well as the isomeric diazoniaanthra[1,2-*a*]anthracenes **VIa–c** and diazoniahexaphene **VII** were prepared by the cyclodehydration synthesis. In particular, it was shown that the cyclodehydration of the substituted bis-pyridinium precursors **VIIIa–c** does not lead to the expected linear diazoniapentacenes **IXa–c**, but proceeds through an aromatic *ipso* substitution

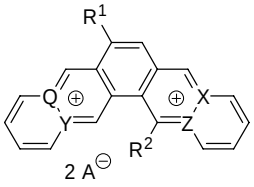

IVa: Q = X = C; Y = Z = N; $R^1 = R^2 = H$
IVb: Q = X = N; Y = Z = C; $R^1 = R^2 = H$
IVc: Q = Z = C; X = Y = N; $R^1 = R^2 = H$
Va: Q = X = N; Y = Z = C; $R^1 = R^2 = CH_3$
Vb: Q = Z = C; X = Y = N; $R^1 = H$; $R^2 = CH_3$

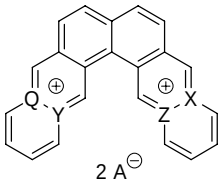

VIa: Q = X = C; Y = Z = N
VIb: Q = X = N; Y = Z = C
VIc: Q = Z = C; X = Y = N

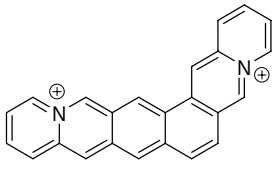

VII 2 A⊖

A = BF_4

and a methyl-group shift in the case of **VIIIa–b**, or bromine elimination in the case of **VIIIc**, and leads to the substituted diazoniapentaphenes **Va–c** (Scheme S2).

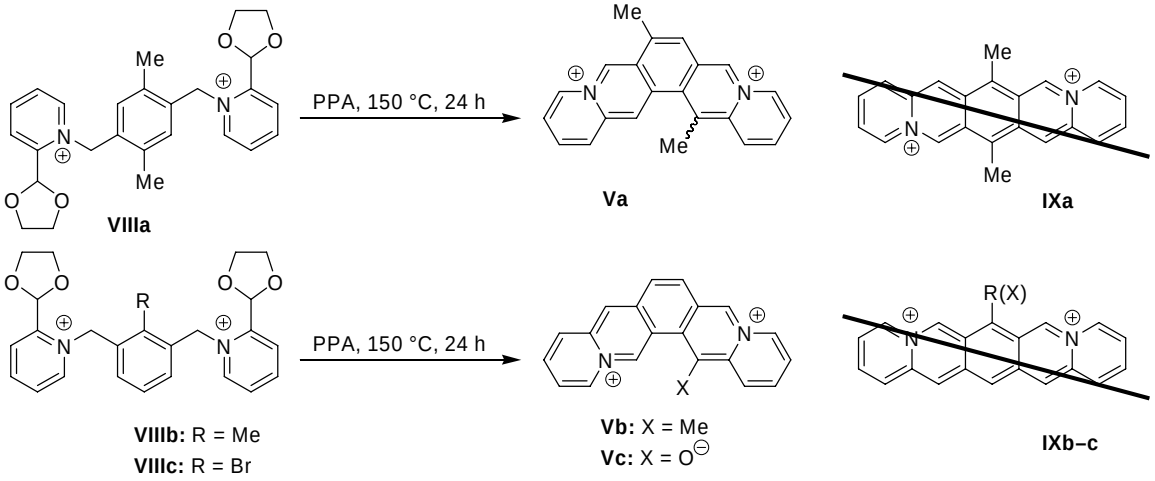

Scheme S2. Synthesis of substituted diazoniapentaphenes **Va–c**.

The interaction of the diazoniapolycyclic salts **IV**–**VII** with double-stranded and triple-helical DNA was investigated by the DNA thermal denaturation experiments as well as by the competition dialysis assay. The results reveal the preferential binding of both diazoniapentaphenes **IV–V** and diazoniaanthra[1,2-*a*]anthracences **VI** to the triple-helical DNA and stabilization thereof. The triplex-binding properties are much more pronounced in the case of the hexacycles **VI**; at the same time, their structural isomer, diazoniahexaphene **VII** shows preferential binding to the duplex structures, especially $[poly(dAdT)]_2$, but not to the triplex DNA. Within the diazoniapentaphene series, the DNA-binding properties remain essentially the same upon variation of the positions of the bridgehead nitrogen atoms or upon substitution with methyl groups. In contrast, significant variations were observed within the isomers **VIa–c**: thus, compound **VIa** shows a marked triplex-*vs.*-duplex selectivity, while the isomers **VIb–c** have slightly higher affinity for the duplex structures. Remarkably, compound **VIa** is one of the most efficient triplex stabilizers described to date, with a 9-fold larger binding affinity for the triplex as compared to the double-stranded DNA. Moreover, the structures **IV** and **VI** represent the first examples of synthetic triplex-DNA binders without additional aminoalkyl side chains.

Conclusion II: Diazoniapolycyclic salts represent novel lead structures, in which preferential, high-affinity binding to the triple-helical DNA may be achieved in the absence of an additional alkaline side chains.

Ligands for Abasic DNA Sites

Two isomeric acridizinium–adenine conjugates **Xa–b**, as well as the three model compounds, acridizinium-9-carboxamides **XIa–c**, were prepared from the corresponding carboxyacridizinium salts. Their affinity towards regular and abasic-site containing DNA structures was investigated by thermal denaturation experiments with synthetic oligodeoxyribonucleotides (TA = regular duplex, TX = abasic duplex).

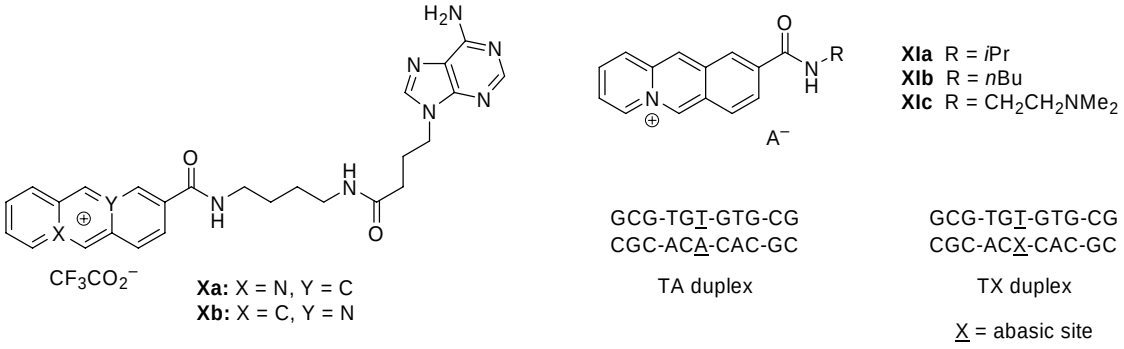

The results show moderate preferential binding of the conjugates **Xa–b** to the abasic oligonucleotides as compared to the regular structures (difference of the induced melting-temperature shifts between the TX and TA duplexes $\Delta\Delta T_m \approx 4$ ºC at the ligand-to-DNA ratio $r = 0.5$). However, the highest selectivity towards abasic sites and the most pronounced binding affinity is achieved by the aminoalkyl derivative **XIc** ($\Delta\Delta T_m = 9.6$ ºC).

Both conjugates **Xa–b** and the acridizinium-9-carboxamides, such as **XIb**, induced DNA single-strand cleavage upon irradiation, as shown by the plasmid-relaxation assay. Notably, the derivative **XIb** has about 50% higher photocleavage efficiency than the acridizinium–adenine conjugates, which is attributed to an enhanced excited-state deactivation in the conjugates **Xa–b** due to the electron transfer to the adenine moiety, that results in a less efficient photosensitized formation of the reactive oxygen species. Experiments with the apurinic plasmid DNA reveal no enhanced photocleavage of abasic DNA structures.

Conclusion III: Acridizinium–adenine conjugates and aminoalkyl-substituted acridizinium-9-carboxamides are capable of selective binding to abasic DNA sites. They readily induce the photo-damage of plasmid DNA, however, without selectivity towards abasic DNA structures.

ZUSAMMENFASSUNG

Im Rahmen dieser Arbeit wurden verschiedene Chinoliziniumderivate, d.h. polycyclische Aromaten, die über ein quartäres Stickstoffatom verfügen, synthetisiert und sowohl auf ihre Eignung als Fluoreszenzsensoren zur Detektion von Biomakromolekülen als auch auf ihre Bindungseigenschaften gegenüber Triplex-DNA und DNA mit abasischen Positionen hin überprüft.

Fluoreszenzsensoren zur Detektion von Biomakromolekülen

Es wurden Derivate des Acridiziniumions mit verschiedenen Substituenten in Position 9 (**I–III**) synthetisiert. Die aminosubstituierten Derivate **II–III** wurden durch eine neuartige nukleophile Substitution des 9-Bromacridiziniumbromids durch Umsetzung mit ausgewählten aliphatischen und aromatischen Aminen dargestellt. Die photophysikalischen Eigenschaften dieser Substanzen wurden mittels Absorptions- und Fluoreszenzspektroskopie untersucht.

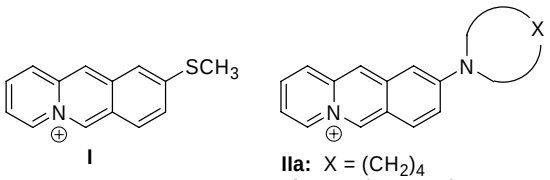

I

IIa: X = $(CH_2)_4$
IIb: X = $(CH_2CH_2)_2O$

IIIa: R = 4-NMe_2 **IIIe:** R = 4-F
IIIb: R = 4-OMe **IIIf:** R = 4-Br
IIIc: R = 4-Me **IIIg:** R = 4-Cl
IIId: R = H **IIIh:** R = 3-Cl

Die Derivate **I** und **II** weisen eine ausgeprägte intrinsische Fluoreszenz auf (Φ_F = 0.2–0.6), wohingegen die *N*-arylsubstituierten Verbindungen **III** keine Fluoreszenz in flüssigen Lösungen zeigen ($\Phi_F \leq 0.01$). Im Gegensatz dazu steigt die Fluoreszenz der halogen-substituierten Derivate **IIIe–h** sowohl in viskosen Medien, wie z.B. in Glycerin-Lösungen, als auch nach Zugabe von doppelsträngiger DNA und ausgewählten Proteinen in wässrigen Lösungen stark an. Besonders bemerkenswert ist dabei das Derivat **IIIh**, dessen Bindung an die DNA zu einer 50-fachen Zunahme der Fluoreszenz führt. Darüber hinaus hat die Wechselwirkung mit Albumin in Gegenwart eines anionischen Tensids (Natriumdodecyl-sulfat) eine 20-fache Zunahme der Fluoreszenzintensität zur Folge. Weiterhin wurden die Wechselwirkungen einiger repräsentativer Derivate mit doppelsträngiger DNA mit Hilfe von spektrophotometrischen Titrationen und LD-Spektroskopie untersucht. Die hierbei erhaltenen Ergebnisse zeigen, dass der bevorzugte Bindungsmodus die Intercalation ist.

Um den Deaktivierungsprozess des angeregten Zustandes der *N*-Aryl-9-aminoacridiziniumderivate zu untersuchen, wurden fluoreszenzspektroskopische Untersuchungen in Medien mit unterschiedlicher Viskosität durchgeführt. Die Deaktivierung des angeregten Zustandes ist die Folge von zwei strahlungslosen Prozessen: (i) Torsionsrelaxation durch eine Drehung um die N–Aryl-Bindung (Schema Z1, Weg a); (ii) Elektronentransferprozess vom Phenylring zum angeregten Acridiziniumkation (Schema Z1, Weg b). Allerdings ist der Elektronentransferprozess nur dann effektiv, wenn der Phenylring Elektronendonorsubstituenten trägt. Die Bindung der Derivate **IIIe–h** an Biomakromoleküle verhindert die Torsionsrelexation, was zu einem Anstieg der Fluoreszenzintensität führt.

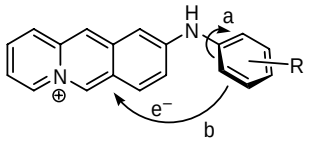

Schema Z1. Deaktivierungsprozess des Anregungszustandes von *N*-aryl-9-aminoacridiziniumderivativen.

Fazit I: Acridiziniumderivate, die in Position 9 einen Donorsubstituenten besitzen, stellen ein viel versprechendes Grundgerüst für die Entwicklung von Fluoreszenzsensoren dar. Insbesondere die substituierten N-*Aryl-9-aminoacridiziniumsalze erscheinen aussichtsreich, da deren Fluoreszenz besonders empfindlich auf kleinste Veränderungen der Viskosität des umgebenden Mediums reagiert.*

Triplex-DNA-stabilisierende Liganden

Eine Reihe von unsubstituierten (**IVa–c**) und methylsubstituierten (**Va–b**) Diazoniapentaphen-Derivaten sowie die isomeren Diazoniaanthra[1,2-*a*]anthracene **VIa–c** und das Diazoniazoniahexaphen **VII** wurden durch Cyclodehydratisierung erhalten. Es wurde gezeigt, dass die Cyclodehydratisierung der entsprechenden Bispyridiniumvorstufen **VIIIa–c** nicht zu den erwarteten linearen Diazoniapentacenen **IXa–c** führt, sondern über eine

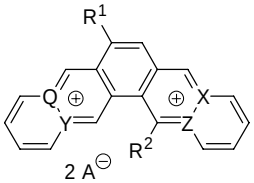

IVa: Q = X = C; Y = Z = N; $R^1 = R^2 = H$
IVb: Q = X = N; Y = Z = C; $R^1 = R^2 = H$
IVc: Q = Z = C; X = Y = N; $R^1 = R^2 = H$
Va: Q = X = N; Y = Z = C; $R^1 = R^2 = CH_3$
Vb: Q = Z = C; X = Y = N; $R^1 = H$; $R^2 = CH_3$

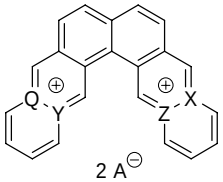

VIa: Q = X = C; Y = Z = N
VIb: Q = X = N; Y = Z = C
VIc: Q = Z = C; X = Y = N

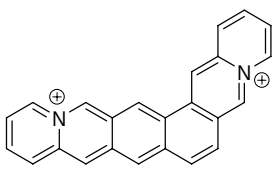

VII 2 A⊖

A = BF_4

aromatische *ipso*-Substitution und die Umlagerung einer Methylgruppe (bei den Substanzen **VIIIa–b**) bzw. über eine Eliminierung (bei **VIIIc**) zu den substituierten Diazoniapentaphenen **Va–c** führt (Schema Z2).

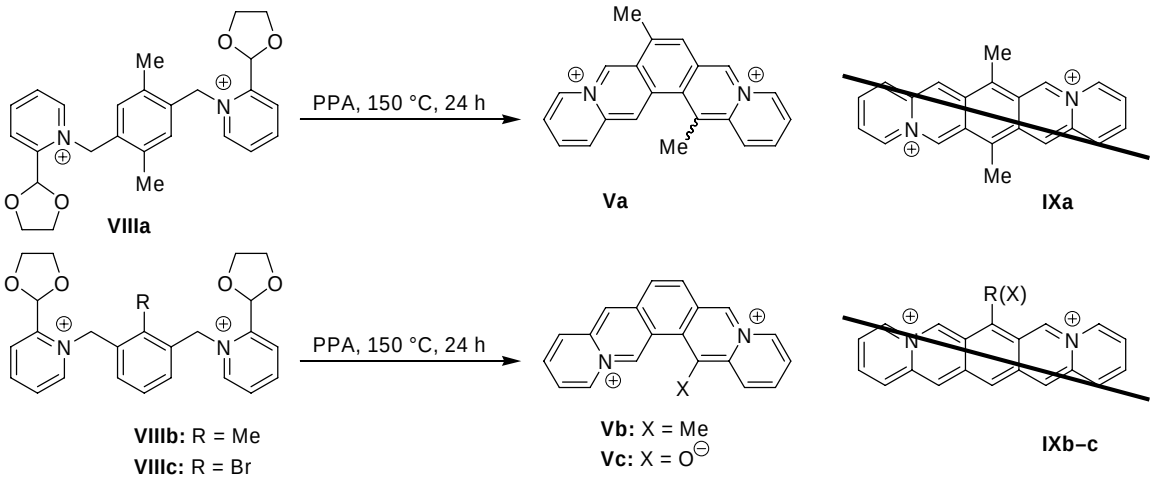

Schema Z2. Synthese der substituierten Diazoniapentaphene **Va–c**.

Die Wechselwirkungen der Diazoniasalze **IV–VII** mit doppelsträngiger DNA und Triplex-DNA wurden mit DNA-Schmelzexperimenten und Konkurrenzdialyse untersucht. Die Ergebnisse zeigen, dass die Diazoniapentaphene **IV–V** und die Diazoniaantra[1,2-*a*]anthracene **VI** bevorzugt an die Triplex-DNA binden und diese auch deutlich stabilisieren. Die triplexbindenden Eigenschaften sind bei den Hexacyclen **VI** viel deutlicher ausgeprägt. Im Gegensatz dazu bindet das Diazoniahexaphen **VII** bevorzugt an doppelsträngige DNA, vor allem an $[poly(dAdT)]_2$, aber nicht an Triplex-DNA. Innerhalb der Reihe der Diazoniapentaphene werden die DNA-bindenden Eigenschaften durch Veränderung der Position der Stickstoffatomen oder durch Substitution mit Methylgruppen nicht beeinflusst. Im Gegensatz dazu wurden signifikante Veränderungen bei den Isomeren **VIa–c** nachgewiesen: so bindet **VIa** mit hoher Selektivität an Triplex-DNA, wohingegen die Isomere **VIb–c** eine leicht erhöhte Affinität gegenüber doppelsträngiger DNA aufweisen. Besonders hervorzuheben ist Verbindung **VIa**, denn sie weist eine 9-fach erhöhte Affinität für tripelhelikale im Vergleich zur doppelsträngigen DNA auf und gehört damit zu den besten bislang bekannten Triplex-Stabilisatoren. Desweiteren repräsentieren die Verbindungen **IV** und **VI** die ersten synthetischen Triplex-DNA-Liganden, die keine zusätzlichen Aminoalkylseitenketten benötigen.

Fazit II: Polycyclische Diazoniasalze repräsentieren neue Leitstrukturen, die mit hoher Affinität eine selektive Bindung an Triplex-DNA aufweisen, ohne dass zusätzliche Aminoalkylseitenketten notwendig sind.

Liganden für DNA mit abasischen Positionen

Zwei isomere Acridizinium–Adenin–Konjugate **Xa–b** sowie drei Modellverbindungen, d.h. Acridizinium-9-carboxamidderivate **XIa–c**, wurden ausgehend von den entsprechenden Carboxyacridiziniumsalzen erhalten. Ihre Bindungsaffinität gegenüber DNA, die entweder eine oder keine abasische Stelle aufweist, wurde mit Hilfe von DNA-Schmelzexperimenten mit synthetischen Oligodesoxyribonukleotiden ermittelt (TA = vollständige Duplex-DNA, TX = DNA mit einer abasischen Position).

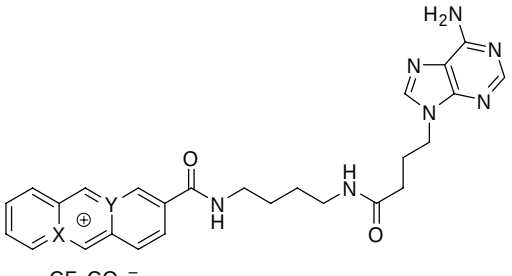

Xa: X = N, Y = C
Xb: X = C, Y = N

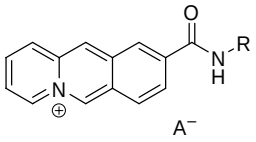

XIa R = *i*Pr
XIb R = *n*Bu
XIc R = $CH_2CH_2NMe_2$

GCG-TG<u>I</u>-GTG-CG
CGC-AC<u>A</u>-CAC-GC
TA Duplex

GCG-TG<u>I</u>-GTG-CG
CGC-AC<u>X</u>-CAC-GC
TX Duplex
<u>X</u> = abasische Position

Die Ergebnisse zeigen eine erhöhte Bindung der Konjugate **Xa–b** an die abasischen Oligonukleotide (Unterschiede der induzierten Verschiebungen der Schmelztemperaturen zwischen TX und TA $\Delta\Delta T_m \approx 4$ °C bei einem Ligand-zu-DNA-Verhältnis $r = 0.5$). Die höchste Selektivität für die Bindung an die abasiche Position und die ausgeprägteste Bindungsaffinität wird jedoch durch das Aminoalkylderivat **XIc** erreicht ($\Delta\Delta T_m = 9.6$ °C). Beide Konjugate **Xa–b** und auch die Acridizinium-9-carboxamide, wie z.B. **XIb**, sind dazu in der Lage, bei Bestrahlung einen DNA-Einzelstrangbruch zu induzieren. Das Derivat **XIb** weist im Vergleich zu den Acridizinium–Adenin–Konjugaten **Xa–b** eine um etwa 50% höhere DNA-Schädigungsrate auf. Dies ist auf eine erhöhte Deaktivierung des angeregten Zustandes von **X** durch einen Elektrontransfer vom Adenin zum angeregten Acridizinium zurückzuführen. Experimente mit apurinischer Plasmid-DNA zeigen jedoch keine erhöhte Photoschädigung der DNA mit abasischen Positionen.

Fazit III: Acridizinium–Adenin–Konjugate und aminoalkylsubstituierte Acridizinium-carboxamide sind in der Lage, an abasische Positionen in DNA zu binden. Sie können die Photoschädigung von Plasmid-DNA auslösen, jedoch gibt es keine selektive Schädigung von DNA mit abasischen Positionen.

1 INTRODUCTION AND LITERATURE SURVEY

1.1 Annelated Quinolizinium Derivatives as DNA Binders

Nucleic acids are important biomacromolecules which offer several binding sites for a variety of guest molecules. The binding interaction between small molecules and nucleic acids often leads to significant changes in the structure of the latter and may have an important influence on their physiological functions.[1] Thus, DNA is a target for many anti-cancer drugs and antibiotics, which suppress the gene replication or transcription in tumor cells.[2] In addition, such a host-guest interaction may be used for detection of nucleic acids when the physical properties of the guest molecule change upon binding and may be easily monitored. Especially useful is DNA staining (*vide infra*), which is based on the change of the color or fluorescence properties of an organic dye upon binding to the macromolecule.

In general, guest molecules may associate with the DNA by two distinct binding modes, namely (i) intercalation, when the ligand molecule is inserted between the adjacent DNA base pairs, and (ii) groove binding in the minor or major DNA grooves. Additionally, a non-specific external binding by the electrostatic interactions with the DNA phosphate backbone should be considered, which is often observed for the ligands with a tendency to self-association. However, in many cases all three binding modes may take place at the same time. In contrast to the outside stacking, which is mainly governed by the electrostatic interactions, groove binding and intercalation result from a supramolecular assembly based on π-stacking, hydrogen bonding, van der Waals, and hydrophobic interactions. Importantly, intercalation has a significant influence on the DNA structure, because the double helix needs to unwind as the intercalator fits between the base pairs. This unwinding leads to the lengthening of the double helix for approximately 3.4 Å per intercalator molecule, and may be used for unambiguous discrimination of the intercalation process from the groove binding, since the latter process does not significantly influence the DNA structure.

Polycyclic aromatic molecules are usually regarded as classical intercalators, with representative examples such as acridine derivatives, *e.g.* proflavine (**1**),[3] phenanthridinium salts, *e.g.* ethidium (**2**),[1,4] or monomethine dyes (*e.g.* Thiazole Orange).[5,6] It has been observed that a cationic charge and a chromophore consisting of at least three aromatic rings are general features of intercalating ligands.[7] In most intercalators, the positive charge is provided by an exocyclic alkylamino side chain or by an endocyclic pyridinium moiety, which are

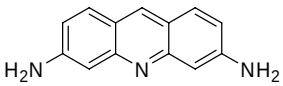

1

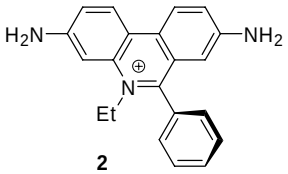

2

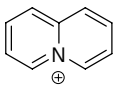

3

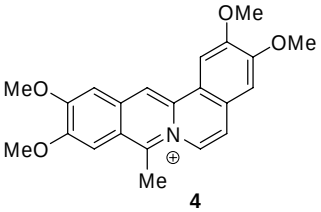

4

quaternized by alkylation or protonation. As a consequence, the pH of the environment has a significant influence on the DNA-binding properties of such ligands.

In contrast, in cationic ligands with a bridgehead nitrogen atom, *e.g.* derivatives of the quinolizinium ion (**3**), the brutto charge is independent of the pH of the environment. Although the structures of this kind are rather rare in comparison with a vast number of the intercalators investigated to date, annelated quinolizinium derivatives represent important lead structures for DNA intercalators and DNA-targeting drugs.[8] Thus, alkaloids of the protoberberine series, in particular coralyne (**4**), exhibit an anti-leukemic activity, which was correlated with its DNA-binding properties.[9] Moreover, coralyne acts as a poison of human topoisomerase I, the enzyme that is responsible for the modification of the tertiary structure of DNA and vital for replication and gene expression.

Recently, the DNA-binding properties of a number of annelated quinolizinium derivatives, such as acridizinium (**5a**) and its amino derivatives, *e.g.* **5b**,[10] naphthoquinolizinium salts **6a−b**,[11] and 12a,14a-diazoniapentaphene **7a**,[12] have been investigated in detail. Thus, it has

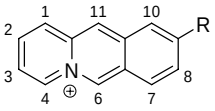

5a: R = H
5b: R = NH_2

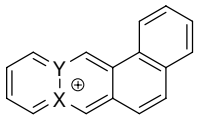

6a: X = C, Y = N
6b: X = N, Y = C

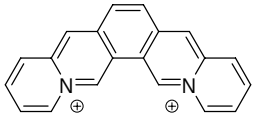

7a

been concluded on the basis of spectrophotometric titrations, circular and linear dichroism spectroscopy and ^{1}H-NMR study of ligand–oligonucleotide complexes that these compounds bind to double-stranded (ds) DNA mainly by intercalation.[13] The parent compound **5a** binds to ct DNA with a rather moderate binding constant ($K = 1.2 \times 10^4$ M^{-1}), whereas the introduction of an amino group in derivative **5b** results in an about 5-fold increase of the binding affinity. An even higher increase of the binding affinity is caused by an extension of the π system in the naphthoquinolizinium salts **6a–b** ($K \approx 2 \times 10^5$ M^{-1}) and in the case of the doubly-charged pentaphene derivative **7a** ($K = 5.7 \times 10^5$ M^{-1}). Moreover, a slightly

preferential binding to GC-rich DNA was demonstrated for these compounds by the comparison of binding constants with $[poly(dGdC)]_2$ and $[poly(dAdT)]_2$. Quinolizinium derivatives **5–7** are fluorescent in the unbound state and, while acridizinium **5a** and its annelated derivatives **6a–b** and **7a** fluoresce in the blue region (400–450 nm) of the visible spectrum, 9-aminoacridizinium **5b** exhibits an intensive fluorescence in the yellow-green region (500–520 nm) and has a large Stokes shift ($\Delta\lambda \approx 120$ nm). This difference is attributed to the significant donor-acceptor interplay in compound **5b**.[14] Nevertheless, the interaction with ds DNA results in an efficient quenching of fluorescence of these salts due to a photoinduced electron-transfer reaction between the excited acridizinium ion and nucleic bases. Therefore, these compounds are hardly useful as DNA probes, since a decrease of fluorescence intensity may be also due to other external stimuli (*e.g.* heavy atoms, aromatic amino acids, other functional groups which assist rapid intersystem crossing, some inorganic ions).

Annelated quinolizinium derivatives, including coralyne and its synthetic analogues **5–7**, are also capable of photoinduced DNA cleavage.[11–12,15–16] Thus, UV-light irradiation of supercoiled plasmid DNA in the presence of these compounds results in single strand breaks, as shown by gel electrophoresis. The mechanism of the photoinduced DNA damage by acridizinium derivatives depends on the presence of molecular oxygen; thus, under aerobic conditions, singlet oxygen is generated by photo-excited acridizinium ions, which leads to oxidation of the DNA bases, primarily guanine. Under oxygen-free conditions, however, hydroxyl radicals are formed upon interaction of excited acridizinium ions with the water molecules, which induce frank breaks of DNA strands by hydrogen abstraction from deoxyribose residues.[15] Photoinduced DNA damage is an important event in cellular systems, often leading to the cell death, mutagenesis, or aging in the absence of DNA repair mechanisms, and finds application as a photodynamic chemotherapy. However, while many organic dyes are known that damage the DNA upon irradiation, the selectivity of this process remains a challenging goal, since the photosensitizers usually show no or just little sequence or structure selectivity with respect to the target DNA.[17] A promising approach to the site-selective DNA photodamage is the tethering of DNA-photocleaving agents and DNA-recognizing moieties, such as triplex-forming oligonucleotides (*vide infra*) or units capable of recognition of specific, *e.g.* abasic DNA sites.

1.2 Fluorescence Probes for Detection of Biomacromolecules

The detection and labeling of biomacromolecules by organic fluorescence probes is widely used in analytical chemistry, biochemistry and medicine, mainly because of the high sensitivity of this method.[18] Recent developments in the near-field microscopy and confocal microscopy techniques allow even the detection of single fluorescent molecules and probing of the microenvironment of the dye molecule.[19] In particular, organic dyes offer the opportunity to design the chemical and photophysical properties of fluorescent probes by a systematic variation of the substitution pattern, and thus provide access to an almost unlimited range of possible applications.

Fluorescent probes whose emission intensity increases upon association with DNA or proteins are useful tools in genomics and proteomics, because the binding event to the host molecule may be followed by the appearance of an intense fluorescence emission ("light-up probes").[20] Their major applications are staining of DNA and proteins in gel electrophoresis and quantification of these biomacromolecules in solution.[21] Thus, for the detection of DNA bands after gel electrophoresis, staining with ethidium bromide (**2**) is the most common approach. However, the strong mutagenic effect of ethidium bromide complicates its handling. At the same time, less toxic dyes are available, such as the bis(benzimidazole) derivatives Hoechst 33258 (**8a**) and Hoechst 33342 (**8b**),[22] as well as the monomethine dyes Thiazole Orange (**9a**) or its oxazole analogue **9b**.[5] Moreover, dimeric mono- and polymethine dyes, such as TOTO (**10a**)[23] and YOYO (**10b**)[23,24] exhibit very pronounced fluorescence enhancement upon binding to ds DNA. Fluorescence quantum yields of widely used DNA stains are summarized in Table 1.1.

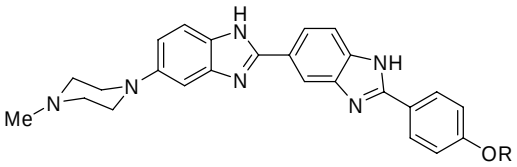

8a: R = H
8b: R = Et

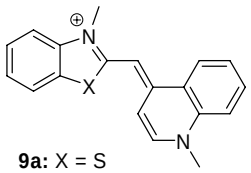

9a: X = S
9b: X = O

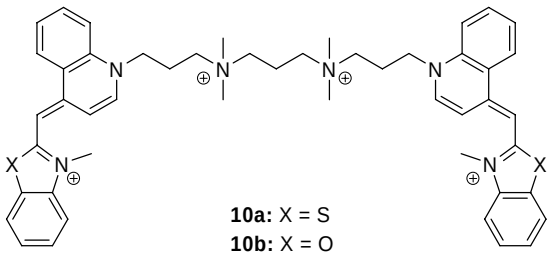

10a: X = S
10b: X = O

Table 1.1. Fluorescence quantum yields of the most widely used fluorescent DNA stains in isotropic solution and in dye–DNA complexes (taken from Ref. 22).

Dye	Φ_f [a]	Φ_{DNA} [b]	Φ_{DNA} / Φ_f [c]
Ethidium bromide (**4**)	0.039	0.35	~ 10
Hoechst 33258 (**8a**)	0.015	0.42	~ 30
Hoechst 33342 (**8b**)	0.034	0.38	~ 10
Thiazole Orange (**9**) [d]	0.0002	0.10	~ 500
TOTO (**10**) [e]	0.0002	0.34	~ 1400
PicoGreen	0.0006	0.64	> 1000
SYBR Gold	0.0006	0.66	> 1000

[a] Fluorescence quantum yield of the uncomplexed dye; [b] fluorescence quantum yield in the presence of DNA (r = 0.1); [c] fluorescence enhancement upon complex formation with DNA; [d] Ref. 5b; [e] Ref. 23.

It should be mentioned that proprietary fluorescent stains, such as PicoGreen and the SYBR dye family[25] have very low intrinsic fluorescence in the absence of DNA, which is enhanced by a factor of more than 1000 upon intercalation. Therefore, these dyes have excellent properties to be applied for DNA quantification in solution and visualization of DNA fragments in gel electrophoresis. However, these stains have been discovered by the exploratory screening rather than by rational design. Thus, studies towards a better understanding of the origin of the fluorescence response of fluorescent probes are scarcely addressed in the literature. For example, the mechanism of the fluorescence enhancement of ethidium bromide upon binding to DNA has been a matter of debate for more than 20 years.[26] Even less studied are the DNA-binding properties of the proprietary fluorescent stains, since their structure is protected and hidden in the patent literature, which does not allow the determination of structure–properties relationships.

Similarly to DNA staining, proteins, that are separated in SDS–polyacrylamide gel electrophoresis[27] or in microchip capillary electrophoresis,[28] need to be visualized to allow band detection. This staining is usually achieved by visible dyes, such as Coomasssie Blue dyes, or by colloidal silver. However, fluorescent stains may be also applied for the detection of proteins, such as Nile Red (**11**),[29] 1-anilino-8-naphthalenesulfonate (1,8-ANS, **12**),[30] or the SYPRO dye family.[31] Moreover, environment-sensitive fluorescent probes, such as 1,8- and 2,6-ANS (**13**) and derivatives thereof, are suitable for probing protein conformations *in vitro* and *in vivo*.[32]

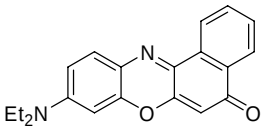

11

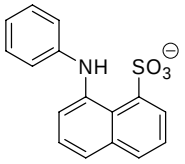

12

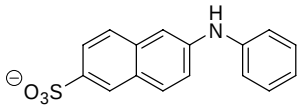

13

At the same time, only few systematic strategies for the rational design of light-up probes or detailed analyses of structure-property relationships are known, since the interaction of organic dyes with proteins is driven by many factors. Sometimes, the fluorescent protein stains, such as SYPRO dyes, are not compatible with anionic surfactants, such as SDS used in proteine gel electrophoresis, so that prolonged washing to remove the surfactant from gels is required. Therefore, the synthesis and investigation of protein-sensitive fluorescent dyes, which would be compatible with most common procedures and tolerant to interference from foreign substances, represents an active research area.[33]

1.3 Triplex-DNA Binders

Triple-helical structures of nucleic acids, DNA as well as RNA, are formed—in either inter- or intra-molecular fashion—when a third strand binds to the major groove of a homopurine DNA region (Figure 1.1, A).[34,35] This binding takes place due to Hoogsten or reverse Hoogsten hydrogen bonding with the nucleic bases in the purine-rich strand (Figure 1.1, B). In the former case, the third strand runs parallel relative to the 3′→5′ direction of the purine strand of the duplex, whereas in the case of reverse-Hoogsten bonding it is oriented in the opposite direction.

It has been demonstrated that the binding of an oligonucleotide to an oligopyrimidine–oligopurine DNA structure is sequence-specific. Such oligonucleotides are referred to as triple helix-forming oligonucleotides (TFOs). Along with synthetic hairpin polyamides that are capable of recognizing short DNA sequences in the minor groove[36] and DNA-binding zinc finger proteins,[37] the triplex-forming oligonucleotides represent an important class of DNA sequence-reading agents. This property may be used to design tools for the manipulation of ds DNA *in vitro* as well as for interfering with the DNA-related processes *in vivo*. Thus, TFOs can interfere with the binding of transcription factors, transcription elongation, or DNA repair.[34] Moreover, TFOs covalently bound to a DNA-cleaving agent, *e.g.* EDTA–Fe^{2+} or phenanthroline–Cu^{2+}, are capable of selective strand scission. Unlike conventional restriction

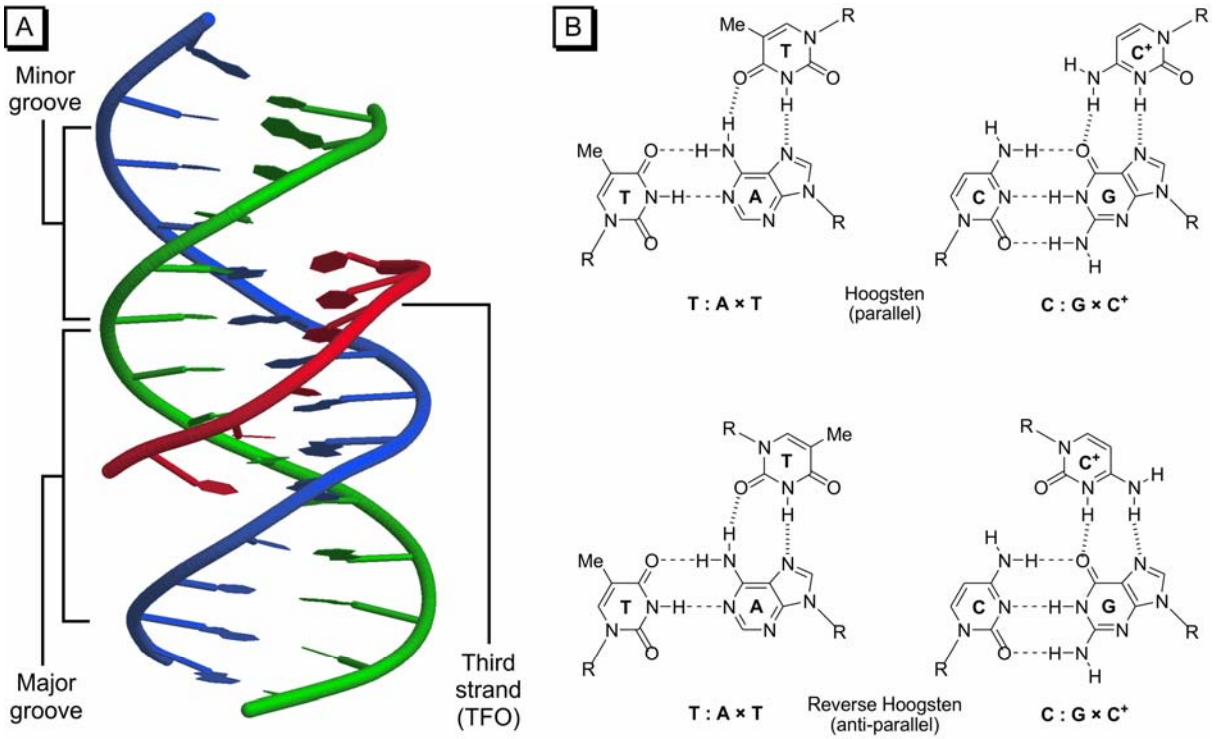

Figure 1.1. (A) Schematic representation of a TFO (red) associated with a DNA duplex (replotted from the PDB ID: 1BWG).[38] (B) Selected Hoogsten and reverse-Hoogsten base triplets. Watson-Crick hydrogen bonds are shown by dashed lines, while Hoogsten hydrogen bonds are shown by hashed lines. R = sugar residue.

enzymes, such conjugates have much longer recognition sequences and cut genomic DNA less frequently and into larger fragments.[39] On the other hand, sequence-specific *photoinduced* DNA damage has been achieved by TFOs that are covalently attached to photosensitizing molecules, such as psoralen or ellipticine.[40] Recently, conjugates of TFOs with a topoisomerase poison, namely camptothecin, have been described, which induce selective DNA cleavage by topoisomerase I at the triplex-binding sites.[41] In general, conjugates of the described type act as sequence-specific artificial endonucleases.

Limitations of the TFO-based approach, however, arise from the low stability of triple-helical DNA structures at physiological conditions. Thus, a relatively high ionic strength or the presence of multivalent ions, *e.g.* Mg^{2+} or protonated polyamines, is required for triplex formation, and even a single base mismatch drastically reduces the triplex stability. Moreover, the protonation of cytosine residues, and consequently an acidic environment ($pH < 6$) is required for the formation of the parallel triplexes. In general, four strategies are available to increase the stability of the triple-helical structures: (i) modification of the structure of the TFO, *e.g.* use of peptide or aminoalkyl-substituted phosphoramidate backbones; (ii) use of modified nucleic bases, which do not require protonation, *e.g.* 5-methylcytosine or

6-oxocytidine, or which are capable of particularly strong hydrogen bonding, *e.g.* 5-fluorodeoxyuracil, (iii) covalent attachment to a TFO of an efficient DNA-binding unit, *e.g.* an acridine derivative or a polyamine, and (iv) use of external, non-conjugated small molecules that bind selectively to the triplex structure and increase its stability.[42,43] A prerequisite for the action of the agents of the latter type is the preferential binding to triplex DNA over the duplex form, since it shifts the equilibrium in the direction of the triplex formation (Scheme 1.1).

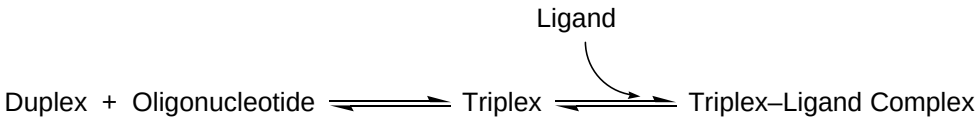

Scheme 1.1. Equilibrium for stabilization of triplexes by triplex-binding ligands.[42c]

Since the discovery of the triplex selectivity of a benzo[*e*]pyridoindole derivative (BePI, **14**),[44] a number of triplex-binding agents have been identified,[42] including benzopyrido- and benzoquinoquinoxalines, *e.g.* **15**,[45] dibenzophenanthrolines, such as **16**,[46] naphthylquinolines,[47] indolocarbazoles,[48] biarylpyrimidines, *e.g.* **17**,[49] 2,6-disubstituted anthraquinones **18**,[50,51] aromatic diamidines,[52] and several alkaloids (coralyne **4**, cryptolepine).[53,54]

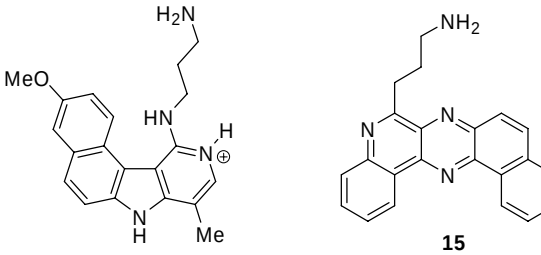

14

15

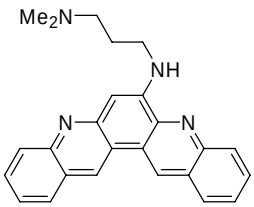

16

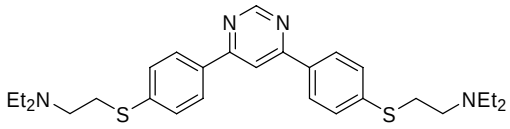

17

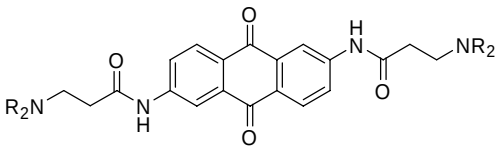

18

Beyond their use for increasing the stability of triple-helical structures, triplex-selective ligands may be combined with DNA-modifying agents. In this approach, a ternary complex between a triplex ligand, TFO, and a target DNA sequence is formed, resulting in a modification of the latter.[55] Thus, conjugates of the EDTA–Fe^{2+} complex with a triplex-

specific benzoquinoquinoxaline derivative were shown to cleave the target DNA sequence in the presence of the corresponding TFO.[55a] As a particular case, the triplex-binding specificity and DNA-photodamaging properties may be combined in one unit, as in the case of amino-substituted dibenzophenanthrolines.[46] Thus, it has been shown that irradiation of a double-stranded plasmid fragment in the presence of a complementary TFO and a triplex-specific photocleavage agent **16** leads to an efficient cleavage of the target duplex in the vicinity of the TFO-binding site. In the absence of the TFO, no photoinduced DNA cleavage has been observed.[46a]

Apart from their use *in vitro*, triplex-DNA binders may show *in vivo* activity. Thus, it was shown that coralyne promotes the formation of short DNA triplexes *in vivo* as well, which provides a possibility for a site-directed mutagenesis.[56] Moreover, since *in viv*o formation of DNA triplexes interferes with the function of topoisomerases,[57] several triplex-DNA binders, *e.g.* cryptolepine, coralyne[53] and indolocarbazoles,[48] have been identified as potent topo-isomerase poisons and thus promising lead structures for anti-cancer drugs.[58]

1.4 Ligands Associating with DNA Abasic Sites

Abasic, or apurinic / apyrimidinic sites (AP-sites), represent one of the most frequent lesions in the DNA.[59] They result from the removal of a heterocyclic nucleic base by the hydrolysis of the *N*-glycosidic bond, leaving deoxyribose residues in the DNA strand (Figure 1.2). Abasic-site formation occurs spontaneously under physiological conditions due to depurination. This process is, however, markedly increased by the modification of purine bases, either by chemical (alkylating agents, antitumor drugs) or physical factors (UV light, γ-radiation). Abasic sites are also produced enzymatically during the base excision repair pathway following the excision of modified or abnormal bases by DNA *N*-glycosylases. Abasic sites are miscoding and non-informative DNA lesions, which have to be repaired prior to replication and transcription; they also appear to interfere with other vital enzymes, such as topoisomerases. If not repaired, the abasic sites can be mutagenic or lethal. Therefore, abasic-site repair is a critical cellular activity. This repair pathway includes DNA breakage at the abasic site by a specific AP-endonuclease, followed by the resynthesis of the DNA by DNA polymerase and ligase.

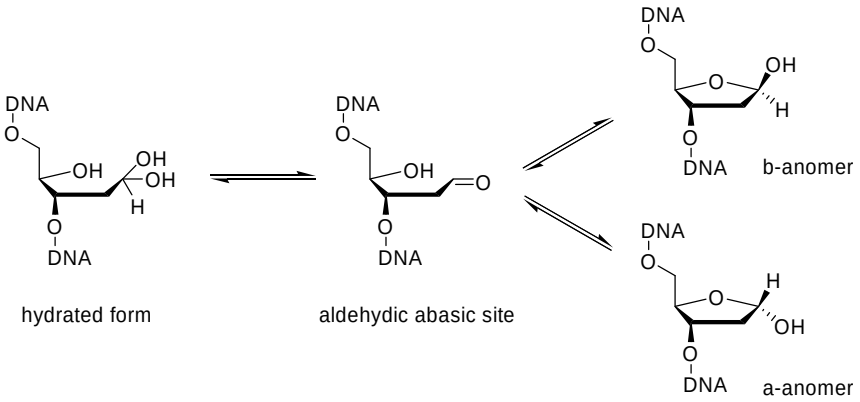

Figure 1.2. Chemical structure of an abasic lesion showing the equilibrium forms.

Due to the biological significance of abasic sites as intermediates in the repair of damaged DNA and as mutagenic or carcinogenic lesions, there is a great challenge to design molecules which could be able to selectively recognize this lesion and suppress its repair process. The AP-endonucleases, which recognize and cleave DNA at these sites at the first stages of the repair process, are interesting target candidates for the potentiation of the action of antitumor drugs, since a deficiency of the repair pathway could result in an enhanced cellular sensitivity to anti-cancer agents, allowing the use of lower doses to achieve comparable therapeutic result.[60] Thus, 9-aminoellipticine (**19**) and the structurally related 3-aminocarbazole, which intercalate into ds DNA, interact with abasic sites by the formation of Schiff bases with the aldehyde group of the latter, and induce DNA cleavage at these sites.[61] These compounds enhance the cytotoxic effect of the alkylating agent, dimethylsulfate, in cell colonies.[61b] The macrocyclic bisacridine **20** was shown to bind to abasic sites by a “threading intercalation”

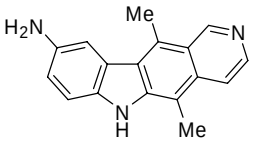

19

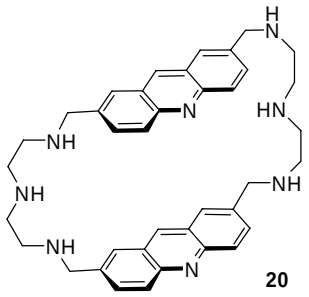

20

mode, sandwiching the base pair opposite to the lesion between the two acridine rings, and leaving the alkaline side chain in the DNA grooves. This cyclobisintercaland also induces selective photocleavage of DNA in the vicinity of the abasic lesion.[62]

Recently, a series of heterodimeric molecules, such as **21**–**25**, that were designed to bind selectively to the abasic sites (Figure 1.3), has been described.[60,63] These compounds include (i) a recognition unit, *i.e.* a nucleic base that inserts into the abasic cavity and forms hydrogen bonds with the complementary base in the opposite strand; (ii) an intercalator, serving for a strong but non-specific binding to DNA; and (iii) a linking chain ("linker") endowed with

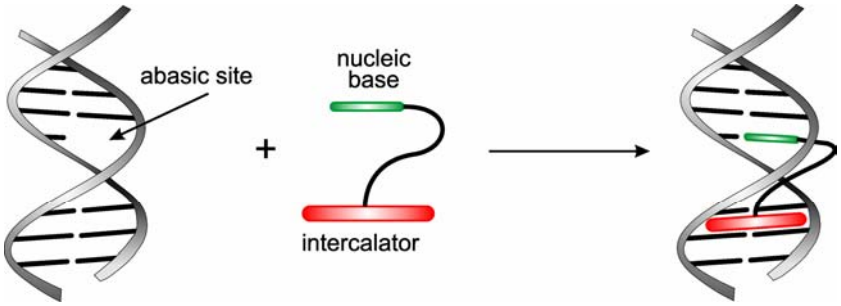

Figure 1.3. Interaction of nucleic base–intercalator conjugates with abasic sites.

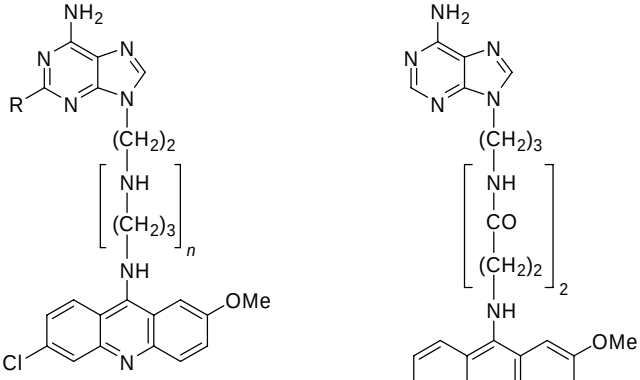

21a: R = H, n = 1
21b: R = NH_2, n = 1
21c: R = H, n = 2
21d: R = NH_2, n = 2

22

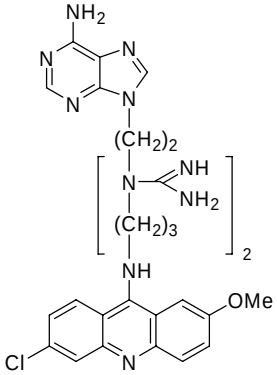

23

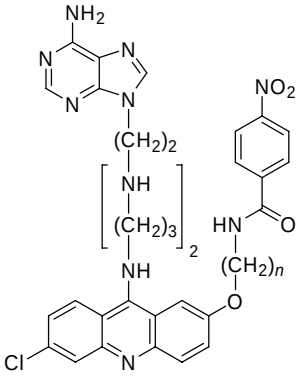

24a: n = 4
24b: n = 6

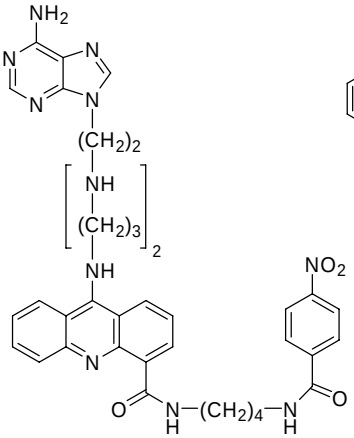

25

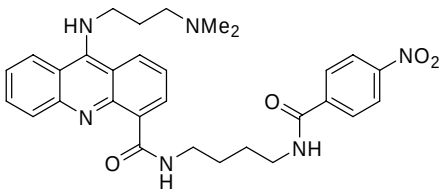

26

DNA-binding and/or DNA-cleaving properties. These molecules may act as artificial nucleases or DNA-repair inhibitors. Thus, compounds **21a–d** with an alkaline linking chain efficiently cleave the abasic DNA strand by the β-elimination mechanism.[64] Within this series, the use of 2,6-diaminopurine as a recognition unit (**21b**, **21d**) increases both the DNA affinity and the cleavage activity. In contrast, compounds **22** and **23** with no secondary amino groups in the linker show no DNA cleavage activity. Conjugate **23**, however, binds strongly to abasic DNA *in vitro* and *in vivo* and acts as an inhibitor of DNA exonulease III. This compound also potentiates the action of bis(chloroethyl)nitrosourea (Carmustine), an alkylating antitumor drug which induces abasic sites in the DNA. Thus, an apparent synergic effect of up to 94% was observed.[63b]

Another approach towards targeting abasic sites makes use of the phenomenon of clustered DNA lesions, or locally multiple damaged sites. These lesions, in close proximity to each other, appear to be very toxic, as they are difficult to be repaired by the cellular enzymes. Hence the production of new lesions in the vicinity of an abasic site is a promising strategy to increase the biological activity of antitumor drugs.[60] This has been realized by introducing a second DNA-damaging or DNA-cleaving group, as in compounds **24** and **25**. Compounds **24a–b** with a nitrobenzamide residue are able to photoinduce DNA damage. Moreover, the alkali-labile strand breaks are produced on both DNA strands in close proximity (1–2 nucleotides) to the abasic site, as shown by DNA footprinting studies. In contrast, compound **25**, consisting of the similar functional moieties, is photobiologically inactive.[65]

Notably, recent studies reveal that the nucleic base unit is not absolutely necessary for the action of the chimeric molecules of the described type. Thus, compound **26**, in which the recognition unit (adenine) was replaced with a simple alkylamine chain, also binds preferentially to abasic DNA sites, as shown by NMR and molecular-dynamics studies of complexes of **26** with oligonucleotides. Upon irradiation with UV light, this ligand efficiently induces alkali-sensitive strand breaks at the abasic sites, provided the unpaired nucleotide is a pyrimidine. No DNA cleavage has been observed when the unpaired base was a purine.[66]

1.5 Methods for Study of DNA–Ligand Interactions

1.5.1 UV/Vis Absorption Spectroscopy

Upon complex formation with DNA, the ligand molecule is positioned in an environment which is different from the one of the uncomplexed molecule in solution. The ligands, especially solvatochromic compounds such as organic dyes, usually have different absorption properties in the complexed and uncomplexed forms.[67] Thus, upon interaction of DNA with a ligand, a shift of the absorption maximum of the latter to longer wavelengths (bathochromic, or "red" shift) and a decrease of the absorbance (hypochromic effect) usually occur. These effects may be utilized to probe the equilibrium binding properties of a ligand with DNA. In practice the association process is monitored by a spectrophotometric titration, during which aliquots of DNA solution are added to a solution of the ligand. The absorption spectra at each dye-to-DNA ratio are determined and superimposed.[67,68]

Further information might be extracted from spectrophotometric titrations if isosbestic points are observed. An isosbestic point appears when each absorption spectrum of the titration has the same absorbance at a particular wavelength, *i.e.* a point of intersection of all superimposed absorption spectra. Such isosbestic points reveal that each absorption spectrum arises from almost exclusively two different absorbing species (*e.g.* complexed and uncomplexed dye). Because it is likely that each binding mode results in different absorption properties, an isosbestic point indicates that mainly one particular binding mode between the DNA and the guest molecule occurs. It should, nevertheless, be noted that a second, but minor, binding mode only contributes marginally to the overall absorption spectrum and might not have a significant influence on the isosbestic points.

Data from spectrophotometric titrations may also be used to determine the association constant between the ligand and DNA. Thus, from the absorbance data at a certain wavelength, concentrations of bound (c_b) and free (c) ligand species may be calculated. Analysis of these data is usually performed using a binding model of McGhee and von Hippel,[69] to access the values of the affinity constant, K, and the binding site size, n. Additionally, the base selectivity of the association may be investigated by spectrophotometric titrations with synthetic polynucleotides such as $[poly(dGdC)]_2$ and $[poly(dAdT)]_2$.

Spectrophotometric titrations have been widely applied for the study of ligand–nucleic acid interactions.[10–12,67] This method is often used as a reference tool to validate the values of binding constants obtained by other techniques, such as competition dialysis (*vide infra*). In

fact, spectrophotometric titrations are one of the few methods that allow determination of the binding site sizes of the ligands, since in this case the investigation is performed in a broad range of ligand-to-DNA ratios.

Unfortunately, a major drawback of photometric titrations is the requirement of relatively large amounts of DNA, which makes it inconvenient for the studies with non-canonical, triplex or quadruplex DNA structures. This problem may be, however, to some extent overpassed by the use of micro- or semimicro spectrophotometric cells. Another disadvantage is the tendency to large errors, which are not intrinsic for the method, but arise in the course of fitting the experimental data to the multi-parametric model. As a consequence, spectrophotometric titrations should be performed several times, in order to obtain reliable values of the binding parameters. For these reasons, spectrophotometric titrations are hardly suitable for the high-throughput screening of potential ligands.

1.5.2 Fluorescence Spectroscopy

If a molecule has pronounced fluorescence emission properties, the interaction with DNA may, as in the case of absorption spectroscopy, result in shifts of the emission maxima and changes of the fluorescence quantum yield.[67,68] In the latter case, either an increase or a decrease of the emission intensity might be observed. Dyes whose fluorescence intensity increases on binding to DNA have especially high potential as DNA stains, or markers (*vide supra*). In the absence of DNA the relatively low fluorescence quantum yield of these dyes results from a radiationless deactivation of the excited state by conformational changes or acid–base reactions with the solvent. On association with DNA, however, a significant suppression of the conformational flexibility and a shielding of the dye from solvent molecules within the complex occur, leading to an increase of the emission intensity.

In contrast, many organic chromophores are known whose fluorescence intensity decreases upon interaction with DNA. The origin of this quenching is usually an electron- or energy-transfer reaction between the excited dye and the DNA.[70] Since organic dyes usually have absorption maxima at longer wavelengths than the DNA bases, energy transfer between the excited dye and DNA is energetically disfavored when the chromophore is excited at these wavelengths. Most often an electron-transfer reaction between the excited dye and the DNA bases occurs, with guanine being the base with the highest propensity to be oxidized.

The change of the emission intensity upon complex formation is followed by spectrofluorimetric titrations, which are performed analogously to spectrophotometric titrations. Nevertheless, it must be considered that the absorption at a particular wavelength may also change upon DNA addition, which also leads to a change of the emission intensity on excitation at this wavelength. To avoid this secondary effect on the emission spectrum, which does not reflect the direct influence of the DNA on the emission properties of the ligand, the fluorophore should be excited at the isosbestic point, which is obtained from the spectrophotometric titrations.

1.5.3 Thermal Denaturation of DNA–Ligand Complexes

Thermal denaturation of the DNA-ligand complexes is a useful tool for a rapid and unambiguous determination of the stabilizing effect of the bound ligands on the double helix.[71] In such an experiment, samples of DNA are heated in a buffer solution of known ionic strength in the presence or in the absence of ligands, while the UV absorbance is monitored at a wavelength of nucleic base absorption (usually 260 nm). The plots of normalized absorbance versus temperature are known as melting curves, or profiles, of DNA. The denaturation (duplex-to-random coil transition) of DNA is accompanied by a sharp increase of UV absorption, while the middle point of this transition, at which one-half of DNA is in the double-helical state, is defined as the melting temperature of the DNA sample, T_m. Ligands that bind to the double-stranded DNA, but not—or weakly—to single-stranded DNA, stabilize the ds DNA against thermal denaturation, and thus increase the corresponding T_m values. The induced shifts of the melting temperature, $\Delta T_m = T_m(\text{DNA}-\text{Ligand}) - T_m(\text{DNA})$, may serve as a characteristic of the DNA affinity of a given ligand. Destabilizing ligands, which preferentially bind to single-stranded DNA, show negative ΔT_m values.

Beyond monitoring the changes in the UV absorption of the DNA, other physical properties, such as the fluorescence emission signal of dye-labeled oligonucleotides (“molecular beacons”),[72] position and intensity of NMR signals, circular dichroism, or Raman signals, that accompany thermal denaturation of the DNA, may be used for detection of the melting event. Recently, a novel modification of the thermal denaturation experiment was proposed, in which the melting event is monitored by the change of the absorption of oligonucleotide-modified gold nanoparticles, which disaggregate as the DNA strands separate.[73] However, UV melting studies are more suitable for high-throughput screening, since they exploit the readily

available natural DNA samples or unmodified synthetic oligo- or polynucleotides. In contrast, the fluorescence melting experiments require oliginucleotides which are modified with fluorescent labels, and, in spite of somewhat higher sensitivity of the method and, consequently, lower amounts of DNA required for a single experiment, remain a highly priced alternative. The above-mentioned points concern also the nanoparticle-modified DNA melting assay, although the sensitivity of the latter method is even higher.

In the case of triplex DNA, the UV melting profiles usually contain two transitions. The low-temperature transition ($T_m^{3\rightarrow2}$) corresponds to the dissociation of the triplex into duplex and a single-strand polynucleotide (Hoogsten transition, Figure 1.4), whereas the high-temperature event ($T_m^{2\rightarrow1}$) represents the denaturation of the remaining double helix (Watson–Crick transition). The comparison of the ligand-induced shifts of these transitions allows accessing the structural selectivity of the ligands, as the triplex-selective ligands increase the $T_m^{3\rightarrow2}$ values, with no or little influence on the temperatures of the Watson–Crick transition. It should be noted that the values of $\Delta T_m^{3\rightarrow2}$ reflect the difference in binding to triplex *vs*. duplex structures and not the strength of the binding to the triplex alone, whereas $\Delta T_m^{2\rightarrow1}$ measures a difference in binding to the duplex *vs*. single strands.[74] Modifications of the thermal denaturation experiment, such as the use of fluorophore-modified[72] or gold nanoparticle-modified oligonucleotides,[73b,75] that increase the sensitivity of the method, have been applied for studies with triplex DNA, too.

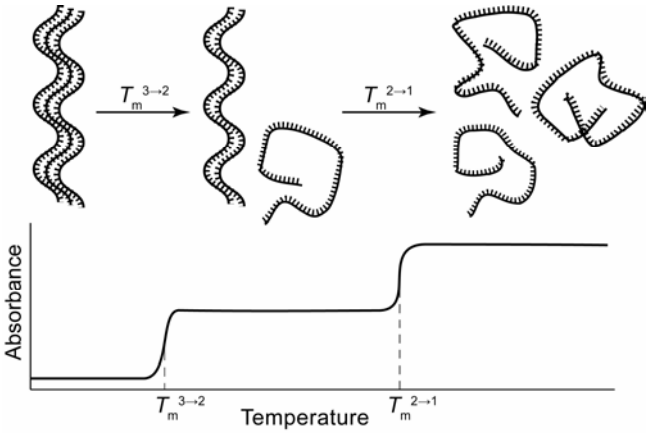

Figure 1.4. Schematic representation of a thermal denaturation experiment with triplex DNA.

The major drawback of the thermal denaturation experiments is that it is not possible to correlate directly the ligand-induced T_m shifts with the thermodynamic affinity constant. Thus, the ΔT_m values depend not only on the affinity constant, but also on the binding-site size, a

possible cooperativity between ligand molecules, ionic strength and pH of the solution, and on the enthalpy of the DNA denaturation. Moreover, the binding constant at the melting temperature, K_{Tm}, usually cannot be correlated with the intrinsic binding constant, K_i, as the enthalpy of the ligand binding (ΔH_b) is hardly accessible. Although several comprehensive numerical models for simulation of DNA melting profiles and prediction of the ΔT_m values have been proposed,[76,77] their use requires the determination of several parameters, primarily ΔH_b, by independent methods, such as microcalorimetry.[78] However, since in the current work the thermal denaturation experiments were performed with a series of structurally very similar ligands, which should have similar thermodynamic parameters of the DNA binding, it may be expected that the ΔT_m values give a reliable characteristic of affinity of ligands to the DNA.

1.5.4 Linear Dichroism Spectroscopy

Linear dichroism (LD) spectroscopy is an efficient tool to evaluate the binding modes between ligands and nucleic acids.[79] In a typical experiment, the DNA molecules are oriented by an external electric or hydrodynamic field ("flow linear dichroism"), while the vector of the field lines is defined as a reference axis. The unbound ligand molecules are usually not oriented by a hydrodynamic field. Therefore, the nucleic bases of the DNA and—in the case of an intercalative binding mode—bound ligand molecules are oriented perpendicular to the reference axis ($\alpha \approx 90°$). Molecules that bind in the DNA grooves show a different orientation with respect to the reference axis ($\alpha \approx 45°$).

Linear dichroism is defined as a differential absorption of light, polarized parallel and perpendicularly to the reference axis ($LD = A_{\parallel} - A_{\perp}$). Since the absorption of polarized light by a chromophore depends on the geometrical orientation of its transition dipole moment—which usually lies in the plane of the chromophore—relative to the polarization plane of the light, linear dichroism allows the determination of angles of chromophore planes with respect to the reference axis. The chromophores, whose transition dipole moments are oriented at an angle $\alpha > 55°$ with respect to the axis (nucleic bases and intercalated ligands), show a negative LD signal, while those with a smaller deviation from the axis (ligands, which are bound in the DNA grooves or stacked to the external phosphate backbone) show a positive LD signal.

By dividing the LD value by the absorbance of the unoriented sample under isotropic conditions (A_{iso}), the "reduced" linear dichroism (LD_r), *i.e.* the wavelength-independent LD, is

obtained. The LD_r signal provides additional information on the average orientation of the transition moment of the dye relative to those of the DNA bases and allows distinguishing between homogeneous and heterogeneous binding.

Linear dichroism spectroscopy has been widely and successfully applied to study the mode of interaction of various ligands with ds DNA.[8,79] However, the disadvantage of the method is the requirement of relative large amounts of polymeric DNA. For this reason, linear dichroism experiments are usually not applied in studies with multi-stranded DNA structures or oligonucleotides. Another hydrodynamic method, namely the viscosimetry of DNA solutions,[80] also provides information on the binding modes of ligands to the DNA; however, it requires comparably large amounts of DNA samples and has a similar scope as LD spectroscopy.

1.5.5 Competition Dialysis

Competition dialysis is a powerful new method that allows the determination of preferential binding of ligands to particular structures or sequences of nucleic acids.[81] The method is based on firm thermodynamic principles and is simple to implement. In the competition dialysis experiment, an array of nucleic acid samples is dialyzed against a mutual ligand stock solution. After equilibration, the amount of ligand bound to each structure or sequence is determined. Since all structures and sequences are in equilibrium with the same concentration of the free ligand, the amount of bound ligand may be correlated with the affinity of the ligand for that particular DNA sample. This method provides a direct and quantitative measure of selectivity, and unambiguously identifies which of the DNA structures or base sequences within the sample array are preferred by a particular ligand.

The competition dialysis assay is based on the fundamental thermodynamic principle of equilibrium dialysis. Thus, at equilibrium, the chemical potential of the free ligand is equal inside and outside the dialysis unit, and any excess ligand on the macromolecule side of the membrane may be attributed to binding to the macromolecule. Therefore, competition dialysis data may be used to calculate the apparent binding constants and free energies of the binding. The apparent binding constants, however, do not correspond to the intrinsic binding constants, since they are derived from a single set of reactant concentrations. They essentially correspond to a single point on a more complete binding isotherm, and have to be validated

using independent complementary methods, such as spectrophotometric or spectrofluorimetric titrations.[81b]

Competition dialysis also proved to be useful for the quantitative study of compounds that bind to higher-order DNA structures. Thus, a variety of compounds with selectivity for triple-helical or quadruplex DNA were studied by this method.[82] Advantages of the method are high throughput and a possibility to use a large number of various DNA structures, provided they are all stable at the experimental conditions. A major drawback of the competition dialysis experiment is that, as in the case of DNA thermal denaturation, the thermodynamic binding constant and the binding-site size are not directly accessible.

2 9-SUBSTITUTED ACRIDIZINIUM SALTS AS FLUORESCENT PROBES

2.1 Objective

As it has been shown in the Introduction, the annelated derivatives of the quinolizinium ion (**3**) represent an interesting, but relatively unexplored structural motif in DNA intercalators. Along these lines, the 9-aminoacridizinium (**5b**) represents a system with attractive photophysical properties, *i.e.* absorption in the near-UV region of the spectrum ($\lambda_{max} \approx 390$ nm), well separated from the one of the nucleic bases; good quantum yield of fluorescence ($\Phi_F = 0.12$ in aqueous solutions); and a large Stokes shift ($\Delta\lambda \approx 120$ nm),[14] allowing an unambiguous detection without re-absorption effects and not interfering with the background fluorescence of biomolecules. However, upon interaction with the DNA bases, the fluorescence of **5b** is significantly quenched due to the photoinduced electron-transfer reaction with the nucleic bases. Therefore, it was planned to modify the structure of **5b** in such a way that it had a very low intrinsic fluorescence, which might increase upon complex formation with DNA or other biomacromolecules.

To impair the intrinsic fluorescence properties of **5b**, an additional deactivation pathway for the excited state needs to be introduced. This could be realized *e.g.* by the introduction of an aryl substituent at the exocyclic nitrogen atom, giving the system **27**. The presence of such a substituent may result in two effects: (i) photoinduced electron-transfer reaction between the electron-rich phenyl substituent and the photo-excited acridizinium chromophore; (ii) rotation about the N-aryl bond, leading to the non-radiative deactivation of the excited state. For comparison, it has been shown that in 2-anilino-6-naphthalenesulfonate (**13**, R = H), the fluorophore widely used to study the conformation of proteins (*cf.* Section 1.2),[32] both effects

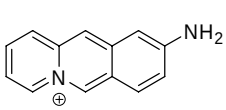

5b

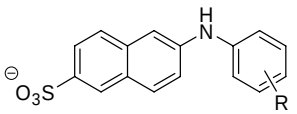

13

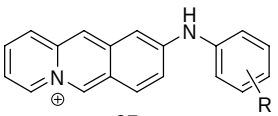

27

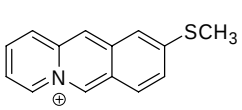

28

take place.[83] It was proposed that the binding of **27** to a host molecule might hinder one or both of the deactivation pathways, resulting in an increase of the fluorescence signal. Moreover, the use of the novel acridizinium-based chromophore may have advantages

compared to the established anilinonaphthalenesulfonate (ANS) system. Thus, the positively-charged acridizinium chromophore (in contrast to the negatively charged ANS) determines the DNA-binding properties of the system, and may also cause the association with the binding sites of proteins which are usually not accessible by the ANS-like probes. In addition, binding to the negatively charged protein–surfactant micelles in the presence of an anionic surfactant (SDS, used in the gel electrophoresis of proteins) may be possible, providing a tool for the visualization of proteins after gel electrophoresis.

Since the photophysical properites of intramolecular donor–acceptor systems, such as **13**, are often influenced by several independent effects, their detailed investigation represents a challenging research field[83] and a systematic study is desirable. This, in part, may be achieved by the synthesis and detailed investigation of a series of derivatives **27** with different substituents in the phenyl ring, such as electron-donating (R = OMe, NMe_2), electron-withdrawing (CF_3, CN), or halogen substituents (F, Cl, Br). Moreover, the substitution pattern may be varied, too. This approach would allow the deduction of a structure-properties relationship and, as a final goal, tuning the photophysical properties of the system in such a way that it could match a particular practical application.

To get insight into the photophysical properties of the system **27** and the parent compound **5b**, it was also planned to synthesize derivatives with the substituents other than aryl groups. Thus, *N*-alkyl- or *N*,*N*-dialkyl-substituted derivatives of **5b** may be useful to study the electron-donating effect of the alkyl groups on the 9-aminoacridizinium chromophore and, on the other hand, to serve as reference compounds for the investigation of the effects of the aryl substituent in compounds **27**. Finally, it was planned to synthesize and investigate a sulfur analogue of **5b**, *e.g.* compound **28** in which the amino group is replaced with a methylthio substituent. Since a methylthio group has different electron-donating properties than the amino substituent in **5b**, it was proposed that compound **28** could represent a complementary donor–acceptor system, which may also be used as a DNA-sensitive fluorescent probe.

2.2 Results

2.2.1 Synthesis of 9-Substituted Acridizinium Salts

2.2.1.1 Synthesis of 9-Amino-Substituted Acridizinium Salts

Similar to the nucleophilic substitution reactions of halogen- and alkoxy-substituted quinolinium[84,85] and quinolizinium salts,[86,87] the *N*-substituted 9-aminoacridizinium derivatives **27a–k** were synthesized by the reaction of the readily available 9-bromo-acridizinium bromide (**29**)[88] with selected amines (Scheme 2.1; Table 2.1). This reaction was unprecedented in the acridizinium system.[89]

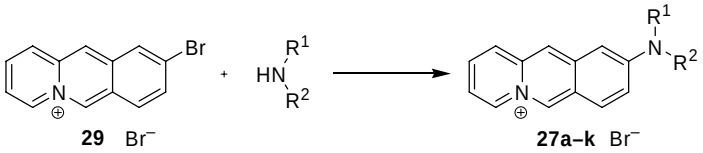

Scheme 2.1. Synthesis of 9-amino-substituted acridizinium salts. For the experimental conditions see Table 2.1.

Table 2.1. Reaction conditions and yields for the synthesis of 9-aminoacridizinium derivatives **27a–k**.

Compound	R^1	R^2	Reaction conditions			Yield / %
			Solvent	Time / h	Temp. / °C	
27a	– $CH_2CH_2OCH_2CH_2$ –		*i*PrOH	2	reflux	24
27b	– $(CH_2)_4$ –		*i*PrOH	2	reflux	30
27c	CH_3	CH_2CH_2OH	*i*PrOH	16	reflux	16 [a]
27d	H	4-$C_6H_4NMe_2$	EtOH	48	reflux	14
27e	H	4-C_6H_4OMe	*i*PrOH	48	reflux	13
27f	H	4-C_6H_4Me	none	6	130	77
27g	H	C_6H_5	none	24	130	23
27h	H	4-C_6H_4F	none	22	120	57
27i	H	4-C_6H_4Br	none	72	150	11
27j	H	4-C_6H_4Cl	none	72	150	15
27k	H	3-C_6H_4Cl	none	72	150	20

[a] Isolated as a hexafluorophosphate and fully characterized as an *O*-acetyl derivative (**27ℓ**).

The reaction proceeds in refluxing isopropanol or ethanol in modest yields with secondary aliphatic amines, to give compounds **27a–c**, and in low yields with donor-substituted anilines, to give the derivatives **27d–e**. In the cases of aniline, toluidine, or halogen-substituted

anilines, the formation of the products **27f–k** required considerably higher temperatures (120–150 ºC). The latter reactions were performed in the absence of the solvent, but in the presence of a Lewis-acid catalyst (BF_3 etherate). The presence of other catalysts such as Lewis acids ($SnCl_4$), Brønsted acids (hydrochloride of the corresponding amine, pyridine hydrochloride) or auxiliary bases, such as 1,8-diazabicyclo[5.4.0]undecene or pyridine, did not improve the yield of the desired products. Moreover, attempts to obtain substitution products with several primary aliphatic amines (benzylamine, ethanolamine, isopropylamine) and with several electron-poor aromatic amines (4-aminobenzonitrile, 4-(trifluoromethyl)aniline, 3-amino-pyridine) were unsuccessful, which limits the scope of this nucleophilic substitution reaction.

In the case of reaction with dialkylamines, the reaction is complicated by the formation of a dark tar, which presumably corresponds to the acridizinium-dialkylamine adducts **30**, obtained by Mörler and Kröhnke,[90] or other products resulting from the destruction of the acridizinium core by the nucleophilic addition to position 6.[91,92] The separation of the substitution product from this tar and from the side product, namely the hydrobromide of the

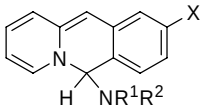

30

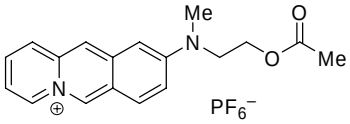

27l

amine, turned out to be difficult. The derivatives **27a–b** were isolated by column chromatography and converted into the corresponding tetrafluoroborates. Due to the high solubility of alcohol **27c** in water, it was isolated by the precipitation as a hexafluoro-phosphate. However, it was found that the latter salt loses HF upon drying. Therefore, for the unambiguous identification and full characterization, compound **27c** was transformed into an *O*-acetyl derivative **27ℓ** by the treatment with acetic anhydride in pyridine. Arylamino-substituted derivatives **27d–k** were isolated as bromide salts by several subsequent crystallization steps. The structures of the acridizinium derivatives **27a–ℓ** were confirmed by ^{1}H- and ^{13}C-NMR spectroscopy, mass-spectrometric data, and elemental analysis.

2.2.1.2 Synthesis of 9-(Methylthio)acridizinium

The synthesis of 9-(methylthio)acridizinium salt **28** followed the general approach for the preparation of substituted acridizinium salts by the cyclodehydration of pyridinium precursors (Scheme 2.2).[14,88] Thus, 4-(methylthio)benzyl bromide (**31b**) was prepared from the commercially available 4-(methylthio)benzyl alcohol (**31a**)[93] and allowed to react with

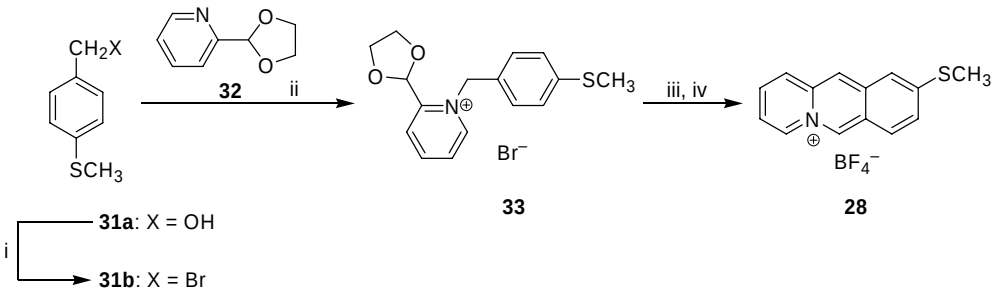

Scheme 2.2. Synthesis of 9-(methylthio)acridizinium **28**. Reagents and conditions: (i) HBr, toluene, 90 °C, 1 h, 98%; (ii) DMSO, room temp., 7 days, 98%; (iii) $MeSO_3H$, 90 °C, 2 h; (iv) aq. $NaBF_4$, 81%.

(1,3-dioxolan-2-yl)pyridine (**32**), to give the quaternary salt **33** in high yield. The cyclodehydration of **33** in PPA, which is most widely used as a cyclization medium in such reactions,[14] gave only moderate yield of the desired product (42%); however, the use of methanesulfonic acid increased the yield on this stage up to 81%. The 9-(methylthio)acridizinium **28**, isolated as a tetrafluoroborate, was prepared in 78% overall yield based on the alcohol **31a**; its structure is supported by the spectroscopic and elemental analysis data.

2.2.2 Photophysical Properties of 9-Substituted Acridizinium Derivatives

2.2.2.1 Absorption and Fluorescence Properties of 9-Amino-substitued Acridizinium Salts

The 9-aminoacridizinium derivatives **27a–ℓ** are colored substances in the solid state and in solution. The compounds **27d** and **27e** form dark-red to black crystals, while the derivatives **27a–c** and **27f–k** are yellow to brick-red in the crystalline state. Diluted solutions of all compounds are yellow. The solutions of the dialkylamino-substituted derivatives **27a–c** and **27ℓ** exhibit a characteristic, strong yellow-green fluorescence similar to the one of the parent 9-aminoacridizinium salt (**5b**).[14] In contrast, the solutions of the arylamino-substituted derivatives **27d–k** in various solvents are virtually non-fluorescent. The salts **27** are well-soluble in protic and polar aprotic solvents, and moderately soluble in halogenated solvents

(chloroform, dichloromethane). Unfortunately, the solubility of these compounds in the solvents with moderate polarity (1,4-dioxane, ethyl acetate) is lower than required for UV/Vis spectroscopy which excludes investigations therein. Representative absorption and emission spectra of dialkyl-substituted salts **27a–b** are shown in Figure 2.1; absorption spectra of aryl-substituted derivatives **27d–k** are presented in Figure 2.2. The complete set of data on the absorption and fluorescence properties of compounds **27a–b** and **27d–k** in different solvents is presented in Table 2.2. Compound **27c** was excluded from the photophysical investigations because of its limited stability; for the compound **27ℓ** only qualitative studies were performed, since the electronic properties of the (2-acetoxyethyl)methylamino substituent are unknown and would not contribute to the derivation of the structure-properties relationship.

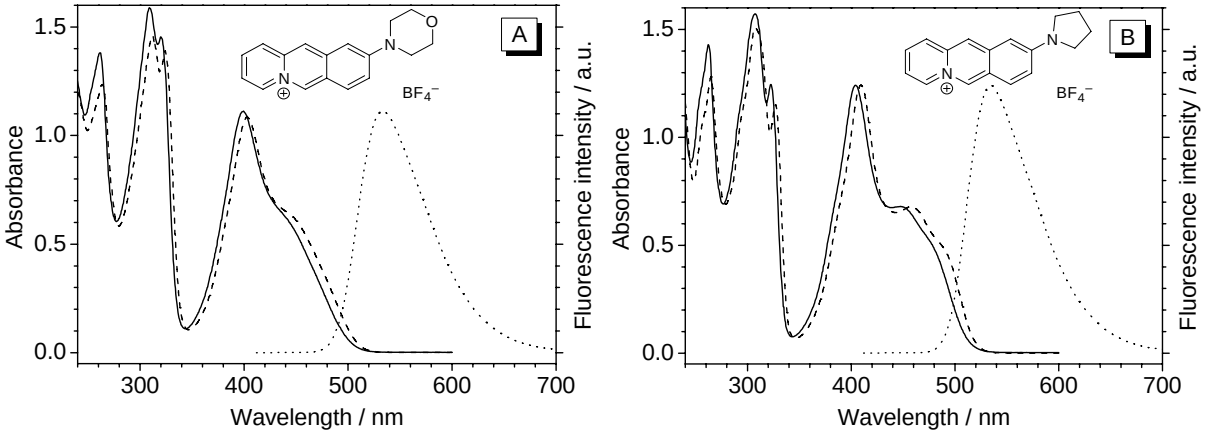

Figure 2.1. Absorption and fluorescence spectra of compounds **27a** (A) and **27b** (B). Solid lines: absorption spectra in MeOH; dashed lines: absorption spectra in dichloromethane, c(**27**) = 50 μM in both cases. Dotted lines: normalized fluorescence emission spectra in MeOH, c(**27**) = 10 μM, excitation wavelength λ_{exc} = 390 nm.

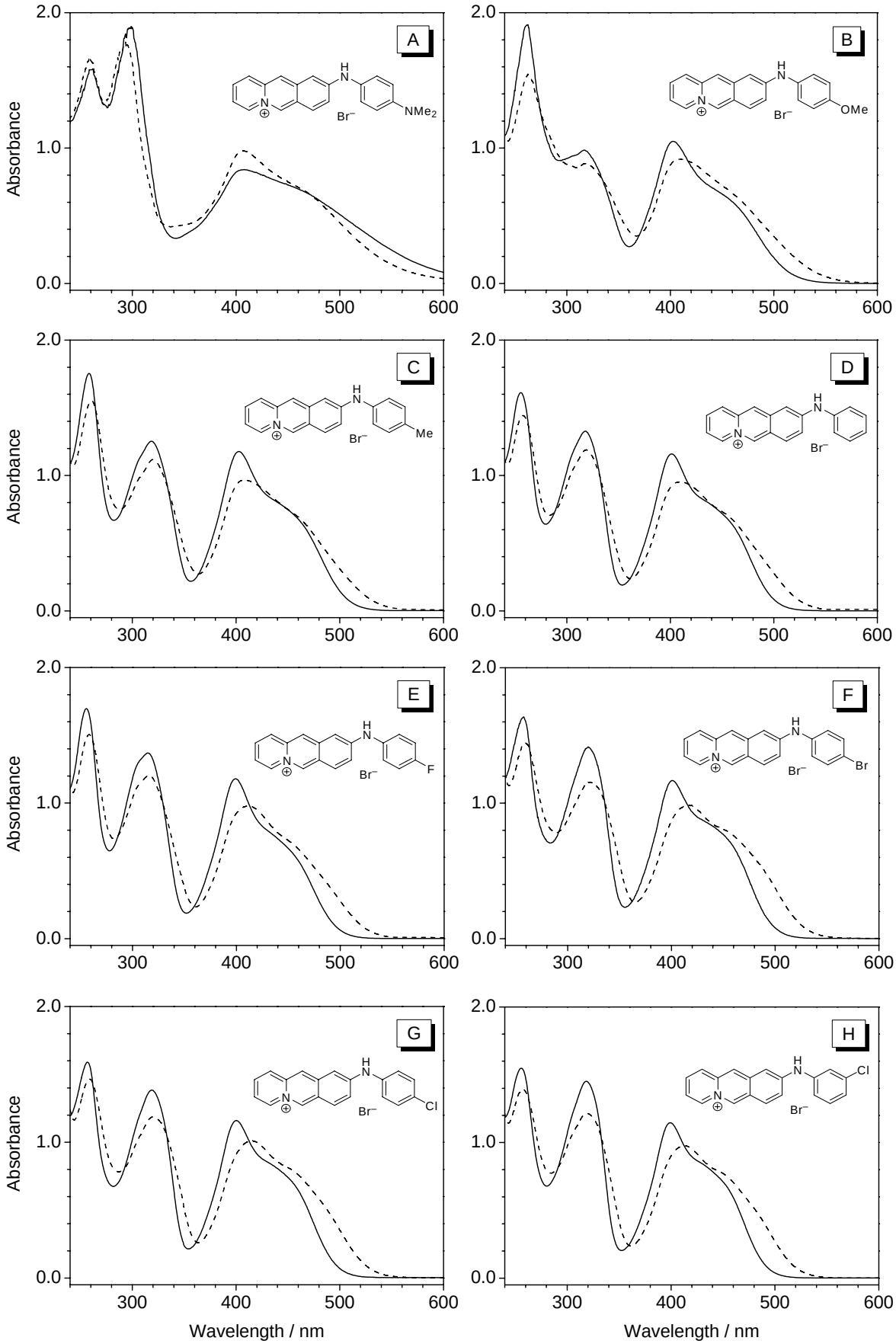

Figure 2.2. Absorption spectra of compounds **27d** (A), **27e** (B), **27f** (C), **27g** (D), **27h** (E), **27i** (F), **27j** (G) and **27k** (H) in methanol (solid lines) and in dichloromethane (dashed lines); *c*(**27**) = 50 μM in all cases.

Table 2.2. Spectrophotometric properties of acridizinium derivatives **27** and **28**.

Solvent [a]	**27a**			**27b**			**27d**		
	λ_{abs} [b] ($\log \varepsilon$ [c])	λ_{fl} [d]	$\Phi_F / 10^{-2}$ [e]	λ_{abs} [b] ($\log \varepsilon$ [c])	λ_{fl} [d]	$\Phi_F / 10^{-2}$ [e]	λ_{abs} [b] ($\log \varepsilon$ [c])	λ_{fl} [d]	$\Phi_F / 10^{-2}$ [e]
H_2O	396 (4.30)	528	40	404 (4.33)	535	36	400 (4.30)	523	0.21
MeOH	400 (4.35)	534	36	404 (4.40)	534	40	407 (4.29)	532	0.11
MeCN	399 (4.34)	536	36	404 (4.40)	537	43	404 (4.29)	535	0.09
DMSO	402 (4.33)	546	29	406 (4.37)	546	41	412 (4.28)	544	0.12
CH_2Cl_2	404 (4.34)	525	61	409 (4.40) 458 (4.13)	526	59	408 (4.23)	522	0.08
$CHCl_3$	399 (4.32)	540	33	404 (4.41) 449 (4.13)	538	53	403 (4.25)	532	0.04
Solvent [a]	**27d-H$^+$**			**27e**			**27f**		
	λ_{abs} [b] ($\log \varepsilon$ [c])	λ_{fl} [d]	$\Phi_F / 10^{-2}$ [e]	λ_{abs} [b] ($\log \varepsilon$ [c])	λ_{fl} [d]	$\Phi_F / 10^{-2}$ [e]	λ_{abs} [b] ($\log \varepsilon$ [c])	λ_{fl} [d]	$\Phi_F / 10^{-2}$ [e]
H_2O	397 (4.34)	523	0.38	399 (4.28)	530	0.02	399 (4.35)	[f]	[f]
MeOH	398 (4.37)	532	0.32	403 (4.32)	[f]	[f]	403 (4.37)	538	0.01
MeCN	396 (4.37)	531	0.41	399 (4.32)	525	[f]	400 (4.36)	506	0.02
DMSO	401 (4.35)	546	0.41	406 (4.32)	[f]	[f]	405 (4.37)	506	0.04
CH_2Cl_2	399 (4.33)	511	9.6	410 (4.26)	522	[f]	409 (4.29)	[f]	[f]
$CHCl_3$	411 (4.30)	530	3.2	402 (4.27)	[f]	[f]	402 (4.31)	556	0.07
Solvent [a]	**27g**			**27h**			**27i**		
	λ_{abs} [b] ($\log \varepsilon$ [c])	λ_{fl} [d]	$\Phi_F / 10^{-2}$ [e]	λ_{abs} [b] ($\log \varepsilon$ [c])	λ_{fl} [d]	$\Phi_F / 10^{-2}$ [e]	λ_{abs} [b] ($\log \varepsilon$ [c])	λ_{fl} [d]	$\Phi_F / 10^{-2}$ [e]
H_2O	398 (4.33)	526	0.01	396 (4.34)	545	0.01	398 (4.33)	550	0.01
MeOH	401 (4.37)	538	0.02	399 (4.37)	541	0.01	401 (4.37)	542	0.02
MeCN	400 (4.35)	522	0.03	397 (4.36)	508	0.02	398 (4.35)	536	0.01
DMSO	403 (4.35)	533	0.08	402 (4.36)	543	0.06	404 (4.36)	552	0.08
CH_2Cl_2	409 (4.28)	534	0.07	411 (4.29)	536	0.04	420 (4.29)	527	0.15
$CHCl_3$	401 (4.29)	530	0.38	401 (4.29)	529	0.23	406 (4.29)	531	0.45
Solvent [a]	**27j**			**27k**			**28**		
	λ_{abs} [b] ($\log \varepsilon$ [c])	λ_{fl} [d]	$\Phi_F / 10^{-2}$ [e]	λ_{abs} [b] ($\log \varepsilon$ [c])	λ_{fl} [d]	$\Phi_F / 10^{-2}$ [e]	λ_{abs} [b] ($\log \varepsilon$ [c])	λ_{fl} [d]	$\Phi_F / 10^{-2}$ [e]
H_2O	397 (4.32)	513	0.07	397 (4.33)	550	0.08	389 (4.17)	493	21
MeOH	401 (4.37)	548	0.01	400 (4.36)	542	0.05	391 (4.24)	498	15
MeCN	397 (4.36)	[f]	[f]	397 (4.36)	536	0.06	391 (4.23)	498	19
DMSO	403 (4.36)	544	0.08	402 (4.33)	552	0.18	393 (4.22)	502	1.1
CH_2Cl_2	415 (4.31)	542	0.07	413 (4.29)	527	0.59	395 (4.22)	486	17
$CHCl_3$	404 (4.29)	531	0.36	403 (4.28)	531	1.40	395 (4.18) 419 (4.02)	474	18

[a] In order of their decreasing E_T^N values;[94] [b] long-wavelength absorption maximum, in nm; $c = 50$ µM; [c] extinction coefficient, $cm^{-1} M^{-1}$; [d] fluorescence emission maximum, $c = 10$ µM; excitation wavelength $\lambda_{ex} = 390$ nm; [e] fluorescence quantum yield relative to Coumarin 153, estimated error ±10%; [f] too low to be determined.

The most remarkable feature of the absorption spectra is the close similarity of the positions and intensities of absorption bands for all derivatives in the series **27a–k**. Thus, the introduction of aryl substituents (**27d–k**) does not result in significant changes in the absorption spectra compared to the dialkyl-substituted derivatives **27a–b**, as can be seen from the examination of Figure 2.1 and Figure 2.2. An especially high similarity is observed between the compounds **27f–k**; thus, in these cases, the variation of the positions of the long-wavelength absorption maximum is less than 5 nm. At the same time, absorption spectra of the derivatives with electron-donating substituents in the phenyl ring (**27d–e**) are broadened as compared to the derivatives **27f–k**, although the positions of the long-wavelength maxima do not change significantly in this case, either (*cf.* Figure 2.2, A–B). For the compound **27d**, absorption spectra were investigated in a broad range of concentrations (1×10^{-5}–1×10^{-3} M in dichloromethane); however, it was observed that the shape of the absorption spectrum does not change significantly within this concentration range (Figure 2.3, A).

The salts **27a–k** exhibit only weak solvatochromism. Thus, in dichloromethane the absorption maxima are most red-shifted and the emission maxima are most blue-shifted for all compounds (*e.g.* for **27k**: the absorption maximum $\lambda_{abs} = 413$ nm in dichloromethane *vs.* 397 nm in water and acetonitrile; emission maximum $\lambda_{em} = 527$ nm in dichloromethane *vs.* 536 nm in acetonitrile and about 550 nm in water; see also Table 2.2). Thus, the Stokes shifts are the smallest in dichloromethane. In the other solvents investigated (water, methanol, acetonitrile, DMSO, chloroform), only minor shifts of the absorption maxima were observed, not exceeding 8 nm for a particular derivative.

The dialkyl-substituted derivatives **27a–b** have significant fluorescence properties, whereas the fluorescence quantum yield is especially high in dichloromethane ($\Phi_F \approx 0.6$ for both derivatives), *i.e.* almost a factor of 2 higher than in other solvents (*e.g.* for **27a** $\Phi_F = 0.36$ both in methanol and acetonitrile). The emission spectra of these derivatives have a maximum at 525–540 nm, depending on the solvent, and a large Stokes shift (120–140 nm) is observed. In contrast, the aryl-substituted derivatives **27d–k** exhibit a very weak fluorescence, usually just slightly exceeding the detection limit of the instrument ($\Phi_F \geq 1 \times 10^{-4}$); sometimes the fluorescence could not be detected (**27e**, **27f**). For most of the aryl-substituted compounds, the fluorescence is slightly enhanced in chloroform solutions, reaching $\Phi_F = 0.014$ in the case of **27k**. The emission spectrum, in the cases when it could be detected, is usually broad and centered at $\lambda_{em} \approx 520$–540 nm, similar to the emission spectra of the highly-fluorescent derivatives **27a–b**. However, in the solid state or in colloid solutions (*e.g.* in ethyl acetate)

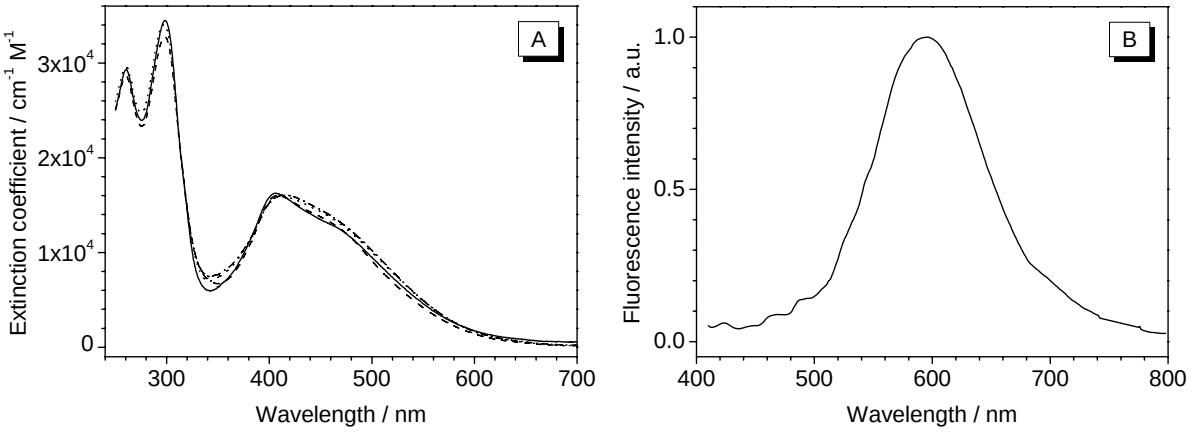

Figure 2.3. (A) Absorption spectra of compound **27d** in dichloromethane at different concentrations: 10 μM (solid line), 50 μM (dashed line), 500 μM (dotted line) and 1 mM (dash-dotted line). (B) Fluorescence emission spectrum of a colloid solution of compound **27j** in ethyl acetate ($c \approx 50$ μM; $\lambda_{exc} = 380$ nm).

compounds **27g–k** show a moderately intensive, orange emission with a broad maximum centered at around 600 nm (Figure 2.3, B).

The absorption and emission properties of the derivative **27d**, which carries a conjugated dimethylamino group, change significantly upon protonation (Table 2.2). The photometric titrations of hydrochloric acid to this compound in the Britton–Robinson buffer (an aqueous buffer solution consisting of phosphoric, boric and acetic acids and providing a smooth pH change in a broad range, $1 \leq pH \leq 8$)[95] revealed the presence of several isosbestic points (Figure 2.4, A). Nevertheless, when **27d** was titrated with trifluoroacetic acid (TFA) in dichloromethane, the long-wavelength isosbestic points were not conserved during the titration (Figure 2.4, B). Remarkably, the position and intensity of the long-wavelength absorption band (around 400 nm) do not change essentially upon protonation, while the other part of the spectrum undergoes significant changes. That is, the long-wavelength tail of the absorption spectrum disappears, and a new band located at 320 nm arises. In the fluorescence spectra, the emission maxima remain essentially unchanged during the acid titration, but the fluorescence intensities increase. This effect is especially large when **27d** is protonated with TFA in dichloromethane (Figure 2.4, C); that is, the fluorescence intensity increases by a factor of ca. 130, and the emission maximum shifts by 11 nm to shorter wavelengths. In other solvents, such as water and DMSO, the fluorescence enhancement is not as pronounced (*cf.* the values of Φ_F for the protonated and basic forms of **27d**, Table 2.2).

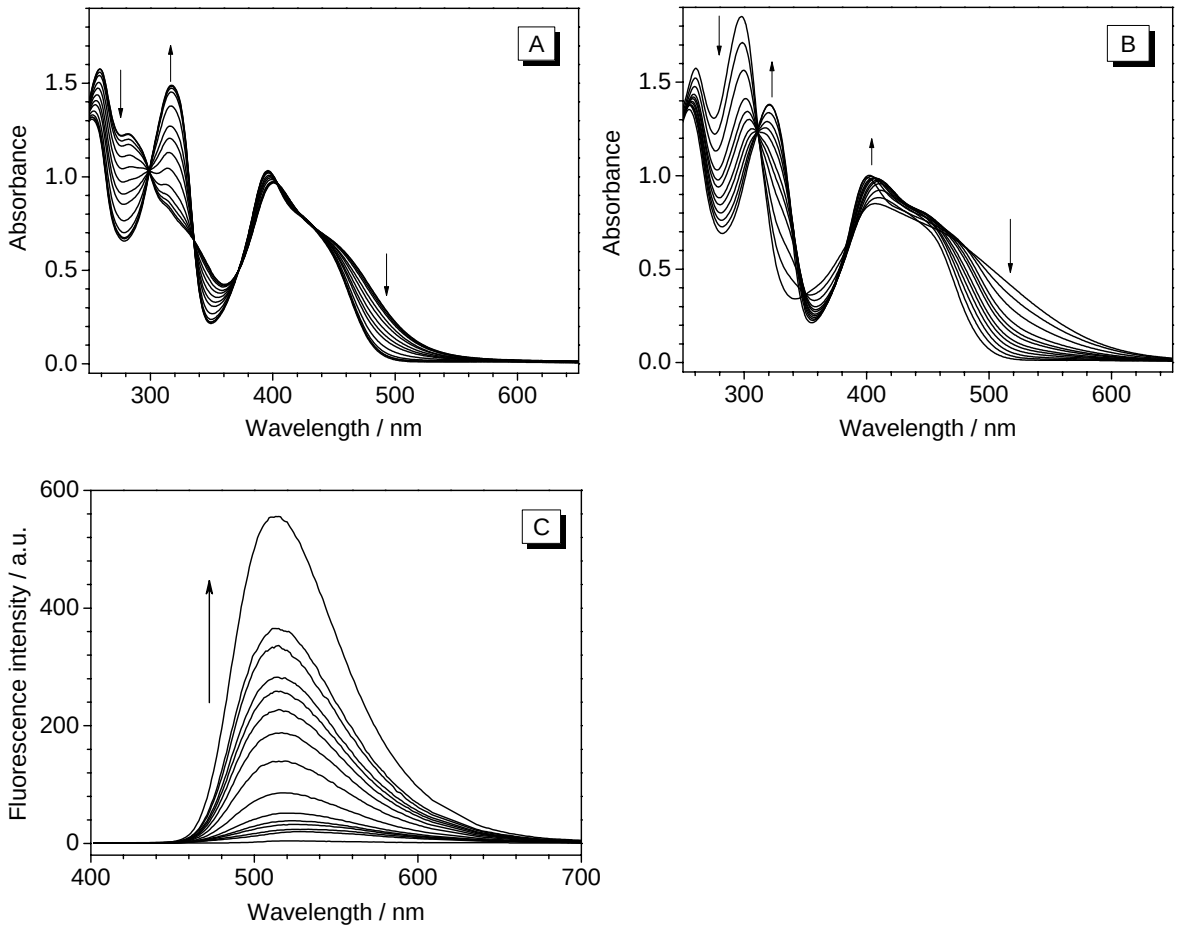

Figure 2.4. (A–B) Spectrophotometric titrations of compound **27d** (50 μM) with HCl in the Britton–Robinson buffer (A) and with TFA in dichloromethane (B). (C) Spectrofluorimetric titration of TFA to **27d** (10 μM in dichloromethane). Arrows indicate change in the spectra upon acidification.

2.2.2.2 Absorption and Fluorescence Properties of 9-(Methylthio)acridizinium

Compound **28**, a sulfur analogue of the 9-aminoacridizinium system, exhibits absorption and fluorescence properties (Figure 2.5, A) that are very similar to the ones of 9-amino-acridizinium (**5b**) and its dialkyl-substituted derivatives **27a–b**. For comparison, the spectra of compound **5b** were measured with an authentic sample of this substance and are shown in Figure 2.5, B. The overall shape of the absorption spectrum of **28** closely resembles the one of the amino analogue, although the intensities of the bands are to some extent redistributed. The long-wavelength absorption band is slightly more structured than in the case of **5b**, and three constituents may be identified. However, the positions of the long-wavelength absorption maxima of these compounds are very close (*e.g.* in methanol λ_{max} = 391 nm for **28** *vs.* 393 nm for **5b**). The solvatochromism of this compound is also negligible (*cf.* the data in Table 1.1); thus, the absorption maximum shifts from 389 nm (in water) to 395 nm (in dichloromethane).

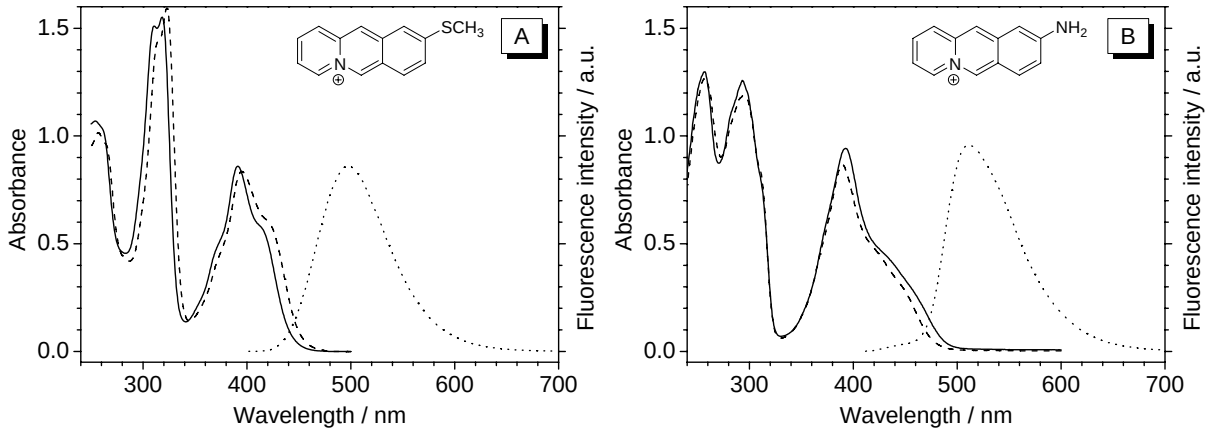

Figure 2.5. Absorption and fluorescence spectra of compounds **28** (A) and **5b** (B). Solid lines: absorption spectra in MeOH; dashed line: absorption spectra in dichloromethane, c = 50 µM in both cases. Dotted line: normalized fluorescence emission spectra in MeOH, c = 10 µM, excitation wavelength λ_{exc} = 390 nm.

The fluorescence spectra of compound **28** have a maximum at 470–500 nm and are thus blue-shifted by 10–20 nm compared to compound **5b**. The Stokes shift (80–110 nm) is large, but slightly smaller than the one observed for the amino analogues. The fluorescence quantum yields are about 0.20 in most solvents and thus slightly smaller than the ones of the *N*,*N*-dialkyl-substituted 9-aminoacridizinium salts **27a–b**, but higher than the fluorescence quantum yield of **5b** (Φ_F = 0.12).[14] Remarkably, in DMSO the fluorescence is efficiently quenched (Φ_F = 0.01), a phenomenon not observed within the series of the amino analogues.

2.2.2.3 Viscosity Dependence of the Fluorescence of N-*Aryl-9-aminoacridizinium Derivatives*

To investigate the mechanism of the radiationless deactivation in the weakly fluorescent aryl-substituted derivatives **27d–k**, the dependence of their fluorescence properties on the viscosity of the medium was studied. The viscosity of the medium was systematically varied by two methods: (i) solvents of different viscosity were used at a constant temperature and (ii) a solvent whose viscosity changes to a large extent upon changes of the temperature was employed at varied temperatures.

The media of varied viscosity were provided by glycerol–water mixtures, since the latter allow investigations in a very broad range of viscosities (from η = 1.005 cP in water to 1499 cP in glycerol at 20.0 °C). The viscosity dependence of such mixtures on their content is well-documented.[96] Moreover, both glycerol and water represent protic solvents with a comparable polarity ($E_T(30)$ = 63.1 and 57.0 for water and glycerol, respectively),[94] allowing to exclude the influence of the factors other than viscosity on the fluorescence. The

fluorescence of solutions of *N*-aryl-9-aminoacridizinium salts in such mixtures increases significantly upon increasing the glycerol content. The representative fluorescence spectra of the *N*-phenyl-substituted derivative **27g** are shown in Figure 2.6, A; the dependence of the fluorescence quantum yield of selected derivatives on the viscosity of the medium is plotted in Figure 2.6, B. The values of Φ_F for selected derivatives in aqueous and glycerol solutions are summarized in Table 2.3.

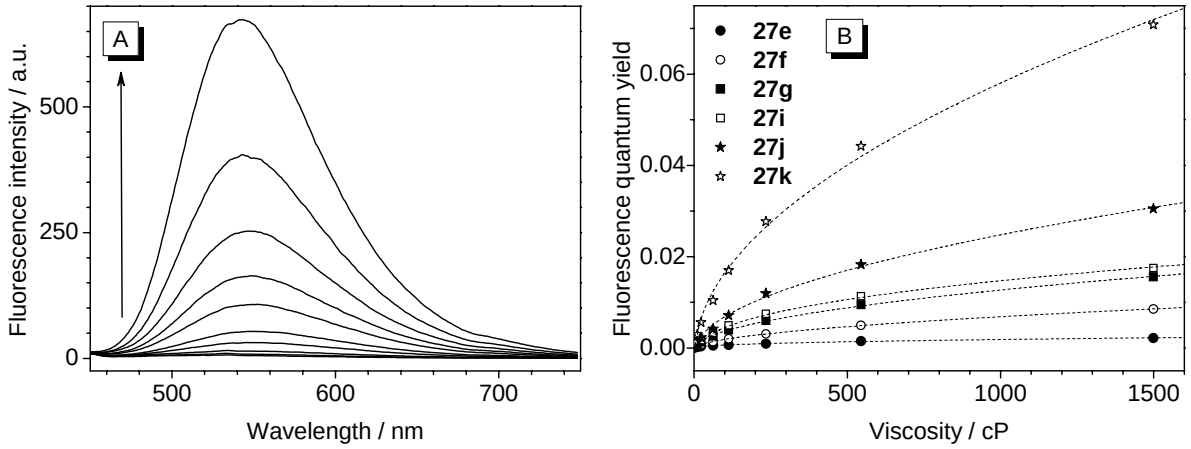

Figure 2.6. (A) Fluorescence emission spectra of compound **27g** in water–glycerol mixtures of varied viscosity. The arrow indicates changes in emission intensity upon increasing the glycerol content from 0 to 100%. (B) Viscosity dependence of fluorescence quantum yields of compounds **27e** (filled circles), **27f** (empty circles), **27g** (filled squares), **27i** (empty squares), **27j** (filled stars) and **27k** (empty stars). For the experimental conditions see the footnote to Table 2.3.

Table 2.3. The fluorescence quantum yields of selected *N*-aryl-9-aminoacridizinium derivatives in water and glycerol solutions.[a]

Compound	Fluorescence quantum yield		$\frac{\Phi_{glycerol}}{\Phi_{water}}$
	Water (η_{20} = 1.005 cP)	Glycerol (η_{20} = 1499 cP)	
27e	0.9×10^{-4}	2.2×10^{-3}	25
27f	1.3×10^{-4}	8.5×10^{-3}	63
27g	1.4×10^{-4}	1.6×10^{-2}	110
27h	1.2×10^{-4}	1.6×10^{-2}	130
27i	1.7×10^{-4}	1.7×10^{-2}	105
27j	1.5×10^{-4}	3.1×10^{-2}	200
27k	3.5×10^{-4}	7.1×10^{-2}	205

[a] Experimental conditions: temperature T = 20.0 °C; concentration c(**27**) = 10 μM; excitation wavelength λ_{ex} = 390 nm in all cases. Fluorescence quantum yields were determined with Coumarin 153 as a reference.

In the case of the methoxy-substituted compound (**27e**), the fluorescence is enhanced by a factor of 25 upon change from water to glycerol. This enhancement is much more pronounced in the case of derivatives **27f–i** (increase by a factor of 60–130) and especially for the chloro-substituted compounds **27j** and **27k** (increase by a factor of 200 for both derivatives).

The effect of the temperature on the fluorescence properties was investigated for the solutions of two representative compounds **27f** and **27j** in glycerol. Upon increase of the temperature from 0 to 100 °C, the viscosity of this solvent decreases non-linearly from 12070 to 14.8 cP.[96] This causes a marked decrease of the fluorescence intensity for both compounds (Figure 2.7). At the same time, the positions of the emission maximum change by 16–19 nm; thus, the emission spectra are most red-shifted at the temperatures 50–60 °C, whereas at lower and at higher temperatures the emission maxima are shifted to the shorter wavelengths. Remarkably, the fluorescence quantum yield of compound **27j** in glycerol at 0 °C reaches the value of 0.17 (*cf.* the insets in Figure 2.7), exceeding the one observed for the parent system, 9-amino-acridizinium (**5b**) in the low-viscosity aqueous solutions (Φ_F = 0.12).

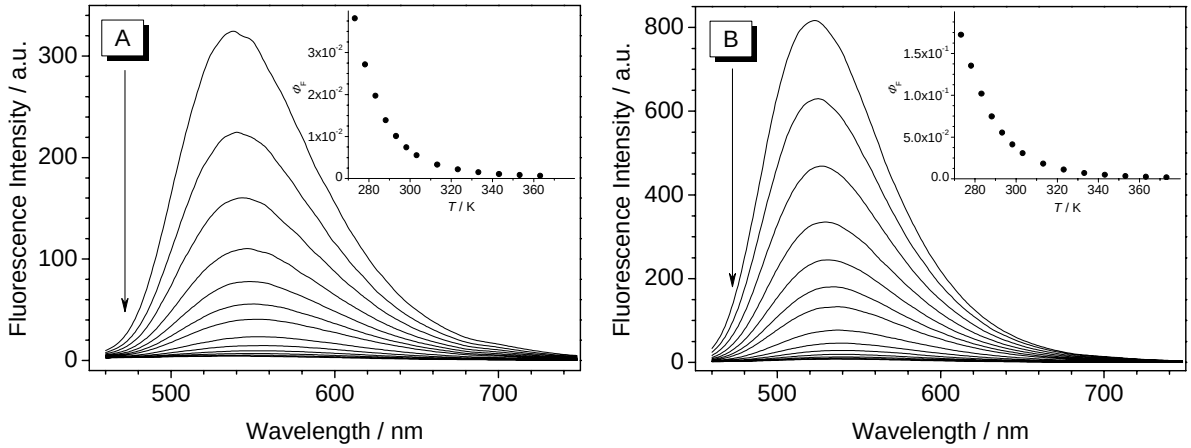

Figure 2.7. Fluorescence emission spectra of compounds **27f** (A) and **27j** (B) in glycerol (c = 50 μM) at different temperatures (0–100 °C); the arrows indicate the changes in the fluorescence intensity with increasing temperature. The insets show the dependence of the fluorescence quantum yield on the temperature.

2.2.3 Interaction of 9-Substituted Acridizinium Derivatives with DNA

2.2.3.1 Spectrophotometric Titrations

The interaction of the representative derivatives **27a**, **27b**, **27d**, **27e**, **27i–k** and **28** with DNA was investigated by spectrophotometric and spectrofluorimetric titrations with ct DNA in

aqueous phosphate buffer solutions at pH 7.0. The changes in the absorption spectra upon addition of ct DNA to the solutions of substituted 9-aminoacridizinium derivatives **27** and the sulfur analogue **28** are shown in Figure 2.8 and Figure 2.9. Upon addition of DNA to the buffered solutions of the acridizinium derivatives, a significant decrease of the absorbance (hypochromic effect) and a red shift (11–15 nm) of the long-wavelength absorption maxima

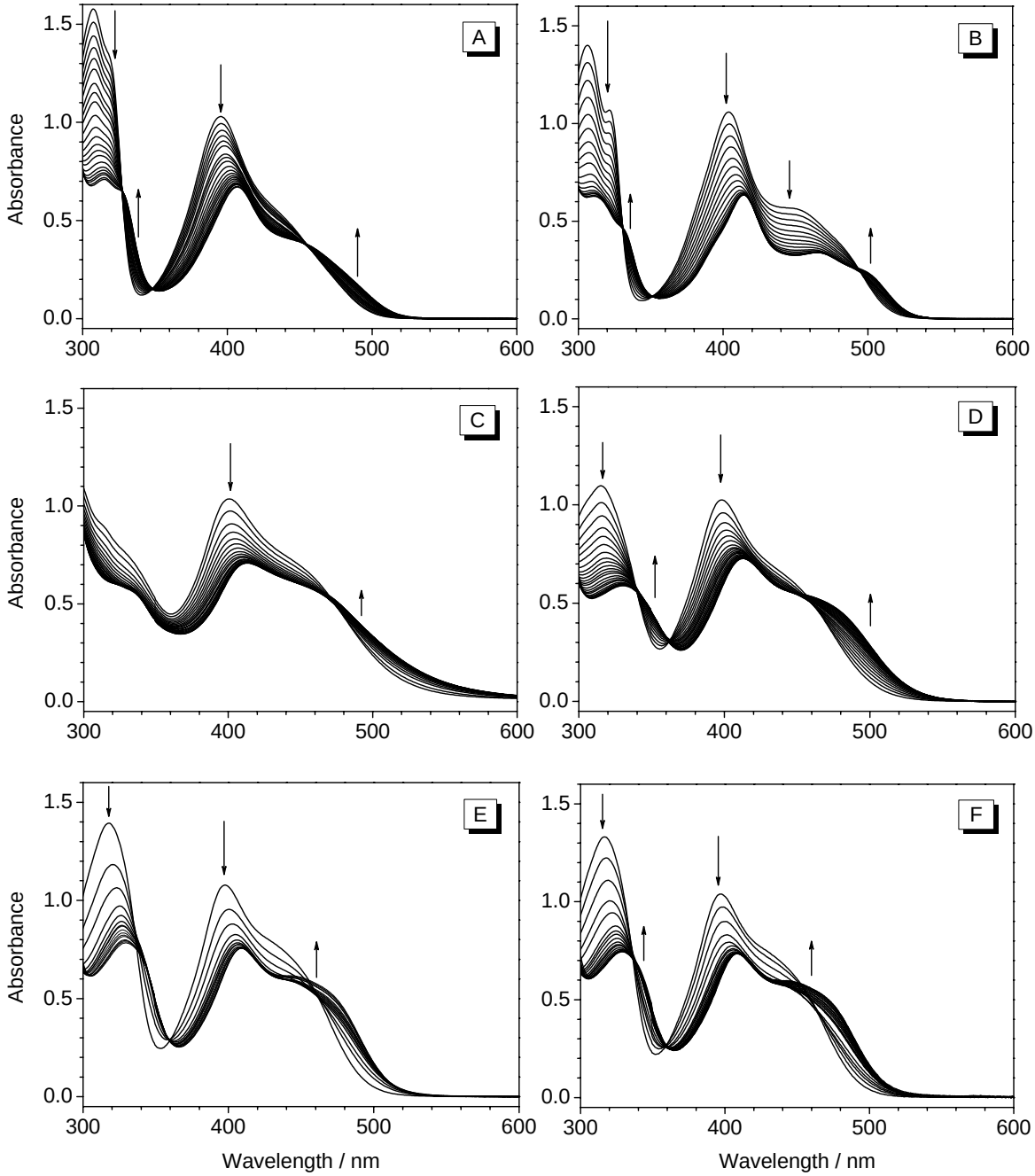

Figure 2.8. Spectrophotometric titrations of ct DNA to compounds **27a** (A), **27b** (B), **27d** (C), **27e** (D), **27i** (E) and **27j** (F) at a dye concentration of 50 μM. Arrows indicate the changes of the intensity of the absorption bands upon addition of the DNA (0–0.5 mM).

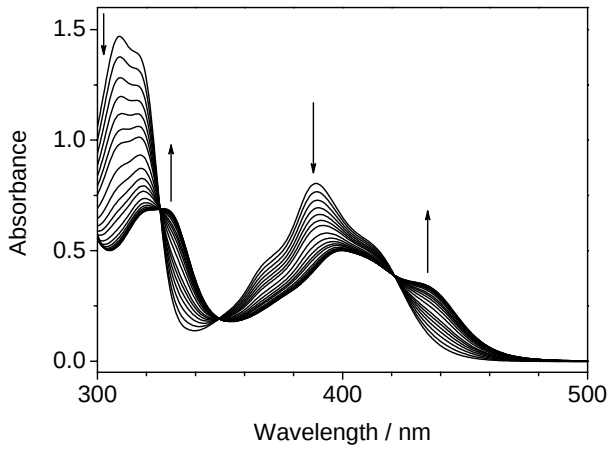

Figure 2.9. Spectrophotometric titrations of ct DNA to compound **28** at a dye concentration of 50 μM. Arrows indicate the changes of the intensity of the absorption bands upon addition of the DNA (0–0.5 mM).

were observed. Simultaneously new weak shoulders at longer wavelengths and one or more isosbestic points were detected. In the case of compound **27d**, the characteristic isosbestic point between 340–370 nm was not observed, and a new absorption band at ~ 330 nm has formed only at low ligand-to-DNA ratios (Figure 2.8, C). Photometric titrations of DNA to the halogen-substituted derivatives **27i–j** at a dye concentration of 50 μM turned out to be problematic, since at the beginning of the titrations, *i.e.* at high ligand-to-DNA ratios ($r > 0.25$), the colored, fibrous DNA-dye complex precipitated from the solution. Nevertheless, upon further addition of DNA ($r \leq 0.16$) the precipitate partly dissolves. This precipitate was not observed, either, when the amount of DNA, which corresponds to a final ligand-to-DNA ratio of less than 0.25, was added in one portion and the solution was thoroughly mixed immediately.

2.2.3.2 Spectrofluorimetric Titrations

Spectrofluorimetric titrations of ct DNA to the acridizinium derivatives **27a–b**, **27e, 27i–k** and **28** were performed in an aqueous buffer solution at a ligand concentration of 10 μM. At these conditions, no precipitation was observed. Since the interaction with DNA also leads to significant changes in the absorption spectra of the dyes (*vide supra*), the excitation wavelengths for the fluorimetric titrations corresponded to the isosbestic points, which were determined from the spectrophotometric titrations. The changes in the fluorescence emission spectra upon addition of ct DNA are presented in Figure 2.10 and Figure 2.12; the plots of the relative change of fluorescence intensity upon addition of DNA are shown in Figure 2.11.

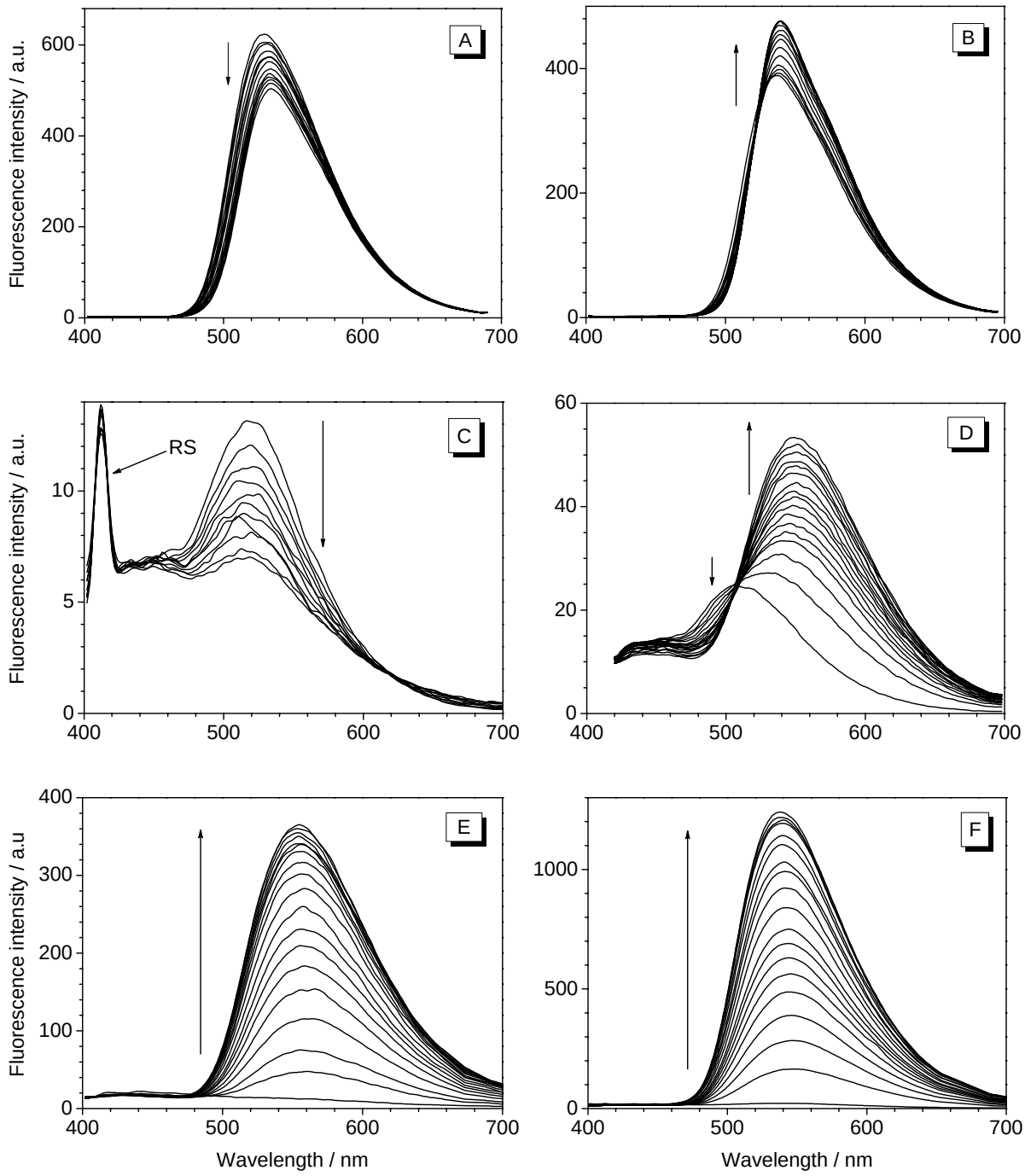

Figure 2.10. Spectrofluorimetric titrations of ct DNA to acridizinium derivatives **27a** (A, λ_{ex} = 348 nm), **27b** (B, λ_{ex} = 351 nm), **27e** (C, λ_{ex} = 362 nm), **27i** (D, λ_{ex} = 360 nm), **27j** (E, λ_{ex} = 336 nm) and **27k** (F, λ_{ex} = 335 nm). Ligand concentration c(**27**) = 10 μM in all cases. Arrows indicate changes in the fluorescence intensity during the titration; RS – peak due to the Raman scattering of the excitation light.

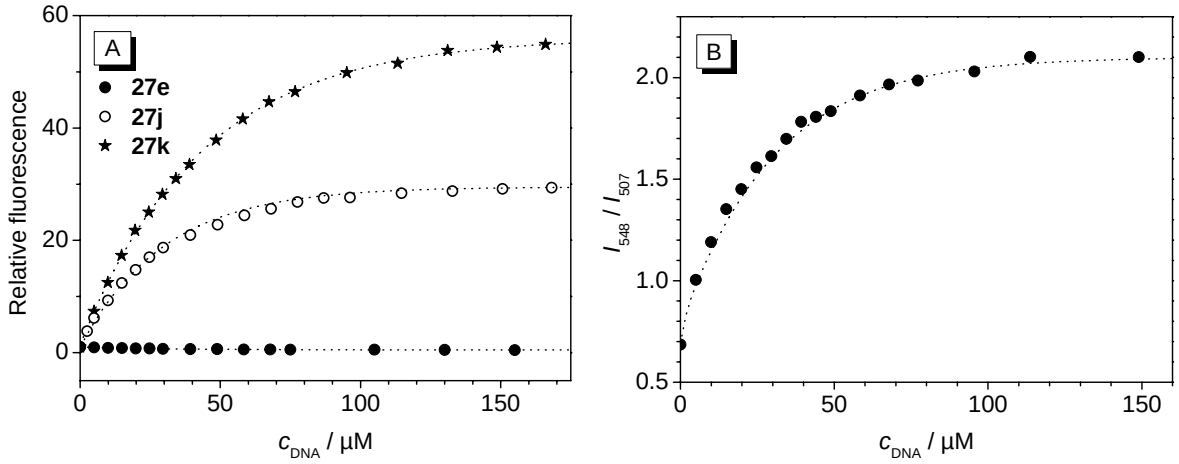

Figure 2.11. (A) Changes of fluorescence intensity upon titrations of ct DNA to the derivatives **27e** (filled circles), **27j** (empty circles) and **27k** (stars). (B) Ratiometric plot for titration of ct DNA to compound **27i**.

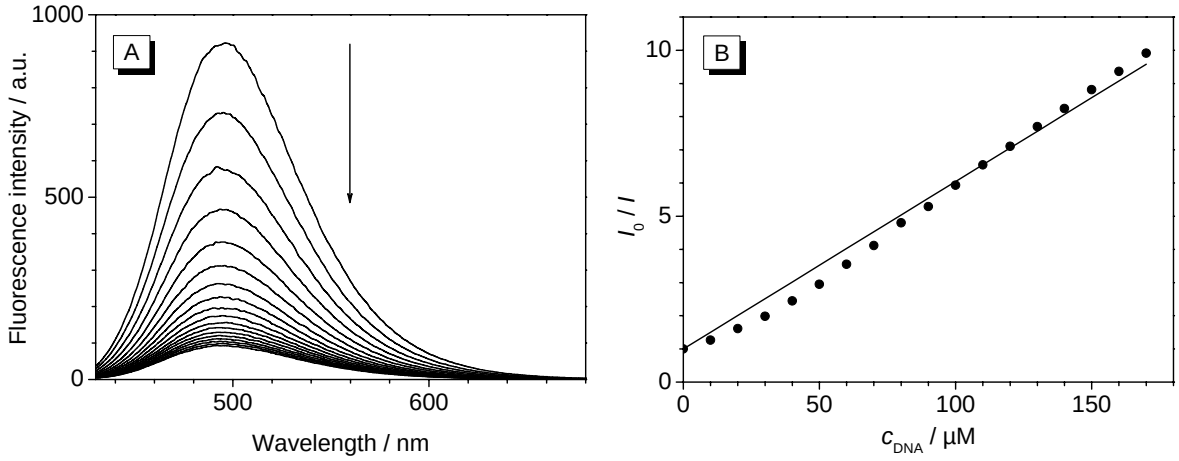

Figure 2.12. (A) Spectrofluorimetric titration of ct DNA to the derivative **28** (c = 10 µM, λ_{ex} = 421 nm); the arrow indicates changes of fluorescence intensity during the titration. (B) Stern–Volmer plot for the titration.

The changes of the fluorescence properties of these compounds upon DNA addition show little regularities. Thus, the dialkyl-substituted compounds **27a–b** show opposite changes of their—intrinsically very high—fluorescence properties. Compound **27a** shows a weak decrease of the fluorescence intensity similarly to the parent compound **5b**, while the fluorescence of **27b** slightly increases (Figure 2.10, A–B). The emission maximum shifts to longer wavelengths in both cases, although the shift is small (5 and 3 nm, respectively).

Upon addition of ct DNA to the methoxy derivative **27e**, its weak intrinsic fluorescence decreases even further. In this case, the experiment reached the detection limit of the instrument (Figure 2.10, C). In the case of the bromo-substituted derivative **27i**, the fluorescence intensity increases by a factor of about 2.3, but remains rather low; at the same

time, the emission maximum shifts by 50 nm to longer wavelengths, and an isoemissive point at λ = 508 nm is observed (Figure 2.10, D). This behavior may be used for the ratiometric detection of DNA (Figure 2.11, B).

The DNA-induced fluorescence enhancement is most pronounced in case of the chloro-substituted derivatives **27j–k** (Figure 2.10, E–F). The very weak fluorescence of these compounds in aqueous solutions increases by factors of approx. 30 and 50, respectively, upon addition of ct DNA (Figure 2.11, A). In the case of derivative **27j**, the emission maximum upon complex formation with DNA is considerably red-shifted with respect to the emission of the unbound compound (555 *vs.* 513 nm). However, for the derivative **27k**, an opposite behavior is observed; thus, the emission maximum undergoes a small hypsochromic shift (539 *vs*. 542 nm).

Upon titration of ct DNA to the solutions of the sulfur analogue **28**, a marked decrease of the fluorescence intensity is observed, whereas the position of the emission band does not change significantly (Figure 2.12, A). The quenching of the fluorescence in this case obeys the Stern–Volmer relationship (Figure 2.12, B; r^2 = 0.986), and the quenching constant was determined to be $K_{SV} = 5.1 \times 10^4$ м$^{-1}$ (bp).

2.2.3.3 Linear Dichroism Spectroscopy

To determine the binding geometry of 9-substituted acridizinium derivatives, the flow LD spectra of two representative derivatives **27a** and **27j** were measured at various ligand-to-DNA ratios (r = 0.04, 0.08 and 0.2). The LD signals of both compounds (Figure 2.13) are negative at all mixing ratios both in the UV region where both the DNA bases and the ligands absorb (< 300 nm) and at wavelengths longer than 350 nm, where only ligands absorb. Such negative LD bands are indicative of an intercalative mode of binding.

The reduced linear dichroism (LD_r) spectra provide information about the average orientation of the ligand transitions relative to the DNA bases transitions. Typically, LD_r spectra are structureless, except in the regions of overlap of transitions with different polarizations. In the case of derivative **27a**, an essentially constant LD_r value between 350 and 500 nm, comparable to the one of the DNA bases (at 280 nm), indicates that a single binding mode, *i.e.* intercalation into DNA, takes place. In contrast, for the compound **27j**, the values of LD_r are slightly smaller than the ones of free DNA, which indicates a certain degree of tilting of the transition moment of the dye, and thus of the aromatic plane of the acridizinium chromophore, relative to the plane of the base pairs.

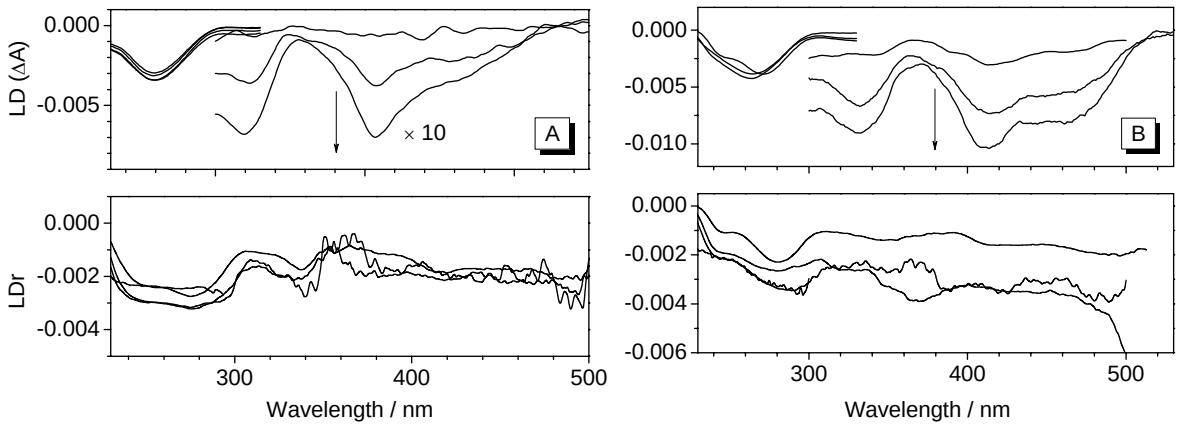

Figure 2.13. Linear dichroism (upper panels) and reduced LD (lower panels) spectra of the compounds **27a** (A) and **27j** (B) in the presence of ct DNA. Arrows indicate the changes in the intensity of the bands with increasing ligand-to-DNA ratios (r = 0.04, 0.08 and 0.2).

From Eq. 5.16 (Experimental Section) it can be estimated that the transition dipole moment of the compound **27j** is tilted by 10–20° relative to the orientation perpendicular to the helix axis. At higher ligand-to-DNA ratios (r > 0.08), the magnitude of the LD_r signal decreases due to the non-specific association of the dyes on the DNA surface with a random orientation.

2.2.4 Interaction of *N*-Aryl-9-aminoacridizinium Derivatives with Proteins

The interaction of the halogen-substituted compounds **27h** and **27j–k** with selected proteins, namely, bovine serum albumin (BSA), human serum albumin (HSA) and chicken egg white albumin (CEA), was studied by spectrophotometric and spectrofluorimetric titrations. Upon titration of these proteins to the aforementioned acridizinium derivatives in aqueous buffer solutions, no significant changes in the absorption spectra of the dyes were observed. However, in most cases an increase of the fluorescence intensity was detected (Figure 2.14, A). It was further observed that, like in the case of some proprietary fluorescent protein probes,[97] the anionic surfactant (SDS) shows a cooperative effect on the protein-induced fluorescence enhancement; therefore, in a preliminary experiment, an optimal concentration of SDS was determined. To do this, a solution of the dye **27k** (10 μM) in the presence of excess protein (500 μg mL^{-1} BSA) was titrated with a stock solution of SDS, and fluorescence spectra were recorded. The concentration of SDS, which induced the most intensive fluorescence signal, was 0.05% w/v (Figure 2.14, B); at lower and at higher surfactant concentration, a decrease of the fluorescence was observed. Therefore, all further fluorimetric titrations of proteins were performed in the presence of 0.05% SDS. It should be noted that, in

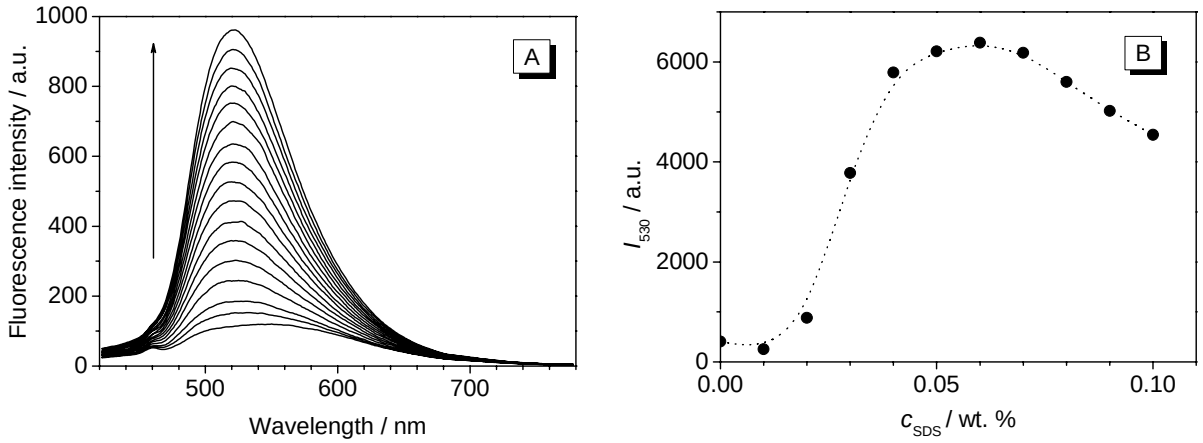

Figure 2.14. (A) Spectrofluorimetric titration of BSA (0–1 mg mL^{-1}) to a solution of **27k** (10 μM in BPE buffer); excitation wavelength λ_{ex} = 397 nm. The arrow indicates changes in the fluorescence intensity upon addition of the protein. (B) Changes in the emission intensity upon titration of SDS to a solution of **27k** (10 μM) and BSA (500 μg mL^{-1}) in BPE buffer.

the absence of proteins, SDS slowly induces the aggregation of the dyes, which causes changes in the fluorescence spectra and irreproducibility of the titrations. Therefore, aliquots of the SDS solution were added to the dye solutions directly before each titration experiment.

The results of the spectrophotometric titrations of different proteins to compounds **27h** and **27j–k** in the presence of SDS are presented in Figure 2.15. Remarkably, all investigated compounds show very similar behavior upon binding to the proteins. Thus, the binding reaches saturation at protein concentrations of 600–800 μg mL^{-1}; at this point, the relative increase of the fluorescence constitutes a factor of about 20 for all compounds, although the *absolute* fluorescence intensities for these dyes are different. The observed difference between various proteins is also minor; thus, of the proteins investigated, BSA induced the steepest increase of fluorescence (Figure 2.15, B–D). It should be noted that the concentrations of the protein solutions used in these titrations were determined by the conventional Bradford assay, which is known to have some protein-to-protein variability,[97] and this may cause some deviations in the actual titration curves.

Remarkably, at low protein concentrations (0–50 μg mL^{-1}), the relationship between the fluorescence intensity of the dyes and the protein concentration is linear, as determined by the fluorimetric titrations with diluted protein solutions (Figure 2.16). This behavior may allow the quantitative fluorimetric detection of the proteins in solution within this concentration range, provided a calibration curve had been constructed prior to the determination. Within the linear range of titration curves, a low protein-to-protein variability is observed, too.

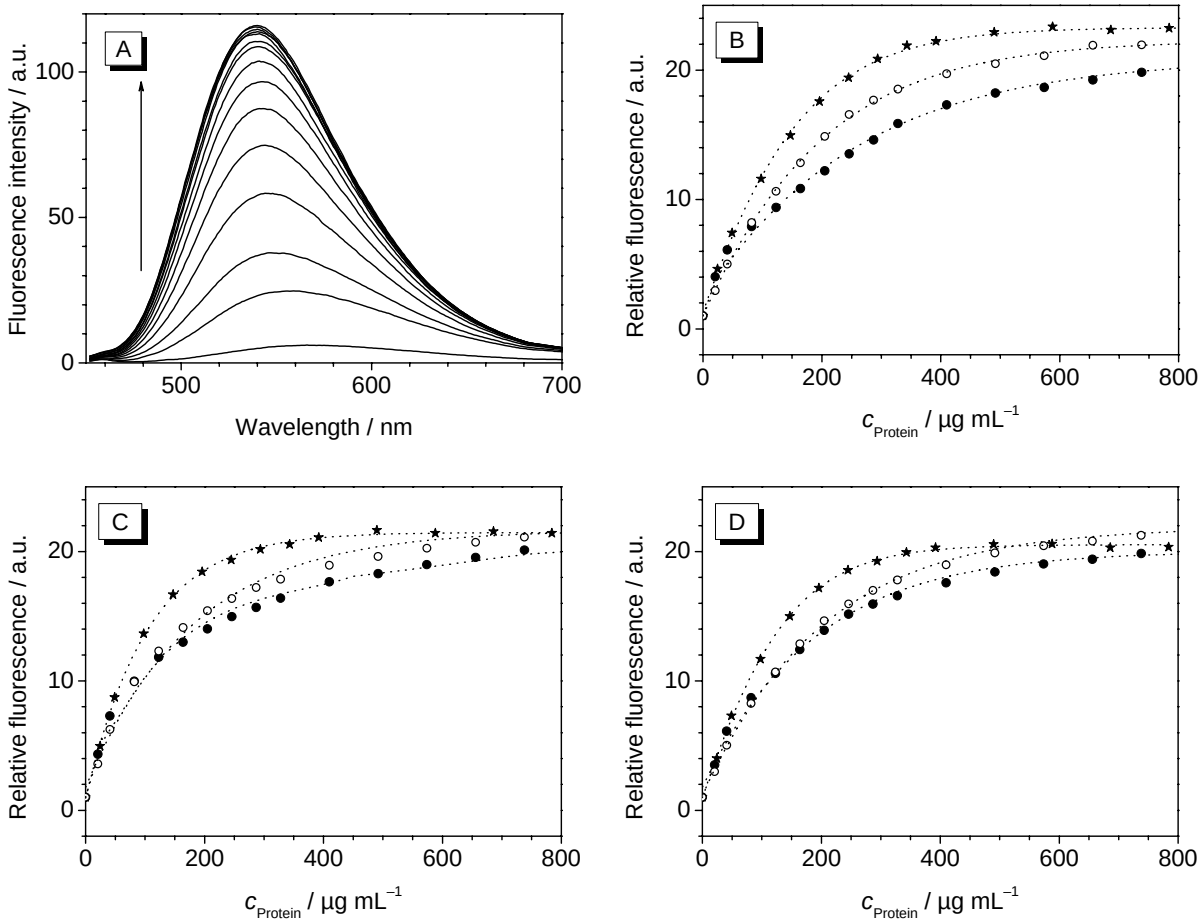

Figure 2.15. (A) Spectrofluorimetric titration of BSA to a solution of **27h** (10 µM in BPE buffer) in the presence of 0.05% SDS; excitation wavelength λ_{ex} = 397 nm. The arrow indicates changes of the fluorescence intensity upon addition of the protein (0–1 mg mL^{-1}). (B–D) Titration curves for the spectrofluorimetric titrations of proteins (filled circles: HSA, empty circles: CEA, stars: BSA) to derivatives **27h** (B), **27j** (C) and **27k** (D) at the conditions indicated in (A).

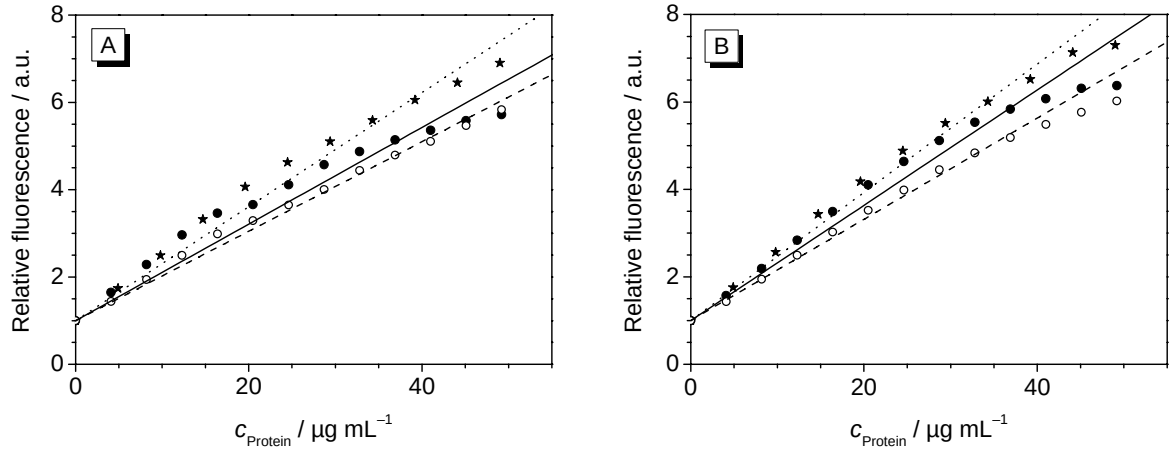

Figure 2.16. Linear regions of the titration curves for the spectrofluorimetric titrations of proteins (filled circles and solid lines: HSA, empty circles and dashed lines: CEA, stars and dotted lines: BSA) to derivatives **27h** (A) and **27j** (B). For the experimental conditions see footnotes to Figure 2.15.

2.3 Discussion

2.3.1 Photophysical Properties of 9-Substituted Acridizinium Derivatives

The series of the 9-substituted acridizinium derivatives, investigated in this work, may be divided into two groups. The parent compound **5b**,[14] its *N*,*N*-dialkyl-substituted derivatives **27a–c** and the sulfur analogue **28** show significant fluorescence properties with moderate to large quantum yields (Φ_F = 0.2–0.6). The second group, the *N*-aryl derivatives **27d–k** exhibit essentially no or very weak fluorescence in solution ($\Phi_F \leq 0.01$). However, despite these substantial differences in the fluorescence properties, the position and the shape of the long-wavelength band ($S_0 \rightarrow S_1$ transition) in the absorption spectra of the compounds from both groups are closely similar ($\lambda_{max} \approx$ 390–410 nm). Moreover, the fluorescence emission spectra of the compounds from the second group—in the cases when an unambiguous detection was possible—are located in the same wavelength region as the ones of the compounds from the second group ($\lambda_{em} \approx$ 510–550 nm).

First group: derivatives with intense intrinsic fluorescence

It has been proposed that the photophysical properties of the 9-aminoacridizinium **5b**, *i.e.* large red shift of the absorption compared to the unsubstituted acridizinium chromophore and a remarkably large Stokes shift of the fluorescence ($\Delta\lambda \approx$ 120 nm) may be rationalized on the basis of two resonance forms **A** and **B** (Scheme 2.3).[14] Thus, in the ground state, canonical structure **A** may be more favored, whereas the first excited state is better represented by structure **B**. The energy difference between these canonical forms determines the absorption shift, as has been demonstrated for cyanine dyes.[98]

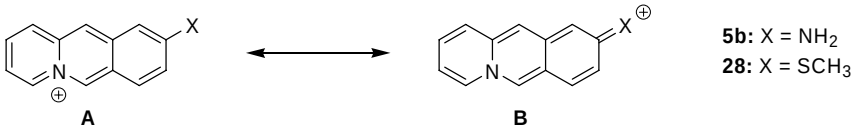

Scheme 2.3. Donor–acceptor interplay in 9-donor-substituted acridizinium derivatives.

This scheme may be applied also to the derivatives **27a–b** and **28**. Thus, the introduction of a stronger electron donor instead of the amino group in **5b**, *e.g.* morpholino (**27a**) or pyrrolidino (**27b**) residues, results in the bathochromic shifts of the $S_0 \rightarrow S_1$ transition by 7 nm (450 cm^{-1}) for **27a** and by 11 nm (690 cm^{-1}) for **27b** (hereafter the data refer to solutions in methanol as a

representative solvent, if not stated otherwise). On the other hand, the replacement of the amino group with a weaker electron donor, *i.e.* the methylthio substituent in compound **28**, results in a small hypsochromic shift by 2 nm (130 cm^{-1}), as compared to compound **5b**. These results are in accordance with the observations that morpholino and especially pyrrolidino substituents are stronger electron donors than the unsubstituted amino group.[99] A quantitative treatment of these data shows a good correlation between the energy of the $S_0 \rightarrow S_1$ transition and the Hammett–Brown substituent parameter σ^+ (Figure 2.17).[100] The use of the σ^+ parameter (which has been determined for the heterocyclic substituents only recently)[100b] is reasonable because it appropriately represents the π-donating properties of the substituents in conjugated systems.

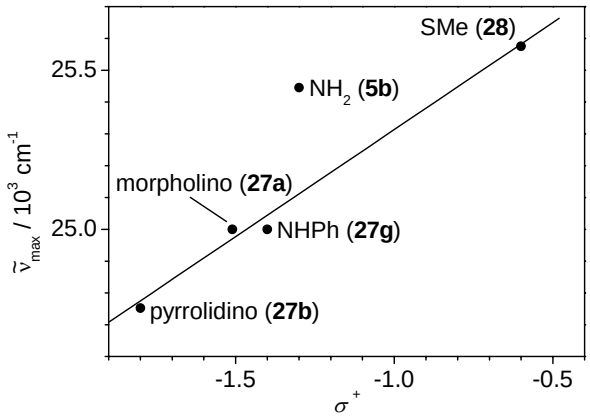

Figure 2.17. Correlation between the energy of the $S_0 \rightarrow S_1$ transition in 9-substituted acridizinium derivatives (in methanol) and the Hammett–Brown substituent parameter σ^+.

It should be noted that the data for the 9-aminoacridizinium **5b** deviate significantly from the trend, presumably due to the specific interaction of the protons of the amino group with the solvent, which change the apparent electron-donor properties of the substituent. Thus, it has been shown that the position of the absorption band of **5b** in protic solvents undergoes a hypsochromic shift, which correlates with the acceptor number, *i.e.* the electron-acceptor properties of the solvent, indicating the formation of the hydrogen bonds.[14]

Remarkably, the values of the shifts of absorption maxima, resulting from the replacement of the amino group with other substituents, are lower than in other donor–acceptor dyes. Thus, it has been shown that in the related donor-substituted quinolinium salts replacement of the amino group (**34a**) with a morpholine residue (**34b**) results in a bathochromic shift by 1090 cm^{-1}, whereas the introduction of an alkylthio group (**34c**) causes a hypsochromic shift

by 850 cm^{-1}.[85] Even a more pronounced effect has been observed in the cationic styrylpyrididinium dyes; thus, replacement of the amino group with a pyrrolidine residue results in a bathochromic shift by ~ 1600 cm^{-1}.[101] The use of wavenumbers for these comparisons allows to disregard the absolute values of the transition energies.

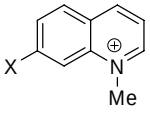

34a: X = NH_2
34b: X = $N(CH_2CH_2)_2O$
34c: X = $SCH_2CH_2CHMe_2$

The minor solvatochromic properties of the 9-donor-substituted acridizinium derivatives may be rationalized assuming a similar polarity of the ground and first excited states of the chromophore. Thus, these compounds, along with the quinolinium analogues **34**, represent the so-called *charge-resonance* chromophores[85] of the D–π–A^+ X^- architecture, which—in contrast to the *charge-transfer* chromophores of the D–π–A type—are relatively insensitive to the polarity of the medium. Indeed, the solvatochromism usually arises from the different stabilization of the ground and excited states of the chromophore by the solvent and, since both structures **A** and **B** (Scheme 2.3) are charged species, no significant difference in the stabilization is possible.[94] However, it was observed that in dichloromethane solutions a significant red shift of the absorption maxima, a blue shift of the emission maxima, and an increase of the fluorescence quantum yield for these derivatives take place (*cf.* the data in Table 2.2). This may be attributed to the high polarizability of this solvent (α = 6.52 $Å^3$),[102] since it facilitates the fast redistribution of the polarizable electrons during excitation. Thus, following the vertical excitation upon photon absorption, the excited Franck–Condon state (S_1-FC, Figure 2.18) is formed, which is immediately subjected to the relaxation process, namely the solvent-cage relaxation to the solvent-relaxed S_1-FC^{SR} state, followed by the geometrical relaxation to the vibrationally relaxed S_1 state. From the latter state the fluorescence and non-radiative processes occur. In the case of a highly polarizable solvent, such as dichloromethane, the vertical electronic excitation is accompanied by an instant rearrangement of the electrons of the solvent cage, leading directly to the S_1-FC^{SR} state and decreasing the apparent energy of the excited FC state. This leads to a bathochromic shift of absorption. In the case of fluorescence emission, the same mechanism takes place, and lowers the apparent energy of the ground FC state, as the fluorescence is accompanied by re-polarization of the solvent cage and finishes at the S_0-FC^{SR} state. This results in an increase of the energy of the radiative $S_1 \rightarrow S_0$ transition (hypsochromic shift). Such anomalous shifts of

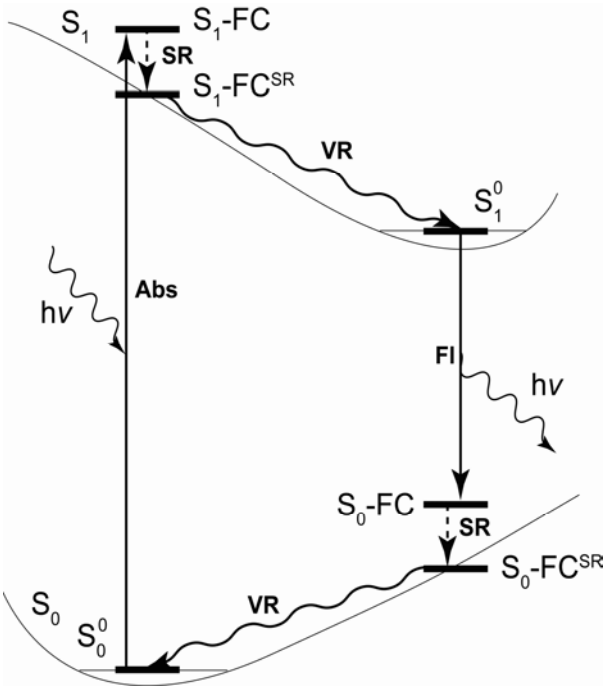

Figure 2.18. A simplified scheme of energy states of a chromophore. Energetic states: S_0^0 = vibrationally-relaxed ground state; S_1-FC = Franck–Condon excited state; S_1-FC^{SR} = solvent-relaxed excited FC state; S_1^0 = vibrationally-relaxed excited state; S_0-FC = Franck–Condon ground state; S_0-FC^{SR} = solvent-relaxed ground FC state. Processes: Abs = light absorption; Fl = fluorescence; SR = relaxation of the solvent cage; VR = vibrational relaxation.

absorption and fluorescence bands and increase of fluorescence quantum yield in dichloromethane have been occasionally observed for cationic dyes, such as **34**,[85,103] but are rarely addressed in the literature, as these effects are usually masked by the more pronounced polarity-dependent solvatochromic shifts and become evident only in the case of polarity-independent charge resonance dyes. Interestingly, chloroform (α = 8.53 Å^3) does not cause a similar effect in this sub-series, although it is observed in the *N*-aryl derivatives **27d–k**.

Finally, the reduced fluorescence quantum yield of the derivative **28** (Φ_F = 0.15–0.20) compared to the amino analogues **27a–b** (Φ_F = 0.30–0.60) may be attributed to the enhanced intersystem crossing rate in **28** due to the presence of the sulfur atom in the chromophore (internal heavy-atom effect).[104] A similar decrease of the fluorescence quantum yield has been observed for the sulfur derivatives of charge-resonance dyes (*cf.* Φ_F = 0.63 and 0.10 for the quinolinium dyes **34a** and **34c**, respectively).[85] The exceptional decrease of fluorescence of **28** in DMSO is presumably due to the lower reduction potential of this chromophore compared to the amino analogues, in combination with the high electronic donor strength of the solvent. A similar quenching in DMSO has also been observed for the unsubstituted acridizinium

cation.[105] Moreover, this is supported by the efficient quenching of fluorescence of **28** by the DNA (*cf.* Figure 2.12).

Second group: derivatives with low intrinsic fluorescence

All *N*-aryl-9-aminoacridizinium salts **27d–k** possess much weaker intrinsic fluorescence than the parent compound **5b** and the above-discussed derivatives. At the same time, the absorption spectra of these derivatives—with the exception of the 4-(dimethylamino)phenylamino derivative **27d**—are closely similar to each other and to the spectra of dialkyl-substituted derivatives **27a–b**. Moreover, the position of the absorption maximum of the *N*-phenyl-substituted derivative **27g** correlates well with the σ^+ parameter for the phenylamino group (Figure 2.17). The fluorescence spectra of these derivatives, in spite of their low intensity, also lay in the same region as the ones of the derivatives **27a–b**.

These observations may be rationalized by the assumption that the aryl substituents in the ground state do not interact and are not conjugated with the chromophore, which is formed by the 9-aminoacridizinium residue *per se*. Instead, in the ground state, the phenyl ring is oriented almost perpendicular relative to the plane of the aminoacridizinium chromophore, similarly to the orientation in 2-*N*-arylamino-6-naphtalenesulfonate derivatives **13**.[83,106] Further support of this hypothesis comes from the analysis of the protolytic equilibria in compound **27d**.

Compound **27d** with a 4-dimethylamino substituent in the phenyl ring shows a very broad absorption band extending up to 600 nm. Since the shape of the absorption spectrum remains essentially unchanged in a broad concentration range (*cf.* Figure 2.3, A), formation of aggregates may be excluded as a possible reason for such band broadening. On the other hand, the long-wavelength part of this band decreases upon acidification (Figure 2.4, A–B). This observation indicates that the long-wavelength absorption is due to a pronounced excited-state charge transfer between the *para*-aminophenyl substituent and the acridizinium chromophore, which disappears as the electron-donating properties of the dimethylamino functionality are suppressed by the protonation. The titration curves may be fitted by a simple 1:1 protolytic equilibrium (Figure 2.19); they give the values of acidity constants (pK_a, at 293 K) of 5.04 (in water) and 4.05 (in dichloromethane). The value in water is very close to the one of *N*,*N*-dimethylaniline (pK_a = 5.15 at 298 K),[107] but is significantly larger than the ones of donor–acceptor systems, such as 4-dimetylamino-4′-cyanobiphenyl (pK_a = 2.35 in EtOH–water)[108] or 9-[(4-dimethylamino)phenyl]-10-methylacridinium perchlorate

(pK_a = 3.38 in water).[109] These data indicate that the 9-aminoacridizinium chromophore *as a whole* acts as a very weak electron acceptor.

While the basic form of **27d** is virtually non-fluorescent, the protonated form exhibits a weak fluorescence with an emission centered at about 510–530 nm (Table 2.2; Figure 2.4, C). This phenomenon is more pronounced in dichloromethane and chloroform solutions, most likely due to the high polarizability of these solvents.

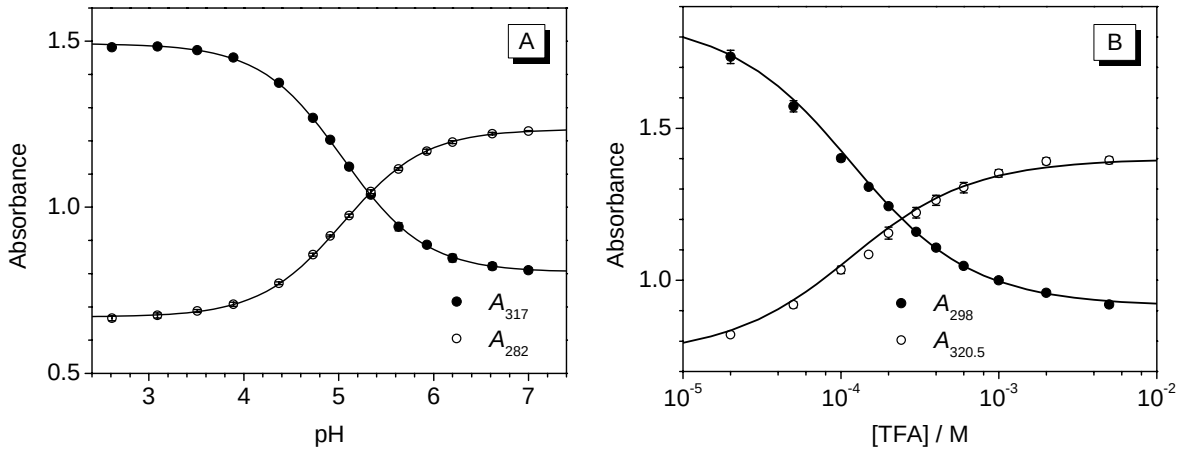

Figure 2.19. Titration curves for the titration of (A) HCl to **27d** in an aqueous buffer solution and (B) TFA to **27d** in dichloromethane. Numerical fits calculated for the values $K_a = 9.1 \times 10^{-6}$ M (in water) and 9.0×10^{-5} M (in dichloromethane).

Deactivation pathways

The fluorescence quantum yield of *N*-aryl-9-aminoacridizinium salts **27d–k** increases drastically with increasing rigidity of the medium, either by using solvent mixtures with increasing viscosity or upon decreasing the temperature (Section 2.2.2.3). A similar behavior has been observed for a large number of dyes that undergo a conformational change in the excited state, such as di- and triphenylmethane dyes,[110] phenyl-substituted heterocycles, such as 3,3-dimethyl-2-phenylindolenine (**35**),[111] and donor–acceptor systems that form a twisted intramolecular charge transfer (TICT) state, in which the orbitals of the donor and acceptor moieties are perpendicular.[112] The ANS derivatives **13** also belong to the latter group.[83,106]

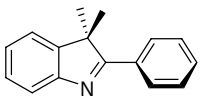

35

Since it was shown above that the fluorescence emission of the *N*-aryl derivatives **27d–k** originates from the 9-aminoacridizinium chromophore, the possibility of the rotation about the acridizinium C9−N bond may be excluded. Moreover, it has been observed that the fluorescence of the parent compound **5b** does not show any significant viscosity dependence.[113] Therefore, it may be proposed that a radiationless deactivation of the excited state in **27d–k** is due to the excited-state rotation about the N–C(aryl) bond. This process was investigated by the studies of the viscosity dependence of fluorescence of *N*-aryl-9-aminoacridizinium derivatives.

It has been shown that in the solutions of medium to high viscosity the internal rotation (torsional relaxation) of the probe molecules is controlled by the free-volume effects rather than by the bulk viscosity of the solutions.[18] Thus, an empirical relationship between viscosity η and the free volume is given by the Doolittle equation (Eq. 2.1).

$$\eta = \eta_0 \exp\left(\frac{V_0}{V_f}\right) \qquad \text{(Eq. 2.1)}$$

In Eq. 2.1 η_0 is a constant, and V_0 and V_f are the van der Waals volume and the free volume of the solvent, respectively. Under assumptions that the only non-radiative process is the rotational relaxation of the chromophore and that the intrinsic radiative lifetime of the excited state is independent of the temperature T and viscosity η, the fluorescence quantum yield is related to the radiative (k_r) and non-radiative (k_{nr}) rate constants by the Eq. 2.2.

$$\Phi_F = \frac{k_r}{k_r + k_{nr}} \qquad \text{(Eq. 2.2)}$$

The non-radiative rate constant is dependent on the free-volume effects according to an empirical expression (Eq. 2.3).[112a]

$$k_{nr} = k_{nr}^0 \exp\left(-x\frac{V_0}{V_f}\right) \qquad \text{(Eq. 2.3)}$$

In Eq. 2.3, k_{nr}^0 is the reorientation rate in the absence of the solvent cage and x is a constant dependent on the geometry and size of the probe molecule. Usually, $x < 1$ and emphasizes the influence of the effective viscosity of the medium, which is less than the bulk viscosity

because of the free-volume effects. Combination of Eq. 2.3 with Eqs. 2.1–2.2 gives a relationship between the fluorescence quantum yield and viscosity of the medium (Eq. 2.4).[18]

$$\frac{\Phi_F}{1-\Phi_F} = a\,(\eta/T)^x \qquad \text{(Eq. 2.4)}$$

Under conditions of the constant temperature and small fluorescence quantum yields ($\Phi_F \ll 1$), Eq. 2.4 may be approximated to the Förster–Hoffmann equation (Eq. 2.5), which reveals the power dependence of the fluorescence quantum yield on the viscosity of the solution.[110b]

$$\Phi_F = C\,\eta^k \qquad \text{(Eq. 2.5)}$$

The dependence of fluorescence quantum yields of selected *N*-aryl-9-aminoacridizinium derivatives on the viscosity of the medium, provided by water–glycerol mixtures at a constant temperature, shows an almost linear fit in the double-logarithmical coordinates (Figure 2.20). This behavior is in good agreement with the Förster–Hoffman equation. Moreover, the results of the regression analysis (Table 2.4) show that the *k* values for the *N*-phenyl derivative **27g** and for the derivatives with weak electron-acceptor substituents (F, Br) in the phenyl group are very close to the value of $k = ⅔$, that has been theoretically derived by Förster and Hoffmann for the rotation of the phenyl group and that has been found for the triphenylmethane dyes and many similar systems, *e.g.* indolenine **35**.[111]

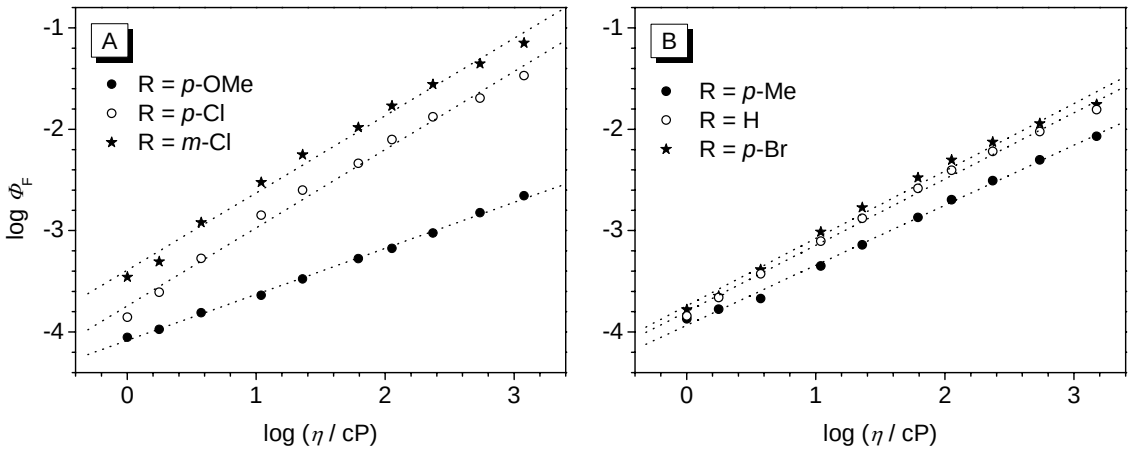

Figure 2.20. Viscosity dependence of fluorescence quantum yields for compounds **27e**, **27j**, **27k** (A) and **27f**, **27g**, **27i** (B). The data for **27h** have been omitted for clarity.

Table 2.4. Results of the regression analysis of log Φ_F over log η.

Compound	Substituent	Slope k	r^2
27e	4-C_6H_4OMe	0.45	0.998
27f	4-C_6H_4Me	0.59	0.997
27g	C_6H_5	0.65	0.996
27h	4-C_6H_4F	0.69	0.996
27i	4-C_6H_4Br	0.66	0.991
27j	4-C_6H_4Cl	0.77	0.991
27k	3-C_6H_4Cl	0.76	0.991

The results of the fluorescence measurements of selected compounds (**27f** and **27j**) in glycerol solutions at varied temperatures, which also provide changes in the viscosity, were treated according to the more exact Eq. 2.4. The results (Figure 2.21, A) show a linear dependence of $\Phi_F/(1 - \Phi_F)$ on the η/T in the double-logarithmical coordinates. Moreover, the values of the exponent (x = 0.62 and 0.68 for **27f** and **27j**, respectively) are in good agreement with the values found from the experiments at a constant temperature and with the ones reported for the other systems with a phenyl group that can undergo a torsional reorientation.[18] Therefore, it may be concluded that one of the excited-state deactivation pathways includes the rotation of the phenyl group.

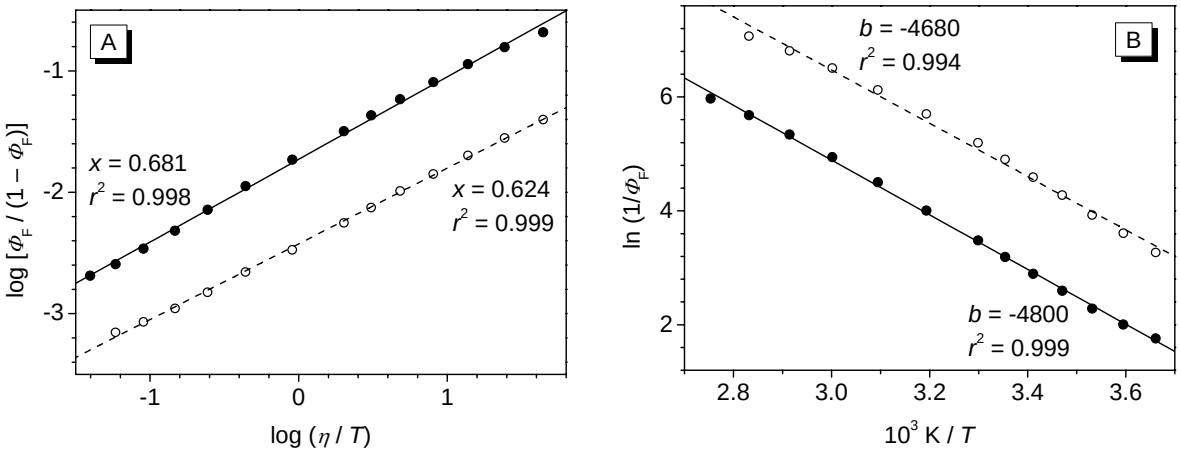

Figure 2.21. Plots of (A) $\log\left(\frac{\Phi_F}{1-\Phi_F}\right)$ *vs.* log (η/T) and (B) ln ($1/\Phi_F$) *vs.* reverse temperature for compounds **27f** (empty circles and dashed lines) and **27j** (filled circles and solid lines) in glycerol; x, b = slopes of the linear fits.

The temperature dependence of the fluorescence quantum yields in glycerol also allows to estimate the height of the potential barrier for the torsional reorientation of the phenyl

substituent. Thus, the dynamics of the reorientational relaxation of molecules in solutions with a significant friction between the rotating molecule and the solvent (as it occurs in a protic solvent) may be described by the Debye–Stokes–Einstein hydrodynamic model,[112a] and the temperature dependence of the observed fluorescence quantum yield, Φ_F, is given by an Arrhenius-type relationship (Eq. 2.6).[112]

$$\Phi_F^{-1} = \frac{\tau\, T}{B\, \Phi_0\, \eta_0} \exp\left(\frac{-\Delta E_a}{RT}\right) \qquad \text{(Eq. 2.6)}$$

In Eq. 2.2, B is the geometry-dependent rotational friction coefficient of the solute molecule, ΔE_a is the activation energy for the rate of rotational relaxation, and Φ_0 is the fluorescence quantum yield at the limit when the internal rotation has ceased, *i.e.* $\eta = \infty$. For the conditions of low or moderate viscosity, Φ_F is significantly smaller than Φ_0. The Arrhenius plots, $\ln(1/\Phi_F)$ *vs.* $1/T$, derived from the temperature dependence of fluorescence for compounds **27f** and **27j** in glycerol solutions, are shown in Figure 2.21, B. It may be observed that a linear dependence is preserved in a wide temperature range (0–90 °C).

The regression analysis gives the values of the activation energy ΔE_a = 38.9 and 39.9 kJ mol^{-1} for the derivatives **27f** and **27j**, respectively, which are essentially the same within the experimental precision. A similar value of 42 ± 2 kJ mol^{-1} was found for the excited-state rotation of the phenyl group in the phenylindolenine **35**.[111] Therefore, these results confirm the assumption that one of the deactivation pathways is due to the rotational reorientation of the phenyl group in the excited state, and does not depend on the nature of the substituent in the phenyl ring. Instead, the energy barrier for the rotation is determined by the steric hindrance between the *o*,*o*′-hydrogen atoms of the phenyl group and the ones of the acridizinium core. It should be noted, however, that the obtained values of the activation energy should be treated with care, since at the conditions of medium-to-high viscosity the Debye–Stokes–Einstein model may be used only with limitations because of the above-discussed free-volume effects.[112a]

The data in Table 2.4 also show that the derivatives with an electron-donor substituent in the phenyl ring have lower k values than *N*-phenyl-9-aminoacridizinium **27g** and the derivatives with electron-acceptor substituents. Thus, k = 0.45 and 0.59 were found for the derivatives **27e** (R = OCH_3) and **27f** (R = CH_3), respectively, while the derivatives with the electron-

acceptor chloro substituents (**27j–k**) have larger *k* values (0.76–0.77) than the compound **27g** (*k* = 0.65). Moreover, the values of the fluorescence quantum yield of the derivatives **27e–k** in glycerol solutions, *i.e.* under conditions when the rotational relaxation of the excited state is strongly suppressed, are not equal (Table 2.3), but show an apparent dependence on the electron-donating strength of the substituent, as characterized by the substituent constant $\sigma_{m/p}$ (Figure 2.22, A).

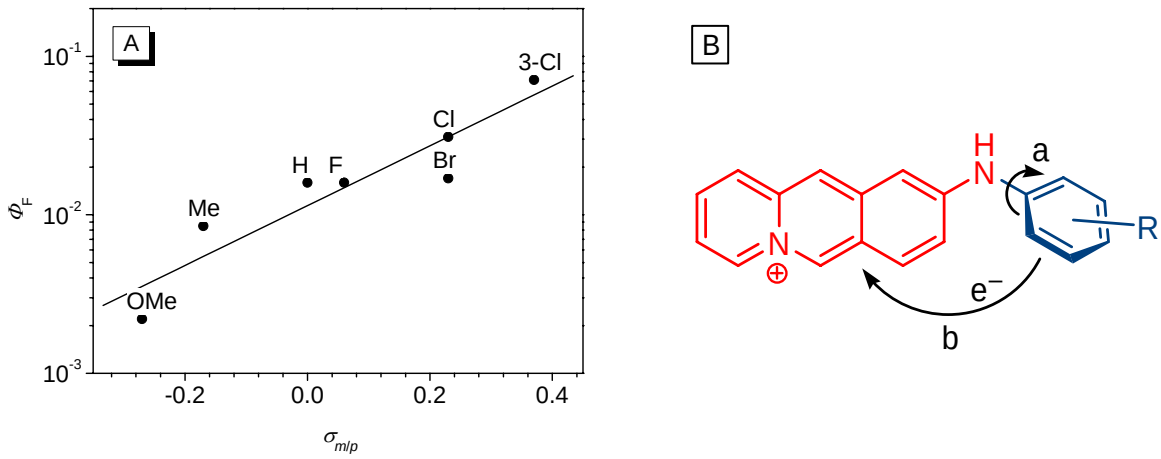

Figure 2.22. (A) Dependence of the fluorescence quantum yield of derivatives **27e–k** in glycerol on the Hammet substituent constant σ. (B) The proposed model for the radiationless deactivation of the excited state in *N*-aryl-9-aminoacridizinium salts, including torsional relaxation of the phenyl group (a) and excited-state electron transfer (b). The chromophore unit is shown red.

Therefore, it may be proposed that there exists another radiationless pathway for the deactivation of the excited state, the efficiency of which is dependent on the electron density on the phenyl ring that is provided by the substituent. Similarly to the ANS system **13**, it may be concluded that this pathway is represented by an excited-state electron transfer from the phenyl group to the photo-excited 9-aminoacridizinium chromophore.

The scheme for the deactivation of the excited state of *N*-aryl-9-aminoacridizinium salts, including both radiationless processes, is presented in Figure 2.22, B. The validity of the proposed mechanism may be demonstrated by the protolytic viscosity dependence of fluorescence of derivative **27d** (Figure 2.23, A).

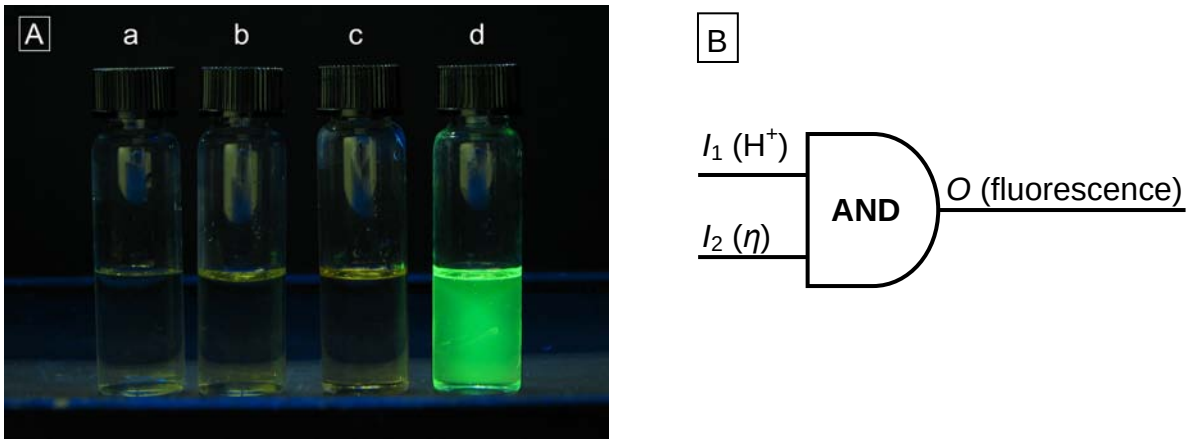

Figure 2.23. (A) Image of solutions of **27d** in water (*a*, pH 7), aq. HCl (*b*, pH ≈ 1), glycerol (*c*), and acidified glycerol (*d*, ca. 0.1 M HCl), under UV illumination (λ_L = 366 nm). Concentration c(**27d**) = 50 μM in all cases. (B) A schematic representation of a logic gate, representing the dye **27d** and transforming two inputs (I_1: protonation, I_2: rigidity of the medium) into one output (*O*).

Thus, the basic form of **27d** is virtually non-fluorescent either in aqueous solutions or at the conditions of increased viscosity (glycerol solutions), where the rotational deactivation pathway is suppressed. The protonation of the dimethylamino group, which transforms it from the electron-donor to the electron-acceptor substituent and thereby blocks the electron-transfer deactivation pathway, does not lead to a significant increase of fluorescence at the low-viscosity conditions, *i.e.* in an aqueous solution. However, when the protonation is performed in a highly viscous glycerol solution, an intense green fluorescence may be observed, as both non-radiative deactivation pathways for the excited state are hindered. Therefore, the salt **27d** may be regarded as a molecular "logic gate" of the AND type that transforms two different input parameters (proton concentratrion and the viscosity of the medium) into one output signal, namely fluorescence (Figure 2.23, B).

Quantum chemical calculations

To support the proposed structure and the excited-state dynamics of *N*-aryl-9-amino-acridizinium derivatives, quantum chemical calculations using a semiempirical AM1 method were performed. This method is a modification of the MNDO (modified neglect of diatomic overlap) approach, offering a more accurate parameterization for polar organic molecules (including heterocyclic compounds) and transition states,[114] and has been widely used for the quantum chemical calculation of cationic organic dyes.[115,116] The calculations were performed for the chloro-substituted derivative **27j**, in order to decrease the electronic density on the

phenyl ring and avoid the charge-transfer effects, which hardly can be represented correctly at the semiempirical level of theory; the anion was excluded from the calculations.

The energy-minimized ground-state structure of **27j** (Figure 2.24) shows that the acridizinium skeleton, the exocyclic nitrogen atom and the NH proton lie in one plane and represent the chromophore of the system. At the same time, the plane of the phenyl group is twisted by an angle $\theta \approx 60°$ with respect to the chromophore plane. Within the acridizinium core, a significant bond length alteration may be observed; thus, the bonds C1–C2, C3–C4 and C7–C8 are considerably shorter (1.36–1.37 Å) than the other C–C bonds (1.41–1.45 Å). A similar bond length alternation has been observed in the solid-state structures of the related quinolizinium derivatives.[117] The length of the C9–N_{exo} bond constitutes 1.365 Å and thus only slightly shorter than a single C_{ar}–N bond; the bond order equals 1.22, as determined by the calculation.

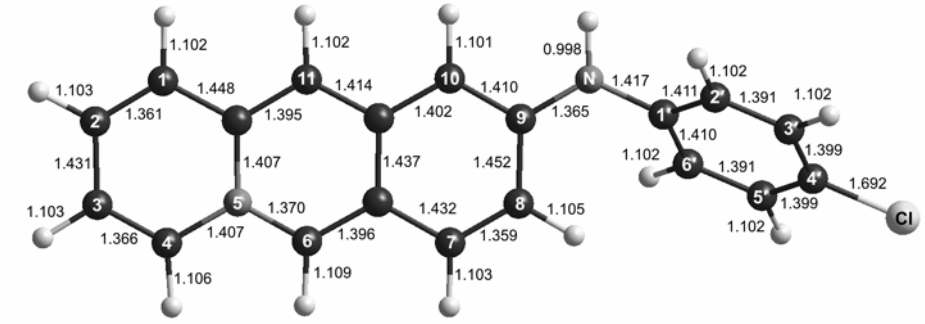

Figure 2.24. Energy-minimized structure of **27j** in the ground state, as determined by AM1 calculations. Bond lengths are indicated.

The molecular orbitals of **27j** were calculated using the optimized ground-state geometry and a closed-shell configuration interaction (CI) method with singly-excited configurations including five highest occupied and five lowest unoccupied orbitals. This was thought to provide a reasonable accuracy, as the long-wavelength part of the electronic spectrum of **27j** results mostly from the π–π^* transitions.

The calculated electronic transitions of **27j** (Figure 2.25, A) are in a good agreement with the experimentally observed spectrum, although the calculated oscillator strength values do not exactly follow the distribution of the absorption bands. However, the match of the positions of the absorption bands with the calculated energies of transitions is remarkable, considering that the calculations were performed for a gas-phase ion and no solvation effects were taken into account. In fact, performing the calculation at a higher level, *i.e.* involving more CI states,

results in a small bathochromic shift of the electronic transitions, since the extensive single-excitation CI treatment lowers the energy of the excited states without affecting the ground-state energy.

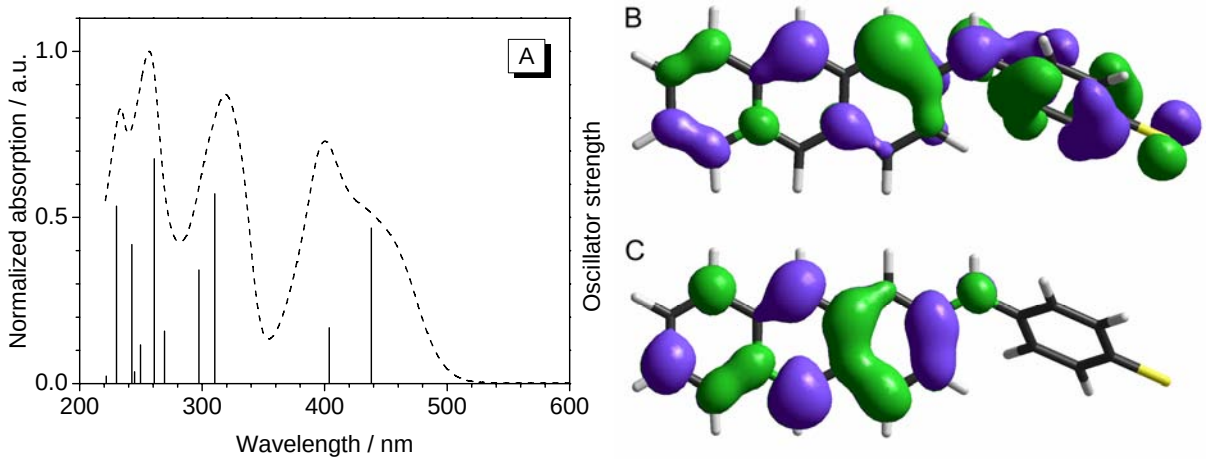

Figure 2.25. (A) Comparison of the experimental electronic absorption spectrum of **27j** (dashed curve, in methanol) with predicted electron transitions (solid lines). (B–C) Plots of the molecular orbitals (B: HOMO, C: LUMO) of **27j**, calculated at CI-AM1 level of theory.

The HOMO and LUMO of **27j** are presented in Figure 2.25, B–C. It may be noted that the HOMO–LUMO transition is accompanied by a significant redistribution of the electron density over the acridizinium chromophore. Remarkably, the spatial distribution of these orbitals over the chromophore part of the molecule closely resembles the one determined for the parent compound **5b** by the density-functional theory (DFT) calculations.[14] The dipole moments of the S_0 and S_1 states are 12.7 and 9.1 D, respectively, and lie in the plane of the chromophore. The magnitude of the HOMO–LUMO transition dipole moment is 6.6 D; its vector is oriented at an angle of 166° relative to the long axis of the acridizinium core.

Finally, the potential energy surfaces for the rotation of the phenyl group were determined for the ground and first excited states of **27j** cation. These surfaces were constructed as a function of the torsion angle, θ(C9–N_{exo}–C1′–C2′), between the planes of the acridizinium chromophore and the phenyl ring, while the torsion angle φ(C8–C9–N_{exo}–C1′) was fixed at 0° (as it is in the energy-minimized conformation). This additional restraint was necessary for the correct treatment of the "saddle points" at which the inversion of the phenyl group takes place.

The calculated potential energy surfaces (Figure 2.26) give evidence that a potential barrier for the rotation of the phenyl group exists both in the ground and in the first excited state. The

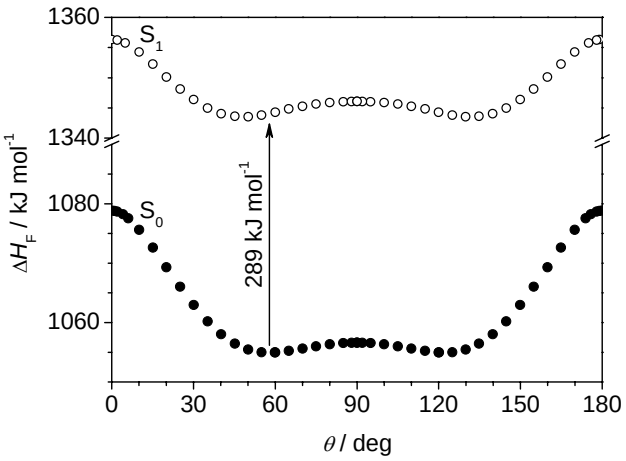

Figure 2.26. Computed potential energy surfaces for the rotation of the phenyl group in the S_0 (filled circles) and S_1 (empty circles) states of **27j**.

energy for the vertical excitation, calculated as the distance between the states at the ground-state minimum, constitutes 289 kJ mol^{-1} (λ = 412 nm) and is in a good agreement with the results of CI calculations and experimental data. At the same time, the height of the barrier in the ground state is significantly larger ($\Delta\Delta H_f$ = 23.9 and 12.8 kJ mol^{-1} for S_0 and S_1 states, repectively). These values are smaller than the experimentally determined value of the activation energy of the fluorescence quantum yield in glycerol (ΔE_a = 39 kJ mol^{-1}). Nevertheless, it may be proposed that, since the energy barrier is almost twice as low in the excited state compared to the ground state, the torsion of the phenyl group takes place in the excited state, leading to a non-radiative deactivation.

Conclusions

The non-radiative deactivation pathways of *N*-aryl-9-aminoacridizinium derivatives include an excited-state rotation of the phenyl group and—in the case of electron-donor substituents in the phenyl ring—an electron transfer from the phenyl ring to the electronically excited acridizinium chromophore. Therefore, these compounds represent fluorescence probes, almost insensitive to the changes in the *polarity* of the medium but with a pronounced susceptibility to the *rigidity* of the environment. Apart from the prospects for the detection of biomacromolecules, which will be discussed below, the aforementioned properties make the *N*-aryl-9-aminoacridizinium derivatives attractive for the applications in which the changes of the probe signal due to the changes in polarity are undesired, as they can obstruct the changes arising from other events, such as fluctuations in the rigidity of the medium. Such applications include *e.g.* on-line monitoring of polymerization reactions and aging of polymers,[85,118]

fluorimetric measurement of viscosity of liquids,[119] and measurement of microviscosity of the cell structures.[120]

2.3.2 Interaction of 9-Substituted Acridizinium Derivatives with DNA

The results of the spectrophotometric titrations of selected 9-substituted acridizinium derivatives with DNA, namely a significant hypochromic effect of the long-wavelength absorption band and the formation of new red-shifted bands indicate binding of these salts to the DNA. The isosbestic points, observed in most cases, indicate that one binding mode takes place almost exclusively. An exception from this behavior show the halogen-substituted derivatives **27i–k**, for which the long-wavelength isosbestic point was not conserved during the titration (Figure 2.8).

The linear dichroism spectroscopy of the dye-DNA complexes reveals that both compounds **27a** and **27j** intercalate into ds DNA, as indicated by the negative LD bands in the presence of DNA (Figure 2.13). The reduced LD spectrum provides further information on the average orientation of the transition moment of the chromophore relative to those of the DNA bases and allows distinguishing between homogeneous and heterogeneous binding. For the *N*,*N*-dialkylamino derivative **27a**, the LD_r spectrum is consistent with a perpendicular orientation of the chromophore plane relative to DNA helix axis, confirming that its orientation, like in the case of the parent compound **5b**,[10] is fully consistent with an intercalation into the DNA. In contrast, the LD_r spectrum of compound **27j** indicates a binding geometry in which the plane of the acridizinium chromophore is tilted by about 10° relative to the DNA bases. This observation indicates that ionic interactions or groove binding also contribute to the overall binding of this compound to the DNA. This heterogeneous binding is confirmed by the loss of the isosbestic point in the UV/Vis titration. Thus, it may be estimated that dialkylamino-substituted derivatives **27a–b**, as well as the parent compound **5b** and the sulfur analogue **28** bind to ds DNA exclusively by intercalation, whereas in the case of most *N*-aryl derivatives the intercalative binding mode prevails at low DNA-to-dye ratios, and at higher DNA concentrations another binding mode with a low binding constant takes place, which may be assigned to the assembly of the dye cations on the surface of DNA.

For the evaluation of the DNA-binding constants and binding-site sizes, the data from spectrophotometric titrations were represented as Scatchard plots (Figure 2.27) and fitted to the neighbor-exclusion model of McGhee and von Hippel (Eq. 5.10 in the Experimental Part).

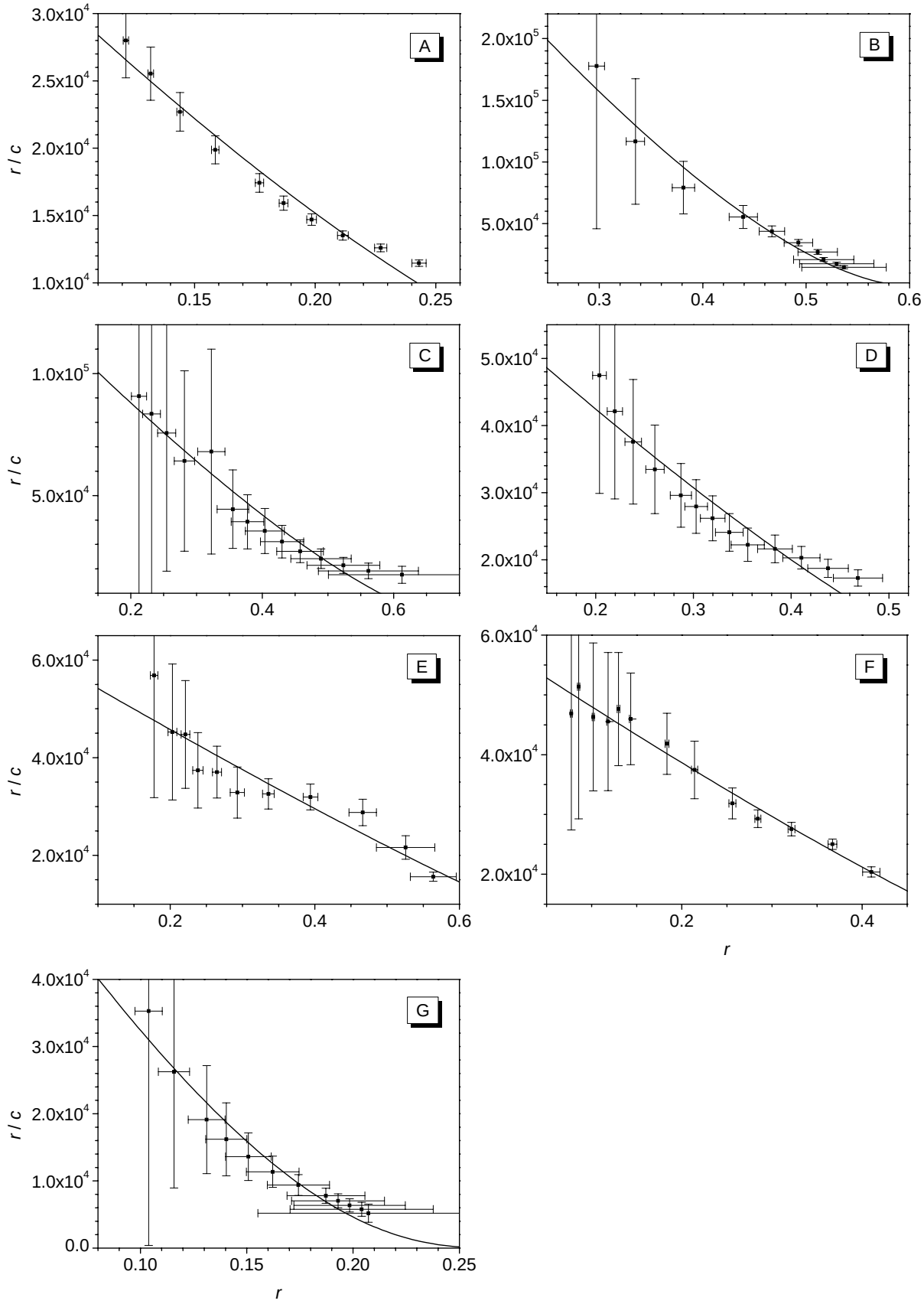

Figure 2.27. Scatchard plots of spectrophotometric titrations of acridizinium derivatives **27a** (A), **27b** (B), **27d** (C), **27e** (D), **27i** (E), **27j** (F) and **28** (G) for the determination of binding constants *K* and exclusion parameters *n*. Solid lines represent the best fits to the theoretical model (Eq. 5.10).

The binding constants of the investigated compounds are in 10^4 M^{-1} range within the experimental error (Table 2.5). Compound **27b** has the largest value of $K = 4.4 \times 10^5$ M^{-1}. In general, the binding-site sizes for the dialkylamino-substituted derivatives **27a–b** and the methylthio derivative **28** are larger than the values for the *N*-aryl derivatives (n = 1.2–1.5), which may be explained by the assumption that the latter compounds, in addition to the intercalation, at high ligand-to-DNA ratios form aggregates which stack along the DNA backbone. The binding of the compounds from the former subgroup is more consistent with the exclusive intercalative mode.

Table 2.5. DNA-binding properties of selected 9-aminoacridizinium derivatives from spectrophotometric and fluorimetric titrations.

	λ_{abs} / nm [a]			λ_{fl} / nm [b]			K [c] / 10^4 M^{-1}	n [d]
	free	bound	shift $\Delta\lambda$	free	bound	shift $\Delta\lambda$		
27a	396	407	11	529	534	5	4.7 ± 0.2	2.4 ± 0.1
27b	404	415	11	537	540	3	44 ± 4	1.7 ± 0.1
27d	401	413	12	524	532	8	14 ± 1	1.5 ± 0.1
27e	398	413	15	519	519	0	6.8 ± 0.4	1.5 ± 0.1
27i	398	410	12	508	558	50	6.3 ± 0.4	1.2 ± 0.1
27j	397	409	12	513	555	42	5.8 ± 0.2	1.4 ± 0.1
27k	397	407	10	542	539	−3	– [e]	– [e]
28	389	400	11	496	492	−4	7.5 ± 0.6	3.7 ± 0.1

[a] Absorption wavelengths that corresponds to the free and bound dye absorption maxima, as well as the shift upon complex formation with DNA; [b] emission maxima for the free and bound dye and the shift upon complex formation with DNA; [c] binding constant (in bp) and [d] binding-site size (in bp), determined from fitting the Scatchard plots to the McGhee–von Hippel model; [e] not determined due to precipitation of DNA-dye complex during titration.

The interaction of the dyes **27a–k** with the DNA has an influence on their emission properties. While this influence is rather weak in the case of compounds **27a–b**, the derivatives **27i–k** with electron-acceptor halogen substituents in the phenyl ring exhibit fluorescence enhancement upon interaction with the DNA. This enhancement is rather weak for **27i** and significant in case of **27j** and **27k** (by factors of 30 and 50, correspondingly). Obviously, intercalation of the acridizinium chromophore into the DNA helix reduces the possibility of free rotation about the *N*-aryl bond, which prevents the non-radiative decay from the excited state. Compared to the derivative **27e**, which has a methoxy substituent in the phenyl ring, it

may be assumed that in the latter case another deactivation pathway, namely the electron-transfer process from the electron-rich phenyl substituent to the acridizinium cation, prevents the fluorescence enhancement upon association with DNA. Smaller fluorescence enhancement of **27i** compared to **27j–k** may be attributed to the internal heavy atom effect in **27i**, since its fluorescence at the high-viscosity conditions, which hinder the torsional relaxation pathway, is also lower than the ones of the chloro-substituted derivatives (*cf.* the data in Table 2.3). A similar effect was found in the structurally similar ANS system.[106c]

These results indicate that—with an appropriate substitution pattern—*N*-aryl-9-amino-substituted acridizinium salts may be used as fluorescent "light-up" probes for DNA detection (Figure 2.28). Notably, the enhancement of fluorescence intensity of **27k** upon addition of DNA is larger than the ones observed for the conventional DNA stains, such as ethidium bromide ($I_{max} / I_0 \approx 10$, *cf.* the data in Table 1.1) and Hoechst 33258 ($I_{max} / I_0 \approx 30$), so that this dye may be used complementary to the already established ones.

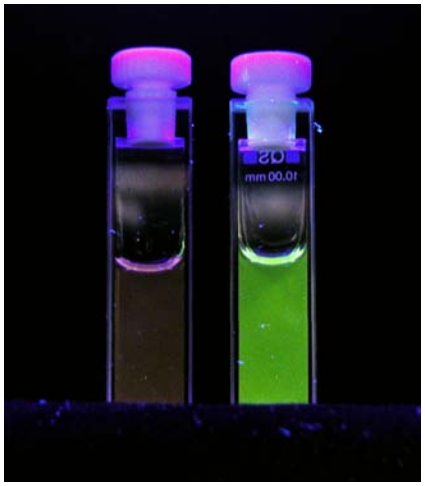

Figure 2.28. Image of aqueous solutions of **27k** in the absence (left) and in the presence (right) of ct DNA under UV illumination (λ_L = 366 nm).

2.3.3 Interaction of *N*-Aryl-9-aminoacridizinium Derivatives with Proteins

The halogen-substituted derivatives **27h** and **27j–k** exhibit a significant fluorescence enhancement upon interaction with the proteins, such as human and bovine serum albumins and egg-white albumin. This fluorescence enhancement becomes more pronounced in the presence of an anionic surfactant (SDS), which is known to denaturate the proteins and form structures, in which the surfactant micelles are distributed along the unfolded protein molecules (necklace and beads model).[121] However, excess SDS leads to a decrease of the

fluorescence, since the surfactant begins to displace the protein-bound probe molecules. A similar dependence of fluorescence on the surfactant concentration has been observed for other fluorescent probes, such as the ANS derivative TNS (**13**, R = CH_3)[121] and Nile Blue,[122] and has been used in some patented fluorescence-based assays for quantification of proteins in solution.[97] It may thereofore be concluded that the role of SDS is the denaturation of the proteins, which provides access to the probe-binding sites which otherwise can not be occupied by the dye molecules.

Remarkably, the fluorescent enhancement factors observed for the different compounds investigated are essentially the same, which leads to the conclusion that these probes occupy the same binding sites. It may be proposed that, like in the case of the interaction with DNA, binding to the proteins reduces the conformational freedom of the probe molecule, leading to hindered rotation of the phenyl group and increase of the fluorescence quantum yield.

The observed fluorescence enhancement ($I_{max} / I_0 \approx 20$) is smaller than the one observed for TNS ($I_{max} / I_0 \approx 100$);[123] however, the fluorescence maxim of acridizinium derivatives are located at longer wavelengths (540 nm *vs.* about 460 nm in the case of TNS) and thus more advantageous for the fluorimetric detection. It should be noted that recently a series of squaraine dyes for the fluorimetric detection of albumins has been described;[124] such dyes possess high sensitivity ($I_{max} / I_0 \approx 80$) and emit at long wavelengths ($\lambda_{fl} \approx 610$ nm), but their application in the presence of surfactants was not tested. Along these lines, *N*-aryl-9-amino-substituted acridizinium derivatives represent fluorescent probes which are consistent with the surfactants used in the protein gel electrophoresis, and may find application for protein detection in gel electrophoresis due to the low protein-to-protein variability.

3 TARGETING TRIPLE-HELICAL DNA WITH DIAZONIAPOLYCYCLIC INTERCALATORS

3.1 Objective

As it has been argued in the Introduction (Section 1.3), the search for the small molecules that selectively bind to and stabilize the triple-helical DNA structures is an active research area. A number of the triplex-selective ligands have been identified. However, in spite of almost 15 years of active research, almost all synthetic triplex-DNA binders are derived from just a handful of lead structures. It is commonly accepted[42] that the general features of triplex-DNA binders are (i) an extended, crescent-shaped polyaromatic system with an aromatic surface area large enough to provide a π overlap with three nucleic bases in the triplex; (ii) a cationic charge on the chromophore; and (iii) a side chain with an alkaline amine functionality. The latter is proposed to provide additional stabilization by the interaction with the phosphate groups in the DNA groove. However, some exceptions from this paradigm are known; thus, substituted anthracenes[125] and anthraquinones[51] bind selectively to the triplex DNA despite their rather limited extension of the π system. Moreover, alkaloids such as coralyne (**4**),[53] berberine and cryptolepine[54] represent examples with a pronounced affinity towards triplex DNA even in the absence of aminoalkyl side chains. In the latter cases, however, the four methoxy substituents may play a role in the DNA-binding properties.

The major drawback of the synthetic triplex-binding intercalators reported so far is the requirement of aminoalkyl substituents. Along with the sometimes tedious synthetic efforts to introduce such substituents, their chemical reactivity needs to be considered: amino groups may act as bases, as nucleophiles, or as electron donors in electron-transfer reactions. Thus, under physiological conditions, several reaction pathways are possible that may lead to the deactivation of a triplex binder, which may limit its application as a drug.

In this context, the interactions of the diazoniapolycyclic salts, namely the diazoniapentaphenes **7a–c**,[126] which closely resemble the structures of triplex-DNA selective lead structures, such as dibenzophenanthroline derivatives **36a–c**[46] and substituted naphthylquinolines (**37**),[47] with double-stranded and triple-helical nucleic acids were planned to be investigated. The diazoniapolycyclic compounds were proposed to have advantageous properties, such as readily availability by the cyclodehydration synthesis and high stability due to the aromatic character and the absence of alkaline side chains. In the case of positive

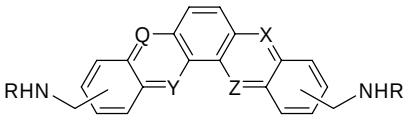

36a: Q = X = C; Y = Z = N
36b: Q = X = N; Y = Z = C
36c: Q = Z = C; X = Y = N

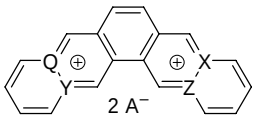

7a: Q = X = C; Y = Z = N
7b: Q = X = N; Y = Z = C
7c: Q = Z = C; X = Y = N

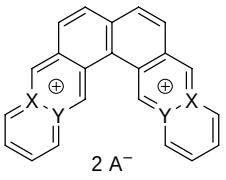

38a: X = C; Y = N
38b: X = N; Y = C

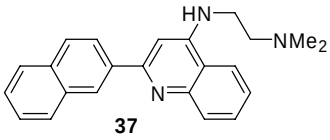

37

results, the series should be expanded into the structurally related diazoniaanthra-[1,2-*a*]anthracenes **38a–b**.[127] Moreover, the series of diazoniapolycyclic salts may be increased by the synthesis of previously unknown derivatives. Thus, linear diazonia-pentacenes **39a–b** could in principle have been synthesized by the cyclodehydration of methyl-substituted precursors **40a–b** (Scheme 3.1).

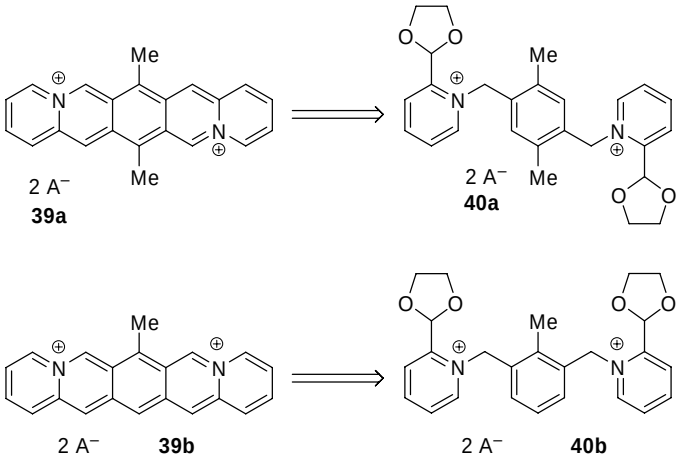

Scheme 3.1. Retrosynthetic analysis of methyl-substituted diazoniapentacenes.

This systematic study should allow the deviation of a structure–properties relationship. Thus, the influence of the ligand shape (angular, helicene-like, linear), number of aromatic rings (five or six), and position of quaternary nitrogen atoms within the polycyclic framework on the duplex- and triplex-DNA binding properties were planned to be studied.

3.2 Results

3.2.1 Synthesis of Diazoniapolycyclic Salts

3.2.1.1 Synthesis of Unsubstituted Diazoniapentaphenes

The synthesis of the previously described unsubstituted isomeric diazoniapentaphenes **7a–c** was accomplished by a modification of the published procedures,[126] starting from the isomeric *α*,*α*′-dibromoxylenes (Scheme 3.2, Table 3.1). These were allowed to react with (1,3-dioxolan-2-yl)pyridine (**32**), to give the corresponding bispyridinium dibromides **41a–c** in high yield. The latter were further converted into tetrafluoroborate salts. The use of bromide salts of these intermediates in the final cyclodehydration step is unfavorable, due to the competing nucleophilic substitution of pyridinium residues with a bromide counter-ion.[126b]

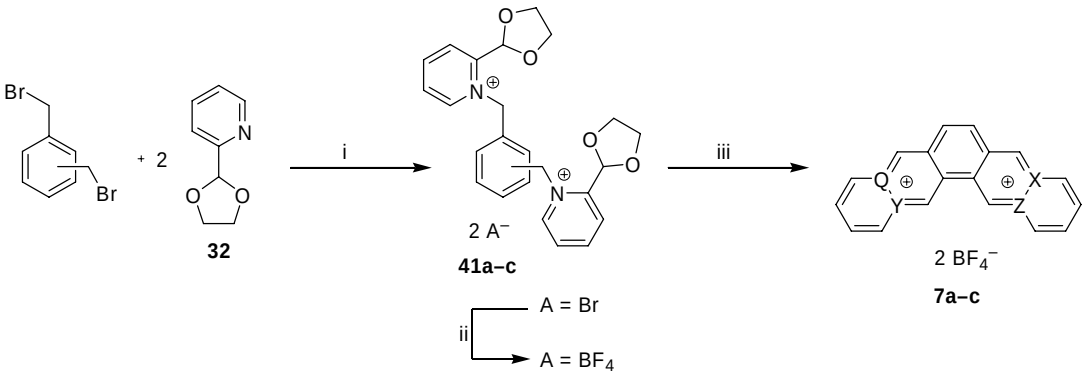

Scheme 3.2. Synthesis of unsubstituted diazoniapentaphenes. Reagents and conditions: (i) DMSO, 7 days, room temp.; (ii) $NaBF_4$ aq.; (iii) PPA, 150 °C, then aq. $NaBF_4$.

Table 3.1. Synthesis of unsubstituted diazoniapentaphenes.

Compound	Substitution pattern					Yield / %		
	41a–c	**7a–c**						
		Q	X	Y	Z	i	ii	iii
7a	1,2	C	C	N	N	85	63	84
7b	1,4	N	N	C	C	97	79	61
7c	1,3	C	N	N	C	80	65	65

3.2.1.2 Synthesis of Substituted Diazoniapentaphenes

In an attempt to prepare linear diazoniapentacenes **39a** and **39b** (Scheme 3.1), the bispyridinium derivatives **40a–b** were synthesized from the corresponding methyl-substituted bis(bromomethyl)arenes **43** and **30c** and 2-(1,3-dioxolan-2-yl)pyridine (**32**), followed by the ion exchange with tetrafluoroborate (Scheme 3.3). Nevertheless, cyclodehydration of **40a (2BF_4^-)** in PPA at 150 °C gave a single product in 30% yield, whose NMR spectra were not consistent with the structure of the desired diazoniapentacene **39a**. Thus, 12 non-equivalent low-field aromatic ^{1}H-NMR signals and 20 non-equivalent ^{13}C-NMR signals, as well as two independent signals for the methyl groups, were detected. In addition, ESI mass spectrometry and elemental analysis revealed that the product is a constitutional isomer of **39a**. The lack of symmetry already indicated a pentaphene structure rather than a pentacene skeleton. In fact, X-ray-diffraction analysis (Section 3.2.2.1) showed that 6,13-dimethyl-4a,8a-diazoniapentaphene **42a** was formed as the reaction product.

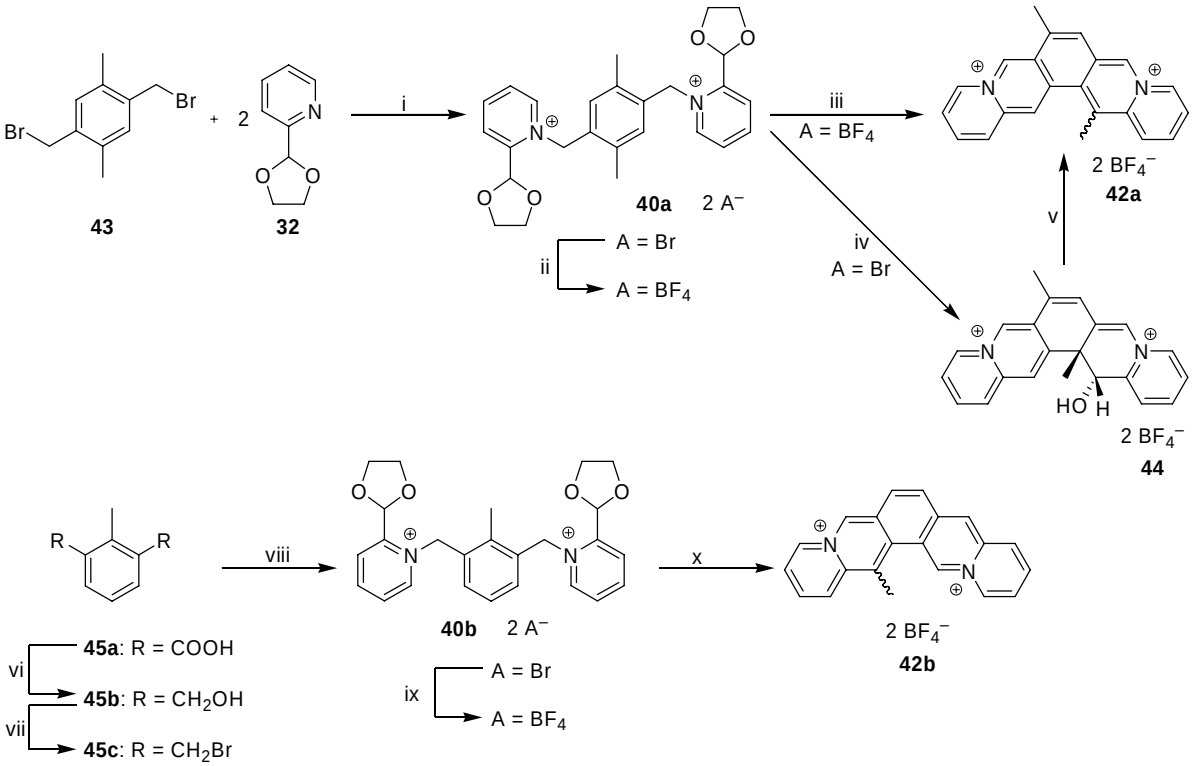

Scheme 3.3. Synthesis of methyl-substituted diazoniapentaphenes. Reagents and conditions: (i) NMP, room temp., 7 days, 95%; (ii) aq. $NaBF_4$, 92%; (iii) PPA, 150 °C, 24 h, 30%; (iv) aq. HBr (48%), reflux, 2 h, then aq. HBF_4, 35%; (v) PPA, 150 °C, 18 h, 91%; (vi) BF_3·THF, THF, 0 °C → room temp., 18 h, 92%; (vii) aq. HBr (48%), 50 °C, 1 h, 85%; (viii) **32**, NMP, room temp., 48 h, 96%; (ix) aq. $NaBF_4$, 93%; (x) PPA, 150 °C, 24 h, 51%.

At the same time, the cyclization of the salt **40a (2Br$^-$)** under slightly milder conditions, *i.e.* in refluxing aqueous HBr, gave the partially saturated product **44**. Although the compound **44** was isolated in rather low yield (35%), the ^{1}H-NMR spectrum of the crude product, obtained by precipitation of the reaction mixture with acetone, did not reveal the presence of any side products. This indicates that the competing nucleophilic substitution of the pyridinium residue with bromide does not take place in this case. Moreover, dehydration of **44** in PPA at 150 °C gave the same diazoniapentaphene **42a** in high yield (91%) without formation of any detectable side products.

The structure of **44 (2BF$_4^-$)** was confirmed by ^{1}H- and ^{13}C-NMR, mass-spectrometric and elemental analyses. Especially characteristic is the coupling of the hydroxyl proton with 13-H ($^3J_{H,H}$ = 4.7 Hz) and the NOE effect between the latter and the methyl group at C13a (Figure 3.1, B). Although compound **44** has two stereogenic centers, the NMR spectra give evidence that only one diastereomer (as a racemate) has formed. Indeed, the integration of the NOE spectra showed that the distance between 13-H and the methyl group at C13a is consistent with the structure of the *anti*–isomer shown on Scheme 3.3. Moreover, this structure was firmly confirmed by the X-ray diffraction analysis (Section 3.2.2.2).

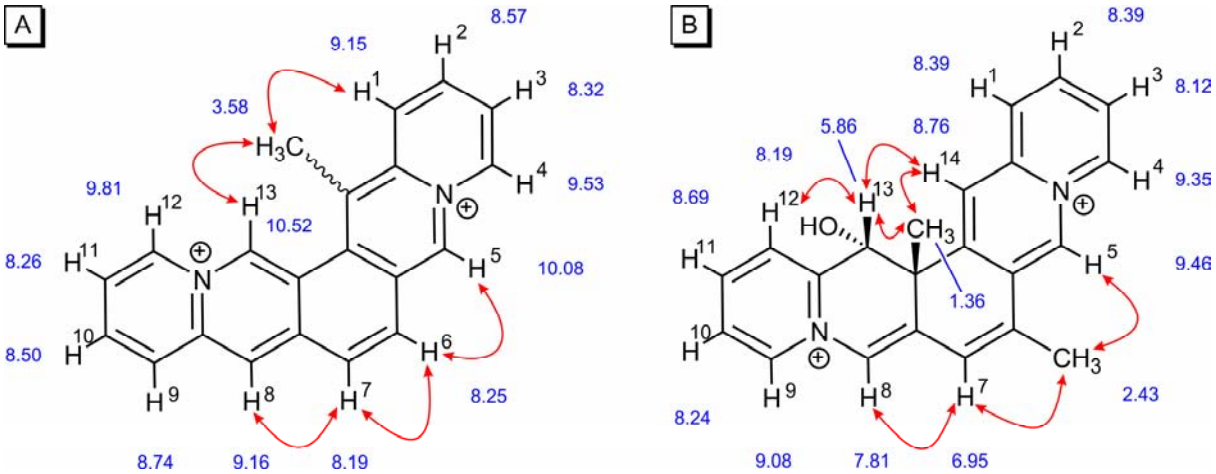

Figure 3.1. ^{1}H-NMR shifts (in [D$_6$]DMSO) and characteristic NOE effects in **42b** (A) and **44** (B).

Similarly to the reaction of **40a**, the cyclodehydration of **40b (2BF$_4^-$)** under the same conditions (PPA, 150 °C, 24 h) gave the 14-methyl-4a,12a-diazoniapentaphene **42b** in 51% yield (Scheme 3.3). Its structure was elucidated on the basis of NOE effects between the methyl group and 13-H, the ^{1}H-NMR signal of which is strongly downfield-shifted (δ = 10.52 ppm), since C13 is directly bound to the positively charged nitrogen (N12a) atom (Figure 3.1, A). The NOE interactions between 6-H and 7-H, whose signals are shifted to

relatively high field (δ = 8.25 and 8.19 ppm), and the neighboring 5-H and 8-H atoms, respectively, also confirmed the assignment of the structure of **42b**.

To investigate the scope of this rearrangement, compounds **40c** and **40d** in which the methyl group is replaced with bromine and trifluoromethyl substituents, respectively, have been prepared (Scheme 3.4). After the cyclization of **40c** at similar conditions (PPA, 150 °C, 36 h), a purple product was isolated in 56% yield which, at first glance, was different from the pale-yellow salts **42a–b**. However, NMR spectra of the product showed 13 non-equivalent low-field ^{1}H signals and 20 distinct ^{13}C signals, which were consistent with an unsymmetric monosubstituted diazoniapentaphene structure. While NMR spectroscopy did not give unambiguous information about the constitution, only a single peak with an *m*/*z* value of 297 was observed in the ESI mass spectra. This ion mass as well as the isotopic pattern was not consistent with a bromo-substituted derivative. On the basis of mass-spectra and elemental analysis, the structure of the semi-betaine **42c** was assigned to the product. This structure is further supported by the ^{13}C-NMR signal of C14 at δ = 164.3 ppm, which is characteristic for pyridinium-3-olates,[128] and by an IR band at $\tilde{\nu}_{max}$ = 1552 cm^{-1}, which is typical for a phenolate C–O^{-} bond. Moreover, this structure assignment is in accordance with the observations that under neutral or alkaline conditions the 11-hydroxybenzo[*b*]quinolizinium forms a purple-colored betaine, whose electronic spectra resemble those of compound **42c**.[129] Notably, the mass-spectrometric analysis gives evidence that compound **42c** reacts with molecular oxygen under ambient conditions, since, after storing a sample solution for several hours, an additional peak with *m*/*z* = 329 was observed. This peak is attributed to formation of the endoperoxide $[M + O_2]^{+}$, as pyridinium betaines are known to react easily with oxygen.[130] The solutions of **42c** in aprotic solvents undergo fading already after a few hours at ambient light conditions, whereas diazioniapentaphes **7a–c** and **42a–b** remain unchanged for weeks.

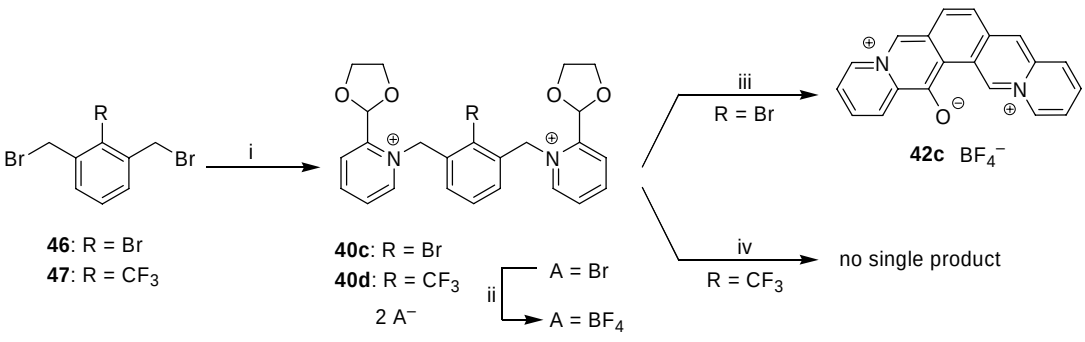

Scheme 3.4. Reagents and conditions: (i) **32**, NMP, room temp., 7 days, **40c**: 91%, **40d**: 72%; (ii) aq. $NaBF_4$, **40c**: 80%, **40d**: 75%; (iii) PPA, 150 °C, 72 h, 56%; (iv) PPA, 160 °C, 48 h.

In contrast, an attempt to cyclize the trifluoromethyl-substituted salt **40d** under similar conditions (PPA, 160 °C, 48 h) gave a non-separable mixture of unidentified products. Heating of **40d** in methanesulfonic acid under slightly milder conditions (120 °C, 3 h) resulted only in deprotection of the aldehyde groups, as judged by the ^{1}H-NMR spectroscopic analysis of the crude product (δ = 6.28 ppm, characteristic for the CH_2N^+ group of the precursor, together with a broad singlet at δ = 10.47 ppm, assigned to the aldehyde group).

3.2.1.3 Synthesis of Hexacyclic Diazoniaarenes

The symmetrical hexacyclic derivatives, namely 14a,16a-diazoniaanthra[1,2-*a*]anthracene **38a** and 4a,10a-diazoniaanthra[1,2-*a*]anthracene **38b** were prepared by slight modification of the published procedures.[127] Similarly to the synthesis of unsubstituted diazoniapentaphenes **7a−c**, the corresponding bis(bromomethyl)naphtalenes were allowed to react with 2-(1,3-dioxolan-2-yl)pyridine (**32**) to give the quaternary salts **48a–b**, followed by the ion exchange with tetrafluoroborate and the cyclodehydration step (Scheme 3.5, Table 3.2). The structures of the products **38a–b** were confirmed by 1D and 2D NMR spectroscopy, since in the previous works the NMR spectroscopic data have not been cited and the structure assignments were made solely on the basis of electronic absorption spectra.[127]

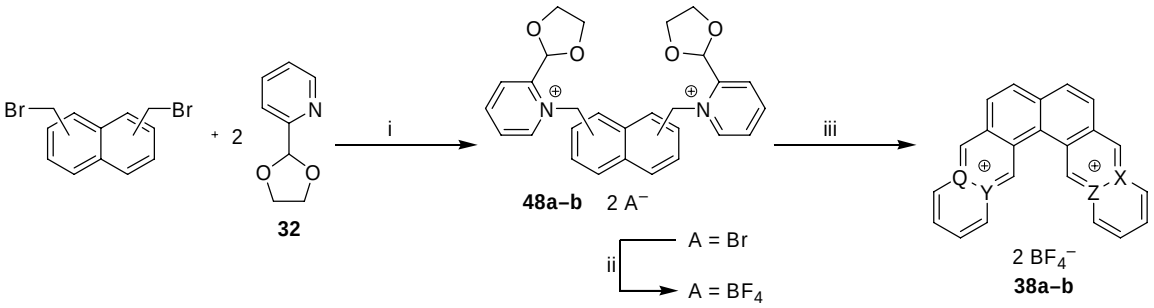

Scheme 3.5. Synthesis of diazoniaanthra[1,2-*a*]anthracenes **38a–b**. Reagents and conditions: (i) DMSO or NMP, 7–12 days, room temp.; (ii) $NaBF_4$ aq.; (iii) PPA, 150 °C, then aq. $NaBF_4$.

Table 3.2. Synthesis of symmetrical diazoniapentaphenes **38a–b**.

Compound	Substitution pattern					Yield / %		
	48a–b	**38a–b**						
		Q	X	Y	Z	i	ii	iii
38a	1,8	C	C	N	N	quant.	70	79
38b	2,7	N	N	C	C	95	78	40

The unsymmetrical isomer **38c** (4a,14a-diazoniaanthra[1,2-*a*]anthracene) has not been described previously. Thus, its synthesis was planned starting from 1,7-dimethylnaphthalene **49** (Scheme 3.6). The latter is commercially available, however, at a relatively high price. Moreover, reported syntheses of **49** are rather tedious and time-consuming.[131,132] Therefore, an efficient preparation of 1,7-dimethylnaphthalene was developed using the method of Leitch *et al.* for the synthesis of substituted 2-methylnaphthalenes.[133]

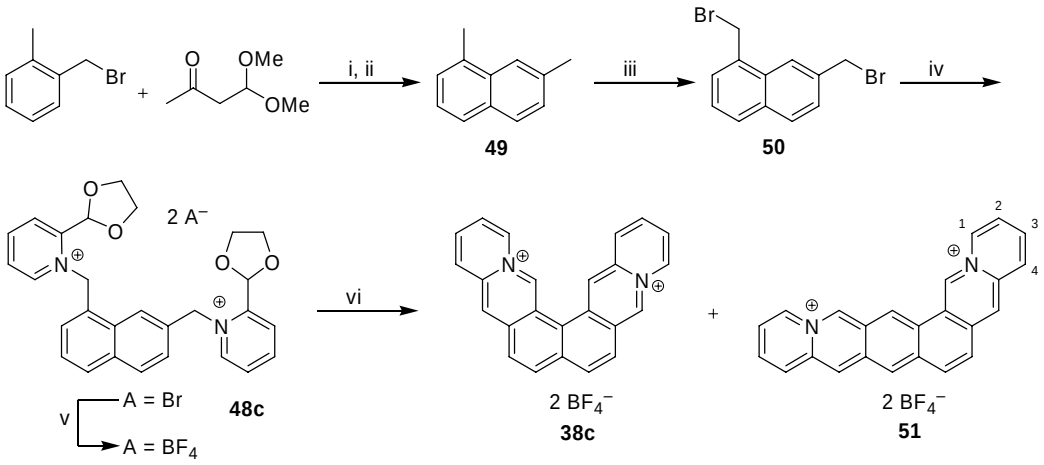

Scheme 3.6. Synthesis of 4a,14a-diazoniaanthra[1,2-*a*]anthracene **38c** and 13a,16a-diazoniahexaphene **51**. Reagents and conditions: (i) Mg, Et_2O; (ii) HBr, AcOH, reflux, 2 h, 38%; (iii) NBS, $(PhCOO)_2$, CCl_4, reflux, 4 h, 49%; (iv) **32**, NMP, room temp., 7 days; (v) aq. $NaBF_4$, 67%; (vi) PPA, 150 °C, 24 h, 95%.

Thus, 2-methylbenzylmagnesium bromide, prepared from the commercially available 2-methylbenzyl bromide, was allowed to react with 4,4-dimethoxybutan-2-one, and the intermediate alcohol was—without further purification—subjected to the cyclodehydration by HBr in acetic acid. This two-step procedure gave 1,7-dimethylnaphthalene (**49**) in 38% yield. Radical dibromination of the latter to 1,7-bis(bromomethyl)naphthalene (**50**), followed by the reaction with two equivalents of **32**, gave the bispyridinium dibromide **48c (2Br⁻)**, which was further converted into the corresponding tetrafluoroborate **48c (2BF_4^-)**. However, the cyclodehydration at the conditions usually employed for the synthesis of diazoniapolycycles (PPA, 150 °C, 24 h) gave a mixture of the desired product **38c** and the isomeric 13a,16a-diazoniahexaphene (**51**). Fortunately, laborious fractional crystallization of this mixture allowed separation of the isomers due to the better solubility of diazoniahexaphene **51**.

The structures of **38c** and **51** were assigned by ^{1}H- and ^{13}C-NMR spectroscopy, {^{15}N, ^{1}H}-correlation NMR spectroscopy, mass-spectrometric and elemental analyses. In particular, the NOE interaction patterns for the two isomers are significantly different (Figure 3.2).

Moreover, the structure of **38c** is firmly supported by a single-crystal X-ray diffraction analysis (Section 3.2.2.3). It should be mentioned that compound **51** is the first isolated and fully characterized azonia analogue of hexaphene.

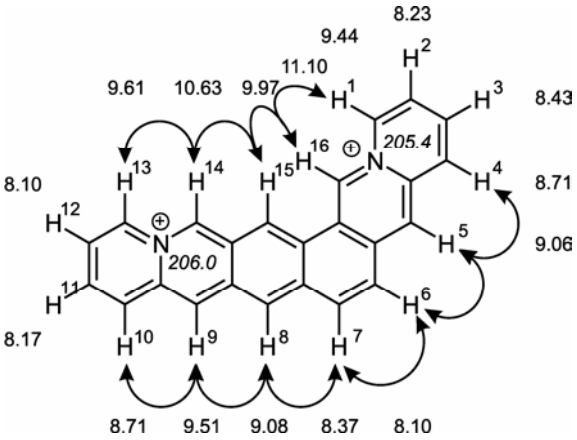

Figure 3.2. ^{1}H- (straight) and ^{15}N-NMR (*italics*) shifts (in [D_6]DMSO) and characteristic NOE effects in **51**.

Since cyclodehydration reactions are often susceptible to the reaction parameters, such as cyclization medium or temperature,[91,134] the influence of different conditions on this reaction was investigated (Table 3.3). Most notably, the cyclodehydration in refluxing aqueous HBr (48%) gave compound **38c** exclusively, which is therefore the preferred method of its preparation. However, the overall yield of the cyclization product in this case was lower (54% *vs.* 80–95% in case of PPA), presumably due to a competing nucleophilic substitution of the pyridinium residues with a bromide ion.[126b] In contrast, the use of anhydrous methanesulfonic acid (MSA) resulted in an enhanced yield of **51** (60%, with a total yield of **3** and **7** of 85%), although the formation of the diazoniaanthra[1,2-*a*]anthracene **38c** could not be avoided completely. As shown in Table 3.3, the reaction temperature has little effect on the ratio of isomers.

Table 3.3. Influence of the reaction conditions on the formation of diazoniahexacycles **38c** and **51**.

Cyclization medium	*T* / °C	Time / h	Overall yield	Ratio **38c** : **51** [a]
PPA	150	24	95%	37 : 63
PPA	180	20	82%	43 : 57
MSA	120	1.5	85%	29 : 71
HBr (aq. 48%)	128 [b]	3.5	54%	> 95 : 5

[a] Determined by ^{1}H-NMR spectroscopy; estimated error ± 5%; [b] reflux.

3.2.2 X-Ray Structure Analysis of Diazoniapolycyclic Salts

3.2.2.1 Structure of **42a** *in the Solid State*

Compound **42a** is chiral, and the racemate crystallizes in the space group $P\bar{1}$ (Table 5.1), with one single crystal containing both enantiomers in a 1:1 ratio (Figure 3.3, A). Due to steric repulsion with the neighboring hydrogen atoms the methyl substituent in position 13 points towards one of the enantiotopic faces of the aromatic plane with a deviation angle of approximately 13°. The distance between the ring planes of the neighboring enantiomeric cations is close to 3.7 Å, due to the π stacking of the cations (Figure 3.3, B). The cations overlap with more than half of the area of their aromatic core. Since the methyl groups at C13 point into opposite directions within such a pair, the distances between the C8 and C13′ atoms are somewhat larger (3.9 Å).

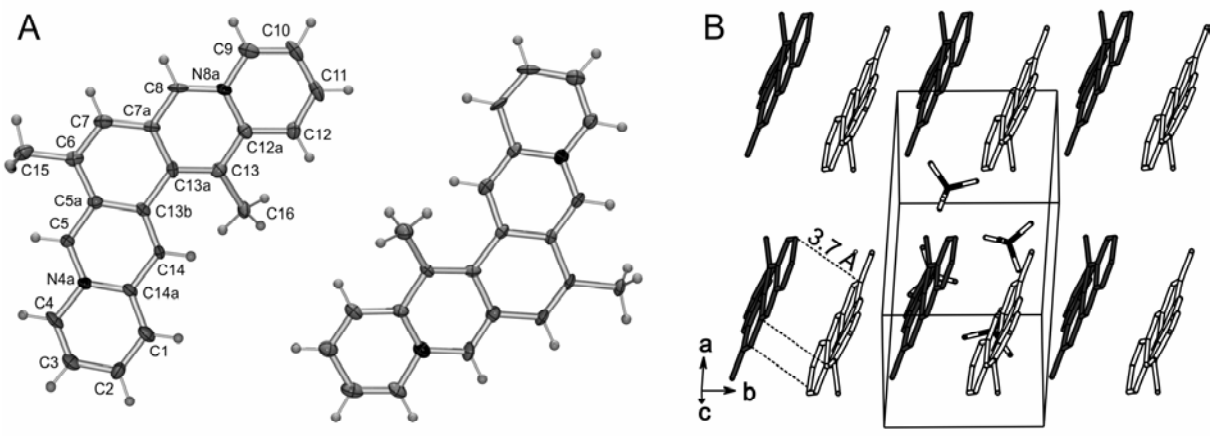

Figure 3.3. (A) The molecular structure (ORTEP view) of an enantiomeric pair of **42a** in the solid state. Except for the hydrogen atoms, the thermal ellipsoids are shown with 50% probability. (B) Crystal packing of **42a** extending along the *b* axis. The hydrogen atoms and selected BF_4^- anions were omitted for clarity. Enantiomers are shown in different colors.

3.2.2.2 Structure of **44** *in the Solid State*

Although compound **44** has two stereogenic centers, only the *anti*-diastereomer was isolated. Thus, the racemic *anti*-**44** crystallizes in the chiral space group $P2_1/n$ (Table 5.1) as a crystalline hydrate with one water molecule per cation. Within the crystal, ordered layers of enantiomers are formed (Figure 3.4).

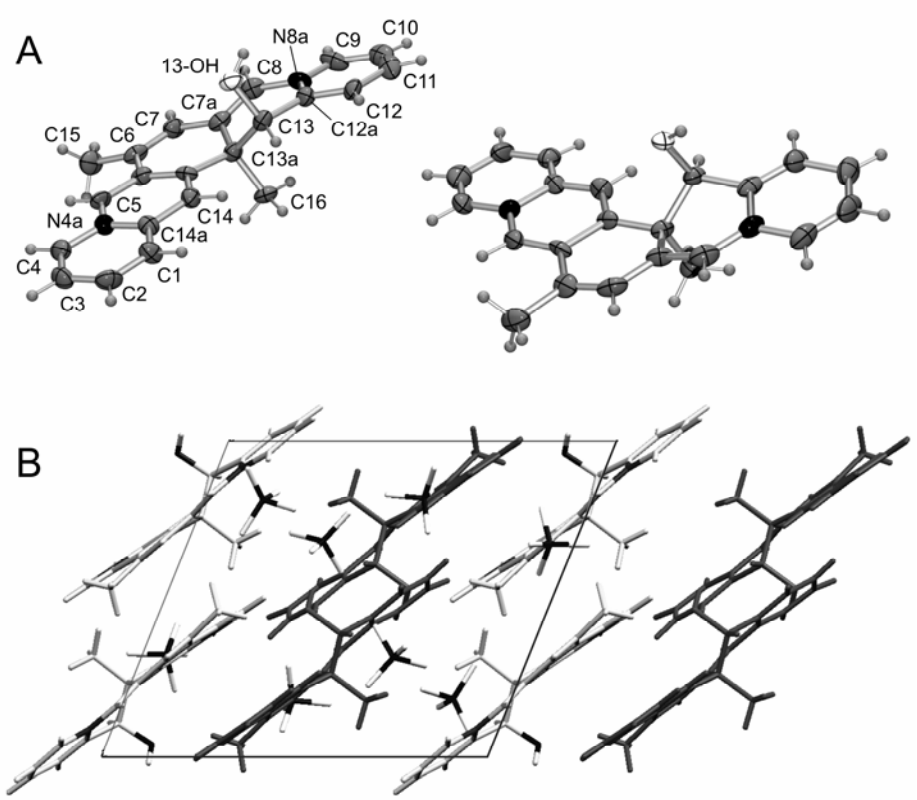

Figure 3.4. (A) The molecular structure (ORTEP view) of the enantiomeric pair of **44** in the solid state. Except for the hydrogen atoms, the thermal ellipsoids are shown with 50% probability. (B) Crystal packing of **44** extending along the *c* axis. Selected BF_4^- anions and water molecules were omitted for clarity. Enantiomers are shown in different colors.

In the case of compound **44**, no π stacking is possible due to the distortion of the ring system and *anti*-configuration of the methyl group at C13a and the hydroxyl group at C13. Hydrogen bonding is observed between the hydroxyl groups of **44** and molecules of the lattice water and between the latter and the tetrafluoroborate anions.

3.2.2.3 Structure of **38c** *in the Solid State*

Compound **38c** crystallizes in the monoclinic space group *C*2/*c* (Table 5.1) with an equal number of P- and M-enantiomers. In the solid state, the intrinsically unsymmetrical dications acquire a two-fold axis through the C7a–C15b bond, which coincides with the crystallographic axis. Therefore, the atoms labeled N4a and C10a (Figure 3.5) occupy alternative positions within the lattice and were refined with occupancy values of 0.5 for both C and N. The same procedure was applied to the atoms labeled C16a and N14a. A refinement of an ordered structure in the lower-symmetric space group *Cc* did not significantly improve the *R*-values and led to serious correlation problems.

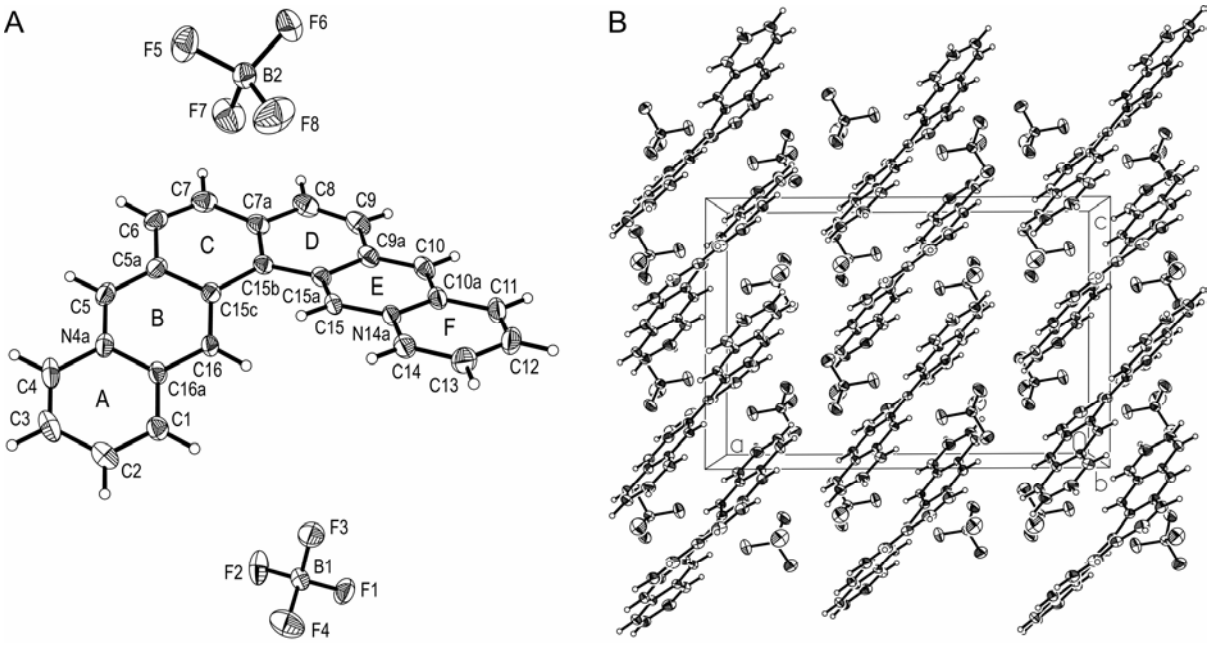

Figure 3.5. (A) The molecular structure of **38c** in the solid state. Except for the hydrogen atoms, the thermal ellipsoids are shown with 50% probability. (B) The crystal packing of **38c** viewed down the *b*-axis.

Similarly to other helicene-like molecules, two benzo[*b*]quinolizinium moieties of the dications of **38c** are twisted against each other to avoid short intramolecular C–H…H–C contacts. The shortest intramolecular contact distance is H15…H16 (1.96 Å). The angle between the planes of the two quinolizinium fragments comprises 30.7°. The C1–C2, C3–C4 and C6–C7 bond lengths are considerably shorter than the remaining C–C bonds. A similar bond length alternation has been observed in related quinolizinium derivatives.[117]

The aromatic cations are connected to the anions by intermolecular C–H…F interactions. There are five C–H…F contacts with H...F distances between 2.27 and 2.52 Å and six additional C–H…F contacts with H…F distances between 2.60 and 2.66 Å. Moreover, an intermolecular π stacking between benzo[*b*]quinolizinium moieties is observed; thus, the distance between the *meso* atoms of ring B of one molecule and ring E of the π-stacked neighboring molecule is 3.82 Å (Figure 2). The remaining rings are separated by a larger distance (ca. 3.9 Å) due to the distortion of the C/D rings.

3.2.3 Photophysical Properties of Diazoniapolycyclic Salts

Diazoniapolycyclic salts are known to have strong absorption in the UV region of the electromagnetic spectrum and significant fluorescence properties.[126a,127a] The spectroscopic data of diazoniapolycyclic salts **7a–c**, **42a–c**, **38a–c** and **51** in aqueous solutions are presented in Table 3.4. Unfortunately, diazoniapolycyclic salts are only soluble in highly polar solvents, and limited solubility in aprotic and protic solvents of low to intermediate polarity prohibited

Table 3.4. Photophysical properties of diazoniapolycyclic salts in aqueous solutions.

Compound	Absorption			Fluorescence	
	λ_{max} / nm [a]	log (ε / cm^{-1} M^{-1})	Assignment	λ_{max} / nm [b]	Φ_F [c]
7a	367	4.53	β	417	0.60
	387	4.58	$\beta + p$	443	
	413	3.69	α	471	
7b	338	4.71	β	459	0.38
	380	4.64	p	487	
	445	3.72	α		
7c	355	4.78	β	433	0.50
	373	4.50	p	460	
	425	3.69	α		
42a	348	4.86	β	483	0.32
	382	4.81	p		
	459	3.73	α		
42b	356	4.80	β	440	0.41
	379	4.54	p	466	
	429	3.65	α		
42c	373	4.52	β	626 [d]	0.03 [d] [e]
	459	4.00	π–π^*		
38a	370	4.49	β	486	0.17
	429	4.04	α		
38b	355	4.62	β	459 [f]	0.34
	451	3.89	α	490 [f]	
38c	365	4.67	β	466 [f]	0.38
	386	4.04	p	497 [f]	
	458	4.05	α		
51	373	4.92	β	471	0.42
	392	4.18	p	503	
	462	4.06	α		

[a] Selected absorption maxima, at c = 20 µM; [b] fluorescence emission maxima, at c = 5 µM; excitation wavelength λ_{ex} = 380 nm; [c] fluorescence quantum yield relative to Coumarin 1, estimated error ± 10%; [d] excitation wavelength λ_{ex} = 480 nm; [e] relative to Cresyl Violet; [f] excitation wavelength λ_{ex} = 368 nm.

the detailed investigation of the solvatochromic properties. Therefore, these compounds were investigated in a rather limited set of solvents; representative data for compound **42b** are given in Table 3.5.

Table 3.5. Spectrophotometric properties of compound **42b** in various solvents.

Solvent [a]	Absorption		Fluorescence	
	λ_{max} / nm [b]	log (ε / cm^{-1} M^{-1})	λ_{max} / nm [c]	Φ_F [d]
DMSO	366	4.65	469	0.03
	387	4.42		
	434	3.69		
Acetonitrile	357	4.77	442	0.21
	380	4.52	468	
	430	3.67		
Ethanol	360	4.79	443	0.15
	382	4.53	470	
	431	3.67		
Methanol	359	4.81	442	0.26
	380	4.55	469	
	431	3.68		
Water	356	4.80	440	0.41
	379	4.54	466	
	429	3.65		

[a] In order of their increasing E_T^N values;[94] [b] characteristic absorption maxima, at c(**42b**) = 20 μM; [c] fluorescence emission maximum, at c(**42b**) = 5 μM; excitation wavelength λ_{ex} = 380 nm; [d] fluorescence quantum yield relative to Coumarin 1, estimated error ± 10%.

To study the effect of the substituents on the electronic spectra of diazoniapentaphenes, the spectral properties of the compounds **42a–b** have been compared with those of the unsubstituted diazoniapentaphenes **7a–c**. Electronic absorption spectra of **42a** and **42b** (Figure 3.6) resemble the ones of the parent compounds and confirm the assignment of diazoniapentaphene structure to these compounds. The absorption spectra of compounds **42a−b** consist of several strong *p*- and *β*-absorption bands in the UV region (log ε > 4.60) and much weaker *α*-bands in the visible region (400–500 nm). However, derivative **42a** shows much less pronounced fine structure in the UV region than the parent unsubstituted compound **7b** (Figure 3.6, A). This confirms the deviation from the planar structure,[135] as it has been previously shown for methyl-substituted phenanthrenes.[136] In the case of derivative **42b**, this effect is less pronounced (Figure 3.6, B).

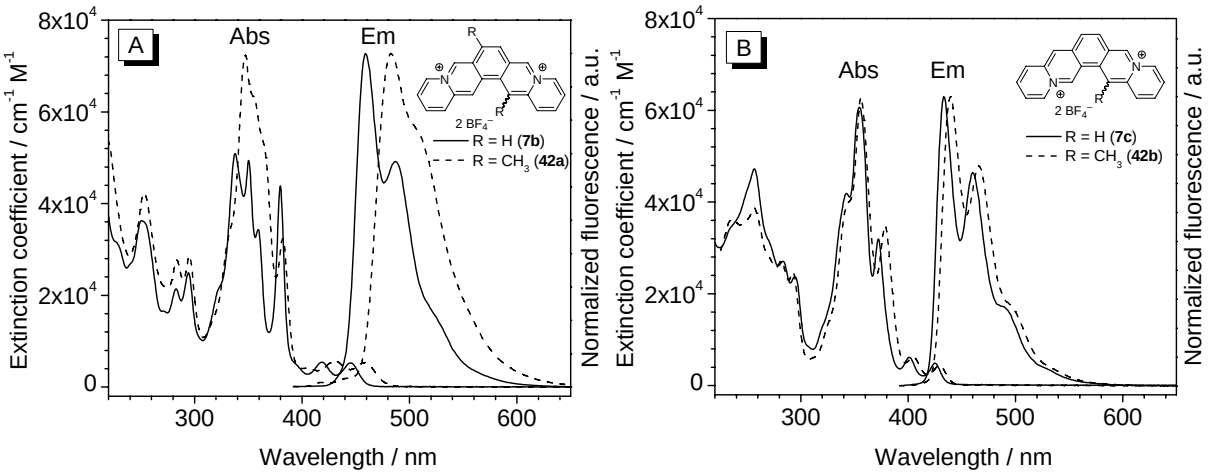

Figure 3.6. (A) Absorption (Abs) and normalized fluorescence emission (Em, λ_{ex} = 380 nm in all cases) spectra of diazoniapentaphenes **7b** (solid line) and **42a** (dashed line) in water. (B) Absorption and normalized fluorescence emission spectra of diazoniapentaphene **7c** (solid line) and its 14-methyl derivative **42b** (dashed line) in water.

The diazoniapolycilcic salts, except for the semi-betaine **42c**, are strongly fluorescent in most solvents, such as water, alcohols and acetonitrile. The fluorescence emission spectra of methyl-substituted diazoniapentaphenes **42a–b** resemble the ones of the parent compounds, while the introduction of two methyl groups in **42a** leads to a bathochromic shift of the emission maximum of about 25 nm and to the reduction of the vibrational structure as compared to the unsubstituted analogue **7b**. At the same time, the introduction of one methyl group in **42b** results in a batochromic shift by only 7 nm, and the shape of the emission spectrum is almost identical with that of the parent compound **7c**.

The largest fluorescence quantum yields for all diazoniapentaphenes are observed in aqueous solutions (*cf.* representative data in Table 3.6). The fluorescence quantum yields of methyl-substituted compounds **42a–b** in aqueous solutions are about 20% smaller than the values for the unsubstituted analogues. In contrast, the fluorescence is strongly quenched in DMSO (Φ_F = 0.01–0.03 for unsubstituted and methyl-substituted diazoniapentaphenes), and the emission spectra are structureless. A similar decrease of fluorescence in DMSO has been observed for the related 3a,9a-diazaperylenium dication[137] as well as for the unsubstituted benzo[*b*]quinolizinium cation,[105] and has been correlated with the high electronic donor strength of this solvent in combination with the low reduction potential of the chromophore.[105]

Notably, compound **44**, in which the fused aromatic system is disrupted by two methylene groups, also shows reasonably strong UV absorption and fluorescence properties. Thus, its

broad, structureless long-wavelength absorption band is located at 386 nm and has a large absorption coefficient (log ε = 4.29, Figure 3.7). The fluorescence emission spectrum is also very broad with a maximum centered at around 480–500 nm. As in the case of the diazoniapentaphenes **7a–c** and **42a–b**, the fluorescence intensity is especially pronounced in the aqueous solution (Φ_F = 0.21), whereas in DMSO it is essentially quenched (Φ_F < 0.01). Thus, with respect to the electronic transitions, **44** may be regarded as a substituted diarylbutadiene with a rigid bridge in the chromophore, whereas the conformational restrictions exclude the photoisomerisation, consequently enhancing the quantum yield of fluorescence.

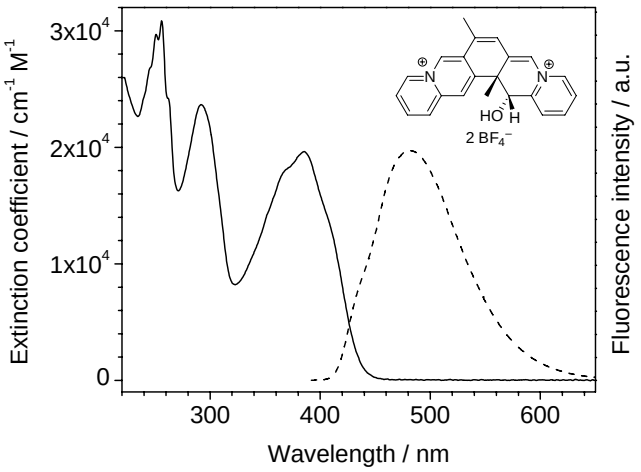

Figure 3.7. Absorption (solid line) and normalized fluorescence emission (dashed line) spectra of **44 (2BF_4^-)** in water. Excitation wavelength λ_{ex} = 380 nm.

The electronic absorption spectra of the semi-betaine **42c** consist of a broad band of moderate intensity (log $\varepsilon \approx$ 4.0) at 460–490 nm and a stronger (log $\varepsilon \approx$ 4.4–4.6), somewhat structured band in the UV region of the spectrum in most solvents. In contrast to the diazoniapentaphenes **7a–c** and **42a–b**, which exhibit only negligible solvatochromism (*vide supra*), the positions and intensities of the absorption bands of **42c** are significantly solvent-dependent (Figure 3.8, A; Table 3.6). Moreover, the energy of the long-wavelength transition shows an almost linear correlation with the Gutmann's acceptor number (AN)[94] of the solvent (r = 0.993; Figure 3.8, B) as well as with the Swain's "acity" parameter (r = 0.996, data not shown), illustrating the ability of the solvent to interact with the negative charge that is localized at the oxygen atom. Thus, the long-wavelength band undergoes a hypsochromic shift by 30 nm when changing form acetone (AN = 12.5) to water (AN = 54.8). Unfortunately, the limited solubility of **42c** in solvents with lower AN values excluded the

investigations therein. As an extreme case, in TFA (AN = 105.3) the spectrum loses its fine structure completely and attains a typical aromatic character, similar to the one of unsubstituted diazoniapentaphenes, with a structured β-band (λ_{max} = 266 nm) and α-band (430 nm; $S_0 \rightarrow S_1$ transition). The latter overlaps to a certain extent with the strongest *p*-band (λ_{max} = 357 nm). This spectrum is attributed to the fully protonated, dicationic form (**42c-H$^+$**).

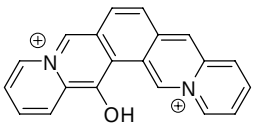

42c-H$^+$

This drastic change is not observed either in acetic acid or in water. Addition of *e.g.* perchloric acid to aqueous solutions of **42c** does not result in such a severe effect as neat TFA, either. Moreover, although acetic acid is more acidic than water, the spectrum is more blue-shifted in water as compared to acetic acid, indicating that the acidity is less important for the stabilization of the semi-betaine **42c** than the overall electrophilic properties characterized by the value of AN.

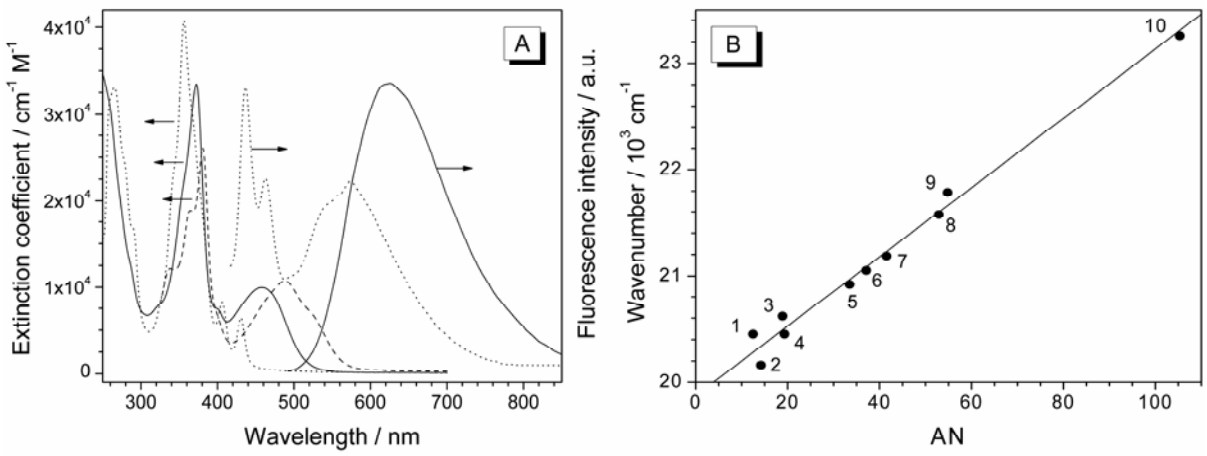

Figure 3.8. (A) Absorption (right-to-left arrows) and normalized fluorescence emission (left-to-right arrows) spectra of **42c** in water (solid lines), acetone (dashed line) and trifluoroacetic acid (dotted lines). Experimental conditions see footnotes to Table 3.6. (B) Correlation of the position of the lowest-energy absorption band of **42c** with the acceptor number of the solvent: (1) acetone, (2) pyridine, (3) acetonitrile, (4) DMSO, (5) 2-propanol, (6) ethanol, (7) methanol, (8) acetic acid, (9) water, (10) TFA.

The semi-betaine **42c** exhibits weak orange-red fluorescence in most solvents, with a broad emission band centered at 620–660 nm (Table 3.6) and quantum yields in the range of 0.03 to

0.07. Similar to the absorption maxima, the emission maxima are solvent-dependent, but do not show any evident correlation with the empiric solvent parameters (solvent polarity function E_T^N, donor- or acceptor numbers). In TFA, a dual fluorescence is observed, with a structured band located at 420–480 nm (blue emission) and a broader band at 580–600 nm (red emission). This blue emission, similar to that of diazoniapentaphenes, is attributed to the fully protonated, dicationic form **42c**-$\mathbf{H}^+$. The red emission, which is observed in all solvents investigated, is attributed to the electronic charge transfer from the phenolate oxygen to the diazoniapentaphene core. The charge-transfer character of this emission is supported by the broadness of the fluorescence band ($\Delta\lambda_{½} \approx 140$ nm) and large Stokes shift values (140–180 nm).

Table 3.6. Solvatochromic properties of compound **42c**.

Solvent [a]	λ_{abs} / nm [b] [log (ε / cm^{-1} M^{-1})]	λ_{em} / nm [c]	Φ_F [d] × 10^2
Acetone	338 (sh [f]); 365 (4.27); 381 (4.42); 489 (4.03)	650	3.9
Pyridine	343 (4.00); 369 (4.11); 387 (4.25); 496 (3.97)	634	7.1
Acetonitrile	335 (4.13); 363 (sh); 380 (4.41); 485 (4.03)	641	2.8
DMSO	337 (sh); 370 (4.23); 385 (4.31); 406 (sh); 489 (3.90)	667	3.3
2-Propanol	380 (4.31); 403 (sh); 478 (3.87)	635	4.4
Ethanol	334 (sh); 379 (4.37); 402 (sh); 475 (3.94)	642	5.4
Methanol	378 (4.35); 400 (sh); 472 (3.90)	644	6.5
Acetic acid	376 (4.51); 464 (3.95)	629	3.8
Water	373 (4.52); 400 (sh); 459 (4.00)	626	3.0
TFA [f]	266 (4.52); 357 (4.61); 406 (3.92); 430 (3.81)	437; 463; 573	[g]

[a] In order of their increasing AN values;[94] [b] absorption maximum, at c(**42c**) = 50 µM; [c] fluorescence emission maximum, at c(**42c**) = 10 µM; excitation wavelength λ_{ex} = 480 nm; [d] fluorescence quantum yield relative to Cresyl Violet, estimated error ± 10%; [e] shoulder; [f] excitation wavelength λ_{ex} = 405 nm; [g] not determined.

Electronic absorption and fluorescence emission spectra of hexacyclic diazoniaarenes **38a–c** and **51** are presented in Figure 3.9 and Figure 3.10. Interestingly, the absorption spectra of the isomeric hexacyclic salts **38c** and **51** (Figure 3.10, A) are to much extent similar and consist of several strong *p*- and *β*-absorption bands in the UV region ($\varepsilon_{max} = 4.68 \times 10^4$ cm^{-1} M^{-1} for **38c** and 8.24×10^4 cm^{-1} M^{-1} for **51**) and much weaker *α*-bands in the visible region (400–500 nm). The spectra of diazoniahexaphene **51** are red-shifted by 4–8 nm compared to isomer **38c** and consist of sharper bands, presumably due to the deviation from planarity in the latter

case.[135] Hence, the electronic absorption spectra are not appropriate to distinguish these two isomers, as it has been done in the former work.[127]

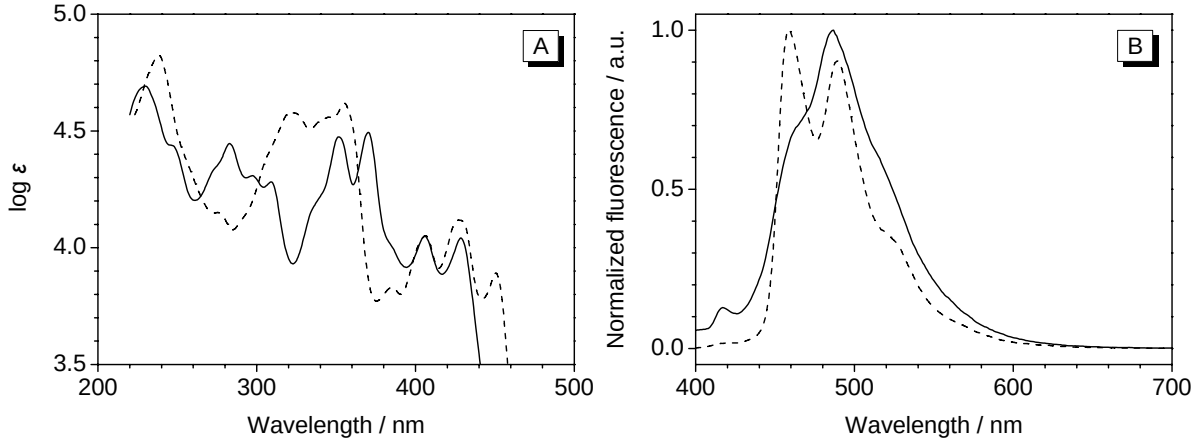

Figure 3.9. Absorption (A) and normalized fluorescence emission (B, λ_{ex} = 380 nm) spectra of diazoniaanthra[1,2-*a*]anthracenes **38a** (solid lines) and **38b** (dashed lines) in water. The absorption spectra are shown on a logarithmic scale to facilitate the comparison of the weak α-bands.

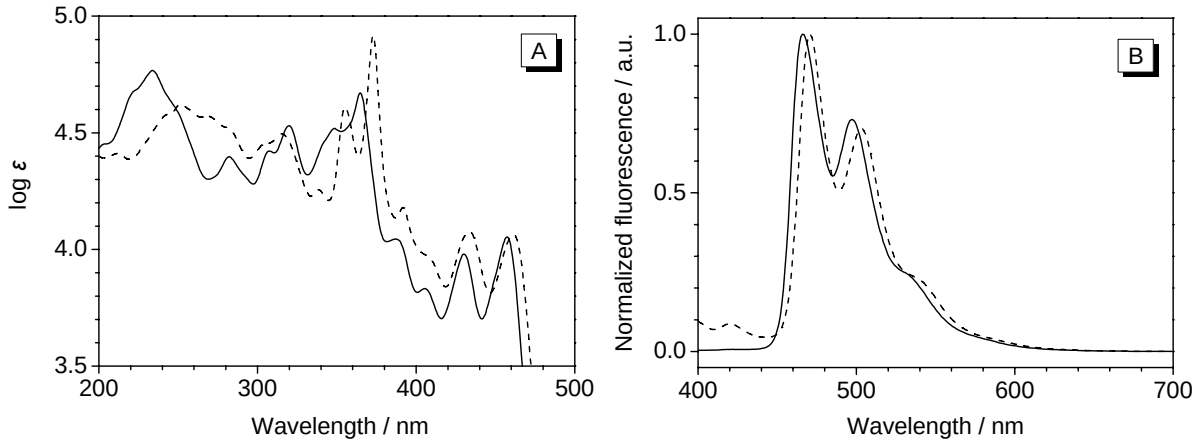

Figure 3.10. Absorption (A) and normalized fluorescence emission (B, λ_{ex} = 368 nm) spectra of diazoniaanthra[1,2-*a*]anthracenes **38c** (solid lines) and **51** (dashed lines) in water. The absorption spectra are shown on a logarithmic scale to facilitate the comparison of the weak α-bands.

Even more pronounced similarity was observed in the fluorescence emission spectra of the isomers **38c** and **51** (Figure 3.10, B). The emission spectra consist of well-resolved bands, and the emission maxima of diazoniahexaphene **51** are red-shifted by 5–6 nm compared to the isomer **38c**. The fluorescence quantum yields in aqueous solutions are 0.38 and 0.42 for **38c** and **51**, respectively, and thus lay in the characteristic range of unsubstituted diazoniapolycycles (*cf.* Table 3.4).

It is noteworthy that the parent hydrocarbon of **38a–c**, namely anthra[1,2-*a*]anthracene, is not persistent under aerobic conditions due to rapid oxidation and could not be purified, so far.[138] In contrast, all diazoniapolycyclic salts, except for the semi-betaine **38c**, are persistent in the solid state and in neutral or acidic aqueous solutions. In fact, no photoreaction was observed upon prolonged irradiation of crystalline **42a** and **38c** with UV light (λ_L = 350 nm), which is surprising considering the favorable intercationic distances in the solid state (Section 3.2.2), since the distance between the aromatic ring planes in photoreactive acridizinium salts usually constitutes 3.8–3.9 Å.[117a] In contrast, in air-saturated aqueous solution diazoniahexacycles **38c** and **51** undergo photodegradation, whereas salt **38c** shows much higher photopersistence than the isomer **51** (Figure 3.11, A). Thus, estimated half-life times at these conditions (*cf.* Experimental Section) are 250 and 37 min for **3** and **7**, respectively. The photodegradation is drastically accelerated in oxygen-free solutions (Figure 3.11, B); moreover, in the latter case, the order of the photopersistence is inversed, *i.e.* diazoniahexaphene **51** is slightly more stable than the isomer **38c**.

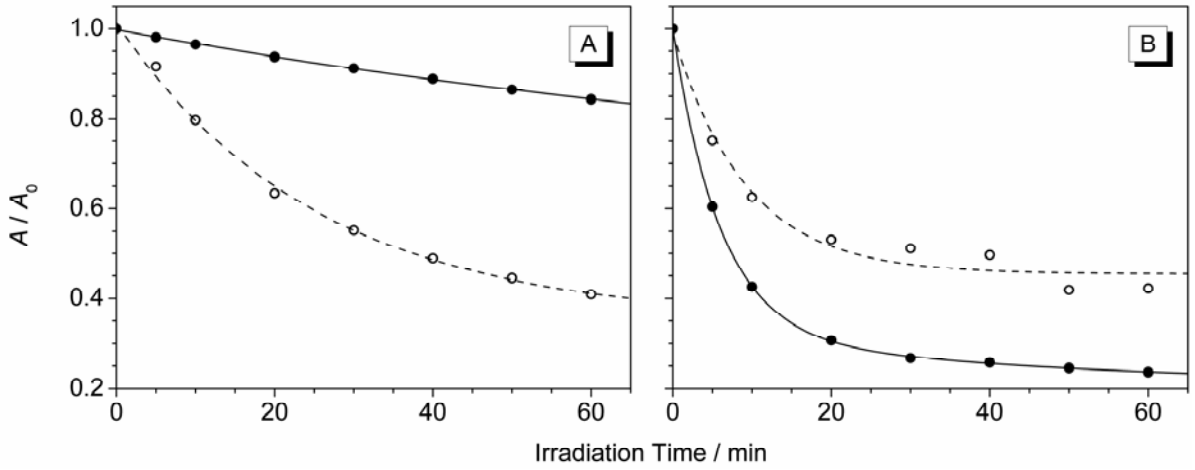

Figure 3.11. Relative decrease of absorption during photodegradation of **38c** (filled circles and solid lines) and **51** (open circles and dashed lines) in (A) air-saturated and (B) deoxygenated aqueous solutions (c = 100 μM); λ_L = 350 nm, irradiance I_L = 7.2 mW cm^{-2}.

3.2.4 Binding of Diazoniapolycyclic Salts to Double-Stranded DNA

3.2.4.1 DNA Thermal Denaturation Studies

The DNA-binding properties of diazoniapolycyclic salts were studied by thermal denaturation experiments with two types of ds DNA, namely calf thymus DNA (ct DNA, 42% GC) and an alternating polynucleotide [poly(dAdT)]$_2$. The stabilizing effect of the ligands was

investigated at incomplete saturation conditions, *i.e.* at ligand-to-DNA ratios $r = 0.2$ and $r = 0.5$, and at low ionic strength of the buffer (BPE buffer, $[Na^+] = 16$ mM), such that the melting transitions could be observed at moderate temperatures, and to allow direct comparison with other known DNA ligands.[139] Proflavine **1**, a known DNA intercalator,[3] was used as a reference. The measured ΔT_m values for the diazoniapolycyclic salts are presented in Table 3.7; the corresponding melting curves are shown in Figure 5.1 and Figure 5.2 (Experimental Part, Section 5.5.3). For two representative ligands, diazoniapentaphene **7b** and diazoniaanthra[1,2-*a*]anthracene **38b**, the influence of the ligand-to-DNA ratios on the DNA melting profiles was studied in a broader range (0.1–2.0) of *r* values (Figure 3.12).

Table 3.7. DNA-binding properties of proflavine and of diazoniapolycyclic salts from thermal denaturation studies.

Ligand	Induced ΔT_m / °C, [a] at ligand-to-DNA ratios *r*				Base selectivity [b]
	ct DNA		$[poly(dAdT)]_2$		
	$r = 0.2$	$r = 0.5$	$r = 0.2$	$r = 0.5$	
Proflavine (**1**)	10.1 [c]	15.6	18.4	24.0	AT
7a	12.1	19.0	11.3	16.2	GC
7b	11.8	17.5	8.5	15.4	GC
7c	12.1	17.6	8.4	15.2	GC
42a	13.0	20.5	10.0	17.0	GC
42b	12.6	18.1	8.3	14.9	GC
38a	15.4	30.2	13.3 [d]	23.3	GC
38b	16.7	30.4	19.6 [d]	32.8	AT
38c	18.7	28.6	18.8 [d]	28.7	none
51	15.1	21.7	25.4	35.0	AT
44 [e]	2.0	5.8	3.4	7.4	AT

[a] Experimental conditions: $c_{DNA} = 40$ μM (bp) in BPE buffer, $[Na^+] = 16$ mM; estimated error ± 0.2 °C; [b] based on comparison of ΔT_m(ct DNA) and $\Delta T_m[poly(dAdT)_2]$ values; [c] literature value: 11.5 °C;[139] [d] biphasic curve, T_m determined from the mid-point of the transition; [e] thermal decomposition of the ligand was observed at temperatures over 70 °C but did not influence the T_m determinations.

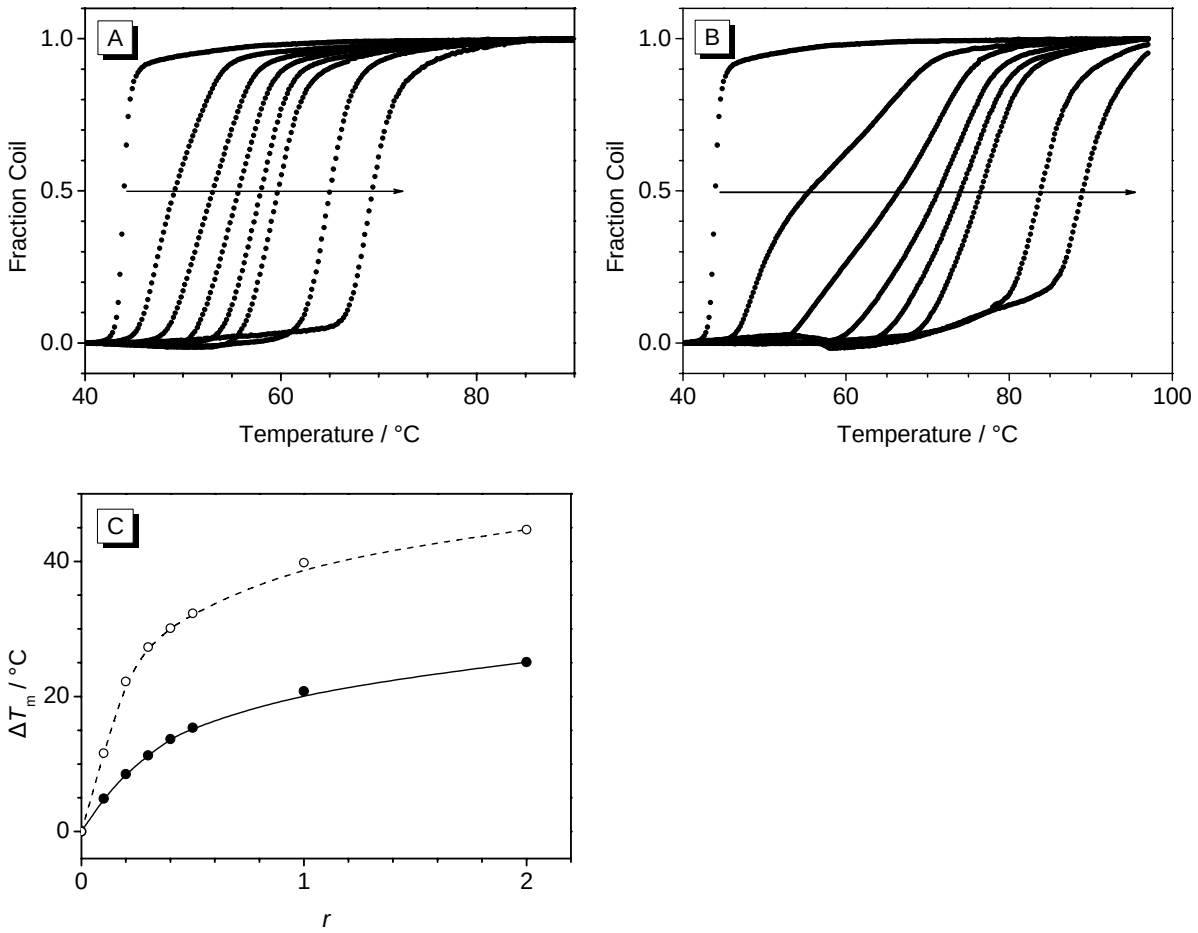

Figure 3.12. (A–B) Thermal denaturation profiles of [poly(dAdT)]$_2$ duplex (c_{DNA} = 40 μM bp in BPE buffer) in the presence of **7b** (A) and **38b** (B) at ligand-to-DNA ratios (*r*) of 0, 0.1, 0.2, 0.3, 0.4, 0.5, 1.0 and 2.0. Arrows indicate the shift of the melting curves with increasing *r* values. (C) Plot of induced T_m shifts *vs.* ligand-to-DNA ratio.

The results show that at low ionic strength all diazoniapolycyclic salts, except for **44**, stabilize the double-helical form of DNA with respect to its thermal denaturation to a very large extent. That is, the diazoniapentaphenes **7a**–**c** and **42a–b** increase the temperatures of helix–coil transition of ct DNA by ΔT_m = 18–20 °C at r = 0.5. This stabilization is comparable to the one induced by proflavine (ΔT_m = 15.6 °C). However, especially large effects are observed for the diazoniaanthra[1,2-*a*]anthracenes **38a**–**c** ($\Delta T_m \approx$ 30 °C at r = 0.5). Comparison of ΔT_m values observed with ct DNA (42% GC) with those obtained with [poly(dAdT)]$_2$ allows to access the sequence selectivity of the ligands. Thus, most diazoniapolycyclic salts exhibit a slightly larger stabilization of ct DNA compared to [poly(dAdT)]$_2$ duplex, presumably due to the preferential binding to GC-rich DNA regions. However, compounds **38b** and **51** display preferential binding to [poly(dAdT)]$_2$ with high affinity. In particular, compound **51** shows an

exceptionally high stabilization of [poly(dAdT)]$_2$ (ΔT_m = 35 °C at r = 0.5), while its binding to ct DNA is less pronounced.

In contrast, compound **44** shows much smaller effects on the melting transition of DNA. The induced T_m shifts (ΔT_m = 5–7 °C at r = 0.5) are in a range which is characteristic of weak to moderate DNA binders, *e.g.* uncharged acridines;[139] and a slight preference for AT-rich DNA sequences is observed. Moreover, a drift in the melting profiles of this compound was observed, which may be attributed to the partial thermal decomposition. For these reasons, this compound was excluded from the further DNA-binding studies.

3.2.4.2 Linear Dichroism Spectroscopy

The flow LD spectra of the representative compound **7c** in the presence of st DNA were measured in aqueous buffer solutions at various ligand-to-DNA ratios (r = 0.04, 0.08 and 0.2) (Figure 3.13, A). The LD signal is negative at all mixing ratios both in the UV region, where the DNA and ligands absorb, and at wavelengths where only ligands absorb (300–450 nm). This observation indicates that within the ligand-DNA complex the transition dipole moment and thus the π-system of the diazoniapentaphene **7c** are coplanar to the ones of the nucleic

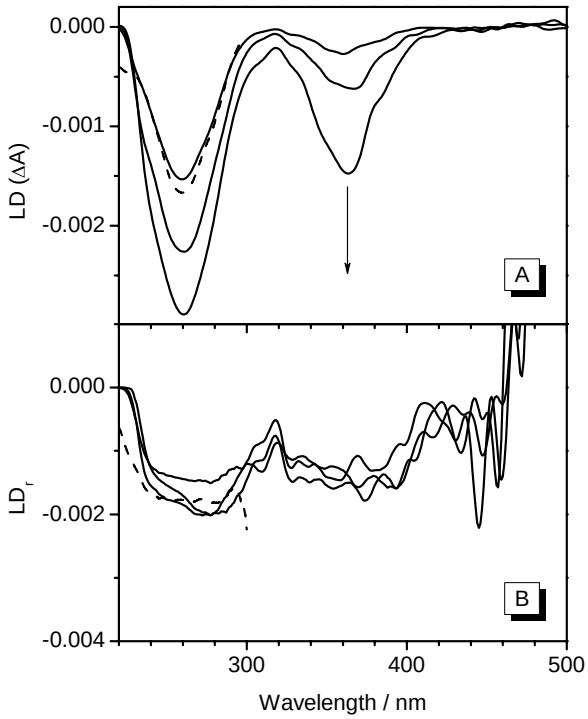

Figure 3.13. Linear dichroism (A) and reduced LD (B) of diazoniapentaphene **7c** in the presence of st DNA. Arrows indicate the changes in the spectra with increasing ligand-to-DNA ratios (r = 0.04, 0.08 and 0.2). Dashed lines represent spectra of the DNA in the absence of ligand.

bases. The intensity of LD signal of the DNA bases at $\lambda_{max} \approx 260$ nm increases significantly upon addiction of the ligand, revealing stiffening of the double helix and a resulting better orientation of the DNA molecules along the flow lines. Moreover, a nearly constant value of the reduced LD signal (LD_r) over the range of 310 nm to 400 nm was observed (Figure 3.13, B), which gives evidence for an almost exclusive intercalation into the DNA. In the region of $\lambda > 400$ nm, a significant fluctuation of the LD_r signal may be observed, appearing because of the low absorbance of the ligand at these wavelengths.

3.2.5 Binding of Diazoniapolycyclic Salts to Triple-Helical DNA

3.2.5.1 DNA Thermal Denaturation Studies

Thermal denaturation studies were also used to investigate the binding of diazoniapolycycles to triple-helical DNA. These initial experiments, aimed to establish the triplex-binding properties of diazoniapolycycles, were performed with the poly(dA)–[poly(dT)]$_2$ triplex, since it is readily prepared from the polynucleotides, poly(dA)–poly(dT) and poly(dT), and is stable at neutral pH values. Such as in reported protocols,[81] thermal denaturation studies with triplex DNA were performed at the conditions of relatively high ionic strength ([Na^+] = 200 mM), because triplex DNA is unstable at low ionic strength. Moreover, interference of otherwise used buffer components, such as polyvalent metal cations (Mg^{2+}) or polyamines that are capable of triplex stabilization, should be avoided.

At the employed conditions, the melting profiles of the poly(dA)–[poly(dT)]$_2$ triplex are biphasic. At $T_m^{3\rightarrow2}$ = 42.8 °C the triplex dissociates into the poly(dA)–poly(dT) duplex and a single-strand poly(dT) (Hoogsten transition), whereas at $T_m^{2\rightarrow1}$ = 74.8 °C the remaining double helix dissociates (Watson–Crick transition). The diazoniapolycyclic salts have a pronounced influence on the melting behavior of the triplex DNA (Figure 3.14, Figure 3.15). Thus, at low ligand-to-DNA ratios ($r \leq 0.5$), the diazoniapentaphenes **7** and **42** induce large shifts of the triplex-to-duplex transition to higher temperatures, $\Delta T_m^{3\rightarrow2}$ = 14–17 °C at r = 0.5 (Table 3.8). At the same time, the temperature of the duplex denaturation is only slightly affected ($\Delta T_m^{2\rightarrow1}$ = 0.7–1.3 °C). These observations show that, at the conditions employed, the salts **7** and **42** are capable of selective binding and stabilization of the triple-helical DNA.

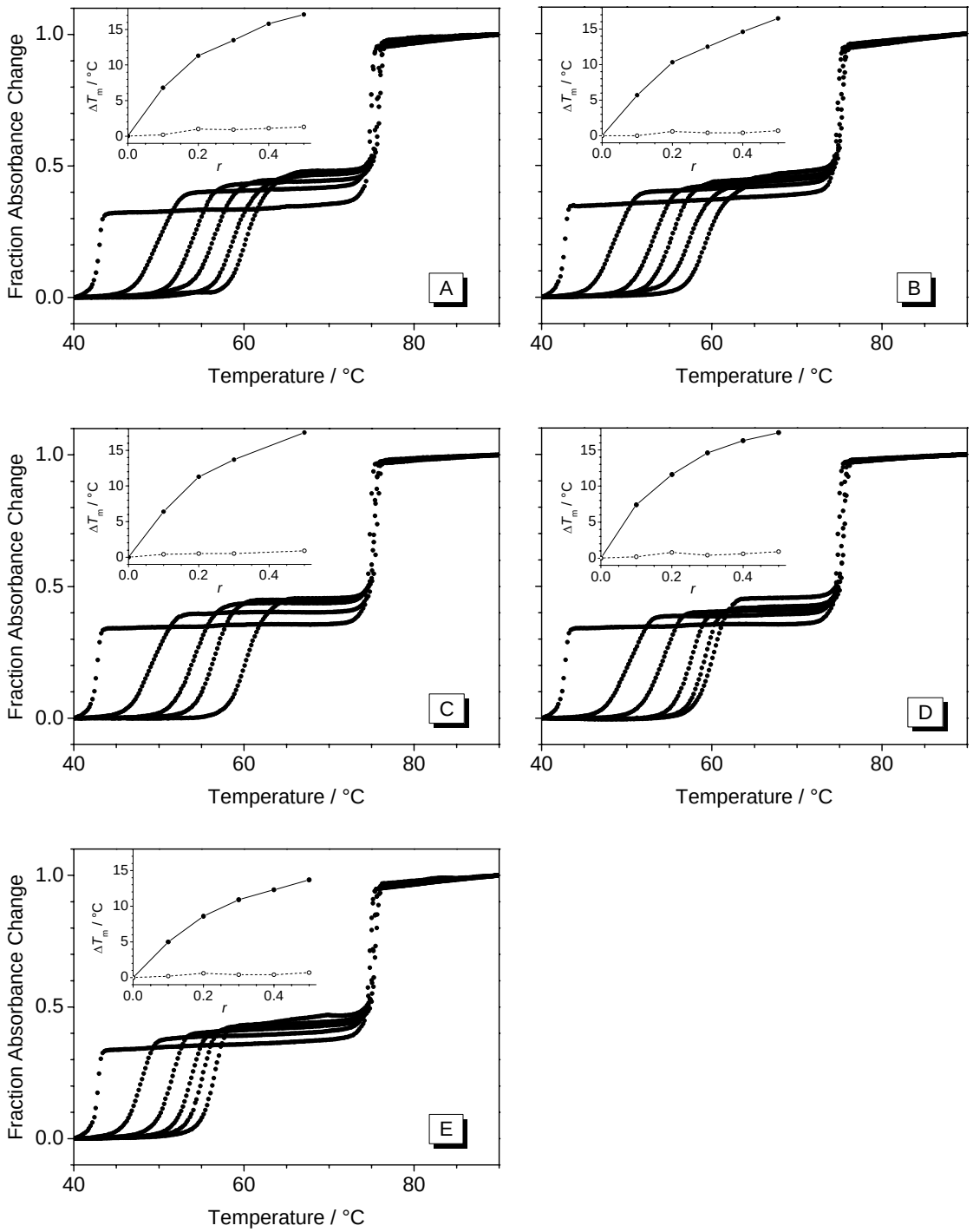

Figure 3.14. Melting profiles of poly(dA)–[poly(dT)]$_2$ in the presence of diazoniapentaphenes **7a** (A), **7b** (B), **7c** (C), **42a** (D) and **42b** (E) at ligand-to-DNA ratios (*r*) of 0, 0.1, 0.2, 0.3, 0.4 (not in C) and 0.5; c_{DNA} = 40 μM (bt) in BPES buffer. Insets show the dependence of T_m shifts ($\Delta T_m^{3\rightarrow2}$: filled circles and solid lines, $\Delta T_m^{2\rightarrow1}$: open circles and dashed lines) on the ligand-to-DNA ratio.

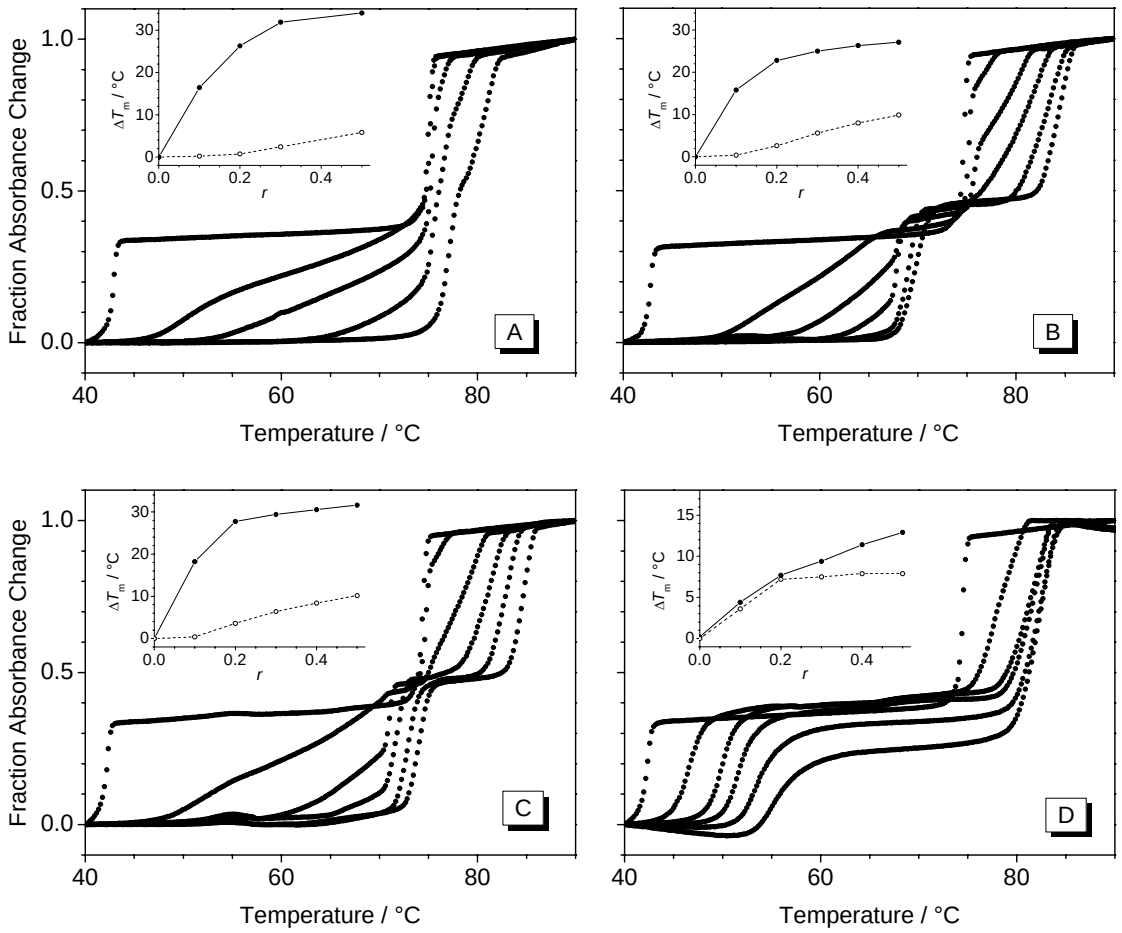

Figure 3.15. Melting profiles of poly(dA)–[poly(dT)]$_2$ in the presence of diazoniaanthra[1,2-*a*]anthracenes **38a** (A), **38b** (B), **38c** (C) and **51** (D) at ligand-to-DNA ratios (*r*) of 0, 0.1, 0.2, 0.3, 0.4 and 0.5; c_{DNA} = 40 μM (bt) in BPES buffer. Insets show the dependence of T_m shifts ($\Delta T_m^{3\rightarrow2}$: filled circles and solid lines, $\Delta T_m^{2\rightarrow1}$: open circles and dashed lines) on the ligand-to-DNA ratio.

Compared to derivatives **7** and **42**, the diazoniaanthra[1,2-*a*]anthracenes **38** have an even more pronounced influence on the thermal stability of the triple-helical DNA. Thus, at ligand-to-DNA ratios of r = 0.5, these compounds increase the temperature of the Hoogsten transition by $\Delta T_m^{3\rightarrow2} \approx 30$ °C; in the case of **38a**, the two melting transitions merge almost completely at $r \geq 0.3$. However, these ligands also induce more severe shifts of the temperature of the duplex-to-coil transitions. This effect is most pronounced in the case of **38b** and **38c** ($\Delta T_m^{2\rightarrow1} \approx 9$–10 °C at r = 0.5), indicating that these compounds have lower triplex-*vs*.-duplex selectivity. The isomer **38a** shows excellent selectivity at low *r* values; that is, at $r = 0.2$ the induced $T_m^{3\rightarrow2}$ shift is 26 °C and thus far larger that those observed with diazoniapentaphenes **7** and **42**, whereas $\Delta T_m^{2\rightarrow1}$ constitutes only 0.7 °C.

Table 3.8. Triplex-DNA stabilizing properties of diazoniapolycycles from thermal denaturation studies [a]

Ligand	r = 0.2		r = 0.5	
	$\Delta T_m^{3\rightarrow2}$	$\Delta T_m^{2\rightarrow1}$	$\Delta T_m^{3\rightarrow2}$	$\Delta T_m^{2\rightarrow1}$
7a	11.3	1.0	17.1	1.3
7b	10.3	0.6	16.5	0.7
7c	11.3	0.5	17.5	0.9
42a	11.6	0.8	17.4	0.9
42b	8.6	0.6	13.7	0.7
38a	26.3	0.7	34.1	5.8
38b	22.8	2.6	27.1	9.9
38c	27.7	3.6	31.6	10.2
51	7.7	7.2	12.9	7.9

[a] Experimental conditions: c_{DNA} = 40 μM bt in BPES buffer, [Na^+] = 200 mM; estimated error in T_m determinations ± 0.2 °C.

Notably, diazoniahexaphene **51** has the lowest triplex-*vs*.-duplex selectivity in the series of diazoniapolycyclic salts. Thus, it stabilizes the triplex DNA to a lesser extent than diazoniapentaphenes and diazoniaanthra[1,2-*a*]anthracenes ($\Delta T_m^{3\rightarrow2}$ = 12.9 °C *vs*. 16–17 °C for compounds **7a–c** at r = 0.5). At the same time, the temperature of the duplex denaturation is increased significantly ($\Delta T_m^{2\rightarrow1}$ = 7.9 °C at r = 0.5), indicating high preference for the duplex form of DNA in this case.

The binding preference of the ligands for triplex DNA as compared to ds DNA was additionally confirmed by monitoring the ligand absorbance during the thermal denaturation of the poly(dA)–[poly(dT)]$_2$ at the wavelength λ = 370 nm where only ligands absorb (Figure 3.16). In the case of **7c**, a hyperchromic effect upon interaction with the DNA is observed at 370 nm, whereas in case of **38a**, a hypochromic effect at this wavelength is detected. As can be seen from the Figure 3.16, the major change of the ligand absorption upon the release of the ligand is centered at the triplex-to-duplex transition. The drift observed in the absorption profiles of the ligands is presumably due to the ligand redistribution within the melting event.

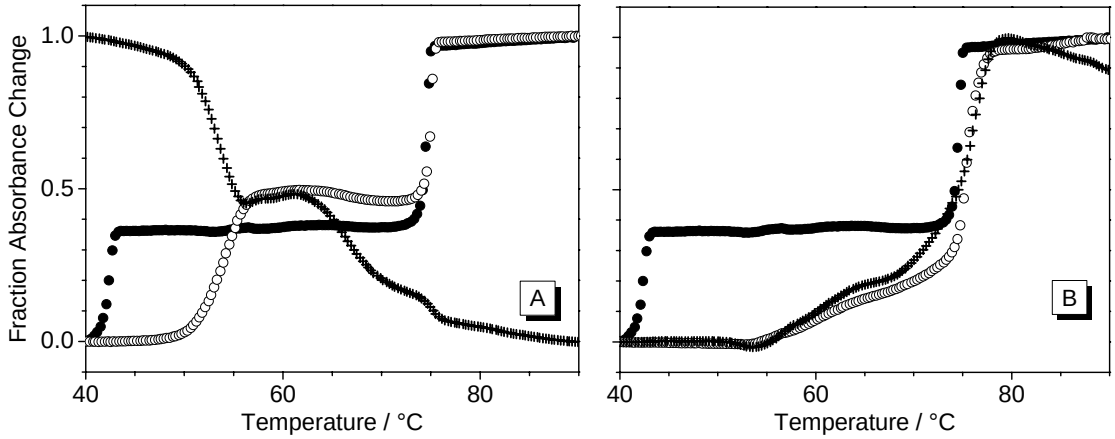

Figure 3.16. Melting profiles of poly(dA)–[poly(dT)]$_2$ in the absence of ligands (filled circles) and in the presence of **7c** (A) and **38a** (B) at a ligand-to-DNA ratio $r = 0.2$, monitored at 260 nm (open circles) and at 370 nm (crosses).

3.2.5.2 Competition Dialysis Assay

To confirm the structural preferences and binding affinities of the diazoniapolycyclic salts, two representative ligands, **7c** and **38a**, were further investigated by the competition dialysis assay. As compared to the original method,[81] a reduced set of nucleic acid structures was used in this work (Figure 3.17). Six nucleic acid samples (at concentration of 75 μM monomeric unit) were dialysed against a solution of the ligand (1 μM in BPES buffer) for 48 h. After this time, ligand–DNA complexes were dissociated by the addition of surfactant (1% SDS), and the concentrations of the ligand accommodated in each dialysis chamber were determined spectrophotometrically.

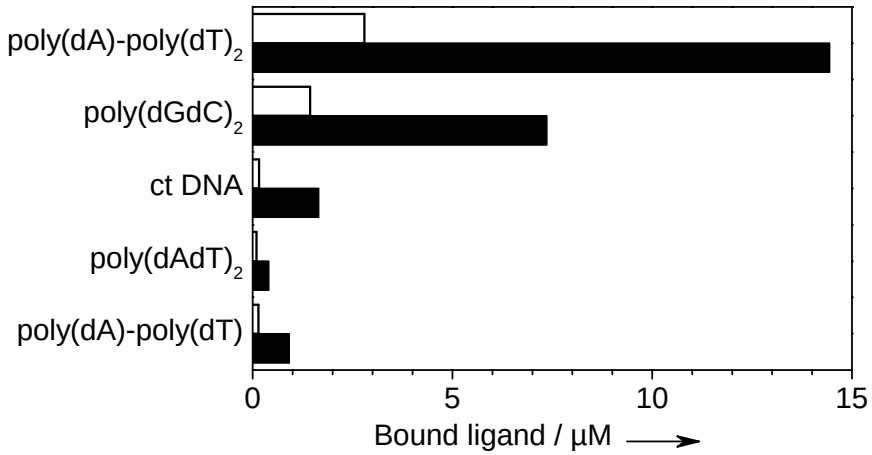

Figure 3.17. Results of the competition dialysis assay for compounds **7c** (empty bars) and **38a** (filled bars). See text for details.

The results confirm the strong preference of both ligands for triple-helical DNA binding (17-fold and 9-fold greater than for natural duplex ct DNA, for **7c** and **38a,** Figure 3). At the same time, overall DNA affinities of the hexacyclic compound **38a** are about 5-fold larger than those of diazoniapentaphene **7c**. In agreement with the thermal denaturation data (Table 3.7), both ligands exhibit a significant preference for GC-rich double-stranded DNAs, $[poly(dAdT)]_2$ < ct DNA (42% GC) < $[poly(dGdC)]_2$.

3.3 Discussion

3.3.1 Rearrangement-Mediated Synthesis of Diazoniapentaphenes

The formation of the diazoniapentaphene derivatives **42a–b** may be rationalized by a cyclo-dehydration which involves an *ipso*-addition of the protonated aldehyde group followed by a methyl migration. Thus, after aldehyde deprotection and the first cyclodehydration sequence, the benzo[*b*]quinolizinium derivative **52a** is the proposed intermediate (Scheme 3.7).

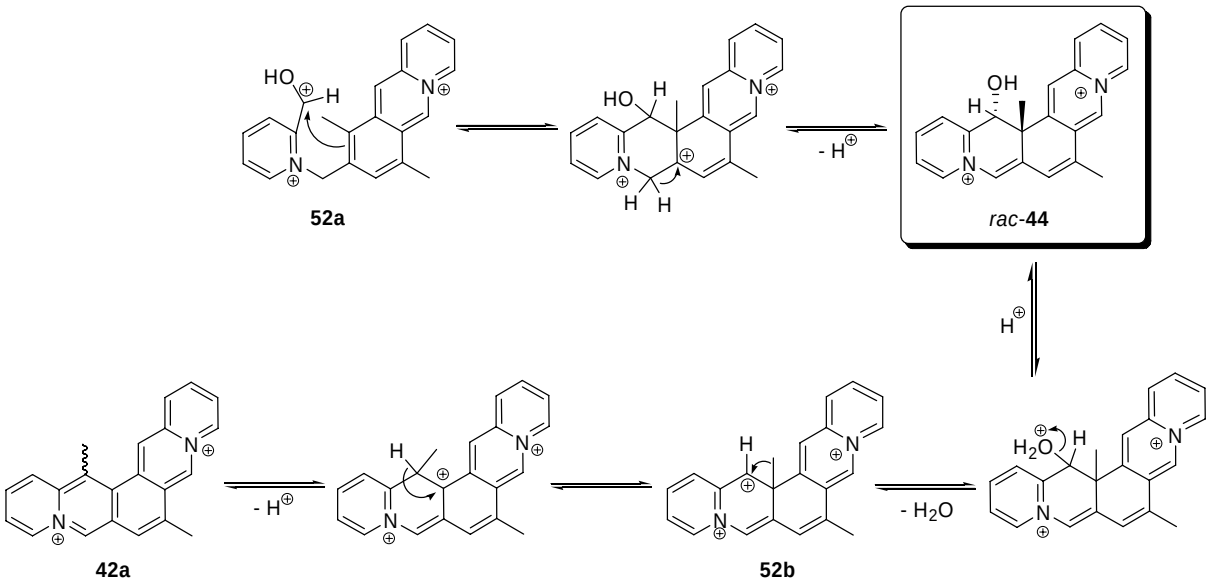

Scheme 3.7. Mechanism of formation of **44** and **42a**.

Apparently, the methyl groups do not protect the positions 7 and 10 of benzo[*b*]quinolizinium **52a** from the electrophilic *ipso* addition, so that an angular annelation takes place along with subsequent deprotonation to give the intermediate **44**. Although there are only few examples for an *ipso* substitution of an *ortho*-alkyl group in the presence of a second hydrogen-substituted *ortho′* position,[140] this addition is in agreement with theoretical and experimental

studies which show that benzo[*b*]quinolizinium derivatives exhibit a significantly higher reactivity towards electrophiles at positions 7 and 10 as compared to positions 8 and 9.[134c] Thus, sulfonation and bromination of the benzo[*b*]quinolizinium cation are reported to occur at position 10,[141] whereas chlorination results in the 7,10-disubstituted product.[142] Under the employed acidic conditions, the hydroxy functionality is protonated and water acts as a leaving group to give the cation **52b**. Finally, a Wagner–Meerwein [1,2]-methyl migration followed by deprotonation leads to the fully aromatic diazoniapentaphene **42a**. Although alkyl migrations are observed extremely rarely upon aromatic *ipso* substitution,[143] the energetically favorable aromatization is probably the driving force for this methyl shift. The proposed mechanism in Scheme 3.7 is supported by the isolation of intermediate **44 ($2BF_4^-$)**, which was formed when the dibromide salt of **40a** was cyclized in refluxing aqueous HBr. Moreover, the final product **42a** is formed upon dehydration of **44** under more severe conditions (PPA, 150 °C).

In the case of the formation of **42b**, a similar mechanism is likely to take place (Scheme 3.8, path *a*); however, with a bromo substituent the aromatization takes place from intermediate **53**

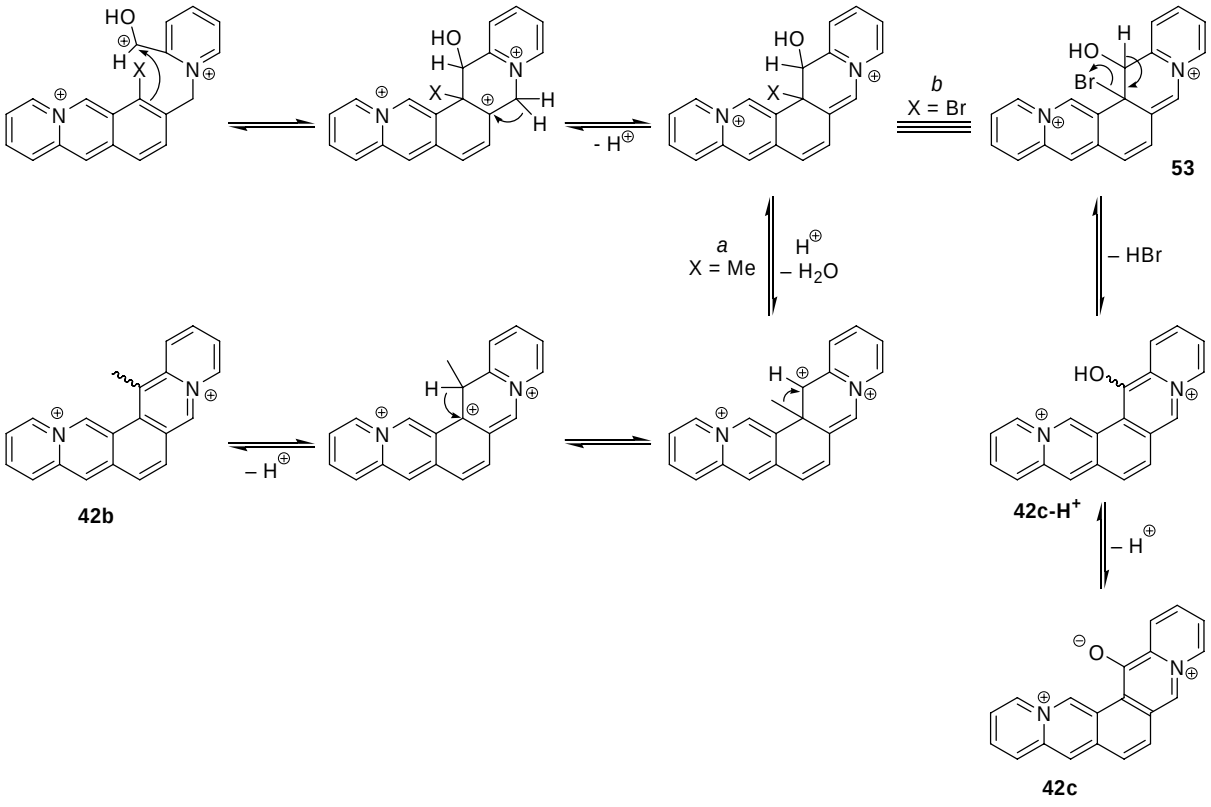

Scheme 3.8. Mechanism of formation of **42b** and **42c**.

by HBr elimination (Scheme 3.8, path *b*). It appears that the acidity of the hydroxy group bound to a doubly charged aromatic system is significantly increased, so that the semi-betaine **42c** is formed as the final product.

In the case of dehydration of **40d**, the strong electron-acceptor property of the trifluoromethyl group deactivates the benzene ring and suppresses the *ipso*- and *ortho*-substitution, so that electrophilic substitution to give the angular pentaphene derivative or the linear pentacene derivative does not take place.

3.3.2 DNA-Binding Properties of Diazoniapolycyclic Salts

3.3.2.1 Binding to Double-Stranded DNA

Diazoniapolycyclic salts, which were investigated in this study, are cationic polyaromatic compounds with a planar structure (**7a–c**, **51**) or having some degree of tilting (**42a–b**, **38a−c**). Considering the general features of DNA intercalators[1] and close structural resemblance of **7a**–**c** to known intercalators dibenzophenanthrolines,[46] it has been proposed that these compounds exhibit strong binding to various types of nucleic acids. It was shown previously[12] by means of spectrophotometric and fluorimetric titrations, linear and circular dichroism spectroscopy that compound **7a** binds to ds DNA with a high binding constant ($K = 5.7 \times 10^5$ M^{-1}) and exclusively by intercalative binding mode. In this work, the interaction of an extended series of diazoniapolycyclic salts with ds DNA was investigated by DNA thermal denaturation studies. As it has been pointed out in the Introduction, results of the thermal denaturation experiments do not correlate directly with the values of association constant of ligands to the DNA, since the ΔT_m values depend also on the binding site size and other thermodynamic parameters of binding. However, since the ligands investigated in this study have high structural resemblance, it may be expected that their binding-site sizes and the values of the binding enthalpy are similar. Therefore, the ΔT_m values were used as an unambiguous measure of binding affinities of the ligands to DNA.

At low ionic strength (16 mM Na^+) all fully aromatic diazoniapolycycles, *i.e.* **7a–c**, **42a–b**, **38a–c** and **51**, bind to ds DNA and stabilize it against thermal denaturation to a large extent, comparable to or extending the one observed with other efficient intercalators, such as proflavine.[139] Notably, the variation of the position of the quaternary nitrogen atoms in isomers **7a**–**c** does not influence the DNA binding affinity significantly, although compound

7a shows slightly stronger binding (*cf.* the ΔT_m values of 19.0, 17.5, 17.6 °C, respectively, for stabilization of ct DNA at $r = 0.5$). Moreover, all compounds from the diazoniapentaphene series show preferential binding to GC-rich DNA structures. These findings may be rationalized by the assumption that the net charges of the ligands are efficiently delocalized within the aromatic system, and specific interactions, *e.g.* hydrogen bonding, between azonia nitrogens and DNA do not take place. Since the introduction of one or two methyl groups into the diazoniapentaphene framework does not result in pronounced changes of induced shifts of DNA melting temperatures as compared to the unsubstituted compounds, it may be concluded that slight deviations from the planar structure in methyl-substituted diazoniapentaphenes do not have any significant effect on the DNA-binding properties.

Diazoniaanthra[1,2-*a*]anthracenes **38a–c** and diazoniahexaphene **51** show even higher degree of stabilization of ds DNA. This observation reflects that, as the net charges of the ligand are identical, the larger aromatic surface area results in an enhanced affinity to ds DNA. At the same time, within the diazoniaanthra[1,2-*a*]anthracenes, a larger variation of affinities and base selectivities is observed than in the diazoniapentaphene series. Thus, compound **38a** shows higher stabilization of GC-containing DNA, while the isomer **38b** stabilizes $[poly(dAdT)]_2$ to a larger extent; in the case of compound **38c**, no base selectivity is observed. The results of the competition dialysis also strongly confirm preferential binding of **7c** and **38a** to GC-rich ds DNA.

The linear dichroism data confirm the intercalative binding mode of diazoniapentaphene **7c** to ds DNA, as it has been shown previously for compound **7a**.[12] It may be expected that other members of the diazoniapentaphene series also bind to ds DNA by the intercalation. However, the outstanding affinity of the diazoniahexaphene **51** for $[poly(dAdT)]_2$, as seen from the thermal denaturation data, allows to expect at least partial contribution from the groove-binding mode, as the minor groove binders bind preferentially to AT-rich DNA sequences.[6,144] Indeed, the elongated, curved shape of the diazoniahexaphene **51** might facilitate its placement in the minor groove of the DNA, although the contribution of the hydrogen bonding with the phosphate backbone could not take place. Unfortunately, the lack of LD data for this compound does not allow to prove this assumption.

The melting curves of DNA in the presence of diazoniapolycyles (Figure 3.12) are biphasic at low ligand-to-DNA ratios ($0 < r \leq 0.2$). This behavior is especially pronounced for the thermal denaturation of DNA in the presence of hexacyclic ligands **38a–c** (*cf.* Figure 5.2). It has been shown that such a shape of the melting curves may be due to ligand redistribution

from the melted loops to the double-stranded regions of DNA in the course of denaturation, and—provided other binding parameters (ligand concentration, binding site size) being similar—becomes especially pronounced for DNA binders with large binding constants.[77] Notably, the saturation of the helix lattice takes place only at relatively high r values ($r \geq 2$), as reflected by the influence of the ligand-to-DNA ratio upon the induced ΔT_m shifts (Figure 3.12, C), while in the other works much smaller ratios, *e.g.* $r = 0.5$, are often referred to as "saturating".[139]

Compound **44** represents a dicationic polycycle where a fully aromatic character is distorted by two sp^3-hybridized carbon atoms. Although the net charge of the chromophore and its geometrical size are similar to the ones of diazoniapentaphenes **42a–b**, the DNA-binding properties of compound **44** are significantly lower than those of fully aromatic diazoniapolycycles (*cf.* data in Table 3.7). Notably, in the series of related, cationic protoberberine derivatives, a completely opposite behavior was observed; thus, 5,6-dihydro-8-desmethylcoralyne binds to double-stranded polynucleotides $[poly(dAdT)]_2$ and $[poly(dIdC)]_2$ much stronger than its fully aromatic analogue, 8-desmetylcoralyne, as determined by DNA thermal denaturation studies.[145]

3.3.2.2 Salt Dependence of Binding

Since the triplex DNA is unstable at low ionic strength in the absence of divalent cations or polyamines, thermal denaturation studies with the poly(dA)–$[poly(dT)]_2$ triplex were performed at higher salt concentration ($[Na^+] = 200$ mM), which is in accordance with established procedures.[81] Nevertheless, the ΔT_m values, obtained at different ionic strength conditions, cannot be directly used for comparison of the binding affinities of the ligands to DNA, since the melting temperature of DNA depends strongly on the salt concentration even in the absence of ligands.[146] On the other hand, binding of the ligands to the double-stranded DNA is also salt dependent due to the counter-ion release that accompanies the binding, as described by Eq. 3.1.[146]

$$\frac{\partial (\log K)}{\partial (\log [Na^+])} = -Z\psi \qquad \text{(Eq. 3.1)}$$

Here ψ is the fraction of the Na^+ ions associated per DNA phosphate residue ($\psi = 0.88$ for B-form of DNA) and Z is the apparent charge on the ligand. Assuming (i) no interaction of the ligands with single-strand polynucleotides and (ii) that the binding sites are distributed

regularly along the lattice, the melting behavior of the DNA in the presence of ligands may be described by Eq. 3.2.[76,77]

$$\frac{1}{T_m{}^0} - \frac{1}{T_m} = \frac{R}{\Delta H_m} \ln \left(1 + K_{Tm} L\right)^{\frac{1}{n}} \qquad \text{(Eq. 3.2)}$$

Here $T_m{}^0$ is the melting temperature of DNA in the absence of ligands, T_m is the melting temperature in the presence of saturating amounts of ligand, ΔH_m is the enthalpy of DNA melting, L is the free ligand concentration, and K_{Tm} is the ligand binding constant at T_m. The latter is connected to the thermodynamical binding constant, K^0, by the van't Hoff equation (Eq. 3.3).

$$\ln\left(\frac{K^0}{K_{Tm}}\right) = -\frac{\Delta H_b}{R}\left(\frac{1}{298} - \frac{1}{T_m}\right) \qquad \text{(Eq. 3.3)}$$

Therefore, the melting temperature of DNA depends on two factors: the ionic strength, as characterized by Na^+ concentration, and on the ligand, characterized by the values of binding constant, $K = f([Na^+], T_m)$, binding-site size, n, and the enthalpy of binding, $\Delta H_b = f(T_m)$. This dependence is complicated and cannot be analyzed completely in the absence of the thermodynamic parameters obtained by independent methods. Moreover, in the present work, mainly sub-saturating ligand concentrations were used, since these allow a better comparison between different ligands. For these reasons, the influence of the salt concentration on the melting behavior of DNA was evaluated empirically by the measurements of T_m values of the double-stranded polynucleotide, $[poly(dAdT)]_2$, in the presence and in the absence of a representative ligand **7b** at the same concentrations, but under various ionic strength conditions (Figure 3.18).

The melting temperature of the $[poly(dAdT)]_2$ duplex in the absence of the ligand is linearly dependent on $\log [Na^+]$ in the range of salt concentrations between 16 and 200 mM, as characterized by the empirical Schildkraut–Lifson equation.[146,147] In the presence of sub-saturating amounts of ligand, T_m expresses a complex behavior; that is, at low Na^+ concentration ($[Na^+] \leq 50$ mM), the melting temperature of ligand–DNA complex is almost independent of the salt concentration. With an increasing salt concentration, the melting temperatures asymptotically approach the ones that are observed in the absence of the ligand. At these salt concentrations the binding constant of a ligand reduces to a level that does not

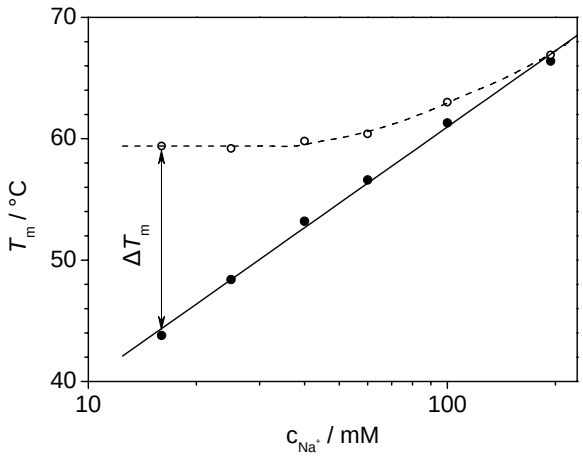

Figure 3.18. Influence of the total Na^+ concentration on the T_m transitions of $[poly(dAdT)]_2$ in the absence (filled circles) and in the presence of **7b** (empty circles, ligand-to-DNA ratio r = 0.5).

significantly contribute to the binding and stabilization of the double helix. It should be emphasized here that the salt influence is especially important for the diazoniapolycyclic ligands, as these are doubly positively charged species (Z = 2).

3.3.2.3 Binding to Triple-Helical DNA

As discussed above, at the high ionic-strength conditions that favor the formation of triple-helical DNA binding of diazoniapolycycles to ds DNA is significantly reduced. Diazoniapolycyclic salts efficiently bind to the poly(dA)–$[poly(dT)]_2$ triplex and stabilize it against thermal denaturation, as characterized by the $\Delta T_m^{3\rightarrow2}$ values (Table 3.8). Most importantly, diazoniapolycycles are able to distinguish between triplex and duplex structures, as can be seen from comparison of the induced T_m shifts ($\Delta T_m^{3\rightarrow2}$ *vs.* $\Delta T_m^{2\rightarrow1}$). Thus, diazoniapentaphenes **7a**–**c** and **42a–b** show very good selectivity at low to near-saturating ligand-to-DNA ratios ($0 < r \leq 0.5$). At the same time, diazoniaanthra[1,2-*a*]anthracenes **38a–c** exhibit much higher binding affinity to the poly(dA)–$[poly(dT)]_2$ triplex, as seen from the thermal denaturation studies and equilibrium dialysis results. Among the hexacyclic derivatives, compound **38a** shows an excellent triplex-*vs*.-duplex selectivity at $r \leq 0.2$; however, at higher ligand concentrations, **38a** and especially **38b** and **38c** bind also to the double helix. Remarkably, the diazoniahexaphene **51** has very poor triplex-*vs*.-duplex selectivity; in fact, at low ligand-to-DNA ratios ($r \leq 0.2$), it stabilizes triple-helical and double-stranded forms of DNA to a similar extent, while at higher r values binding to the triplex form prevails.

As in the case of the duplex binding, the variation of the position of heteroatoms in the series **7a**–**c** has almost no influence on the triplex-binding properties, and the introduction of methyl groups in derivatives **42a** and **42b** results only in minor differences, except for somewhat poorer triplex-stabilizing properties in the case of **42b**. It has been shown that the positions of the heteroatoms have a large influence on the triplex DNA-binding properties in the recently reported series of pyridoindole and pyridoquinoxaline derivatives[45] and in the case of dibenzophenanthrolines.[46] However, in the case of the diazoniapolycycles, presented in this study, the heteroatoms are not available for hydrogen bonding with the DNA phosphate backbone. Moreover, it may be assumed that the charges contributed by the quaternary nitrogen atoms are efficiently delocalized within the aromatic ring system, as it has been shown for the benzo[*b*]quinolizinium ion.[14]

It has been shown that the extension of the aromatic ring system from tetracyclic to pentacyclic hetarenes favors triplex stabilization due to larger surface area available for the π-stacking interactions.[74] It may be suggested that, in a similar way, further extension of the π system from the diazoniapentaphene series to the six-membered diazoniaanthra[1,2-*a*]anthracene structure (**38**) facilitates the triplex-binding properties. However, the diazoniahexaphene **51** represents an exception from this trend, since, although its aromatic surface area is similar to the one of diazoniaanthra[1,2-*a*]anthracenes, it shows much worse selectivity for the triplex DNA compared to the latter compounds.

On the other hand, it has been suggested that aminoalkyl-substituted naphthylquinolines are efficient triplex-DNA binders due to some degree of torsional flexibility in the molecule.[47a] In fact, it was shown by NMR and X-ray diffraction studies of triple-helical DNA structures that the nucleic bases in a triplet are not coplanar, but deviate considerably from the mean plane, inclined by angles of up to 33° ("propeller twist").[35,148] Diazoniaanthra[1,2-*a*]anthracenes are non-planar compounds, as can be seen from the X-ray structure analysis of the derivative **38c** (Section 3.2.2.3). Moreover, the observed value of an angle between the quinolizinium moieties of the dication (30.7°) matches almost perfectly the propeller twist of the nucleic bases. Therefore, it may be suggested that the non-planarity of diazonia-anthra[1,2-*a*]anthracenes facilitates their interaction with the triple-helical DNA for geometrical reasons. It may be also suggested that binding of these compounds to triplex DNA is associated with a unidirectional P/M-racemization, since the interconversion barrier should be rather low. Thus, this system may be considered as an annelated [4]helicene, the racemization barrier of which was estimated to be about 4 kcal mol^{-1}.[149]

The non-planarity of the nucleic bases in triple-helical DNA may also be the reason for the reduced triplex-*vs*.-duplex selectivity of diazoniahexaphene **51**, as compared to diazonia-anthra[1,2-*a*]anthracenes. Thus, its large aromatic surface area favors the interaction with duplex DNA, compared to the five ring-membered diazoniapentaphenes **7a–c**; however, its planar shape does not facilitate the interaction with triplex DNA. Therefore, it may be concluded that a twisted shape of the chromophore is more important for the triplex-binding properties than the simple extension of the planar π system.

Comparison with other reported triplex-DNA binders

Diazoniaanthra[1,2-*a*]anthracene **38a** shows the highest triplex-DNA affinity among the diazoniapolycycles investigated in this study and is superior to the ligands such as first-generation naphthylquinolines **37** ($\Delta T_m^{3\rightarrow2} \approx 35$ °C, $\Delta T_m^{2\rightarrow1} \approx 5$ °C at $r = 0.2$ and nearly identical conditions).[47a] Thus, the $\Delta T_m^{2\rightarrow1}$ values for **38a** are significantly lower and, although the $\Delta T_m^{3\rightarrow2}$ values are slightly larger for the naphthylquinolines, compound **38a** exhibits a significantly higher selectivity for triplex stabilization. This selectivity of diazonia-anthra[1,2-*a*]anthracene **38a** is comparable to that of a recently reported improved series of naphthylquinoline derivatives.[47b] It is also very close to the ligand DB359 from the series of polyaromatic diamidines ($\Delta T_m^{3\rightarrow2} \approx 27$ °C, $\Delta T_m^{2\rightarrow1} \approx 1$ °C at $r = 0.2$ and identical conditions), which has been described as “one of the most triplex selective compounds discovered”.[52]

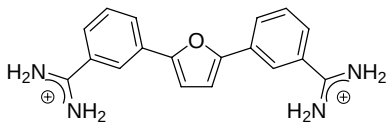

DB359

However, in contrast to the majority of the reported triplex-DNA binders, in the diazoniapolycyclic salts the two full positive charges, which are essential for the DNA binding, are located on the aromatic core, and not on protonable nitrogen atoms. Therefore, the brutto charge of the intercalator and thus its DNA-binding properties are independent of the pH of the environment, excluding strongly alkaline media which may lead to decomposition of azonia salts due to formation of leucobases.

In summary, it was shown that diazoniapolycycles represent a structural motif with remarkably high selectivity towards triple-helical DNA. The DNA affinity is mainly

determined by the shape of the polycyclic system and the two cationic charges, whereas the position of the heteroatoms has only little influence on the DNA-binding properties. Diazoniapolycyclic salts are—up to date—the only triplex-binding aromatic heterocycles that do not need side-chain substituents and therefore represent a promising lead structure for the design of drugs whose mode of action involves the stabilization of triplex DNA.

4 TARGETING DNA ABASIC SITES WITH ACRIDIZINIUM–NUCLEIC BASE CONJUGATES

4.1 Objective

Since the apurinic / apyrimidinic DNA lesions (AP, or “abasic” sites) represent one of the most frequent types of DNA damage resulting from the action of chemotherapeutical agents or physical anti-tumor treatment, it is of large importance to design small molecules that bind selectively to such lesions and prevent their repair by cellular mechanisms (*cf.* Section 1.4). Such drugs, as *e.g.* quinacrine–adenine conjugates **21a** and **21d**, enhance the susceptibility of the tumor cells to the alkylating agents and thus augment the action of certain anti-cancer drugs.[59,60]

A promising approach along these lines is the generation of clustered DNA lesions, or locally multiple-damaged sites. These closely located lesions are highly toxic to the cell, as they are difficult to repair by the cellular enzymes. The generation of such lesions, in part, may be achieved by the use of multifunctional molecules that combine the affinity to the abasic sites with the DNA-damaging or DNA-photocleaving properties. Thus, the conjugates **24** and **26** with a photoactive nitrobenzamide unit represent examples of such multifunctional DNA binders.[65,66]

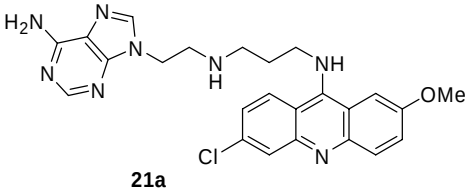

21a

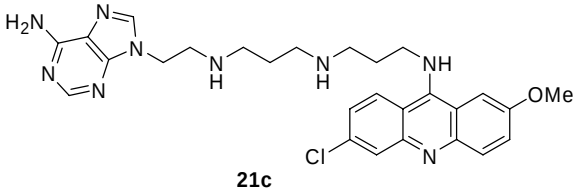

21c

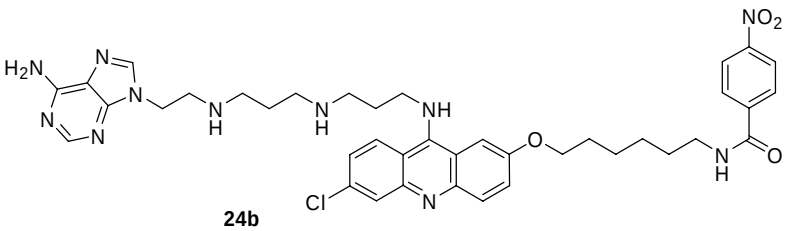

24b

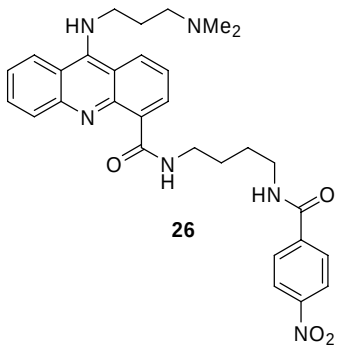

26

Considering the DNA-binding and DNA-photodamaging properties of the acridizinium derivatives,[8,16] it was proposed to prepare compounds of the aforementioned type, in which the DNA-intercalating and DNA-photodamaging functions are combined in *one* structural unit, namely the acridizinium ion. In the first attempts, adenine may be used as nucleic-base unit, because the synthetic protocols to connect it to the linker chain are known. The connection of the adenine–linker part to the acridizinium ion may, in principle, be realized in various ways, including the bridging *via* a secondary amino group as in the conjugates **21** and **24**, or with an amide functionality. However, the results of Chapter 2 of this work show that, in contrast to the 9-substituted acridines, the nucleophilic substitution in the acridizinium derivatives does not proceed with primary aliphatic amines and the reactions with secondary aliphatic amines proceed with rather modest yields. Therefore, it was proposed to use another approach for the synthesis of acridizinium–adenine conjugates, namely, the connection of the parts of the molecule with amide linkages. Thus, acridizinium–adenine conjugates **54a–b** were planned to be synthesized.

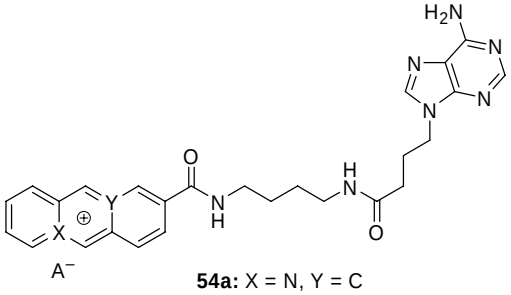

54a: X = N, Y = C
54b: X = C, Y = N

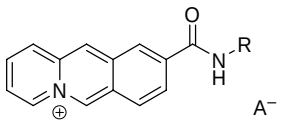

55 R = alkyl

In the preliminary investigations, the use of the amido group in the linker, in contrast to the secondary amino group in compounds **21** and **24**, would allow to avoid the cleavage of the DNA backbone by the β-elimination mechanism and study only the photoinduced DNA damage. Finally, the variation of the position of the quaternary nitrogen atom in the acridizinium part (isomers **54a** and **54b**) should allow to study the effect of the substitution pattern on the DNA-binding and DNA-photodamaging properties of the acridizinium derivatives.

Since acridizinium carboxamides have not been described, so far, it was also planned to synthesize simple amides **55** as model compounds. Their synthesis should allow the development of the synthetic methodology for the preparation of more complex salts **54a–b**. Moreover, the study of the DNA-binding and DNA-photocleavage activity of the model

compounds would be necessary to reveal the effect of the nucleic base in the conjugates **54a–b**. Thus, it was planned to investigate the binding affinities and the photocleavage activity of the conjugates **54a–b** and the acridizinium-9-carboxamides **55** towards double-stranded regular and abasic DNA structures.

4.2 Results

4.2.1 Synthesis of the Model Compounds and Acridizinium–Adenine Conjugates

4.2.1.1 Synthesis of Acridizinium-9-carboxamides

The acridizinium-9-carboxamides were prepared by the reaction of the readily available acridizinium-9-carboxylic acid[150] with selected amines (Scheme 4.1, Table 4.1).

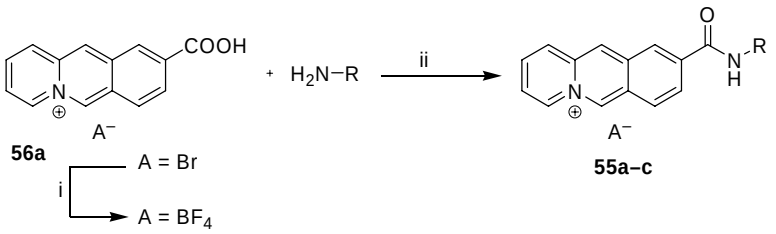

Scheme 4.1. Synthesis of acridizinium-9-carboxamides. Reagents and conditions: (i) HBF_4 aq., 98%; (ii) NMM, *i*BuOCOCl, MeCN, –20 °C → room temp., 18 h.

Table 4.1. Synthesis of the model acridizinium-9-carboxamides

Compound	R	A	Yield / %
55a	*i*Pr	BF_4	70
55b	*n*Bu	BF_4	31
55c [a]	$(CH_2)_3NMe_2$	Cl	70

[a] Reaction performed in the presence of one equivalent of pyridine hydrochloride.

To afford the solubility of the acid **56** in organic solvents, it had first to be converted into the tetrafluoroborate salt by treatment with aqueous HBF_4. The tetrafluoroborate **56 (BF_4^-)** is soluble in polar aprotic solvents such as acetonitrile and DMF. However, it was observed that amidation of this acid by several methods, such as the dicyclohexylcarbodiimide (DCC) method or the reaction in the presence of *N*,*N*′-carbonyldiimidazole (CDI), which are known to give good yields of peptides in the most cases,[151] lead to decomposition of the acridizinium

core by nucleophilic addition of amines to the position 6 of the acridizinium ion, and no amide could be isolated. Further experiments revealed that the desired compounds may be prepared in good yields by the mixed-anhydride (Wieland–Sehring) method.[151,152] Thus, the treatment of the acid **56 (BF_4^-)** with isobutyl chloroformate in acetonitrile in the presence of a very mild base (*N*-methylmorpholine, NMM) afforded a salt of the mixed anhydride, which was allowed to react with selected amines *in situ*, to give the amides **55a–b**. The use of stronger bases, such as ethyldiisopropylamine ("Hünig's base") or *N*-ethylpiperidine, inevitably led to the formation of large amounts of decomposition products. In the case of *N*,*N*-dimethyl-1,3-diaminopropane, the diamine was added in the presence of one equivalent of the acid (pyridine hydrochloride), to partly neutralize the diamine and avoid the decomposition of the acridizinium ion. The crude amides were subjected to ion exchange and isolated as tetrafluoroborates (**55a–b**) or as a dichloride (**55c**); their structures were confirmed by IR, ^{1}H- and ^{13}C-NMR spectroscopy, mass-spectrometric and elemental analysis data.

4.2.1.2 Synthesis of Acridizinium-3-carboxylic Acid

The previously unknown acridizinium-3-carboxylic acid (**56b**) was prepared following the general strategy for the synthesis of acridizinium derivatives by the cyclodehydration of pyridinium precursors (Scheme 4.2).[89]

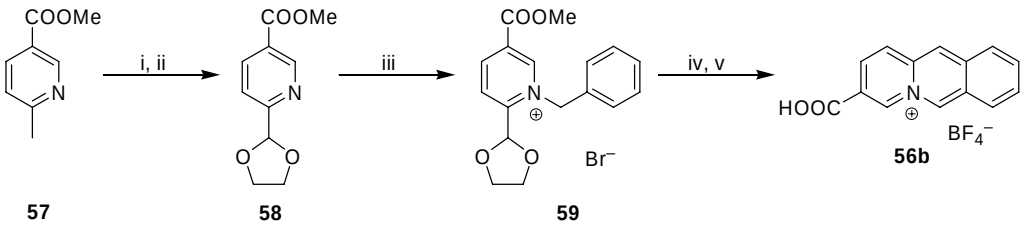

Scheme 4.2. Synthesis of acridizinium-3-carboxylic acid. Reagents and conditions: (i) SeO_2, 1,4-dioxane–water, 65 °C, 1 h; (ii) $HO(CH_2)_2OH$, *p*-TsOH, toluene, reflux, 20 h, 36%; (iii) $PhCH_2Br$, DMSO, room temp., 13 days, 54%; (iv) aq. HBr, reflux, 20 h, 90%; (v) aq. HBF_4, 77%.

Thus, the commercially available methyl 6-methylnicotinate (**57**) was oxidized with selenium dioxide in water–dioxane to methyl 6-formylnicotinate, and the aldehyde was immediately let to react with ethylene glycol under acid catalysis, to give the acetal **58** in 36% yield. The latter compound was quaternized with benzyl bromide to give the salt **59** in a moderate yield (59%). This reflects the lower reactivity of the ester **58** as compared to the acetal **32**, which could be quaternized almost quantitatively (*cf.* Sections 2.2.1.2 and 3.2.1). The cyclodehydration of the salt **59** in refluxing aqueous (48%) HBr, accompanied by the saponification

of the ester group, gave the desired acid **56b (Br⁻)** in 90% yield, which was further converted into the tetrafluoroborate salt **56b (BF_4^-)** by treatment with aqueous HBF_4. The overall yield of the salt **56b (BF_4^-)** comprised 13%, based on the ester **57**; its structure was supported by the ^{1}H- and ^{13}C-NMR spectroscopy, mass-spectrometric and elemental analysis data.

4.2.1.3 Synthesis of the Acridizinium–Adenine Conjugates

Since it was found that the synthesis of acridizinium carboxamides is a reaction sensitive to bases, and no high yields could be achieved, the preparation of the conjugates **54a–b** started from the attachment of a linker chain to the adenine residue, with coupling to the acridizinium ion in the last step (Scheme 4.3).

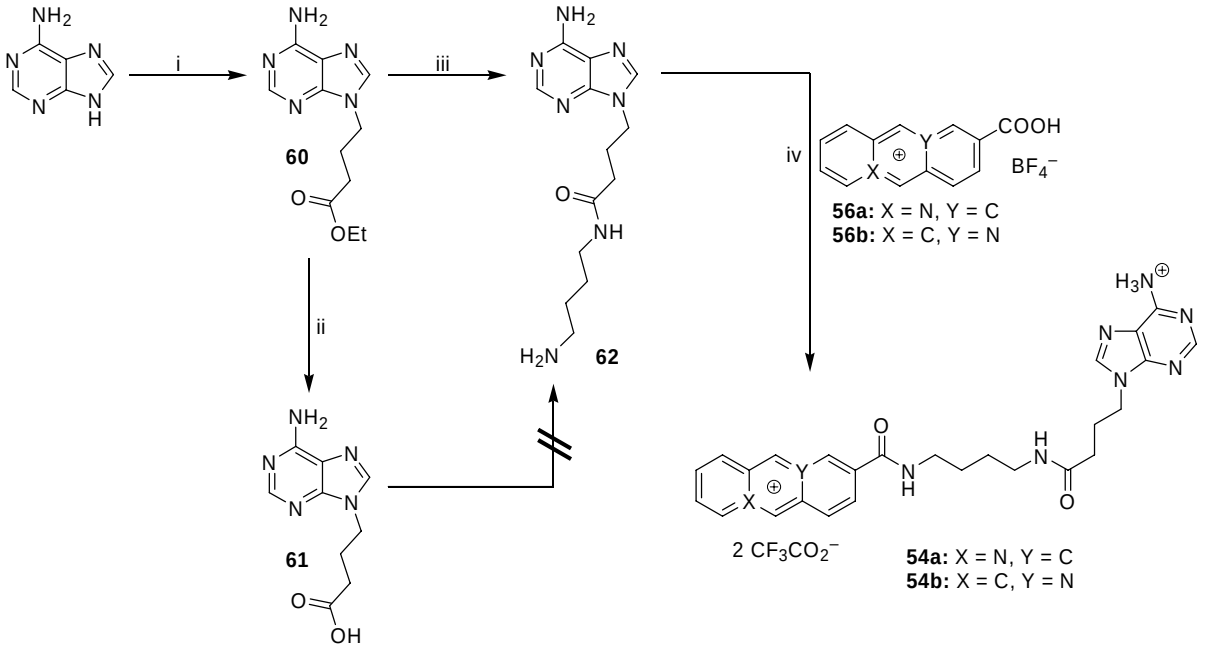

Scheme 4.3. Synthesis of the acridizinium–adenine conjugates **54a–b**. Reagents and conditions: (i) $Br(CH_2)_3COOEt$, NaH, DMF, room temp., 48 h, 74%; (ii) aq. NaOH, room temp., 18 h, 81%; (iii) $H_2N(CH_2)_4NH_2$, *n*PrOH, reflux, 10 h, 86%; (iv) NMM, *i*BuOCOCl, DMF, –20 °C → room temp., 18 h, **54a**: 47%, **54b**: 54%.

Thus, following the published procedures, ethyl 4-(adenin-9-yl)butyrate (**60**) was prepared by the treatment of sodium adenylate (prepared *in situ* from adenine and NaH) with ethyl 4-bromobutyrate.[153] The ester **60** can be readily saponified to the 4-(adenin-9-yl)butyric acid (**61**). However, although the preparation of amides of this acid has been described in the literature,[153b,154] preliminary attempts to prepare the amide **62** from the acid **61** failed due to the very low solubility of the acid **61** in aprotic solvents. Moreover, the reaction *via* the corresponding acyl azide (Schotten–Baumann method), performed in an aqueous medium,

gave a mixture of non-separable products. On the contrary, the treatment of the ester **60** with 1,4-diaminobutane in refluxing *n*-propanol or in ethylene glycol at 100 °C offered a facile approach for the synthesis of the desired amide **62**. In this reaction, a large excess of the diamine has to be used to decrease the formation of the di-substitution product.

The adenine derivative **62** was allowed to react with the isomeric acridiziniumcarboxylic acids **56a** and **56b** at the conditions previously used for the synthesis of the model amides **55a–b**; however, in this case, the reaction was performed in anhydrous DMF because of the low solubility of the intermediate **62** in acetonitrile. The acridizinium–adenine conjugates **54a** and **54b** were purified by the reversed-phase MPLC, eluting with aq. TFA–acetonitrile, and isolated as bis(trifluoroacetate) salts. Their structures were supported by ^{1}H- and ^{13}C-NMR spectroscopy, mass-spectrometric and elemental analysis data.

4.2.2 Photophysical Properties of Acridizinium-9-carboxamides and Acridizinium–Adenine Conjugates

Due to the presence of acridizinium chromophore the acridizinium-9-carboxamides **55** and acridizinium–adenine conjugates **54** show significant absorption in the near-UV region of the spectrum. Absorption and fluorescence emission spectra of these compounds (Figure 4.1) were measured in aqueous solutions of moderate ionic strength ([Na^+] = 38.1 mM, pH 7); the photophysical data determined from the UV/Vis and fluorescence spectroscopy are summarized in Table 4.2.

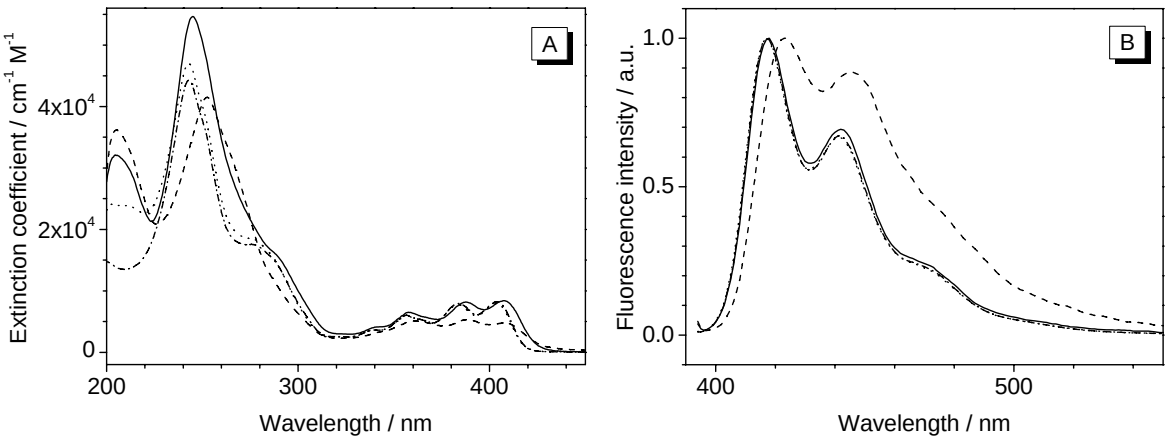

Figure 4.1. Absorption (A, c = 50 μM) and normalized fluorescence emission (B, c = 10 μM) spectra of compounds **54a** (solid lines), **54b** (dashed lines), **55a** (dotted lines) and **55b** (dash-dotted lines) in aqueous buffer solutions (pH 7). Excitation wavelength for the fluorescence spectroscopy λ_{ex} = 390 nm.

Table 4.2. Photophysical properties of acridizinium–adenine conjugates **54a–b** and acridizinium-9-carboxamides **55a-b**.[a]

Compound	Absorption		Fluorescence	
	λ_{max} / nm [b]	log (ε / cm^{-1} M^{-1})	λ_{max} / nm [c]	Φ_F [d]
54a	408	3.92	418	0.041
54b	408	3.68	423	0.064
55a	403	3.90	417	0.51
55b	404	3.92	417	0.50

[a] In aqueous sodium phosphate buffer, [Na^+] = 38.1 mM, pH 7; [b] long-wavelength absorption maxima, c = 50 μM; [c] fluorescence emission maxima, c = 10 μM; excitation wavelength λ_{ex} = 390 nm; [d] fluorescence quantum yield relative to Coumarin 1, estimated error ± 5%.

Inspection of the spectra in Figure 4.1 reveals that the *N*-alkyl-substituted acridizinium-9-carboxamides **55a** and **55b** have virtually identical absorption and emission properties, with a long-wavelength absorption maximum at λ_{abs} = 403–404 nm (0–0 transition), similar to the one of the unsubstituted acridizinium ion.[155] The fluorescence emission spectra of both derivatives are well-structured, represent a mirror image of the $S_0 \rightarrow S_1$ transition bands and have maxima at λ_{em} = 417 nm; the values of the fluorescence quantum yield are almost equal (0.50–0.51).

At the same time, the acridizinium–adenine conjugates **54a–b** reveal a slight bathochromic shift of the long-wavelength absorption band (λ_{abs} = 408 nm for both compounds). Additionaly, compound **54b** shows a significant hypochromism of the long-wavelength absorption band ($H \approx 41\%$), as compared to the isomer **54a** and amides **55a–b**. The fluorescence of both conjugates is quenched by a factor of about 10 (Φ_F = 0.041 and 0.064 for **54a** and **54b**, respectively), as compared to the amides **55a–b** (Table 4.2). The emission spectrum of compound **54a** lies in the same region as the ones of the amides **55a–b** (λ_{em} = 418 nm), whereas the one of the isomer **54b** undergoes a slight bathochromic shift (λ_{em} = 423 nm). Additional experiments showed that the absorption and fluorescence emission spectra of the conjugates **54a–b** remain unchanged in a broad temperature range, from 10 to 80 °C (data not shown).

4.2.3 DNA-Binding Properties of Acridizinium-9-carboxamides and Acridizinium–Adenine Conjugates

4.2.3.1 Binding to Regular and Abasic Oligonucleotides

The interaction of the model compounds **55a–c** and acridizinium–adenine conjugates **54a–b** with the fully paired and abasic-site-containing double-stranded DNA structures was studied by the thermal denaturation of synthetic oligodeoxyribonucleotides (ODNs) in the absence and in the presence of these compounds. The advantage of the thermal denaturation method is that it requires relatively small amounts of the modified synthetic ODNs and provides a direct comparison of relative binding affinities within a series of similar ligands. Because of the instability of the natural abasic sites and in accordance with established protocols,[63] the abasic oligonucleotide (ODN3) contained a chemically stable tetrahydrofuran analogue of the deoxyribose residue (Figure 4.2). Thus, annealing of an equimolar mixture of the strand ODN1 and the modified strand ODN3 produced a duplex containing an apurinic site and designated as TX duplex (Figure 4.2), in which the nucleic base opposite to the lesion, *i.e.* thymine, may pair with the base (adenine) of the conjugates **54a–b**. Annealing of the strand ODN1 with the complementary oligonucleotide ODN2 gave a regular, fully paired double helix designated as TA duplex. Thermal denaturation experiments were performed by monitoring the changes in the absorption at 260 nm of the oligonucleotide–ligand mixtures in aqueous sodium phosphate buffer solutions of moderate ionic strength ($[Na^+]$ = 38.1 mM; pH 7.0). These conditions were selected to ensure the comparison with the published data on the other related intercalator–nucleic base conjugates.[63]

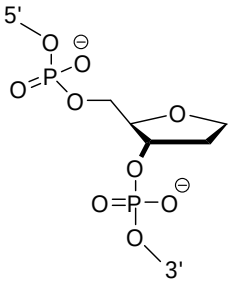

ODN1: GCG-TG**T**-GTG-CG
ODN2: CGC-AC**A**-CAC-GC
TA duplex

ODN1: GCG-TG**T**-GTG-CG
ODN3: CGC-AC**X**-CAC-GC
TX duplex

Figure 4.2. Structure of the tetrahydrofuran abasic-site analogue (**X**) and sequences of the oligonucleotides used in this work.

At the conditions employed, the TX duplex denaturates at T_m = 26.3 ± 0.5 °C and the TA duplex at 52.8 ± 0.5 °C. The recorded melting temperatures of both oligonucleotides are lower than the ones reported for them at the identical conditions previously (T_m = 36.9 and

56.0 °C for the TX and TA duplexes, respectively), presumably due to the ambiguous composition of the buffer solution in the cited work.[63a] The melting profiles of the oligonucleotides in the presence of a representative ligand **55c** at various ligand-to-DNA ratios, $r = c_L / c_{ODN}$, are shown in Figure 4.3. The plots of the induced shifts of the melting temperatures, $\Delta T_m = T_m(\text{ODN}) - T_m(\text{ODN-Ligand})$, against the ligand-to-DNA ratio r are shown in Figure 4.4; representative data are also given in Table 4.3. It should be noted that in the case of experiments with oligonucleotides the r values refer to the molar concentration of the oligonucleotide duplexes, and not to the concentration of nucleic base pairs.

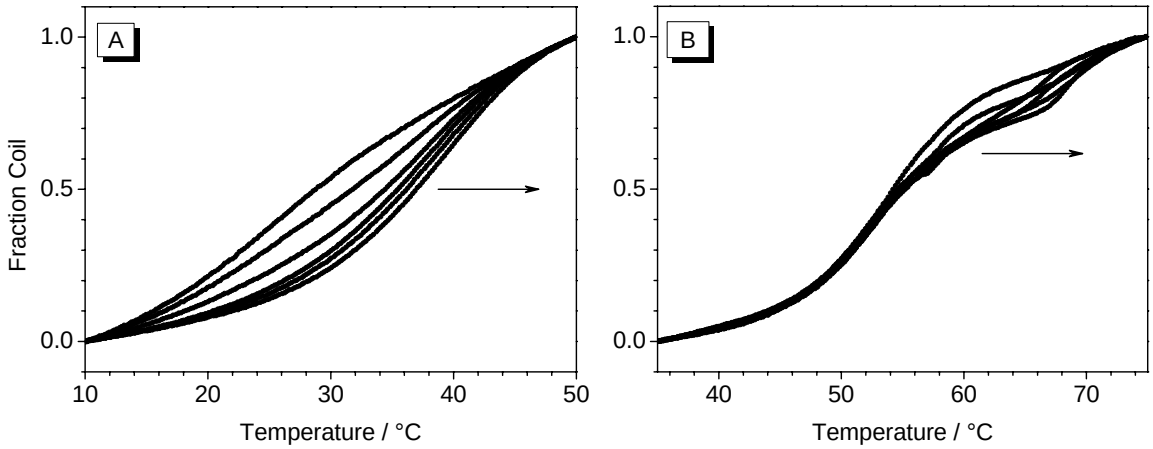

Figure 4.3. Thermal denaturation profiles of TX duplex (A) and TA duplex (B) (c_{DNA} = 5 μM in ODN buffer, [Na^+] = 38.1 mM) in the presence of compound **55c** at ligand-to-DNA ratios (r) of 0, 0.2, 0.5, 1.0, 1.5 and 2.0. Arrows indicate the shift of the melting curves with increasing r values.

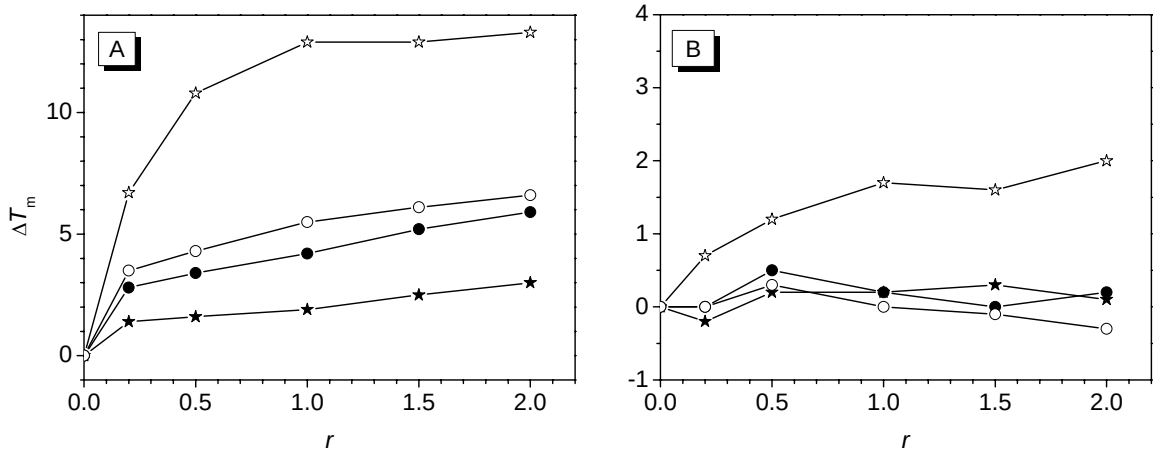

Figure 4.4. Plots of induced T_m shifts of TX duplex (A) and TA duplex (B) by compounds **54a** (filled circles), **54b** (empty circles), **55b** (filled stars) and **55c** (empty stars) *vs.* ligand-to-DNA ratio r.

Table 4.3. Binding affinities of acridizinium–adenine conjugates **54a–b** and acridizinium-9-carboxamides **55b–c** to TX and TA duplexes, as determined from the thermal denaturation studies.

Ligand	Induced ΔT_m / °C, [a] at ligand-to-DNA ratios r			
	TX duplex		TA diplex	
	r = 0.5	r = 2.0	r = 0.5	r = 2.0
54a	3.4	5.9	0.5	0.2
54b	4.3	6.6	0.3	−0.3
55b	1.6	3.0	0.2	0.1
55c	10.8	13.3	1.2	2.0

[a] Experimental conditions: c_{DNA} = 5 μM in ODN buffer, [Na^+] = 38.1 mM; estimated error ± 0.5 °C.

The results of the thermal denaturation studies reveal that none of the compounds investigated, except for **55c**, has an influence on the denaturation of the fully paired TA duplex, since the observed ΔT_m(TA) values lie within the experimental error range (± 0.5 °C). In the case of the aminoalkyl-substituted carboxamide **55c**, a slight stabilizing effect is observed (ΔT_m = 2.0 °C at r = 2.0), indicative of binding of this compound to the TA duplex.

At the same time, compounds **54a–b** and **55b** show a slight, but significant stabilization of the abasic site-containing TX duplex, and the observed induced shifts of the melting temperature regularly increase with the increasing concentration of the ligand. Thus, the acridizinium–adenine conjugates **54a**–**b** have ΔT_m values of about 7 °C at r = 2.0, while the compound **54b** is slightly more efficient than the isomer **54a** (*cf.* the plots in Figure 4.4, A). The *N*-butyl-acridizinium-9-carboxamide **55b** stabilizes the TX duplex to a lesser extent (ΔT_m = 3.0 °C). In contrast, an efficient stabilization is achieved by the compound **55c**, which shows a ΔT_m value of 13.3 °C at r = 2.0.

The selectivity of the ligands for the abasic site may be expressed quantitatively by the $\Delta\Delta T_m$ values ($\Delta\Delta T_m = \Delta T_m(TX) - \Delta T_m(TA)$ at a certain ligand concentration). These values provide a differential comparison of the effects of the presence of an abasic site on the binding of the ligands and reflect their selectivity for the abasic site. These data are presented in Figure 4.5. Thus, compound **55c** has a significant preference for the DNA that contains an abasic site, with saturation of the binding at $r \geq 1.0$. The selectivity of the conjugates **54a–b** is less pronounced, and the saturation does not take place even at r = 2.0. The $\Delta\Delta T_m$ values of these compounds, as well as the ones of compound **55b**, reflect the absence of affinity for the fully paired TA duplex.

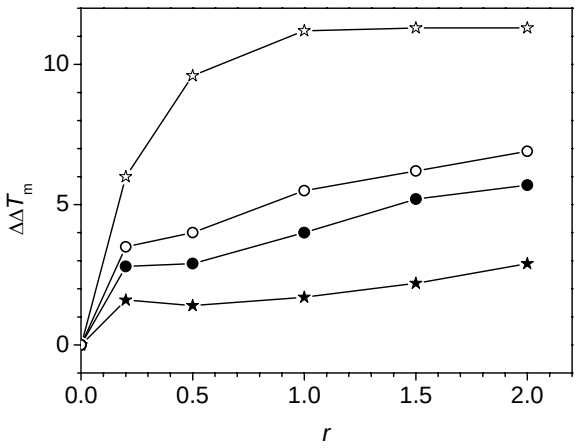

Figure 4.5. Plot of the $\Delta\Delta T_m$ values [$\Delta\Delta T_m = \Delta T_m(TX) - \Delta T_m(TA)$] for compounds **54a** (filled circles), **54b** (empty circles), **55b** (filled stars) and **55c** (empty stars) *vs.* ligand-to-DNA ratio *r*.

4.2.3.2 Binding to Double-Stranded Polynucleotides

The binding affinities of acridizinium-9-carboxamides **55a–b** to double-stranded polynuleotides were determined by the spectrophotometric titrations with ct DNA as well by the thermal denaturation studies with ct DNA and the synthetic polynucleotide $[poly(dAdT)]_2$. The changes in the absorption spectra upon addition of DNA to the solutions of compounds **55a–b** are shown in Figure 4.6. Upon interaction with DNA, a pronounced decrease of the intensity (hypochromic effect) of all long-wavelength absorption maxima was observed. The 0–0 transition bands of both derivatives undergo blue shifts by about 5 nm, simultaneously with the formation of new red-shifted shoulders. Remarkably, the complete binding of the

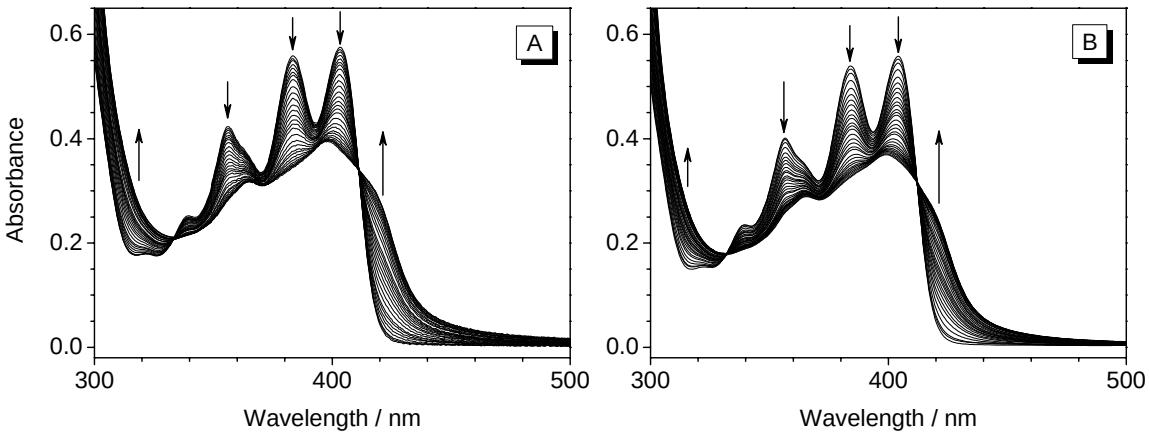

Figure 4.6. Spectrophotometric titrations of ct DNA to compounds **55a** (A) and **55b** (B) at a ligand concentration of 50 μM. Arrows indicate the changes of the intensity of the absorption bands upon addition of the DNA (0–1.0 mM).

ligands is achieved only upon addition of relatively large amounts of the DNA (~ 1.2 mM bp, which corresponds to the DNA-to-ligand ratio $r^{-1} \geq 20$). Even so, the clear isosbestic points are conserved in the full range of DNA concentrations.

The results of the thermal denaturation experiments with compounds **55a–b** are presented in Table 4.4. An intercalator with known binding properties, proflavine (**1**),[3] as well as the parent compound, acridizinium bromide (**5a**) were included as references.

Table 4.4. Binding affinities of proflavine and acridizinium-9-carboxamides **55a–b** to polymeric ds DNA, as determined from the thermal denaturation studies.

Ligand	Induced ΔT_m / °C, [a] at ligand-to-DNA ratios r			
	ct DNA		$[poly(dAdT)]_2$	
	$r = 0.2$	$r = 0.5$	$r = 0.2$	$r = 0.5$
Proflavine (**1**)	10.1 [b]	15.6	18.4	24.0
Acridizinium **(5a)**	1.2	2.6	1.6	3.5
55a	0.4	0.5	nd [c]	nd [c]
55b	0.2	0.8	0.5	0.9
55c	7.4	11.9	8.5	15.9

[a] Experimental conditions: c_{DNA} = 40 μM bp in BPE buffer, $[Na^+]$ = 16 mM; estimated error ± 0.2 °C; r values refer to the concentration of DNA (bp); [b] literature value: 11.5 °C;[139] [c] not determined.

The results of thermal denaturation studies indicate that the *N*-alkyl-substituted amides **55a–b** have only minor effect on the stabilization of ds DNA, much less than proflavine (ΔT_m = 15.6 °C for **1** and < 1 °C for **55a–b** in the case of ct DNA, r = 0.5), and even less than the unsubstituted acridizinium cation (ΔT_m = 2.6 °C at r = 0.5). It is noteworthy that acridizinium **5a** has much less affinity to ds DNA than proflavine, in spite of the similarity of the geometrical shapes of these intercalators. In contrast, the aminoalkyl-substituted acridizinium-9-carboxamide **55c** stabilizes the ds DNA against thermal denaturation to a large extent, although smaller than the one achieved by proflavine, together with a slight preference to AT-rich DNA, as judged from comparison of ΔT_m obtained for ct DNA and $[poly(dAdT)]_2$ (ΔT_m = 11.9 and 15.9 °C, respectively).

4.2.4 Photoinduced DNA Cleavage by Acridizinium-9-carboxamides and Acridizinium–Adenine Conjugates

The photocleavage properties of selected acridizinium-9-carboxamides and of acridizinium–adenine conjugates **54a–b** towards fully paired and abasic DNA were investigated with a conventional plasmid-relaxation assay. In this case, the supercoiled plasmid DNA (pBR322) is the target. The photo-induced single-strand cleavage ("nicking") of the supercoiled DNA converts it to a relaxed, open-circular form, while double-strand cleavage may produce linear DNA fragments (Figure 4.7). The DNA forms are readily separated by agarose gel electrophoresis followed by detection by fluorescent staining and quantification by densitometry. This assay is highly sensitive since even a single cleavage event occurring anywhere in the molecule is sufficient to cause the change to circular or linear forms. However, no information is obtained from this method with regard to the preferred cleavage sequences.[17]

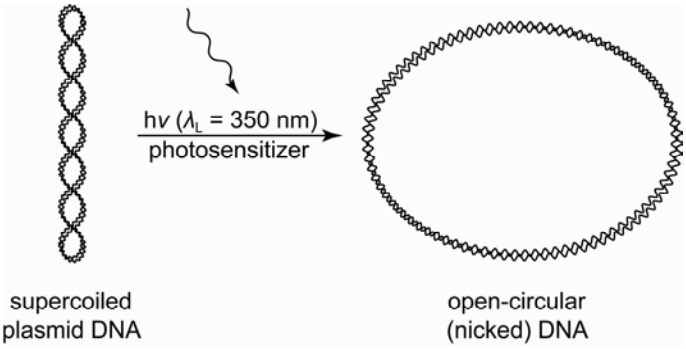

Figure 4.7. Schematic representation of a plasmid photocleavage experiment.

The abasic plasmid DNA was prepared by depurination of intact pBR322 DNA under controlled conditions (heating in an acidic sodium acetate buffer, pH 4.9, at 70 °C for 20 min). This treatment has been reported to produce an average of 1.8 apurinic sites per DNA molecule.[64]

The regular and apurinic plasmid samples were irradiated in the presence of the photosensitizers, namely amide **55b** and conjugates **54a–b**, in buffered aqueous solutions under conditions of reduced oxygen content. The photolysates were analyzed by gel electrophoresis without further work-up (*cf.* Figure 5.4 in the Experimental Part); the quantitative analysis of the electrophoregrams is presented in Figure 4.8.

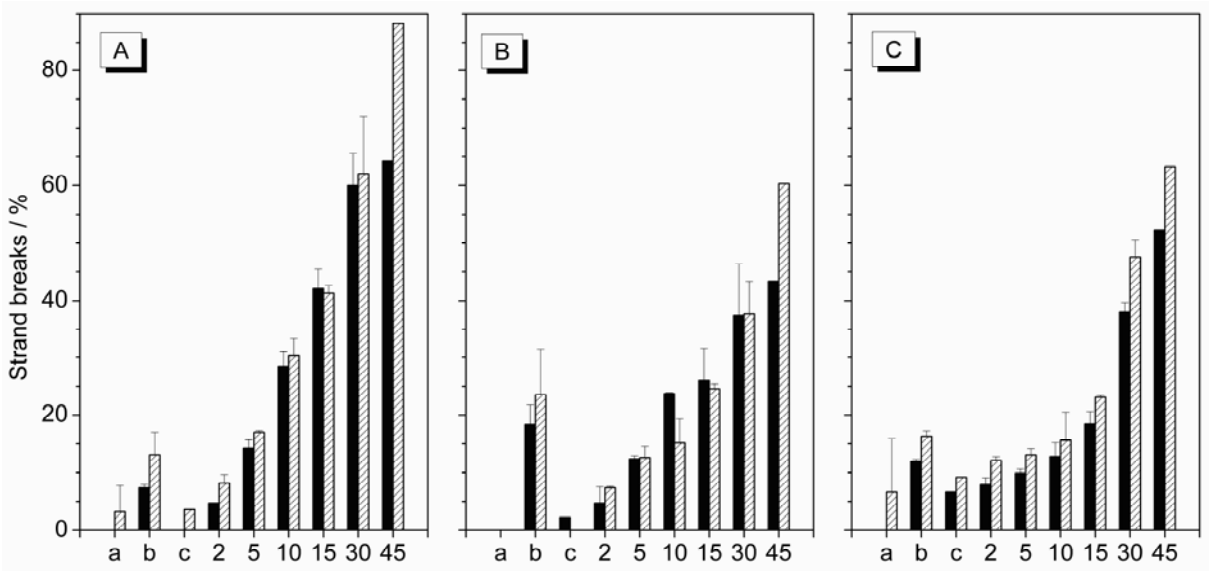

Figure 4.8. Single-strand cleavage of regular (black bars) and apurinic (hatched bars) pBR322 DNA upon irradiation in the presence of compounds **55b** (A), **54a** (B) and **54b** (C). Labels along the *x* axis: (a) non-irradiated reference samples; (b) samples irradiated for 45 min in the absence of photosensitizers; (c) samples incubated for 45 min in the presence of photosensitizers in the dark; numbers specify the irradiation times of samples in the presence of photosensitizers.

Upon incubation in the dark, neither amide **55b** nor the conjugates **54a–b** cause significant nicking of the supercoiled DNA. However, irradiation of plasmid DNA in the presence of these compounds results in single-strand cleavage and formation of the relaxed DNA, the relative amount of which increases with increasing irradiation times. It should be noted that prolonged (45 min) irradiation of the DNA even in the absence of the photosensitizer causes a significant (up to 20%) single-strand cleavage. The most efficient photocleavage of DNA (~ 40% in 15 min) is achieved by compound **55b**, while the conjugates **54a–b** are less efficient (20–25% cleavage in 15 min). At the same time, no significant difference can be observed between the photoclavage of the regular and apurinic plasmid DNA forms.

4.3 Discussion

4.3.1 Photophysical Properties

Absorption and fluorescence spectroscopy data reveal that the photophysical properties of the acridizinium-9-carboxamides **55a–b** resemble the ones of the unsubstituted acridizinium cation **5a**, as can be seen from the similarity of the absorption and emission bands and nearly identical fluorescence quantum yield values (*cf.* Φ_F = 0.50–0.51 for **55a–b** and Φ_F = 0.52 for

5a in water).[105] This leads to the conclusion that the introduction of the carboxamido functionality even in the position 9, conjugated with the quaternary bridgehead nitrogen atom, does not change the photophysical properties of the acridizinium chromophore.

However, the attachment of a nucleic base, adenine in compounds **54a–b**, with a moderately long amidoalkyl linking chain (about 14 Å in the stretched state) leads to a significant (10-fold) quenching of the fluorescence of the acridizinium moiety. Since adenine absorbs at wavelength shorter than the emission of the acridizinium ion ($\lambda_{abs} \approx 260$ nm), a resonance energy-transfer process may be excluded as a possible reason for such quenching. In contrast, a photoinduced electron transfer from the excited acridizinium cation to the adenine moiety seems to take place, as it happens upon intercalation of acridizinium **5a** into ds DNA. A prerequisite for such a process is the inter- or intramolecular π stacking of the conjugates in aqueous solutions. However, since no changes were observed in the absorption and emission spectra of the conjugates at increasing temperatures, it may be concluded that no intermolecular aggregation takes place. On the other hand, the length of the linker is appropriate for an intramolecular stacking arrangement, as may be seen from the molecular model of the compound **54b** (Figure 4.9, A). In particular, the distance between the aromatic planes of the acridizinium and adenine residues constitutes about 3.7 Å, according to the geometry optimization using the MM+ force field.

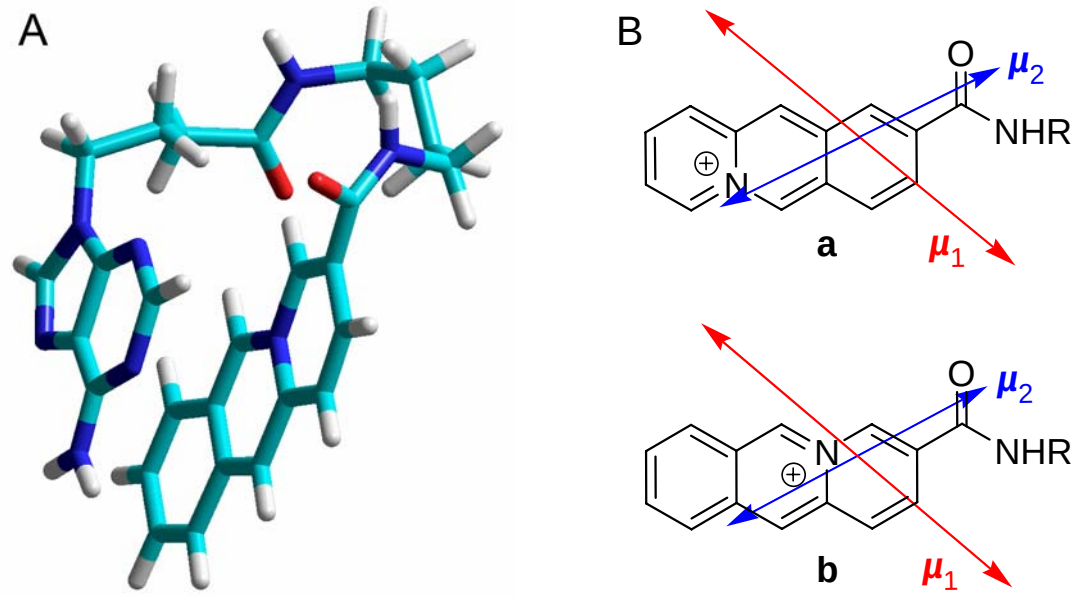

Figure 4.9. (A) Molecular model of compound **54b**, as determined from the molecular mechanics optimization using the MM+ force field. (B) Dipole moments of the first (red) and second (blue) singlet transitions of acridizinium-9-carboxamide (**a**) and of the 3-substituted isomer (**b**), calculated by the CI method (51 singly-excited configurations) using AM1-optimized ground-state geometries.

The intramolecular π stacking leads to the dipole–dipole interaction of the acridizinium and adenine parts of the molecule and causes the bathochromic shift of the long-wavelength absorption bands of the conjugates, as it has been shown for related acridine–nucleic base conjugates.[156] The origin of this red shift is the enhanced polarizability of the excited state of the acridizinium chromophore upon interaction with the π orbitals of adenine, which causes an increase of dispersion forces and a lowers the apparent energy of the excited state.[70]

Nevertheless, it should be noted that compound **54b** undergoes a more severe change of the photophysical properties than the isomer **54a**; that is, it exhibits a pronounced hypochromism of the long-wavelength absorption band and a bathochromic shift of the emission spectrum, as compared to compounds **54a** and **55a–b**. The origin of this different behavior of the isomeric conjugates is not clear, since the results of quantum-chemical calculations show that the transition dipole moments of 9- and 3-carboxamido-substituted acridizinium cations are almost identical (Figure 4.9, B). Therefore, the variation of the attachment point of the linker–adenine moiety between these two positions should not have an effect on the dipole–dipole interaction between the acridizinium and adenine chromophores. Remarkably, the orientations of the calculated transition dipole moments of the isomeric acridizinium-carboxamides closely resemble the ones calculated for the unsubstituted acridizinium ion (**5a**) by *ab initio* methods,[157] confirming that the carboxamido substituent has little, if any, influence on the photophysical properties of the acridizinium ion.

4.3.2 DNA-Binding and DNA-Photocleaving Properties

4.3.2.1 Binding to Regular and Abasic DNA Structures

The results of the spectrophotometric titrations of acridizinium-9-carboxamides **55a–b** with DNA, namely the significant hypsochromic effect of the long-wavelength absorption bands, clearly indicate binding of these salts to the DNA. Moreover, the isosbestic points, observed in both cases, indicate that one binding mode takes place almost exclusively. The fitting of the binding isotherms to the neighbor-exclusion model[69] (Figure 4.10) gives the values of the DNA-binding constants $K = (2–3) \times 10^4$ м$^{-1}$ (bp), which is in a good agreement with the value reported for the unsubstituted acridizinium salt (**5a**, $K = 2.5\times 10^4$ м$^{-1}$ bp).[10] At the same time, the values for the exclusion parameter ($n = 7–10$) are unexpectedly large, whereas most "classical" intercalators have $n \approx 2$ (*cf.* Chapter 2, Section 2.3.2).

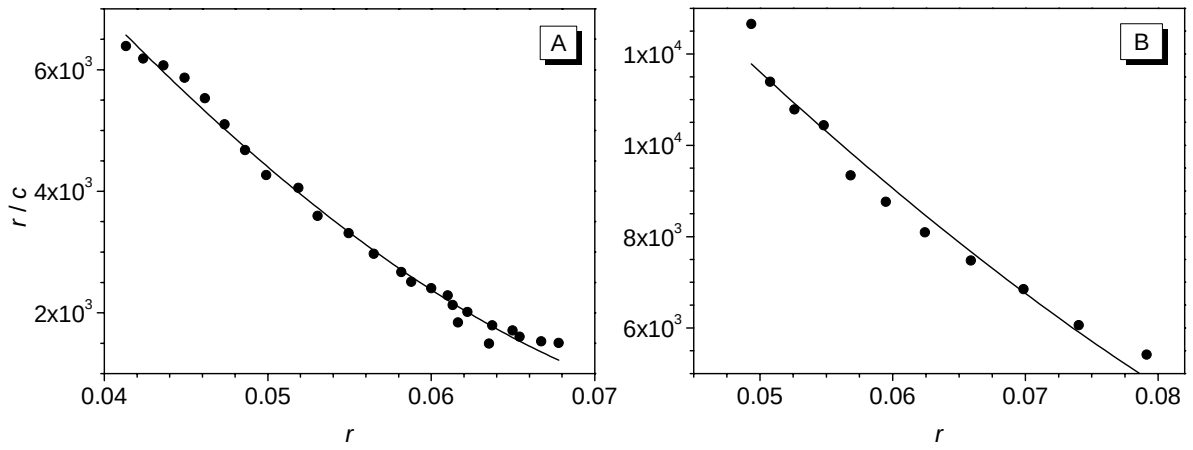

Figure 4.10. Scatchard plots of spectrophotometric titrations of ct DNA to acridizinium derivatives **55a** (A) and **55b** (B) for the determination of binding constants *K* and exclusion parameters *n*. Solid lines represent the fits to the theoretical model, calculated for the values $K = 2.1 \times 10^4$ м$^{-1}$, $n = 10$ (A) and $K = 2.7 \times 10^4$ м$^{-1}$, $n = 6.8$ (B).

The results of the thermal denaturation studies indicate that acridizinium-9-carboxamides **55a–b** show only a minor stabilization of double-stranded polynucleotides against thermal denaturation, as compared to an intercalator such as proflavine, and even smaller than the unsubstituted acridizinium ion (**5a**). In agreement with these results, no effect on the thermal denaturation of the fully-paired double-stranded oligonucleotide (TA duplex) by compound **55b** was observed. At the same time, the latter compound has a minor effect on the stabilization of the abasic double-stranded oligonucleotide (TX duplex), presumably by the intercalation at the abasic position.

The deficiency of the stabilization of ds DNA by acridizinium and acridizinium-9-carboxamides **55a–b** is surprising, considering the reasonable values of their DNA-binding constants. On the one hand, these values are significantly lower than the ones reported for proflavine **1** ($K_a = 8.8 \times 10^4$ м$^{-1}$)[158] and the amino derivatives of the acridizinium ion [$K_a = (5–6) \times 10^4$ м$^{-1}$],[10] which may be the reason for a weaker stabilization against the thermal denaturation of DNA. On the other hand, the small ΔT_m values may be due to a significant binding affinity of **5a** and **55a–b** to the single-stranded polynucleotides, as the ΔT_m values reflect a difference in binding to the duplex *vs*. single strands, and not the binding affinity to the duplex *per se*.[71] Therefore, it may be that the thermal denaturation experiments are not appropriate to study the DNA-binding properties of these particular compounds, although they may be successfully applied in many other cases (*cf.* Chapter 3 of this work and Refs. 72–73).

The even reduced affinity of the *N*-alkylacridizinium-9-carboxamides **55a–b** for association with ds DNA, as compared to the parent compound **5a**, may be due to the steric hindrance of the amido group that suppresses the intercalation into ds DNA. The alkyl substituents seem to have no impact on the magnitudes of the DNA-binding constants of the intercalators, although they have some influence on the values of the exclusion parameter *n*, as it has been shown for a series of *N*-alkylsubstituted 9-aminoacridine derivatives.[159] In contrast, the aminoalkyl substituent in compound **55c**, which is protonated in neutral aqueous solutions, provides the high affinity to double-stranded oligo- and polynucleotides, which results in an efficient stabilization of duplex structures against thermal denaturation. This effect is obviously due to an additional cationic charge of the ligand, which provides an additional stabilization through electrostatic interactions with the negatively charged phosphate groups of the DNA backbone in the grooves. Indeed, while acridine itself has a poor DNA affinity, acridine-4-carboxamide **63** (DACA), bearing the (dimethylamino)ethyl substituent, similar to the one in compound **55c**, is an efficient intercalator with a value of the DNA-binding constant of 1.3×10^6 M^{-1}.[7]

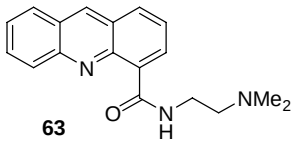

63

The introduction of the adenine residue in conjugates **54a–b** results in an enhanced affinity to abasic DNA structures, while the binding to the fully-paired oligonucleotides remains negligible, as shown by the results of the thermal denaturation experiments with TX and TA oligonucleotides. Therefore, it may be concluded that the adenine moiety interacts with the unpaired nucleic base of the abasic DNA, contributing to the overall DNA-binding properties of the conjugate. However, the stabilization of the TX oligonucleotide achieved by the acridizinium–adenine conjugates **54a–b** is much less than the one provided by the quinacrine–adenine conjugates **21a** and **21c** at similar conditions (*cf.* the $\Delta\Delta T_m$ values of 10.5 and 4.3 °C for **21c**[63] and **54b** at $r = 0.5$, respectively). The reason for such poor stabilization may be the weak DNA-binding properties of the acridizinium moiety, as compared to the quinacrine intercalator, as well as the replacement of the polycationic linking chain, as in conjugates **21a–d**, with an uncharged alkylamido linker, which does not provide additional stabilization by the interaction with the DNA backbone.

Remarkably, the most efficient stabilization of the abasic oligonucleotide is achieved by compound **55c**, which has no adenine part. Although this compound also shows the most pronounced binding to the fully paired polynucleotides among the acridizinium carboxamides, its significant selectivity for the abasic structures is clearly evidenced by the $\Delta\Delta T_m$ value of 9.6 °C at $r = 0.5$, which makes it comparable with the tailor-made conjugates **21a** and **21c**. This fact is in line with the very recent observations that the aminoalkyl-substituted acridine derivative **26**, lacking an adenine moiety, has a high preference towards abasic sites in the DNA.[66] It may be suggested that, as it has been shown for compound **26**, upon interaction with abasic oligonucleotides the intercalating part of the ligand **55c**, *i.e.* the acridizinium ion, is located in the abasic pocket, while the aminoalkyl residue resides in a minor groove, providing additional stabilization of the ligand–DNA complex. These findings urge to revise the existing concepts for the development of the ligands, aimed at the recognition of abasic sites. In particular, it may be supposed that aminoalkyl substituents, providing an additional positive charge, are essential for the overall DNA-binding properties. At the same time, the recognition of an abasic pocket may be achieved not only by the nucleic bases or base-analogues, but also by intercalators which have no specific interaction with the unpaired base opposite to the lesion, but rather an appropriate geometrical shape and π-stacking properties. Moreover, in the case of intercalator–nucleic base conjugates, such as **21a–d** and **54a–b**, a competition between the intercalator moiety and the nucleic base for the occupation of the abasic site should be considered, which may limit the abasic-site selectivity of such conjugates.

4.3.2.2 Photoinduced DNA Damage

Irradiation of supercoiled plasmid DNA in the presence of amide **55b** as well as conjugates **54a–b** at anaerobic conditions results in an efficient single-strand cleavage of the DNA, as shown by the gel-electrophoretic analysis of the photolysates. At the same time, no significant difference is observed between the photocleavage of regular and abasic-site containing plasmid forms by either photosensitizer. Moreover, amide **55b** which has lower affinity towards abasic DNA structures than the conjugates **54a–b** (*cf.* the results of the thermal denaturation experiments) induces the most efficient cleavage of both regular and abasic plasmid DNA, about 50% more efficient than the acridizinium–adenine conjugates.

The lack of the preferential photocleavage of abasic DNA by the acridizinium–adenine conjugates may be due to two reasons. Firstly, the affinity of these conjugates to abasic sites is not very pronounced, as compared to the quinacrine–adenine conjugates **21a–d**. Secondly, it

has been shown that the photoinduced DNA damage by acridizinium derivatives is mainly due to the species that are *not* intercalated into the DNA.[16] Thus, under anaerobic conditions, similar to the ones used in the current work, the irradiation of acridizinium ions results in generation of reactive oxygen species, such as hydroxyl radicals, which lead to the DNA strand cleavage by hydrogen abstraction from the sugar residues. At the same time, the intercalated species undergo an efficient excited-state deactivation by the photoinduced energy transfer to the stacked DNA bases, followed by a fast back electron-transfer process, and do not contribute significantly to the overall DNA damage.

In line with these observations, it may be supposed that the binding of the conjugates **54a–b** to the apurinic DNA samples takes place at abasic sites, but the bound conjugate species are not involved in the photoinduced DNA damage. The latter, instead, is caused by the photosensitizer species that are present in a surrounding solution and generate reactive oxygen species upon irradiation. The latter cleave the regular and abasic-site containing plasmid molecules randomly and with an equal efficiency.

The above considerations may be also applied for the explanation of the higher photocleavage efficiency of the amide **55b**, as compared to the conjugates **54a–b**. Thus, it may be supposed that the introduction of the adenine residue results in a pronounced shortening of the excited-state lifetime of the acridizinium chromophore due to an efficient deactivation pathway, namely the electron-transfer reaction with the attached adenine residue. This assumption is confirmed by a 10-fold reduction of the fluorescence quantum yield of acridizinium–adenine conjugates, as compared to the *N*-alkylamides **55a–b** and the unsubstituted acridizinium ion. Since the reactive oxygen species, such as hydroxyl radicals, are generated upon interaction of the photo-excited acridizinium ions with the solvent molecules, it may be expected that the shorter excited-state lifetimes of the conjugated **54a–b** result in a less efficient production of the former species. As a consequence, the overall DNA damage by the conjugates **54a–b** is reduced, as compared with the alkylamide **55b**.

In summary, it may be concluded that the intercalator–nucleic base conjugates represent an inefficient approach for the site-selective DNA cleavage, as long as the intercalating species do not contribute to the DNA damage. Instead, this task may be achieved *e.g.* by the combination of two identical acridizinium units with an aminoalkyl linker, such as in compounds **64a–b**. In such an approach, one acridizinium unit should provide the recognition

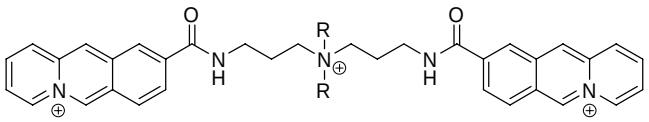

64a: R = H
64b: R = Me

of the abasic sites, as it was shown for compound **55c**. The other acridizinium moiety, which should be in a dynamic equilibrium between the intercalated and threading states, should generate reactive oxygen species upon photo-excitation, and thus cause the DNA damage. In particular, quaternization of the amino group of the linker, such as in compound **64b**, may be necessary to avoid the light-independent DNA cleavage by such compounds *via* the *β*-elimination mechanism.

5 EXPERIMENTAL PART

5.1 General Remarks

5.1.1 Instruments and Methods

The melting points were measured with a melting point apparatus (Büchi 510K) and are uncorrected. Mass-spectra (ESI in the positive-ion mode, source voltage 6 kV) were recorded with a Finnigan LCQ Deca instrument; only *m*/*z* values in the range of 100–2000 units were analyzed. NMR spectra were measured on a Bruker AC200 (^{1}H: 200 MHz, ^{13}C: 50 MHz) and Bruker Avance 400 (^{1}H: 400 MHz, ^{13}C: 100 MHz, ^{19}F: 376 MHz) spectrometer at 20 °C; chemical shifts are given in ppm (δ) values (internal standards TMS for ^{1}H- and ^{13}C-NMR spectroscopy and hexaflurobenzene, $\delta_F = -162.8$ ppm, for ^{19}F-NMR spectroscopy). Unambiguous proton NMR assignments were established with the help of {^{1}H, ^{1}H}-COSY and, if necessary, (R)NOESY (t_{mix} = 1.00 s) experiments. Infrared spectra were obtained with a Perkin–Elmer 1750 Fourier-transform spectrometer in KBr pellets; only significant and characteristic frequencies are given. Elemental microanalyses of all new compounds were performed with a HEKAtech EuroEA combustion analyzer by Mr. H. Bodenstedt (Institut für Organische Chemie, Universität Siegen). UV-visible spectra were recorded on a Varian Cary 100 double-beam spectrophotometer; fluorescence emission spectra were recorded on a Varian Cary Eclipse fluorescence spectrometer. The pH of aqueous solutions was measured with a calibrated pH-meter (Qph 70, VWR). TLC of acridizinium derivatives was performed on silica gel sheets (Macherey-Nagel Polygram Sil G/UV$_{254}$), eluent: $CHCl_3$–MeOH–AcOH 80:20:1, v/v (system A), or on RP-18 silica gel sheets (Macherey-Nagel Alugram RP-18W/UV$_{254}$), eluent: 1 M aq. HCl–MeCN 80:20, v/v (system B).

5.1.2 Reagents and Solvents

All commercially available chemicals were reagent grade and used without further purification. Diethyl ether and THF were distilled from sodium wire; DMF and DMSO were dried with calcium hydride and vacuum-distilled prior to use; ethanol and ethyl acetate were purified by rectification. Other solvents were analytical or HPLC grade and used without further purification. NMP was a generous gift from BASF AG, Ludwigshafen, Germany. If

not stated otherwise, distilled water was used for experiments. The term "purified water" refers to e-Pure™ water (resistivity 18 MΩ cm^{-1}).

The following compounds were obtained according to the published procedures: 9-bromoacridizinium bromide (**29**),[88] 9-carboxyacridizinium bromide (**56a**),[150] 4-(methylthio)benzyl bromide (**31b**),[93] 2-(1,3-dioxolan-2-yl)pyridine (**32**),[160] 2-methyisophthalic acid (**45a**),[161,162] 2,6-bis(bromomethyl)bromobenzene (**46**),[163] 2,6-bis(bromomethyl)benzotrifluoride (**47**),[164] 1,8- and 2,7-bis(bromomethyl)naphthalenes,[133,165,166] ethyl 4-(adenin-9-yl)butyrate (**60**).[153] Several attempts to prepare 1,4-bis(bromomethyl)-2,5-dimethylbenzene (**43**) by bromomethylation of *p*-xylene in 48% aq. HBr gave only 40% yield in contrast to 97% claimed by the authors.[167] It was found that the reaction with 33% HBr in glacial acetic acid gives better yield of this product.[168]

5.2 Syntheses

5.2.1 Synthesis of 9-Substituted Acridizinium Derivatives

General procedure for the reaction of 9-bromoacridizinium bromide with secondary aliphatic amines (GP-1). Salt **29** (0.34 g, 1.0 mmol) and the corresponding amine (2.0 mmol) in *i*PrOH (5 mL) were stirred under reflux for 2 h. After cooling to room temperature, the reaction mixture was evaporated to dryness and the product was isolated by column chromatography (alumina neutral, activity grade I; eluent $CHCl_3$–MeOH, 90:10 v/v). The green-fluorescing fraction was collected. The eluate was evaporated, and the residue was recrystallized from MeOH–AcOEt to give 9-*N*,*N*-dialkylaminoacridizinium bromide. The corresponding tetrafluoroborates or hexafluorophosphates were prepared by addition of aqueous HBF_4 (50%) or concentrated aqueous $NaPF_6$ solution to the solution of the bromide in minimal amount of water, followed by recrystallization of the precipitate from MeCN–AcOEt.

9-(Morpholin-4-yl)acridizinium bromide [27a (Br^-)]: yield 82 mg (24%), peach-colored needles, m.p. 140–142 °C. **27a (BF_4^-):** Orange prisms; R_f = 0.45 (system A); m.p. 256–260 °C; ^{1}H-NMR (200 MHz, CD_3OD): δ = 3.66 (m, 4 H, CH_2N), 3.89 (m, 4 H, CH_2O), 7.32 (d, ^4J = 2 Hz, 1 H, 10-H), 7.48 (dd, ^3J = 7 Hz, 1 H, 3-H), 7.72 (dd, ^3J = 9 Hz, ^3J = 7 Hz, 1 H, 2-H), 7.88 (dd, ^3J = 10 Hz, ^4J = 2 Hz, 1 H, 8-H), 8.10 (d, ^3J = 9 Hz, 1 H, 1-H), 8.21 (d, ^3J = 10 Hz, 1 H, 7-H), 8.41 (s, 1 H, 11-H), 8.79 (d, ^3J = 7 Hz, 1 H, 4-H), 9.71 (s, 1 H, 6-H);

^{13}C-NMR (100 MHz, [D$_6$]DMSO): δ = 49.5, 65.7, 101.9, 118.5, 119.1, 120.5, 122.9, 125.5, 129.6, 129.8, 133.5, 137.4, 137.8, 138.2, 153.4; MS (ESI$^+$): *m*/*z* (%) = 265 (100) [*M*]$^+$; elemental analysis calcd (%) for $C_{17}H_{17}BF_4N_2O \times ½\ H_2O$ (361.2): C 56.54, H 5.02, N 7.76; found C 56.56, H 4.76, N 7.70.

9-(Pyrrolidin-1-yl)acridizinium bromide [27b (Br$^-$)]: yield 0.10 g (30%), orange crystals. **27b (BF$_4^-$):** Orange needles; R_f = 0.57 (system A); m.p. 248–250 °C; ^{1}H-NMR (200 MHz, CD_3OD): δ = 2.15 (m, 4 H, CH_2CH_2), 3.55 (br m, 4 H, NCH_2), 6.73 (d, ^4J = 2 Hz, 1 H, 10-H), 7.30 (dd, ^3J = 7 Hz, 1 H, 3-H), 7.46 (dd, ^4J = 2 Hz, ^3J = 9 Hz, 1 H, 8-H), 7.55 (dd, ^3J = 9 Hz, ^3J = 7 Hz, 1 H, 2-H), 7.89 (d, ^3J = 9 Hz, 1 H, 1-H), 8.04 (d, ^3J = 9 Hz, 1 H, 7-H), 8.06 (s, 1 H, 11-H), 8.59 (d, ^3J = 7 Hz, 1 H, 4-H), 9.44 (s, 1 H, 6-H); ^{13}C-NMR (100 MHz, CD_3OD): δ = 26.5, 49.6, 101.1, 118.6, 119.5, 122.0, 124.3, 126.9, 130.4, 131.2, 134.3, 139.0, 139.2, 139.9, 152.9; MS (ESI$^+$): *m*/*z* (%) = 249 (100) [*M*]$^+$; elemental analysis calcd (%) for $C_{17}H_{17}BF_4N_2$ (329.2): C 60.74, H 5.10, N 8.33; found C 60.40, H 5.08, N 8.26.

9-[(2-Hydroxyethyl)methylamino]acridizinium hexafluorophosphate [27c (PF$_6^-$)]: yield 16%, orange amorphous solid; R_f = 0.37 (system A); m.p. 132–134 (shrinks at 80) °C (methyl ethyl ketone); ^{1}H-NMR (200 MHz, CD_3CN): δ = 3.22 (s, 3 H, NCH_3), 3.73–3.79 (m, 4 H, CH_2CH_2), 6.93 (d, ^4J = 2 Hz, 1 H, 10-H), 7.30 (dd, ^3J = 7 Hz, ^3J = 8 Hz, 1 H, 3-H), 7.56 (dd, ^3J = 9 Hz, ^3J = 8 Hz, 1 H, 2-H), 7.67 (dd, ^3J = 10 Hz, ^4J = 2 Hz, 1 H, 8-H), 7.87 (d, ^3J = 9 Hz, 1 H, 1-H), 8.02 (d, ^3J = 10 Hz, 1 H, 7-H), 8.06 (s, 1 H, 11-H), 8.42 (d, ^3J = 7 Hz, 1 H, 4-H), 9.21 (s, 1 H, 6-H); ^{13}C-NMR (100 MHz, CD_3CN): δ = 40.0 (CH_3), 55.3 (CH_2), 60.22 (CH_2), 101.0, 118.7, 119.6, 121.5, 123.8, 126.6, 130.3, 130.4, 134.0, 138.5, 139.0, 139.6, 154.9; MS (ESI$^+$): *m*/*z* (%) = 253 (100) [*M*]$^+$; satisfactory elemental analysis could not be obtained due to HF elimination upon drying in vacuo.

General procedure for the reaction of 9-bromoacridizinium bromide with electron-rich aromatic amines (GP-2). A solution of salt **29** (0.68 g, 2.0 mmol) and the corresponding aniline derivative (6.0 mmol) in *i*PrOH (10 mL) was stirred under reflux for 48 h. After cooling to room temperature, the reaction mixture was concentrated to approximately one-half of its original volume and poured into Et_2O (200 mL); the red precipitate was separated and recrystallized from *i*PrOH or MeOH until an analytically pure sample was obtained.

9-[4-(Dimethylamino)phenylamino]acridizinium, bromide (27d): yield 0.10 g (14%), black crystals; R_f = 0.59 (system A); m.p. 218–219 °C (*i*PrOH); ^{1}H-NMR (400 MHz,

[D$_6$]DMSO): δ = 2.94 (s, 6 H, CH_3), 6.83 (d, ^3J = 8 Hz, 2 H, 3′-H, 5′-H), 7.10 (s, 1 H, 10-H), 7.23 (d, ^3J = 8 Hz, 2 H, 2′-H, 6′-H), 7.48 (dd, ^3J = 6 Hz, 1 H, 3-H), 7.59 (d, ^3J = 9 Hz, 1 H, 8-H), 7.69 (dd, ^3J = 9 Hz, ^3J = 6 Hz, 1 H, 2-H), 8.01 (d, ^3J = 9 Hz, 1 H, 1-H), 8.16 (d, ^3J = 9 Hz, 1 H, 7-H), 8.35 (s, 1 H, 11-H), 8.84 (d, ^3J = 6 Hz, 1 H, 4-H), 9.65 (s, 1 H, NH), 9.83 (s, 1 H, 6-H); ^{13}C-NMR (100 MHz, [D$_6$]DMSO): δ = 40.3 (2 CH_3), 98.4 (CH), 113.1 (2 C, CH), 117.6 (CH), 118.6 (CH), 121.0 (C_q), 124.1 (2 CH), 125.3 (2 CH), 127.6 (C_q), 129.8 (CH), 129.9 (CH), 133.5 (CH), 137.5 (C_q), 137.8 (CH), 138.5 (C_q), 148.3 (C_q), 151.4 (C_q); MS (ESI$^+$): *m*/*z* (%) = 314 (100) $[M]^+$, 299 (61) $[M - CH_3]^+$; elemental analysis calcd (%) for $C_{21}H_{20}BrN_3 \times ½\ H_2O$ (403.3): C 62.54, H 5.25, N 10.42; found C 62.56, H 5.19, N 10.41.

9-(4-Methoxyphenylamino)acridizinium bromide (27e): yield 0.10 g (13%), dark-red prisms; R_f = 0.53 (system A); m.p. 131–132 °C (MeOH); ^{1}H-NMR (200 MHz, [D$_6$]DMSO): δ = 3.81 (s, 3 H, OCH_3), 7.07 (d, ^3J = 9 Hz, 2 H, 2′-H, 6′-H), 7.20 (d, ^4J = 2 Hz, 1 H, 10-H), 7.35 (d, ^3J = 9 Hz, 2 H, 3′-H, 5′-H), 7.53 (dd, J = 7 Hz, 1 H, 3-H), 7.63 (dd, ^3J = 9 Hz, ^4J = 2 Hz, 1 H, 8-H), 7.74 (dd, ^3J = 7 Hz, ^3J = 9 Hz, 1 H, 2-H), 8.06 (d, ^3J = 9 Hz, 1 H, 1-H), 8.22 (d, ^3J = 9 Hz, 1 H, 7-H), 8.43 (s, 1 H, 11-H), 8.88 (d, ^3J = 7 Hz, 1 H, 4-H), 9.74 (s, 1 H, NH), 9.89 (s, 1 H, 6-H); ^{13}C-NMR (50 MHz, [D$_6$]DMSO): δ = 55.4, 98.9, 114.9 (2 C), 118.0, 118.9, 121.1, 124.2 (2 C), 125.3, 125.4, 130.0, 130.1, 131.7, 133.6, 137.5, 138.0, 138.5, 150.9, 156.7; MS (ESI$^+$): *m*/*z* (%) = 301 (100) $[M]^+$; elemental analysis calcd (%) for $C_{20}H_{17}BrN_2O \times H_2O$ (399.3): C 60.16, H 4.80, N 7.02; found: C 60.29, H 5.05, N 7.02.

General procedure for the reaction of 9-bromoacridizinium bromide with electron-poor aromatic amines (GP-3). Salt **29** (1.70 g, 5.00 mmol) and the corresponding aniline derivative (20.0 mmol) were stirred in the presence of boron trifluoride–diethyl ether complex (0.20 mL) and under argon atmosphere at 150 °C for 72 h. After cooling to room temperature, the melt was triturated with Et_2O (3 × 50 mL) until a brown friable powder was obtained. The solid was separated, washed thoroughly with diethyl ether and ethyl acetate, dried and recrystallized from acetic acid (with charcoal) and then several times from methanol or water until an analytically pure sample was obtained.

9-(4-Toluidino)acridizinium bromide (27f): yield 1.40 g (77%), orange needles; R_f = 0.40 (system A); m.p. (dec.) 255 °C (MeOH); ^{1}H-NMR (400 MHz, [D$_6$]DMSO): δ = 2.35 (s, 3 H, CH_3), 7.28–7.34 (m, 5 H, 4 Ar-H + 10-H), 7.54 (dd, ^3J = 7 Hz, 1 H, 3-H), 7.65 (dd, ^3J = 9 Hz, ^4J = 2 Hz, 1 H, 8-H), 7.75 (dd, ^3J = 7 Hz, ^3J = 9 Hz, 1 H, 2-H), 8.08 (d, ^3J = 9 Hz, 1 H, 1-H), 8.22 (d, ^3J = 9 Hz, 1 H, 7-H), 8.47 (s, 1 H, 11-H), 8.89 (d, ^3J = 7 Hz, 1 H, 4-H), 9.80 (s, 1 H,

NH), 9.91 (s, 1 H, 6-H); ^{13}C-NMR (100 MHz, [D$_6$]DMSO): δ = 20.6, 99.5, 118.3, 119.0, 121.2, 121.9 (2 C), 125.5 (2 C), 130.0, 130.1 (2 C), 133.5, 133.9, 136.5, 137.5, 138.0, 138.4, 150.2, 153.6; MS (ESI$^+$): *m*/*z* (%) = 285 (100) [*M*]$^+$; elemental analysis calcd (%) for $C_{20}H_{17}BrN_2$ (365.3): C 65.76, H 4.69, N 7.67; found: C 65.53, H 4.58, N 7.65.

9-(Phenylamino)acridizinium bromide (27g): yield 0.40 g (23%), orange needles; R_f = 0.33 (system A); m.p. (dec.) 110–112 °C (AcOH–H_2O); ^{1}H-NMR (400 MHz, [D$_6$]DMSO): δ = 7.22 (dd, ^3J = 7 Hz, 1 H, Ar-H), 7.43–7.50 (m, 5 H, 4 Ar-H + 10-H), 7.55 (dd, ^3J = 7 Hz, 1 H, 3-H), 7.69 (dd, ^3J = 9 Hz, ^4J = 2 Hz, 1 H, 8-H), 7.76 (dd, ^3J = 7 Hz, ^3J = 9 Hz, 1 H, 2-H), 8.10 (d, ^3J = 9 Hz, 1 H, 1-H), 8.26 (d, ^3J = 9 Hz, 1 H, 7-H), 8.52 (s, 1 H, 11-H), 8.94 (d, ^3J = 7 Hz, 1 H, 4-H), 9.87 (s, 1 H, NH); 9.98 (s, 1 H, 6-H); ^{13}C-NMR (100 MHz, [D$_6$]DMSO): δ = 100.0 (CH), 118.6 (CH), 119.1 (CH), 121.3 (C$_q$), 121.5 (2 CH), 124.4 (CH), 125.5 (CH), 125.6 (CH), 129.6 (2 CH), 130.1 (CH), 133.6 (CH), 137.5 (C$_q$), 138.2 (C$_q$), 138.3 (CH), 139.3 (C$_q$), 149.7 (C$_q$); MS (ESI$^+$): *m*/*z* (%) = 271 (100) [*M*]$^+$; elemental analysis calcd (%) for $C_{19}H_{15}BrN_2 \times ½\ H_2O$ (360.3): C 63.35, H 4.48, N 7.78; found: C 63.00, H 4.36, N 7.73.

9-(4-Fluorophenylamino)acridizinium bromide (27h): yield 1.05 g (57%), brick-red needles; R_f = 0.47 (system A); m.p. > 250 °C (MeCN–EtOH); ^{1}H-NMR (400 MHz, [D$_6$]DMSO): δ = 7.31–7.35 (m, 3 Ar-H), 7.45–7.49 (m, 2 Ar-H), 7.57 (dd, ^3J = 7 Hz, 1 H, 3-H), 7.66 (dd, ^3J = 9 Hz, ^4J = 2 Hz, 1 H, 8-H), 7.77 (dd, ^3J = 7 Hz, ^3J = 9 Hz, 1 H, 2-H), 8.11 (d, ^3J = 9 Hz, 1 H, 1-H), 8.26 (d, ^3J = 9 Hz, 1 H, 7-H), 8.51 (s, 1 H, 11-H), 8.92 (d, ^3J = 7 Hz, 1 H, 4-H), 9.84 (s, 1 H, NH); 9.94 (s, 1 H, 6-H); ^{13}C-NMR (100 MHz, [D$_6$]DMSO): δ = 99.6 (CH), 116.4 (d, 2 CH, $^2J_{C,F}$ = 22.6 Hz), 118.5 (CH), 119.2 (CH), 121.3 (C$_q$), 124.1 (d, 2 CH, $^3J_{C,F}$ = 8.3 Hz), 125.4 (CH), 125.5 (CH), 130.1 (CH), 133.6 (CH), 135.5 (d, C$_q$, $^4J_{C,F}$ = 2.6 Hz), 137.4 (C$_q$), 138.1 (C$_q$), 138.3 (CH), 150.1 (C$_q$), 159.0 (d, C$_q$, $^1J_{C,F}$ = 241.6 Hz); ^{19}F-NMR (376 MHz, [D$_6$]DMSO): δ = −117.6 (sept, *J* = 4.3 Hz, Ar-F); MS (ESI$^+$): *m*/*z* (%) = 289 (100) [*M*]$^+$; elemental analysis calcd (%) for $C_{19}H_{14}BrFN_2 \times 0.2\ H_2O$ (372.8): C 61.21, H 3.89, N 7.51; found: C 61.16, H 3.82, N 7.57.

9-(4-Bromophenylamino)acridizinium bromide (27i): yield 0.10 g (11%), yellow-red prisms; R_f = 0.50 (system A); m.p. (dec.) 240–242 °C (*i*PrOH–MeOH); ^{1}H-NMR (400 MHz, [D$_6$]DMSO): δ = 7.41 (d, ^3J = 9 Hz, 2 H, 2′-H, 6′-H), 7.51 (d, ^4J = 1 Hz, 1 H, 10-H), 7.60 (dd, ^3J = 7 Hz, 1 H, 3-H), 7.64 (d, ^3J = 9 Hz, 2 H, 3′-H, 5′-H), 7.69 (dd, ^3J = 9 Hz, ^4J = 1 Hz, 1 H, 8-H), 7.80 (dd, ^3J = 9 Hz, ^3J = 7 Hz, 1 H, 2-H), 8.15 (d, ^3J = 9 Hz, 1 H, 1-H), 8.28 (d, ^3J = 9 Hz, 1 H, 7-H), 8.56 (s, 1 H, 11-H), 8.95 (d, ^3J = 7 Hz, 1 H, 4-H), 9.95 (s, 1 H, NH), 9.99 (s, 1 H, 6-H); ^{13}C-NMR (50 MHz, [D$_6$]DMSO): δ = 100.7, 115.8, 119.0, 119.1, 119.5,

121.5, 121.9, 123.2 (2 C), 125.7, 130.1, 130.3, 132.4 (2 C), 133.7, 137.5, 138.3, 138.9, 149.0; MS (ESI^+): *m*/*z* (%) = 349 (100) $[M]^+$, 270 (7) $[M - Br]^+$; elemental analysis calcd (%) for $C_{19}H_{14}Br_2N_2$ (430.1): C 53.05, H 3.28, N 6.51; found: C 52.57, H 3.19, N 6.46.

9-(4-Chlorophenylamino)acridizinium bromide (27j): yield 0.29 g (15%), fine bright-orange needles; R_f = 0.56 (system A); m.p. 149–151 °C; ^{1}H-NMR (400 MHz, [D$_6$]DMSO): δ = 7.45–7.52 (m, 5 H, 10-H + 4 Ar-H), 7.59 (dd, ^3J = 7 Hz, 1 H, 3-H), 7.70 (d, ^3J = 9 Hz, 1 H, 8-H), 7.79 (dd, ^3J = 7 Hz, ^3J = 9 Hz, 1 H, 2-H), 8.14 (d, ^3J = 9 Hz, 1 H, 1-H), 8.26 (d, ^3J = 9 Hz, 1 H, 7-H), 8.55 (s, 1 H, 11-H), 8.95 (d, ^3J = 7 Hz, 1 H, 4-H), 9.99 (br s, 2 H, NH + 6-H); ^{13}C-NMR (100 MHz, [D$_6$]DMSO): δ = 100.5, 118.9, 119.4, 121.4, 122.8 (2 C), 125.6 (2 C), 127.8, 129.5 (2 C), 130.0, 130.2, 133.6, 137.5, 138.2, 138.4, 149.1; MS (ESI^+): *m*/*z* (%) = 305 (100) $[M]^+$; elemental analysis calcd (%) for $C_{19}H_{14}BrClN_2$ (385.7): C 59.17, H 3.66, N 7.26; found C 59.06, H 3.71, N 7.23.

9-(3-Chlorophenylamino)acridizinium bromide (27k): yield 0.39 g (20%), yellow prisms; R_f = 0.56 (system A); m.p. 277–279 °C; ^{1}H-NMR (400 MHz, [D$_6$]DMSO): δ = 7.23 (d, ^3J = 8 Hz, 1 H, 6′-H), 7.41–7.51 (m, 3 Ar-H), 7.56 (d, ^4J = 2 Hz, 1 H, 10-H), 7.61 (dd, ^3J = 7 Hz, 1 H, 3-H), 7.72 (dd, ^3J = 9 Hz, ^4J = 1.7 Hz, 1 H, 8-H), 7.81 (dd, ^3J = 7 Hz, ^3J = 9 Hz, 1 H, 2-H), 8.16 (d, ^3J = 9 Hz, 1 H, 1-H), 8.28 (d, ^3J = 9 Hz, 1 H, 7-H), 8.63 (s, 1 H, 11-H), 8.97 (d, ^3J = 7 Hz, 1 H, 4-H), 10.02 (br s, 2 H, NH + 6-H); ^{13}C NMR (100 MHz, [D$_6$]DMSO): δ = 101.1, 119.3, 119.4, 119.5, 120.3, 121.5, 123.7, 125.6 (2 C), 130.0, 130.2, 131.2, 133.6, 133.8, 137.4, 138.1, 138.3, 141.1, 148.7; MS (ESI^+): *m*/*z* (%) = 305 (100) $[M]^+$; elemental analysis calcd (%) for $C_{19}H_{14}BrClN_2 \times ½\ H_2O$ (394.7): C 57.82, H 3.83, N 7.10; found C 58.04, H 3.61, N 7.13.

9-[(2-Acetoxyethyl)methylamino]acridizinium hexafluorophosphate [27ℓ (PF_6^-)]: A solution of **27c (PF_6^-)** (80 mg, 0.20 mmol) in pyridine (0.50 mL) was treated with acetic anhydride (0.50 mL) and the reaction mixture was stirred for 18 h at room temperature, while an orange precipitate has formed. Methanol (5 mL) was added carefully, and the mixture was evaporated to dryness in vacuo. The orange solid residue was recrystallized from ethanol, to give analytically pure product (64 mg, 73%) as maroon prisms, m.p. (dec.) 182–184 °C; R_f = 0.51 (system A); ^{1}H-NMR (200 MHz, CD_3CN): δ = 1.91 (s, 3 H, CH_3CO), 3.21 (s, 3 H, NCH_3), 3.87 (t, ^3J = 6 Hz, NCH_2), 4.32 (t, ^3J = 6 Hz, 2 H, CH_2OAc), 6.98 (d, ^4J = 2 Hz, 1 H, 10-H), 7.33 (dd, ^3J = 7 Hz, 1 H, 3-H), 7.59 (dd, ^3J = 7 Hz, ^3J = 9 Hz, 1 H, 2-H), 7.66 (dd, ^3J = 10 Hz, ^4J = 2 Hz, 1 H, 8-H), 7.91 (d, ^3J = 9 Hz, 1 H, 1-H), 9.07 (d, ^3J = 10 Hz, 1 H, 7-H),

8.12 (s, 1 H, 11-H), 8.46 (d, ^3J = 7 Hz, 1 H, 4-H), 9.27 (s, 1 H, 6-H); ^{13}C-NMR (100 MHz, CD_3CN): δ = 21.0 (*C*H_3CO), 39.9 (NCH_3), 51.7 (CH_2OAc), 62.1 (NCH_2), 101.2, 119.1, 119.8, 121.5, 123.4, 126.6, 130.5 (2 C), 134.0, 138.6, 138.9, 139.5, 154.4, 171.7 (COO); IR (KBr): $\tilde{\nu}_{max}$ = 839 (PF_6^-), 1510s, 1614m, 1635s, 1731s (CO) cm^{-1}; MS (ESI$^+$): *m*/*z* (%) = 295 (100) [*M*]$^+$, 235 (6) [*M* − CH_3COO]; elemental analysis calcd (%) for $C_{18}H_{19}F_6N_2O_2P$ (440.3): C 49.10, H 4.35, N 6.36; found C 49.01, H 4.12, N 6.41.

2-(1,3-Dioxolan-2-yl)-1-[4-(methylthio)benzyl]pyridinium bromide (33): A solution of 4-(methylthio)benzyl bromide (**31b**; 11.9 g, 51.1 mmol) and 2-(1,3-dioxolan-2-yl)pyridine (**32**; 8.50 g, 56.2 mmol) in DMSO (10 mL) was stirred at room temperature under argon for 7 days and then poured into AcOEt (250 mL). After stirring for 30 min, the solvent was decanted, and the residual oil was triturated with acetone until a white solid has formed. It was collected, washed with acetone, anhydrous Et_2O, and dried in vacuo / P_2O_5 to give 18.5 g (98%) of a white amorphous product, which was used without further purification. An analytically pure sample was obtained by crystallization from *i*PrOH–AcOEt; large prisms, m.p. 113–115 °C; ^{1}H-NMR (400 MHz, CD_3OD): δ = 2.49 (s, 3 H, SCH_3), 4.21 (s, 4 H, OCH_2), 6.00 (s, 2 H, CH_2N^+), 6.46 (s, 1 H, C*H*($OCH_2)_2$), 7.33 (br s, 4 H, Ar-H), 8.11 (dd, ^3J = 6 Hz, ^3J = 8 Hz, 1 H, 5′-H), 8.39 (dd, ^3J = 8 Hz, ^4J = 1 Hz, 1 H, 3′-H), 8.68 (dd, ^3J = 8 Hz, ^3J = 8 Hz, 1 H, 4′-H), 8.92 (d, ^3J = 6 Hz, 1 H, 6′-H); ^{13}C-NMR (100 MHz, CD_3OD): δ = 15.1, 61.7, 67.4, 99.0, 127.3, 127.7, 129.6, 130.2, 130.5, 142.9, 147.9, 148.2, 154.2; elemental analysis calcd (%) for $C_{16}H_{18}BrNO_2S$ (368.3): C 52.18, H 4.93, N 3.80, S 8.71; found: C 52.25, H 4.92, N 3.87, S 8.99.

9-(Methylthio)acridizinium tetrafluoroborate (28): Salt **33** (5.50 g, 15.0 mmol) in methanesulfonic acid (20 mL) was stirred under argon at 80 °C for 1 h. After cooling to 40 °C, the reaction mixture was poured onto crushed ice (60 g). The solution was treated with $NaBF_4$ (6.60 g, 60.0 mmol) in water (6 mL). The yellow precipitate was collected, washed with cold water (3 × 10 mL) and dried in vacuo / P_2O_5, to give 3.80 g (81%) of the product. A sample was recrystallized from MeCN–AcOEt; yellow prisms; m.p. (dec.) 204–206 °C; R_f = 0.50 (system A); ^{1}H-NMR (200 MHz, [D_6]DMSO): δ = 2.73 (s, 3 H, SCH_3), 7.79–7.89 (m, 2 H, 3-H, 8-H), 7.97 (s, 1 H, 10-H), 8.03 (d, ^3J = 7 Hz, 1 H, 2-H), 8.29 (d, ^3J = 9 Hz, 1 H, 7-H), 8.46 (d, ^3J = 9 Hz, 1 H, 1-H), 8.88 (s, 1 H, 11-H), 9.14 (d, ^3J = 7 Hz, 1 H, 4-H), 10.21 (s, 1 H, 6-H); ^{13}C-NMR (50 MHz, [D_6]DMSO): δ = 14.1 (SCH_3), 117.9, 121.5, 121.6, 123.8,

126.6, 127.6, 130.2, 131.2, 134.3, 135.6, 138.1, 139.6, 149.4; MS (ESI^+): *m*/*z* (%) = 226 (100) $[M]^+$, 211 (9) $[M - CH_3]^+$, 539 (16) $[2M + BF_4]^+$; elemental analysis calcd (%) for $C_{14}H_{12}BF_4NS$ (313.1): C 53.70, H 3.86, N 4.47, S 10.24; found C 53.56, H 3.84, N 4.62, S 10.37.

5.2.2 Synthesis of Diazoniapolycyclic Salts

2,6-Bis(hydroxymethyl)toluene (45b): Although this compound has been previously prepared by esterifiction of the 2-methylisophthalic acid (**45a**), followed by reduction of the diester with lithium aluminium hydride,[161,162] or by two-step reduction of 2,6-dicyano-toluene,[169] in the current work the acid **45a** was reduced directly to compound **45b** by the action of borane–THF complex.[170] Indeed, this reduction has proved to be less labor-consuming and gave the desired product in 92% yield, thus improved with respect to the 87% obtained by the two-step sequence.

A solution of the acid **45a** (7.21 g, 40.0 mmol) in anhydrous THF (100 mL) was cooled to 0 °C and deoxygenated by passing argon gas through the solution. To a stirred solution, borane (100 mL of 1 M THF-complex, 100 mmol) was added dropwise under argon atmosphere within 4 h, whereas the reaction mixture has turned into a jelly-like bulk. After standing for 18 h at room temperature, water (100 mL) was added carefully. After hydrogen evolution has ceased, the solution was saturated with solid potassium carbonate. The organic layer was separated; the aqueous layer was extracted with diethyl ether (3 × 30 mL) and the combined organic layers were washed with water and dried with anhydrous magnesium sulfate. After removal of the solvents in vacuo, **45b** (5.60 g, 92%) was obtained as a white solid, m.p. 116–118 °C (lit.[161,169] 122–124 °C), which was used without further purification; ^{1}H-NMR (200 MHz, [D$_6$]DMSO): δ = 2.15 (s, 3 H, CH_3), 4.49 (d, ^3J = 5 Hz, 4 H, CH_2), 5.05 (t, ^3J = 5 Hz, 2 H, OH), 7.11 (m, 1 H, 4-H), 7.25 (m, 2 H, 3-H, 5-H); ^{13}C-NMR (50 MHz, [D$_6$]DMSO): δ = 13.8 (CH_3), 62.1 (CH_2OH), 125.9 (C4), 127.0 (C3, C5), 134.0 (C1), 140.3 (C2, C6).

2,6-Bis(bromomethyl)toluene (**45c):** Dialcohol **45b** (5.40 g, 35.5 mmol) in 48% aq. HBr (45 mL) was stirred at 50 °C for 60 min. After cooling to room temperature, the solid was separated, dissolved in benzene and dried with Al_2O_3. After filtration, the solvent was removed in vacuo, to leave the product (8.42 g, 85%) as an off-white solid, which was used in

the next step without further purification; m.p. 85–87 °C (lit.[161,162] 94–95 °C); ^{1}H-NMR (200 MHz, $CDCl_3$): δ = 2.44 (s, 3 H, CH_3), 4.53 (s, 4 H, CH_2Br), 7.15 (t, ^{3}J = 7 Hz, 1 H, 4-H), 7.30 (d, ^{3}J = 7 Hz, 2 H, 3-H, 5-H); ^{13}C-NMR (50 MHz, $CDCl_3$): δ = 14.2 (CH_3), 32.4 (CH_2Br), 126.4 (CH, C4), 130.8 (2 CH, C3, C5), 136.8 (C_q, C1), 136.9 (2 C_q, C2, C6).

1,7-Dimethylnaphthalene (49): 2-Methylbenzylmagnesium bromide was prepared by dropwise addition of 2-methylbenzyl bromide (58.6 g, 42.5 mL, 317 mmol), dissolved in anhydrous diethyl ether (200 mL), to magnesium turnings (9.20 g, 380 mmol), suspended in anhydrous diethyl ether (50 mL). After addition was complete (1.5 h), the reaction mixture was heated under reflux for 30 min and cooled to room temperature. A solution of acetylacetaldehyde dimethyl acetal (40.2 g, 304 mmol) in anhydrous ether (65 mL) was added dropwise within 30 min under vigorous stirring, whereas a clammy, voluminous pale-yellow precipitate has formed. After addition was complete, the reaction mixture was heated under reflux for 15 h, whereas the precipitate became orange-red. After cooling, the reaction mixture was poured onto a mixture of ice (125 g) and saturated NH_4Cl solution (190 mL). The solid mass from the reaction flask was triturated and also transferred into aqueous NH_4Cl–diethyl ether mixture, and the latter was stirred until almost all solid dissolved. The emulsion was filtered through a paper filter and transferred into a separatory funnel. The organic layer was separated. The aqueous layer was extracted with diethyl ether (3 × 130 mL), and organic layers were combined, washed with water (100 mL), brine (150 mL) and dried with anhydrous Na_2SO_4. After removal of the solvent in vacuo, the yellow oily residue (55.2 g) was dissolved in acetic acid (320 mL), and 48% aq. HBr (250 mL) was added. The reaction mixture was stirred at 105–110 °C (weak reflux) for 2 h. After cooling to 50 °C, a part of the solvent (ca 250 mL) was evaporated in vacuo (50 mbar, 50–60 °C), and the black residue was poured onto ice (320 g). The mixture was extracted with dichloromethane (3 × 250 mL); the combined organic layers were washed with water (100 mL) and dried with anhydrous Na_2SO_4. After removal of the solvent in vacuo, the residual oil was vacuum-distilled (14–15 mbar), and the fraction boiling at 125–130 °C was collected. Colorless liquid; yield 17.8 g (38%); n_D = 1.6056 (lit.[131] 1.6068); ^{1}H-NMR (400 MHz, $CDCl_3$): δ = 2.59 (s, 3 H), 2.71 (s, 3 H), 7.32–7.37 (m, 3 H), 7.70 (d, ^{3}J = 7 Hz, 1 H), 7.77–7.80 (m, 2 H); ^{13}C-NMR (100 MHz, $CDCl_3$): δ = 19.6 (CH_3), 22.3 (CH_3), 123.4 (CH), 124.8 (CH), 126.3 (CH), 126.8 (CH), 127.9 (CH), 128.5 (CH), 131.9 (C_q), 132.9 (C_q), 133.7 (C_q), 135.5 (C_q).

1,7-Bis(bromomethyl)naphthalene (50): To a boiling solution of 1,7-dimethylnaphthalene (**49**; 6.25 g, 40.0 mmol) in carbon tetrachloride (150 mL), a mixture of NBS (15.0 g, 84.0 mmol) and benzoyl peroxide (0.10 g) was added in several portions within 30 min. After completion of addition, the reaction mixture was stirred under reflux for further 3½ h and cooled to room temperature. The mixture was filtered and the residue was washed with dichloromethane (5 × 20 mL). The filtrate was evaporated in vacuo; the residue was dissolved in dichloromethane (ca. 200 mL) and washed with ice-cold water (3 × 50 mL). The organic layer was dried over anhydrous Na_2SO_4 and the solvent removed in vacuo, to give pale yellow residue (11.9 g). The crude product was recrystallized from chloroform–*n*-hexane (1:1), yielding 6.10 g (49%) of fine colorless needles, m.p. 129–130 °C (lit.[166a] 132 °C); R_f = 0.57 (SiO_2; *n*-hexane–ethyl acetate 8:2); ^{1}H-NMR (400 MHz, $CDCl_3$): δ = 4.72 (s, 2 H, C7−CH_2Br), 4.95 (s, 2 H, C1−CH_2Br), 7.42 (dd, ^3J = 8 Hz, ^3J = 8.3 Hz, 1 H, 3-H), 7.55–7.57 (m, 2 H, 2-H, 6-H), 7.82 (d, ^3J = 8 Hz, 1 H, 4-H), 7.88 (d, ^3J = 8 Hz, 1 H, 5-H), 8.12 (s, 1 H, 8-H); ^{13}C-NMR (100 MHz, $CDCl_3$): δ = 31.6 (CH_2Br), 34.3 (CH_2Br), 123.9 (CH), 126.3 (CH), 127.4 (CH), 128.5 (CH), 129.7 (CH), 129.9 (CH), 131.1 (C_q), 133.6 (C_q), 133.9 (C_q), 136.1 (C_q).

General procedure for quaternizations of bis(bromomethyl)arenes with 2-(1,3-dioxolan-2-yl)pyridine (GP-4). To a solution of bis(bromomethyl)arene (20.0 mmol) in a minimal amount of DMSO or NMP (usually 15–20 mL), 2-(1,3-dioxolan-2-yl)pyridine **32** (7.25 g, 48.0 mmol) was added. The reaction mixture was stirred for 5–7 days under moisture protection, whereas a white precipitate has formed. The reaction mixture was poured into ethyl acetate (300 mL), the solid was separated, washed several times with ethyl acetate and anhydrous diethyl ether, and dried in vacuo / P_2O_5, to give the white, amorphous, usually hygroscopic dibromide salt **40 (2Br$^-$)**, **41 (2Br$^-$)**, or **48 (2Br$^-$)**.

A part of the crude dibromide salt (10.0 mmol) was dissolved in minimal amount of water (ca. 10 mL) and treated with concentrated aqueous solution of $NaBF_4$ (4.40 g, 40.0 mmol). The milky reaction mixture was heated gently until a clear solution was obtained. Upon slow cooling to +5 °C, the corrsponding bis(tetrafluoroborate) separated almost quantitatively as a crystalline solid. It was separated, washed with cold water, and dried in vacuo over P_2O_5.

1,2-Bis{[1-(1,3-dioxolan-2-yl)pyridinium]methyl}benzene dibromide [41a (2Br$^-$)] was prepared from *α*,*α*′-dibromo-*o*-xylene; yield 9.62 g (85%); m.p. 182–183 °C (EtOH; lit.[126a] 185–186 °C). **41a (2BF_4^-):** m.p. 194–195 °C (water); ^{1}H-NMR (400 MHz, [D_6]DMSO):

δ = 4.09 (m, 8 H, CH(OCH_2)$_2$), 6.09 (s, 4 H, CH_2N^+), 6.46 (s, 2 H, CH(OCH$_2$)$_2$), 6.84 (AA′BB′, 2 H, 3-H, 6-H), 7.45 (AA′BB′, 2 H, 4-H, 5-H), 8.26 (dd, ^3J = 8 Hz, ^3J = 6 Hz, 2 H, 5′-H), 8.40 (d, ^3J = 8 Hz, 2 H, 3′-H), 8.79 (dd, ^3J = 8 Hz, 2 H, 4′-H), 8.89 (d, ^3J = 6 Hz, 2 H, 6′-H).

1,4-Bis{[1-(1,3-dioxolan-2-yl)pyridinium]methyl}benzene dibromide [41b (2Br$^-$)] was prepared from α,α'-dibromo-*p*-xylene; yield 11.0 g (97%); m.p. 196–198 °C (EtOH; lit.[126a] 195–199 °C). **41b (2BF$_4^-$):** m.p. (dec.) 195 °C (water); ^{1}H-NMR (400 MHz, [D$_6$]DMSO): δ = 4.10 (m, 8 H, CH(OCH_2)$_2$), 6.00 (s, 4 H, CH_2N^+), 6.46 (s, 2 H, CH(OCH$_2$)$_2$), 6.84 (AA′BB′, 2 H, 3-H, 6-H), 7.38 (s, 4 H, 2-H, 3-H, 5-H, 6-H), 8.20 (dd, ^3J = 8 Hz, ^3J = 6 Hz, 2 H, 5′-H), 8.33 (d, ^3J = 8 Hz, 2 H, 3′-H), 8.72 (dd, ^3J = 8 Hz, 2 H, 4′-H), 9.02 (d, ^3J = 6 Hz, 2 H, 6′-H).

1,3-Bis{[1-(1,3-dioxolan-2-yl)pyridinium]methyl}benzene dibromide [41c (2Br$^-$)] was prepared from α,α'-dibromo-*m*-xylene; yield 9.0 g (80%); m.p. (dec.) 93–94 °C (EtOH; lit.[126a] 95.5–97 °C). **41c (2BF$_4^-$):** m.p. 94–96 °C (water); ^{1}H-NMR (200 MHz, [D$_6$]DMSO): δ = 4.08 (s, 8 H, CH(OCH_2)$_2$), 5.98 (s, 4 H, CH_2N^+), 6.43 (s, 2 H, CH(OCH$_2$)$_2$), 7.21 (s, 1 H, 2-H), 7.37 (d, ^3J = 7 Hz, 2 H, 4-H, 6-H), 7.52 (dd, ^3J = 7 Hz, 1 H, 5-H), 8.21 (dd, ^3J = 8 Hz, ^3J = 6 Hz, 2 H, 5′-H), 8.32 (d, ^3J = 8 Hz, 2 H, 3′-H), 8.73 (dd, ^3J = 8 Hz, 2 H, 4′-H), 9.01 (d, ^3J = 6 Hz, 2 H, 6′-H).

1,4-Bis{[1-(1,3-dioxolan-2-yl)pyridinium]methyl}-2,5-dimethylbenzene dibromide [40a (2Br$^-$)] was prepared from **43**; yield 11.3 g (95%); m.p. (dec.) 186–188 °C (EtOH). **40a (2BF$_4^-$):** m.p. 240–242 °C (EtOH–MeCN); ^{1}H-NMR (400 MHz, [D$_6$]DMSO): δ = 2.20 (s, 6 H, CH_3), 4.11 (s, 8 H, CH(OCH_2)$_2$), 5.95 (s, 4 H, CH_2N^+), 6.46 (s, 2 H, CH(OCH$_2$)$_2$), 6.73 (s, 2 H, 3-H, 6-H), 8.20 (dd, ^3J = 7 Hz, ^3J = 6 Hz, 2 H, 5′-H), 8.37 (d, ^3J = 7 Hz, 2 H, 3′-H), 8.74–8.90 (m, 4 H, 4′-H, 6′-H); ^{13}C-NMR (100 MHz, [D$_6$]DMSO): δ = 18.1 (CH_3), 57.8 (CH_2N^+), 65.6 (CH(O*C*H$_2$)$_2$), 97.1 (*C*H(OCH$_2$)$_2$), 126.2 (CH), 128.7 (CH), 129.9 (CH), 132.4 (C_q), 134.7 (C_q), 146.7 (CH), 147.4 (CH), 152.2 (C_q); elemental analysis calcd (%) for $C_{26}H_{30}B_2F_8N_2O_4$ (608.1): C 51.35, H 4.97, N 4.61; found: C 51.14, H 4.90, N 4.64.

2,6-Bis{[1-(1,3-dioxolan-2-yl)pyridinium]methyl}toluene dibromide [40b (2Br$^-$)] was prepared from **45c**; yield 11.1 g (96%); m.p. (dec.) 130–133 °C (EtOH). **40b (2BF$_4^-$):** m.p. 174–176 °C (water); ^{1}H-NMR (400 MHz, [D$_6$]DMSO): δ = 2.23 (s, 3 H, CH_3), 4.11 (s, 8 H, CH(OCH_2)$_2$), 6.07 (s, 4 H, CH_2N^+), 6.50 (s, 2 H, CH(OCH$_2$)$_2$), 6.86 (d, ^3J = 8 Hz, 2 H, 3-H, 5-H), 7.29 (t, ^3J = 8 Hz, 1 H, 4-H), 8.20 (dd, ^3J = 8 Hz, ^3J = 6 Hz, 2 H, 5′-H), 8.38 (d,

^3J = 8 Hz, 2 H, 3′-H), 8.74–8.78 (m, 4 H, 4′-H, 6′-H); ^{13}C-NMR (100 MHz, [D$_6$]DMSO): δ = 14.2 (CH_3), 58.4 (CH_2N^+), 65.6 (CH(O*C*H$_2$)$_2$), 97.1 (*C*H(OCH$_2$)$_2$), 126.2 (CH), 127.3 (CH), 128.7 (CH), 128.8 (CH), 132.7 (C_q), 135.3 (C_q), 146.5 (CH), 147.4 (CH), 152.3 (C_q); elemental analysis calcd (%) for $C_{25}H_{28}B_2F_8N_2O_4$ (594.1): C 50.54, H 4.75, N 4.72; found: C 50.57, H 4.52, N 4.72.

2,6-Bis{[1-(1,3-dioxolan-2-yl)pyridinium]methyl}bromobenzene dibromide [40c (2Br$^-$)] was prepared from **46**; yield 11.7 g (91%); m.p. 175–178 °C (EtOH). **40c (2BF$_4^-$):** m.p. 196–200 °C (water); ^{1}H-NMR (400 MHz, [D$_6$]DMSO): δ = 4.07 (s, 8 H, CH(OC*H*$_2$)$_2$), 6.11 (s, 4 H, CH_2N^+), 6.49 (s, 2 H, C*H*(OCH$_2$)$_2$), 6.91 (d, ^3J = 8 Hz, 2 H, 3-H, 5-H), 7.44 (t, ^3J = 8 Hz, 1 H, 4-H), 8.26 (dd, ^3J = 8 Hz, ^3J = 6 Hz, 2 H, 5′-H), 8.39 (d, ^3J = 8 Hz, 2 H, 3′-H), 8.80 (dd, ^3J = 8 Hz, 2 H, 4′-H), 8.96 (d, ^3J = 6 Hz, 2 H, 6′-H); ^{13}C-NMR (100 MHz, [D$_6$]DMSO): δ = 60.6 (CH_2N^+), 65.6 (CH(O*C*H$_2$)$_2$), 97.2 (*C*H(OCH$_2$)$_2$), 123.2 (C_q), 126.4 (CH), 128.8 (CH), 129.1 (CH), 129.8 (CH), 134.4 (C_q), 147.3 (CH), 147.8 (CH), 152.3 (C_q); elemental analysis calcd (%) for $C_{24}H_{25}B_2BrF_8N_2O_4$ (659.0): C 43.74, H 3.82, N 4.25; found: C 43.39, H 3.77, N 4.21.

2,6-Bis{[1-(1,3-dioxolan-2-yl)pyridinium]methyl}benzotrifluoride dibromide [40d (2Br$^-$)] was prepared from **47**; yield 9.2 g (72%); m.p. 149–151 °C (EtOH). **40d (2BF$_4^-$):** m.p. 196–198 °C (water); ^{1}H-NMR (400 MHz, [D$_6$]DMSO): δ = 4.05 (m, 8 H, CH(OC*H*$_2$)$_2$), 6.27 (s, 4 H, CH_2N^+), 6.43 (s, 2 H, C*H*(OCH$_2$)$_2$), 6.85 (d, ^3J = 8 Hz, 2 H, 3-H, 5-H), 7.62 (t, ^3J = 8 Hz, 1 H, 4-H), 8.29 (dd, ^3J = 8 Hz, ^3J = 6.0 Hz, 2 H, 5′-H), 8.40 (d, ^3J = 8 Hz, 2 H, 3′-H), 8.82 (dd, ^3J = 8 Hz, 2 H, 4′-H), 9.01 (d, ^3J = 6 Hz, 2 H, 6′-H); ^{13}C-NMR (100 MHz, [D$_6$]DMSO): δ = 58.3 (q, $^4J_{C,F}$ = 6 Hz, CH_2N^+), 65.5 (CH(O*C*H$_2$)$_2$), 97.1 (*C*H(OCH$_2$)$_2$), 124.4 (q, $^2J_{C,F}$ = 30 Hz, C_q), 124.5 (q, $^1J_{C,F}$ = 277 Hz, CF_3) 126.5 (CH), 128.9 (CH), 129.4 (CH), 133.5 (C_q), 133.8 (CH), 147.8 (CH), 148.0 (CH), 152.3 (C_q); ^{19}F-NMR (376 MHz, [D$_6$]DMSO): δ = −144.0 (BF_4^-), −48.1 (CF_3); elemental analysis calcd (%) for $C_{25}H_{25}B_2BrF_{11}N_2O_4$ (648.1): C 46.33, H 3.89, N 4.32; found: C 46.57, H 3.69, N 4.35.

1,8-Bis{[1-(1,3-dioxolan-2-yl)pyridinium]methyl}naphthalene dibromide [48a (2Br$^-$)] was prepared from 1,8-bis(bromomethyl)naphthalene; yield 12.3 g (quant.); m.p. 132–134 °C (EtOH; lit.[127a] 136–138 °C). **48a (2BF$_4^-$):** m.p. 195–196 °C (water); ^{1}H-NMR (200 MHz, [D$_6$]DMSO): δ = 4.01–4.04 (m, 8 H, CH(OC*H*$_2$)$_2$), 6.35 (s, 4 H, CH_2N^+), 6.52 (br s, 2 H, C*H*(OCH$_2$)$_2$), 6.89 (d, ^3J = 7 Hz, 2 H, 2-H, 7-H), 7.60 (dd, ^3J = 8 Hz, 2 H, 3-H, 6-H), 8.19 (d, ^3J = 8 Hz, 4-H, 5-H), 8.25 (dd, ^3J = 8 Hz, ^3J = 6 Hz, 2 H, 5′-H), 8.42 (d, ^3J = 8 Hz, 2 H, 3′-H), 8.78–8.86 (m, 4 H, 4′-H, 6′-H).

2,7-Bis{[1-(1,3-dioxolan-2-yl)pyridinium]methyl}naphthalene dibromide [48b (2Br$^-$)] was prepared from 2,7-bis(bromomethyl)naphthalene; yield 11.5 g (93%); m.p. 69–72 °C (lit.[127b] "syrup"). **48b (2BF$_4^-$):** m.p. (dec.) 190–191 °C (water); ^{1}H-NMR (400 MHz, [D$_6$]DMSO): δ = 4.11–4.13 (m, 8 H, CH(OC*H*$_2$)$_2$), 6.16 (s, 4 H, CH$_2$N$^+$), 6.54 (br s, 2 H, C*H*(OCH$_2$)$_2$), 7.55 (d, ^3J = 9 Hz, 2 H, 3-H, 6-H), 7.84 (s, 2 H, 1-H, 8-H), 8.04 (d, ^3J = 8 Hz, 4-H, 5-H), 8.21 (dd, ^3J = 8 Hz, ^3J = 6 Hz, 2 H, 5′-H), 8.36 (d, ^3J = 8 Hz, 2 H, 3′-H), 8.74 (dd, ^3J = 8 Hz, 2 H, 4′-H), 9.07 (d, ^3J = 6 Hz, 2 H, 6′-H); ^{13}C-NMR (100 MHz, [D$_6$]DMSO): δ = 60.0 (CH$_2$N$^+$), 65.7 (CH(O*C*H$_2$)$_2$), 97.1 (*C*H(OCH$_2$)$_2$), 126.1 (CH), 126.4 (CH), 127.7 (CH), 128.6 (CH), 128.9 (CH), 132.2 (C$_q$), 132.4 (C$_q$), 132.5 (C$_q$), 147.3 (CH), 147.4 (CH), 152.3 (C$_q$).

1,7-Bis{[1-(1,3-dioxolan-2-yl)pyridinium]methyl}naphthalene dibromide [48c (2Br$^-$)] was prepared from 1,7-bis(bromomethyl)naphthalene (**50**); yield 12.4 g (quant.); extremely hygroscopic solid. **48c (2BF$_4^-$):** m.p. 120–121 °C (water); ^{1}H-NMR (400 MHz, [D$_6$]DMSO): δ = 4.11–4.15 (m, 8 H, CH(OC*H*$_2$)$_2$), 6.16 (s, 2 H, CH$_2$N$^+$), 6.40 (s, 2 H, CH$_2$N$^+$), 6.47 [s, 1 H, C*H*(OCH$_2$)$_2$], 6.50 [s, 1 H, C*H*(OCH$_2$)$_2$], 7.19 (d, ^3J = 7 Hz, 1 H, Ar-H), 7.58–7.64 (m, 2 H, Ar-H), 7.87 (s, 1 H, Ar-H), 8.10–8.21 (m, 4 H, Ar-H), 8.33 (d, ^3J = 8 Hz, 1 H, Ar-H), 8.41 (d, ^3J = 8 Hz, 1 H, Ar-H), 8.72–8.78 (m, 3 H, Ar-H), 9.04 (d, ^3J = 6 Hz, 1 H, Ar-H); ^{13}C-NMR (100 MHz, [D$_6$]DMSO): δ = 57.9 (CH$_2$N$^+$), 60.2 (CH$_2$N$^+$), 65.7 [4 C, CH(O*C*H$_2$)$_2$], 97.1 [*C*H(OCH$_2$)$_2$], 97.2 [*C*H(OCH$_2$)$_2$], 123.0 (CH), 126.1 (2 CH), 126.3 (CH), 126.8 (CH), 128.1 (CH), 128.6 (CH), 128.8 (CH), 129.0 (C$_q$), 129.8 (CH), 129.9 (C$_q$), 130.2 (CH), 132.4 (C$_q$), 133.2 (C$_q$), 146.5 (CH), 147.2 (CH), 124.3 (CH), 147.4 (CH), 151.9 (C$_q$), 152.1 (C$_q$); elemental analysis calcd (%) for C$_{28}$H$_{28}$B$_2$F$_8$N$_2$O$_4$ (630.1): C 53.37, H 4.48, N 4.45; found: C 53.49, H 4.55, N 4.50.

General procedure for synthesis of diazoniapolycycles by cyclodehydration in PPA (GP-5). The corresponding bis(tetrafluoroborate) **40a–c (2BF$_4^-$)**, **41a–c (2BF$_4^-$)**, or **48a (2BF$_4^-$)** (2.00 g) in PPA (20 g) was slowly heated under argon atmosphere to 150 °C, and the reaction mixture was stirred at this temperature for 24–36 h. After cooling to ~ 100 °C, water (40 mL) was carefully added and the mixture was stirred at this temperature for 30 min to hydrolyse the PPA. The mixture was cooled to room temperature and treated with excess of NaBF$_4$ (15–30 mmol, concentrated aqueous solution). In the cases when a large amount of precipitate has formed, the latter was separated, washed with water (3 × 20 mL), dried in vacuo / P$_2$O$_5$, and recrystallized from a suitable solvent. Otherwise, the dark solution was

extracted with nitromethane (4 × 40 mL). The organic phases were combined, washed with water (20 mL) and evaporated in vacuo; the residue was recrystallized from a suitable solvent, to give the diazoniapolycycle as a bis(tetrafluoroborate) salt.

12a,14a-Diazoniapentaphene bis(tetrafluoroborate) (7a) was prepared from **41a (2BF_4^-)**; yield 1.32 g (84%), recrystallization from acidified (one drop HBF_4) MeOH–water; dark-brown crystalline solid; m.p. > 350 °C; ^{1}H-NMR (400 MHz, [D_6]DMSO): δ = 8.28 (dd, ^3J = 7 Hz, ^3J = 8 Hz, 2 H, 2-H, 11-H), 8.39 (s, 2 H, 6-H, 7-H), 8.50 (dd, ^3J = 8 Hz, 2 H, 3-H, 10-H), 8.80 (d, ^3J = 8 Hz, 2 H, 4-H, 9-H), 9.25 (s, 2 H, 5-H, 8-H), 9.35 (d, ^3J = 7 Hz, 2 H, 1-H, 12-H), 10.97 (s, 2 H, 13-H, 14-H); ^{13}C-NMR (100 MHz, [D_6]DMSO): δ = 121.9 (C_q), 124.6 (CH), 125.9 (CH), 127.5 (CH), 132.1 (CH), 135.0 (CH), 136.1 (C_q), 136.5 (CH), 136.6 (CH), 141.3 (C_q); elemental analysis calcd (%) for $C_{20}H_{14}B_2F_8N_2$ (456.0): C 52.68, H 3.09, N 6.14; found: C 52.28, H 3.04, N 6.09.

4a,8a-Diazoniapentaphene bis(tetrafluoroborate) (7b) was prepared from **41b (2BF_4^-)**; yield 0.96 g (61%), recrystallization from EtOH–water, dark-yellow crystalline solid; m.p. (dec.) 299 °C; ^{1}H-NMR (200 MHz, [D_6]DMSO): δ = 8.26 (s, 2 H, 6-H, 7-H), 8.32 (dd, ^3J = 7 Hz, ^3J = 8 Hz, 2 H, 3-H, 10-H), 8.54 (dd, ^3J = 8 Hz, 2 H, 2-H, 11-H), 8.76 (d, ^3J = 8 Hz, 2 H, 1-H, 12-H), 9.55 (d, ^3J = 7 Hz, 2 H, 4-H, 9-H), 10.18 (s, 2 H, 13-H, 14-H), 10.26 (s, 2 H, 5-H, 8-H); ^{13}C-NMR (100 MHz, [D_6]DMSO): δ = 123.9, 125.1, 126.4, 128.0 (2 C), 132.4, 136.4, 136.6, 137.7, 140.3; elemental analysis calcd (%) for $C_{20}H_{14}B_2F_8N_2 \times 2\ H_2O$ (492.0): C 48.83, H 3.69, N 5.69; found: C 48.50, H 3.25, N 5.51.

4a,12a-Diazoniapentaphene bis(tetrafluoroborate) (7c) was prepared from **41c (2BF_4^-)**; yield 1.00 g (65%), recrystallization from MeCN–water, dark-brown crystalline solid; m.p. > 350 °C; ^{1}H-NMR (400 MHz, [D_6]DMSO): δ = 8.27–8.31 (m, 3 H, 3-H, 7-H, 11-H), 8.39 (d, ^3J = 9 Hz, 1 H, 6-H), 8.48–8.54 (m, 2 H, 2-H, 10-H), 8.74 (d, ^3J = 9 Hz, 1 H, 1-H), 8.78 (d, ^3J = 9 Hz, 1 H, 9-H), 9.22 (s, 1 H, 8-H), 9.38 (d, ^3J = 7 Hz, 1 H, 12-H), 9.54 (d, ^3J = 7 Hz, 1 H, 4-H), 9.98 (s, 1 H, 14-H), 10.29 (s, 1 H, 5-H), 11.16 (s, 1 H, 13-H); ^{13}C-NMR (100 MHz, [D_6]DMSO): δ = 121.5 (2 C), 124.1, 124.4, 125.1, 125.6, 127.1, 127.3, 129.0, 130.8, 132.7, 136.3, 136.4 (2 C), 136.5, 136.7, 137.1, 138.1, 140.1, 141.4; elemental analysis calcd (%) for $C_{20}H_{14}B_2F_8N_2 \times ½\ H_2O$ (465.0): C 51.66, H 3.25, N 6.02; found: C 51.72, H 3.51, N 5.95.

6,13-Dimethyl-4a,8a-diazoniapentaphene bis(tetrafluoroborate) (42a) was prepared from **40a (2BF_4^-)**; yield 0.44 g (30%), recrystallization from MeCN–water, brown crystalline solid;

m.p. > 350 °C; ^{1}H-NMR (400 MHz, [D$_6$]DMSO): δ = 2.83 (s, 3 H, C6–CH$_3$), 3.53 (s, 3 H, C13–CH$_3$), 7.94 (s, 1 H, 7-H), 8.31 (dd, ^{3}J = 7 Hz, 1 H, 10-H), 8.35 (dd, ^{3}J = 7 Hz, 1 H, 3-H), 8.54 (dd, ^{3}J = 9 Hz, ^{3}J = 7 Hz, 1 H, 11-H), 8.56 (dd, ^{3}J = 9 Hz, ^{3}J = 7 Hz, 1 H, 2-H), 9.05 (d, ^{3}J = 9 Hz, 1 H, 1-H), 9.13 (d, ^{3}J = 9 Hz, 1 H, 12-H), 9.54 (d, ^{3}J = 7 Hz, 1 H, 9-H), 9.66 (d, ^{3}J = 7 Hz, 1 H, 4-H), 9.78 (s, 1 H, 14-H), 9.90 (s, 1 H, 8-H), 10.19 (s, 1 H, 5-H); ^{13}C-NMR (100 MHz, [D$_6$]DMSO): δ = 18.8 (CH$_3$), 19.8 (CH$_3$), 124.7, 125.2, 125.8, 126.5, 126.9, 128.3, 128.4, 130.7, 133.1, 133.5, 134.3, 135.2, 135.9, 136.2, 136.3, 136.3, 137.0, 139.4, 140.6; MS (ESI$^+$): *m*/*z* (%) = 155 (100) $[M]^{2+}$, 309 (48) $[M - H]^+$, 320 (25) $[M + F]^+$, 397 (26) $[M + BF_4]^+$, 881 (38) $[2M + 3BF_4]^+$, 1364 (6) $[3M + 5BF_4]^+$; IR (KBr): $\tilde{\nu}_{max}$ = 524 (BF_4^-), 792s, 1062s (BF_4^-), 1389s, 1502, 1646s cm^{-1}; elemental analysis calcd (%) for $C_{22}H_{18}B_2F_8N_2$ (484.0): C 54.59, H 3.75, N 5.79; found: C 54.46, H 3.61, N 5.85.

14-Methyl-4a,12a-diazoniapentaphene bis(tetrafluoroborate) (42b) was prepared from **40b (2BF$_4^-$)**; yield 0.81 g (51%), recrystallization from MeCN–water, dark-brown fine crystalline solid; m.p. > 300 °C; ^{1}H-NMR (400 MHz, [D$_6$]DMSO): δ = 3.58 (s, 3 H, CH$_3$), 8.19 (d, ^{3}J = 9 Hz, 1 H, 7-H), 8.25 (d, ^{3}J = 9 Hz, 1 H, 6-H), 8.26 (dd, ^{3}J = 7 Hz, 1 H, 11-H), 8.32 (dd, ^{3}J = 7 Hz, 1 H, 3-H), 8.50 (dd, ^{3}J = 9 Hz, ^{3}J = 7 Hz, 1 H, 10-H), 8.57 (dd, ^{3}J = 9 Hz, ^{3}J = 7 Hz, 1 H, 2-H), 8.74 (d, ^{3}J = 9 Hz, 1 H, 9-H), 9.15 (d, ^{3}J = 9 Hz, 1 H, 1-H), 9.16 (s, 1 H, 8-H), 9.53 (d, ^{3}J = 7 Hz, 1 H, 4-H), 9.81 (d, ^{3}J = 7 Hz, 1 H, 12-H), 10.08 (s, 1 H, 5-H), 10.52 (s, 1 H, 13-H); ^{13}C-NMR (100 MHz, [D$_6$]DMSO): δ = 18.3 (CH$_3$), 121.0, 122.3, 123.3, 123.4, 124.4, 125.0, 125.5, 127.9, 129.8, 130.0, 133.1, 134.0, 135.6, 135.9, 136.0, 136.4, 137.1, 138.8, 139.7, 139.8; MS (ESI$^+$): *m*/*z* (%) = 148 (59) $[M]^{2+}$, 295 (100) $[M - H]^+$, 315 (21) $[M + F]^+$, 383 (13) $[M + BF_4]^+$, 853 (18) $[2M + 3BF_4]^+$; IR (KBr): $\tilde{\nu}_{max}$ = 523 (BF_4^-), 1056s (BF_4^-), 1343, 1449, 1641w cm^{-1}; elemental analysis calcd (%) for $C_{21}H_{16}B_2F_8N_2$ (470.0): C 53.67, H 3.43, N 5.96; found: C 53.73, H 3.43, N 6.31.

4a,12a-Diazoniapentaphen-14-olate tetrafluoroborate (42c) was prepared from **40c (2BF$_4^-$)**; yield 0.65 g (56%), recrystallization from nitromethane, purple needles, m.p. > 300 °C; ^{1}H-NMR (400 MHz, [D$_6$]DMSO): δ = 7.53 (d, ^{3}J = 9 Hz, 1 H, 7-H), 7.58 (d, ^{3}J = 9 Hz, 1 H, 6-H), 7.77–7.82 (m, 3 H, 2-H, 3-H, 11-H), 7.97 (dd, ^{3}J = 9 Hz, ^{3}J = 8 Hz, 1 H, 10-H), 8.15 (d, ^{3}J = 9 Hz, 1 H, 9-H), 8.23 (s, 1 H, 5-H), 8.37–8.39 (m, 2 H, 1-H, 8-H), 8.80–8.84 (m, 1 H, 4-H), 9.28 (d, ^{3}J = 7 Hz, 1 H, 12-H), 11.46 (s, 1 H, 13-H); ^{13}C-NMR (100 MHz, [D$_6$]DMSO): δ = 110.2 (C$_q$), 113.6 (CH, C5), 122.5 (CH), 122.6 (CH), 123.9 (CH), 124.1 (CH), 125.3 (C$_q$), 126.1 (CH, C9), 127.4 (CH, C7), 128.6 (C$_q$), 129.8 (CH), 132.9 (CH, C6), 133.0 (CH), 133.3 (CH), 133.9 (CH, C4), 135.6 (CH, C12), 137.0 (C$_q$), 138.1 (C$_q$), 164.2 (C$_q$,

C14); MS (ESI^+): *m*/*z* (%) = 297 (100) $[M]^+$, 329 (24) $[M + O_2]^+$; IR (KBr): $\tilde{\nu}_{max}$ = 480, 522 (BF_4^-), 1061s (BF_4^-), 1185, 1459s, 1510, 1552s (C–O phenolate), 1640w cm^{-1}; elemental analysis calcd (%) for $C_{20}H_{13}BF_4N_2O$ (384.1): C 62.53, H 3.41, N 7.29; found: C 62.66, H 3.34, N 7.49.

14a,16a-diazoniaanthra[1,2-*a*]anthracene bis(tetrafluoroborate) (38a) was prepared from **48a (2BF_4^-)**; yield 1.27 g (79%), recrystallization from MeCN–water, dark-yellow prisms, m.p. > 350 °C; ^{1}H NMR (400 MHz, [D_6]DMSO): δ = 8.26 (dd, ^3J = 8 Hz, ^3J = 7 Hz, 2 H, 2-H, 13-H), 8.39 (dd, ^3J = 9 Hz, ^3J = 8 Hz, 2 H, 3-H, 12-H), 8.69 (AB, ^3J = 9 Hz, 4 H, 6-H, 7-H, 8-H, 9-H), 8.82 (d, ^3J = 9 Hz, 2 H, 4-H, 11-H), 9.50 (s, 2 H, 5-H, 10-H), 9.53 (d, ^3J = 7 Hz, 2 H, 1-H, 14-H), 11.42 (s, 2 H, 15-H, 16-H); ^{13}C NMR (100 MHz, [D_6]DMSO): δ = 122.0 (C_q), 123.1 (CH), 123.7 (C_q), 124.7 (CH), 126.8 (CH), 129.3 (CH), 133.7 (CH), 134.6 (C_q), 134.9 (CH), 135.8 (CH), 136.0 (C_q), 138.1 (C_q), 140.2 (CH); elemental analysis calcd (%) for $C_{24}H_{16}B_2F_8N_2$ (506.0): C 56.97, H 3.19, N 5.54; found C 56.66, H 3.03, N 5.64.

6,13a-Dimethyl-13,13a-dihydro-4a,8a-diazoniapentaphen-13-ol bis(tetrafluoroborate) (44): A solution of the dibromide **40a (2Br^-)** (3.57 g, 6.00 mmol) in 48% aq. HBr (35 mL) was stirred under reflux for 2 h, and 20 mL of liquid were distilled off. The residue was poured into acetone (200 mL); the yellow precipitate was collected and washed with acetone. It was dissolved in 5% aq. HBr (5 mL) and diluted with 96% ethanol (500 mL); the suspension was filtered, and the filtrate concentrated in vacuo. The residue was diluted with water (15 mL) and treated with 50% aq. HBF_4 (3 mL), to afford **44 (2BF_4^-)** (1.05 g, 35%) as dark-yellow crystalline solid; m.p. > 300 °C (MeCN–water); ^{1}H-NMR (400 MHz, [D_6]DMSO): δ = 1.36 (s, 3 H, C13a–CH_3), 2.43 (s, 3 H, C6–CH_3), 5.86 (d, ^3J = 5 Hz, 1 H, 13-H), 6.83 (d, ^3J = 5 Hz, 1 H, OH), 6.95 (s, 1 H, 7-H), 7.81 (s, 1 H, 8-H), 8.10–8.14 (m, 1 H, 3-H), 8.19 (d, ^3J = 8 Hz, 1 H, 12-H), 8.24 (dd, ^3J = 6 Hz, ^3J = 9 Hz, 1 H, 10-H), 8.37–8.40 (m, 2 H, 1-H, 2-H), 8.69 (dd, ^3J = 8 Hz, ^3J = 9 Hz, 1 H, 11-H), 8.76 (s, 1 H, 14-H), 9.08 (d, ^3J = 6 Hz, 1 H, 9-H), 9.35 (d, ^3J = 7 Hz, 1 H, 4-H), 9.46 (s, 1 H, 5-H); ^{13}C-NMR (100 MHz, [D_6]DMSO): δ = 18.8 (C6–*C*H_3), 26.1 (C13a–*C*H_3), 41.7 (C_q, C13a), 69.4 (CH, C13), 123.0 (CH), 124.0 (CH), 125.0 (CH), 126.3 (CH), 126.5 (CH), 128.2 (CH), 128.8 (C_q), 128.9 (CH), 132.8 (CH), 134.1 (C_q), 135.5 (C_q), 137.0 (CH), 137.6 (CH), 141.7 (C_q), 143.4 (CH), 146.2 (C_q), 147.1 (CH), 147.2 (C_q); MS (ESI^+): *m*/*z* (%) = 148 (16) $[M – OH – CH_3]^{2+}$, 327 (100) $[M – H]^+$, 415 (14) $[M + BF_4]^+$, 917 (14) $[2M + 3BF_4]^+$; IR (KBr): $\tilde{\nu}_{max}$ = 485, 522 (BF_4^-),

1054s (BF_4^-), 1374, 1413, 1502s, 1637s cm^{-1}; elemental analysis calcd (%) for $C_{22}H_{20}B_2F_8N_2O$ (502.0): C 52.63, H 4.02, N 5.58; found: C 52.73, H 3.92, N 5.67.

Synthesis of 42a by dehydration of 44 in PPA: Salt **44** (0.251 g, 0.500 mmol) in PPA (2.50 g) was stirred under argon atmosphere for 18 h at 150 °C. After cooling to 100 °C, a solution of $NaBF_4$ (0.110 g, 1.00 mmol) in water (6 mL) was added, and the reaction mixture was stirred at 80–100 °C for 15 min. After cooling to room temperature, the solution was extracted with nitromethane (4 × 5 mL). The combined organic layers were washed with water (2 × 5 mL), and the solvent was removed in vacuo, to give pure **42a ($2BF_4^-$)** (0.220 g, 91%) as a yellow solid; spectroscopic data are identical with those given above.

General procedure for synthesis of diazoniaanthra[1,2-*a*]anthracenes by cyclo-dehydration in aqueous HBr (GP-6). A solution of the dibromide **48b–c ($2Br^-$)** (0.50 g, 0.81 mmol) in 48% aq. HBr (4.0 mL) was stirred under reflux for 3½ h. After cooling to 80 °C, a solution of $NaBF_4$ (0.50 g, 4.5 mmol) in water (4 mL) was added, whereas yellow precipitate has formed. After cooling to 4 °C, the solid was collected, washed with water (2 × 5 mL), acetone (2 × 5 mL) and recrystallized from acidified (one drop HBF_4) MeCN–water.

4a,10a-Diazoniaanthra[1,2-*a*]anthracene bis(tetrafluoroborate) (38b) was prepared from **48b ($2Br^-$)**; yield 0.16 g (40%); yellow needles, m.p. > 350 °C; ^{1}H NMR (400 MHz, [D$_6$]DMSO): δ = 8.21 (dd, J = 8 Hz, J = 7 Hz, 2 H, 3-H, 12-H), 8.41 (dd, J = 9 Hz, J = 8 Hz, 2 H, 2-H, 13-H), 8.53 (d, J = 9 Hz, 2 H, 7-H, 8-H) 8.74 (d, J = 9 Hz, 4 H, 6-H, 9-H), 8.97 (d, J = 9 Hz, 2 H, 1-H, 14-H), 9.50 (d, J = 7 Hz, 2 H, 4-H, 11-H), 10.32 (s, 2 H, 15-H, 16-H), 10.57 (s, 2 H, 5-H, 10-H); ^{13}C NMR (100 MHz, [D$_6$]DMSO): δ = 121.6 (C$_q$), 123.6 (CH), 124.6 (CH), 126.3 (C$_q$), 128.1 (CH), 130.9 (CH), 132.0 (CH), 132.6 (C$_q$), 133.2 (CH), 134.8 (CH), 138.8 (C$_q$), 139.3 (C$_q$), 139.4 (CH); elemental analysis calcd (%) for $C_{24}H_{16}B_2F_8N_2$ (506.0): C 56.97, H 3.19, N 5.54; found C 56.97, H 3.14, N 5.72.

4a,14a-Diazoniaanthra[1,2-*a*]anthracene bis(tetrafluoroborate) (38c) was prepared from **48c ($2Br^-$)**; yield 0.22 g (54%); pale-yellow prisms, m.p. > 350 °C; ^{1}H-NMR (400 MHz, [D$_6$]DMSO): δ = 8.20–8.27 (m, 2 H, 3-H, 13-H), 8.36–8.42 (m, 2 H, 2-H, 12-H), 8.55 (d, ^3J = 9 Hz, 1 H, 7-H), 8.64 (d, ^3J = 9 Hz, 1 H, 8-H), 8.68–8.73 (m, 2 H, 6-H, 9-H), 8.79 (d, ^3J = 9 Hz, 1 H, 11-H), 8.83 (d, ^3J = 9 Hz, 1 H, 1-H), 9.47 (s, 1 H, 10-H), 9.51 (d, ^3J = 7 Hz,

1 H, 4-H), 9.77 (d, ^3J = 7 Hz, 1 H, 14-H), 10.46 (s, 1 H, 16-H), 10.60 (s, 1 H, 5 H), 11.30 (s, 1 H, 15-H); ^{13}C-NMR (100 MHz, [D$_6$]DMSO): δ = 122.5 (C$_q$), 122.6 (C$_q$), 123.0 (CH, C13), 123.6 (CH, C3), 125.0 (CH, C10), 125.7 (CH, C16), 126.2 (C$_q$), 126.8 (CH, C11), 128.0 (CH, C1), 129.6 (CH, C6), 130.6 (CH, C9), 131.7 (C$_q$), 131.8 (CH, C7), 133.1 (CH, C13), 133.8 (CH, C3), 134.8 (CH, C4), 135.0 (CH, C8), 136.0 (C$_q$), 136.2 (CH, C14), 137.0 (C$_q$), 138.2 (C$_q$), 138.7 (C$_q$), 139.1 (2 CH, C15, C16); ^{15}N-NMR (HMBC, [D$_6$]DMSO): δ = 204.9 (1 N, N-4a), 205.8 (1 N, N-14a); MS (ESI$^+$): *m*/*z* (%) = 166 (5) [*M*]$^{2+}$, 331 (100) [*M* – H]$^+$, 419 (53) [*M* + BF$_4$]$^+$, 925 (12) [2*M* + 3BF$_4$]$^+$; elemental analysis calcd (%) for $C_{24}H_{16}B_2F_8N_2$ (506.0): C 56.97, H 3.19, N 5.54; found: C 57.14, H 3.10, N 5.53.

13a,16a-Diazoniahexaphene bis(tetrafluoroborate) (51): Bis(tetrafluoroborate) **48c (2BF$_4^-$)** (2.00 g, 3.17 mmol) in PPA (20 g) was heated under argon atmosphere to 150 °C, and the reaction mixture was stirred at this temperature for 24 h. After cooling to about 100 °C, water (30 mL) was carefully added and the mixture was stirred at this temperature for 30 min to hydrolyse the PPA. The mixture was cooled to room temperature and treated with a solution of NaBF$_4$ (3.30 g, 30.0 mmol) in water (5 mL). After cooling to 4 °C, the precipitate was collected, washed with water (2 × 10 mL) and acetone (2 × 10 mL) and dried in vacuo, to give 1.53 g (95%) of a mixture of **3** (37%; determined by ^{1}H-NMR spectroscopy) and **51** (63%) as a yellow powder. Fractional crystallization from nitromethane (3-fold) afforded almost pure **38c** (less soluble compound), the spectroscopic properties are identical with those given above. The mother liquor contained ca. 92% (^{1}H-NMR-spectroscopically) of **51** and was evaporated; the residue was recrystallized from MeCN–water, to give analytically pure **51** (85 mg) as brown microcrystalline solid, m.p. > 340 °C; ^{1}H-NMR (400 MHz, [D$_6$]DMSO): δ = 8.09–8.11 (m, 2 H, 6-H, 12-H), 8.17 (dd, ^3J = 7 Hz, ^3J = 9 Hz, 1 H, 11-H), 8.23 (dd, ^3J = 7 Hz, 1 H, 2-H), 8.37 (d, ^3J = 9 Hz, 1 H, 7-H), 8.43 (dd, ^3J = 8 Hz, ^3J = 8 Hz, 1 H, 3-H), 8.71 (d, ^3J = 9 Hz, 2 H, 4-H, 10-H), 9.06 (s, 1 H, 5-H), 9.08 (s, 1 H, 8-H), 9.44 (d, ^3J = 7 Hz, 1 H, 1-H), 9.51 (s, 1 H, 9-H), 9.61 (d, ^3J = 7 Hz, 1 H, 13-H), 9.97 (s, 1 H, 15-H), 10.63 (s, 1 H, 14-H), 11.10 (s, 1 H, 16-H); ^{13}C NMR (100 MHz, [D$_6$]DMSO): δ = 122.7 (CH, C12), 123.8 (CH, C2), 124.2 (C$_q$), 124.3 (C$_q$), 124.5 (CH, C5), 125.0 (CH, C15), 125.4 (CH, C9), 127.0 (CH, C4 or C10), 127.1 (CH, C4 or C10), 128.2 (CH, C8), 128.3 (CH, C6),128.6 (C$_q$), 131.3 (CH, C11), 133.6 (C$_q$), 134.7 (CH, C13), 135.1 (CH, C7), 135.2 (CH, C16), 135.5 (C$_q$), 135.9 (CH, C3), 136.4 (CH, C1), 136.9 (C$_q$), 137.7 (C$_q$), 140.9 (C$_q$), 141.6 (CH, C14); ^{15}N NMR (HMBC, [D$_6$]DMSO): δ = 205.4 (1 N, N-16a), 206.0 (1 N, N-13a); MS (ESI$^+$): *m*/*z* (%) = 331 (100)

$[M - H]^+$, 351 (29) $[M + F]^+$, 419 (10) $[M + BF_4]^+$, 925 (6) $[2M + 3BF_4]^+$; elemental analysis calcd (%) for $C_{24}H_{16}B_2F_8N_2$ (506.0): C 56.97, H 3.19, N 5.54; found: C 56.71, H 3.43, N 5.57.

5.2.3 Synthesis of Acridizinium-9-carboxamides and Acridizinium–Nucleic Base Conjugates

Methyl 6-(1,3-dioxolan-2-yl)nicotinate (58):[171] Selenium dioxide (freshly sublimed from HNO_3) (2.32 g, 20.9 mmol) dissolved in mixture of 1,4-dioxane (12 mL) and water (2 mL) was added dropwise within 30 min to a stirred at 60–65 °C solution of methyl 6-methylnicotinate (**57**; 3.14 g, 20.8 mmol) in 1,4-dioxane (6 mL). After completion of the addition, the reaction mixture was stirred at 60–65 °C for 1 h, cooled to tome temperature, and filtered through a pad of Celite. The filtrate was evaporated to dryness, dissolved in toluene (40 mL), and ethylene glycol (2.30 mL, 2.59 g, 41.8 mmol) was added, followed by *p*-toluenesulfonic acid monohydrate (1.19 g, 6.26 mmol). The reaction mixture was heated to reflux with a Dean–Stark water separator for 20 h, cooled to room temperature and poured into saturated aqueous Na_2CO_3 solution (50 mL). After separation of the organic layer, the aqueous layer was extracted with toluene (3 × 20 mL). The combined organic layers were washed with water (20 mL), dried with anhydrous Na_2SO_4, and the solvent was removed in vacuo. The residue was purified by flash chromatography (SiO_2; eluent: CH_2Cl_2–MeOH, 98:2 v/v). After evaporation of the solvents in vacuo, ester **58** (1.56 g, 36%) was obtained as a pale-yellow low-melting solid; ^{1}H-NMR (200 MHz, $CDCl_3$): δ = 3.95 (s, 3 H, CH_3), 4.11–4.16 (m, 4 H, OCH_2), 5.90 (s, 1 H, C*H*$(OCH_2)_2$), 7.62 (d, ^3J = 8 Hz, 1 H, 5-H), 8.33 (dd, ^3J = 8 Hz, ^4J = 2 Hz, 1 H, 4-H), 9.21 (d, ^4J = 2 Hz, 1 H, 2-H).

1-Benzyl-2-(1,3-dioxolan-2-yl)-5-carbomethoxypyridinium bromide (59): A solution of the ester **58** (1.05 g, 5.00 mmol) and benzyl bromide (1.28 g, 0.89 mL, 7.50 mmol) in anhydrous DMSO (2 mL) was stirred under argon atmosphere for 13 days and then poured into AcOEt (50 mL). The white precipitate was collected, washed with acetone (2 × 10 mL) and Et_2O (2 × 10 mL), and dried in vacuo / P_2O_5, to give 1.02 g (54 %) of salt **59** as white amorphous solid. Crystallization from EtOH–AcOEt afforded fine colorless needles, m.p. 134–136 °C; ^{1}H-NMR (400 MHz, CD_3OD): δ = 4.01 (s, 3 H, CH_3), 4.21 (s, 4 H, CH_2CH_2), 6.14 (s, 2 H, CH_2N^+), 7.40–7.50 (m, 5 H, Ar-H), 8.52 (d, ^3J = 8 Hz, 1 H, 5-H), 9.12 (dd, ^3J = 8 Hz, ^4J = 2 Hz, 1 H, 4-H), 9.39 (d, ^4J = 2 Hz, 1 H, 2-H); ^{13}C-NMR (100 MHz, CD_3OD):

δ = 54.2 (CH_3), 62.8 (CH_2N^+), 67.5 (2 C, CH_2CH_2), 98.9 (CH), 127.8 (CH), 129.9 (CH), 130.8 (CH), 131.0 (CH), 132.3 (C_q), 133.7 (C_q), 147.9 (CH), 148.9 (CH), 157.4 (C_q), 162.9 (CO); elemental analysis calcd (%) for $C_{17}H_{18}BrNO_4$ (380.2): C 53.70, H 4.77, N 3.68; found: C 54.17, H 4.81, N 3.68.

3-Carboxyacridizinium bromide (56b): A solution of the salt **59** (0.87 g, 2.30 mmol) in 48% aq. HBr (10 mL) was heated under reflux for 20 h. After this time, 3 mL of HBr were distilled off, the residue was cooled to room temperature and THF (40 mL) was added. The yellow precipitate was collected, washed with THF (2 × 10 mL), Et_2O (2 × 10 mL), and dried in vacuo / P_2O_5, giving 0.63 g (90%) of **56b (Br^-)** as a yellow crystalline solid; m.p. (dec.) 265–270 °C (EtOH–H_2O); ^{1}H-NMR (400 MHz, [D_6]DMSO): δ = 8.08 (dd, ^3J = 8 Hz, ^3J = 8 Hz, 1 H,8-H), 8.23 (dd, ^3J = 7 Hz, ^3J = 9 Hz, 1 H, 9-H), 8.32 (dd, ^3J = 9 Hz, ^4J = 2 Hz, 1 H, 2-H), 8.46 (d, ^3J = 9 Hz, 1 H, 10-H), 8.51 (d, ^3J = 8 Hz, 1 H, 7-H), 8.64 (d, ^3J = 9 Hz, 1 H, 1-H), 9.35 (s, 1 H, 11-H), 9.94 (s, 1 H, 4-H), 10.74 (s, 1 H, 6-H), 14.43 (br s, 1 H, COOH); ^{13}C-NMR (400 MHz, [D_6]DMSO): δ = 124.7 (CH, C11); 125.0 (C_q); 125.9 (C_q); 127.1 (CH, C1); 127.3 (CH, C10); 128.5 (CH, C7); 128.9 (CH, C2); 131.4 (CH, C8); 135.7 (CH, C9); 136.2 (C_q); 137.5 (CH, C4); 137.8 (C_q); 142.3 (CH, C6); 164.1 (COOH); MS (ESI^+) *m*/*z* (%) = 224 (100) $[M]^+$, 447 (80) $[2M - H]^+$, 670 (42) $[3M - 2H]^+$.

General procedure for the conversion of carboxyacridizinium bromides into tetrafluoroborates (GP-7). Salt **56 (Br^-)** (0.480 g, 1.58 mmol) was dissolved in boiling water (10 mL) and treated with 50% aq. HBF_4 (2 mL). After slow cooling to room temperature, the tetrafluoroborate separated as yellow crystalline precipitate, which was collected, washed with cold water, and dried in vacuo / P_2O_5.

9-Carboxyacridizinium tetrafluoroborate [56a (BF_4^-)]: yield 98%, bright-yellow needles, m.p. (dec.) 236–240 °C; anal. calcd. for $C_{14}H_{10}BF_4NO_2$ (311.0): C 54.06, H 3.24, N 4.50; found: C 54.01, H 3.14, N 4.47.

3-Carboxyacridizinium tetrafluoroborate [56b (BF_4^-)]: yield 77%, lemon-yellow needles, m.p. (dec.) 240–244 °C; anal. calcd. for $C_{14}H_{10}BF_4NO_2$ (311.0): C 54.06, H 3.24; N 4.50, found: C 54.18, H 3.38, N, 4.51.

General procedure for the synthesis of acridizinium-9-carboxamides (GP-8). To a warm (50–60 °C) solution of the salt **56a (BF_4^-)** (0.62 g, 2.0 mmol) in MeCN (30 mL), NMM (0.24 mL, 0.22 g, 2.2 mmol) was added, while a yellow precipitate has separated. The suspension was cooled to –20 °C under argon atmosphere and treated with isobutyl chloroformate (0.29 mL, 0.30 g, 2.2 mmol). The reaction mixture was stirred at this temperature for 10 min, while the precipitate slowly dissolved. The amine (2.0 mmol) was added dropwise under vigorous stirring. The reaction mixture was stirred for 2 h at –20 °C and warmed to room temperature during 18 h. The suspension was evaporated to dryness; the residue was dissolved in ca. 15 mL of warm (50–60 °C) water and treated with a concentrated aqueous solution of $NaBF_4$ (2.0 g, 18 mmol). The yellow precipitate was collected, washed with water (2 × 5 mL), diethyl ether (2 × 10 mL) and dried in vacuo / P_2O_5. Further purification was achieved by column chromatography (alumina neutral, activity grade I; eluent $CHCl_3$–MeOH–AcOH, 90:10:1), followed by evaporation of the solvent and crystallization of residue from MeCN–AcOEt.

***N*-Isopropylacridizinium-9-carboxamide tetrafluoroborate (55a):** yield 0.49 g (70%); fine pale-yellow needles; R_f = 0.18 (system B); ^{1}H-NMR (400 MHz, [D$_6$]DMSO): δ = 1.26 (d, ^3J = 7 Hz, 6 H, CH_3), 4.21 (m, ^3J = 7 Hz, 1 H, C*H*Me$_2$), 8.03 (dd, ^3J = 7 Hz, 1 H, 3-H), 8.15 (dd, ^3J = 9 Hz, ^3J = 7 Hz, 1 H, 2-H), 8.29 (d, ^3J = 9 Hz, ^4J = 1 Hz, 1 H, 8-H), 8.53 (d, ^3J = 9 Hz, 1 H, 7-H), 8.66 (d, ^3J = 9 Hz, 1 H, 1-H), 8.80 (s, 1 H, 10-H), 8.90 (d, ^3J = 8 Hz, 1 H, NH), 9.34–9.38 (m, 2 H, 11-H, 4-H), 10.52 (s, 1 H, 6-H); ^{13}C-NMR (50 MHz, [D$_6$]DMSO) : δ = 22.3 (2 CH_3), 41.7 (*C*HMe$_2$), 122.9 (CH), 126.1 (CH), 126.2 (C_q), 126.5 (CH), 127.1 (CH), 128.4 (CH), 129.1 (CH), 131.6 (CH), 134.6 (CH), 134.8 (C_q), 137.9 (C_q), 139.2 (C_q), 140.2 (CH), 164.1 (CO); IR (KBr): $\tilde{\nu}_{max}$ = 1546 (amide II), 1653s (amide I) cm^{-1}. **55a (Cl^-):** fine yellow needles, m.p. 230–235 °C; elemental analysis calcd (%) for $C_{17}H_{17}ClN_2O \times H_2O$: C 64.05, H 6.01, N 8.79; found C 63.91, H 5.91, N 8.81.

***N*-Butylacridizinium-9-carboxamide tetrafluoroborate (55b):** yield 0.23 g (31%); fine pale-yellow needles, m.p. 131–133 °C; R_f = 0.11 (system B); ^{1}H-NMR (400 MHz, [D$_6$]DMSO): δ = 0.95 (t, ^3J = 7 Hz, 3 H, CH_3), 1.40 (m, 2 H, CH_2), 1.59 (qi, ^3J = 7 Hz, 2 H, CH_2), 3.37 (m, overlap with H_2O, C*H*$_2$NH), 8.03 (dd, ^3J = 7 Hz, 1 H, 3-H), 8.15 (dd, ^3J = 9 Hz, ^3J = 7 Hz, 1 H, 2-H), 8.29 (d, ^3J = 9 Hz, 1 H, 8-H), 8.54 (d, ^3J = 9 Hz, 1 H, 7-H), 8.66 (d, ^3J = 9 Hz, 1 H, 1-H), 8.79 (s, 1 H, 10-H), 9.09 (t, ^3J = 5 Hz, 1 H, NH), 9.35–9.37 (m, 2 H, 11-H, 4-H), 10.51 (s, 1 H, 6-H); ^{13}C-NMR (100 MHz, [D$_6$]DMSO) : δ = 13.6 (CH_3), 19.6 (CH_2), 31.0 (CH_2), 39.0 (CH_2), 122.8 (CH), 125.9 (CH), 126.0 (C_q), 126.2 (CH), 126.9 (CH),

128.4 (CH), 128.8 (CH), 131.5 (CH), 134.4 (CH), 134.7 (C_q), 137.8 (C_q), 139.0 (C_q), 140.0 (CH), 164.7 (CO); MS (ESI^+) *m*/*z* (%) = 279 (100) $[M]^+$, 645 (5) $[2M + BF_4]^+$; elemental analysis calcd (%) for $C_{18}H_{19}BF_4N_2O \times {}^1\!/_4\, H_2O$ (370.7): C 58.33, H 5.30, N 7.56; found C 58.21, H 5.18, N 7.56.

***N*-(3-Dimethylaminopropyl)acridizinium-9-carboxamide chloride (55c):** To a warm (50–60 °C) solution of the salt **56a (BF_4^-)** (933 mg, 3.00 mmol) in MeCN (45 mL), NMM (363 µL, 333 mg, 3.30 mmol) was added, while a yellow precipitate has separated. The suspension was cooled to −10 °C under argon atmosphere and treated with isobutyl chloroformate (429 µL, 451 mg, 3.30 mmol). The reaction mixture was stirred at this temperature for 15 min, while the precipitate slowly dissolved. *N*,*N*-Dimethyl-1,3-diaminopropane (413 µL, 337 mg, 3.30 mmol) and pyridine hydrochloride (381 mg, 3.30 mmol) in anhydrous DMF (10 mL) were added dropwise within 10 min under vigorous stirring. The reaction mixture was stirred for 2 h in at −10 °C and warmed to room temperature during 18 h. The yellow hygroscopic precipitate was collected, washed with acetonitrile (5 mL) and diethyl ether (2 × 5 mL), dissolved in MeOH (5 mL) and passed through an ion-exchange column (Dowex 1 × 8, in chloride form). After an additional filtration and removal of the solvent in vacuo, the residue was recrystallized from *i*PrOH–MeOH, to give 0.80 g (70%) of **55c (2 Cl^-)** as dirty-yellow amorphous solid, m.p. (dec.) 248–249 °C; R_f = 0.33 (system B); ^{1}H-NMR (400 MHz, CD_3OD): δ = 2.15 (dt, ^3J = 7 Hz, ^3J = 7 Hz, 2 H, $CH_2CH_2CH_2$), 2.96 (s, 6 H, CH_3), 3.31 (m, overlap with MeOD, CH_2NH), 3.61 (t, ^3J = 7 Hz, 2 H, CH_2NMe_2), 7.98 (dd, ^3J = 7 Hz, 1 H, 3-H), 8.13 (dd, ^3J = 9 Hz, ^3J = 7 Hz, 1 H, 2-H), 8.32 (d, ^3J = 9 Hz, 1 H, 8-H), 8.53 (d, ^3J = 9 Hz, 1 H, 7-H), 8.60 (d, ^3J = 9 Hz, 1 H, 1-H), 8.87 (s, 1 H, 10-H), 9.30–9.32 (m, 2 H, 11-H, 4-H), 10.36 (s, 1 H, 6-H); ^{13}C-NMR (100 MHz, CD_3OD): δ = 26.0 (CH_2), 38.0 (CH_2), 43.6 (2 CH_3), 56.8 (CH_2), 124.4 (CH), 127.9 (CH), 128.0 (CH), 128.4 (C_q), 128.5 (CH), 129.7 (CH), 130.3 (CH), 132.9 (CH), 135.6 (CH), 136.9 (C_q), 139.9 (C_q), 140.4 (C_q), 141.0 (CH), 168.4 (CO); MS (ESI^+) *m*/*z* (%) = 308 (100) $[M]^+$, 651 (5) $[2M + Cl]^+$; elemental analysis calcd (%) for $C_{19}H_{22}ClN_3O \times$ ½ HCl (362.1): C 63.03, H 6.26, N 11.61; found C 63.30, H 6.16, N 11.43.

4-(Adenin-9-yl)butyric acid (61): A solution of the ester **60** (2.50 g, 10.0 mmol) in 25 mL 1 N aqueous NaOH (25 mL) was stirred at room temperature for 18 h. The reaction mixture was cooled in an ice bath, and acetic acid (5 mL) was added. The white precipitate was

collected, washed with plenty of water, and dried in vacuo, to give the acid **61** (1.80 g, 81%) as a white amorphous solid, m.p. 291–294 °C (lit.[153] 296–297 °C). ^{1}H-NMR (400 MHz, [D$_6$]DMSO): δ = 2.05 (m, 2 H, $CH_2CH_2CH_2$), 2.24 (t, ^3J = 7 Hz, 2 H, CH_2CO), 4.18 (t, ^3J = 7 Hz, 2 H, CH_2N), 7.24 (bs, 2 H, NH_2), 8.15 (s, 1 H, Ade-H), 8.16 (s, 1 H, Ade-H); ^{13}C-NMR (100 MHz, [D$_6$]DMSO): δ = 25.1 (CH_2), 30.8 (CH_2), 42.5 (CH_2), 118.7 (C_q), 141.0 (C_q), 149.6 (CH), 152.5 (CH), 155.9 (C_q), 173.8 (COOH).

***N*-(4-Aminobutyl)-4-(adenin-9-yl)butyramide (62):** A solution of the ester **60** (1.00 g, 4.00 mmol) and 1,4-diaminobutane (2.82 g, 32.0 mmol) in *n*PrOH (8 mL) was heated under reflux for 10 h, while the reaction was monitored by TLC. After evaporation of all volatile components in vacuo, the residue was triturated with Et_2O (15 mL), the solid was collected, washed with Et_2O (5 mL) and MeCN (2 × 5 mL) and dried in vacuo / KOH, to give **62** (1.00 g, 86%) as white hygroscopic amorphous solid, which was used without further purification; R_f = 0.79 (system B); ^{1}H-NMR (400 MHz, CD_3OD): δ = 1.45–1.50 (m, 4 H, CH_2), 2.16–2.21 (m, 4 H, CH_2), 2.64 (t, ^3J = 7 Hz, 2 H, CH_2NH_2), 3.12 (t, ^3J = 7 Hz, 2 H, CH_2NHCO), 4.28 (t, ^3J = 7 Hz, 2 H, CH_2–Ade), 8.13 (s, 1 H, Ade-H), 8.21 (s, 1 H, Ade-H); ^{13}C-NMR (100 MHz, CD_3OD): δ = 27.2 (CH_2), 27.7 (CH_2), 30.9 (CH_2), 33.8 (CH_2), 40.2 (CH_2), 42.1 (CH_2), 44.4 (CH_2), 120.0 (C_q, C5), 142.8 (CH, C8), 150.8 (C_q, C4), 153.7 (CH, C2), 157.3 (C_q, C6), 174.4 (CO); MS (ESI$^+$) *m*/*z* (%) = 147 (28) $[M + 2H]^{2+}$, 292 (100) $[M + H]^+$. **Dipicrate**, m.p. 200–202 °C (EtOH); elemental analysis calcd (%) for $C_{13}H_{21}N_7O \times 2\ C_6H_3N_3O_7$ (749.6): C 40.06, H 3.63, N 24.29; found: C 40.00, H 3.55, N 23.88.

General procedure for the synthesis of acridizinium–adenine conjugates (GP-9). Carboxyacridizinium tetrafluoroborate **56a (BF$_4^-$)** or **56b (BF$_4^-$)** (311 mg, 1.00 mmol) was dissolved in anhydrous DMF (10 mL) and treated with NMM (121 µL, 110 mg, 1.10 mmol). The solution was cooled to −25 °C under argon atmosphere and treated with isobutyl chloroformate (143 µL, 150 mg, 1.10 mmol). After stirring for 10 min at this temperature, amine **62** (0.350 g, 1.20 mmol), dissolved in anhydrous DMF (15 mL), was added dropwise within 10 min. The reaction mixture was stirred at −25 °C for 2 h and warmed to room temperature during 18 h. Hydrogen chloride (2.5 mL of 1 M in Et_2O, 2.5 mmol) was added and, after stirring for 30 min at room temperature, the reaction mixture was evaporated to the final volume of ca. 2 mL. The residue was triturated with MeCN (25 mL), and the pale-yellow

precipitate was collected, washed with MeCN (3 × 10 mL) and AcOEt (2 × 10 mL) and dried in vacuo / P_2O_5, yielding the crude dichloride salt. A portion of the product was purified by MPLC (RP-18; eluent: 1% aq. TFA–MeCN, 85:15 v/v). The eluate was evaporated to dryness, and the residue was recrystallized from MeOH–AcOEt, to give analytically pure bis(trifluoroacetate) salt.

***N*-{4-[4-(Adenin-9-yl)butyrylamino]butyl}acridizinium-9-carboxamide bis(trifluoroacetate) (54a):** yield of the crude dichloride 270 mg (47%). Purified sample: lemon-yellow microcrystalline solid; m.p. (dec.) 181–184 °C; R_f = 0.24 (system B); ^{1}H-NMR (400 MHz, CD_3OD): δ = 1.57–1.64 (m, 2 H, Acr–CONH–$CH_2CH_2CH_2CH_2$NH); 1.68–1.75 (m, 2 H, Acr–CONH–$CH_2CH_2CH_2$), 2.19–2.29 (m, 4 H, Ade–$CH_2CH_2CH_2$CO), 3.21 (t, ^3J = 7 Hz, 2 H, Acr–CONH–$CH_2CH_2CH_2CH_2$NH), 3.50 (t, ^3J = 7 Hz, 2 H, Acr–CONH–CH_2), 4.35 (t, ^3J = 7 Hz, 2 H, Ade–CH_2), 7.97 (dd, ^3J = 7 Hz, ^3J = 8 Hz, 1 H, 3-H), 8.12 (dd, ^3J = 8 Hz, 1 H, 2-H), 8.27 (dd, ^3J = 9 Hz, ^4J = 1 Hz, 1 H, 8-H), 8.33 (s, 1 H, Ade-H), 8.37 (s, 1 H, Ade-H), 8.50 (d, ^3J = 9 Hz, 1 H, 7-H), 8.58 (d, ^3J = 9 Hz, 1 H, 1-H), 8.74 (s, 1 H, 10-H), 9.23 (s, 1 H, 11-H), 9.27 (d, ^3J = 7 Hz, 1 H, 4-H), 10.31 (s, 1 H, 6-H); ^{13}C-NMR (100 MHz, CD_3OD): δ = 27.0 (CH_2), 27.8 (CH_2), 27.9 (CH_2), 33.7 (CH_2), 40.1 (CH_2), 41.1 (CH_2), 45.0 (CH_2), 119.8 (C_q), 124.4 (CH), 127.7 (CH), 127.8 (CH), 128.4 (CH), 128.5 (C_q), 129.7 (CH), 130.3 (CH), 132.9 (CH), 135.6 (CH), 137.0 (C_q), 140.0 (C_q), 141.0 (CH), 141.1 (C_q), 145.4 (CH), 145.6 (CH), 150.5 (C_q), 152.0 (C_q), 167.9 (CO), 174.4 (CO); MS (ESI^+) *m*/*z* (%) = 498 (100) $[M]^+$; m.p. (dec.) 181–184 °C (MeOH–AcOEt); elemental analysis calcd (%) for $C_{31}H_{30}F_6N_8O_6$ (724.6): C 51.38, H 4.17, N 15.46; found: C 51.05, H 4.13, N 15.16.

***N*-{4-[4-(Adenin-9-yl)butyrylamino]butyl}acridizinium-3-carboxamide bis(trifluoroacetate) (54b):** yield of the crude dichloride 305 mg (54%). Purified sample: lemon-yellow prisms; m.p. 88–90 °C; R_f = 0.21 (system B); ^{1}H-NMR (400 MHz, CD_3OD): δ = 1.57–1.64 (m, 2 H, Acr–CONH–$CH_2CH_2CH_2CH_2$NH); 1.68–1.75 (m, 2 H, Acr–CONH–$CH_2CH_2CH_2$), 2.18–2.28 (m, 4 H, Ade–$CH_2CH_2CH_2$CO), 3.20 (t, ^3J = 7 Hz, 2 H, Acr–CONH–$CH_2CH_2CH_2CH_2$NH), 3.51 (t, ^3J = 7 Hz, 2 H, Acr–CONH–CH_2), 4.33 (t, ^3J = 7 Hz, 2 H, Ade–CH_2), 8.06 (dd, ^3J = 7 Hz, ^3J = 9 Hz, 1 H, 8-H), 8.19 (dd, ^3J = 7 Hz, ^3J = 9 Hz, 1 H, 9-H), 8.27 (s, 1 H, Ade-H), 8.29–8.31 (m, 2 H, 2-H, Ade-H), 8.41 (d, ^3J = 9 Hz, 1 H, 10-H), 8.50 (d, ^3J = 9 Hz, 1 H, 7-H), 8.55 (d, ^3J = 9 Hz, 1 H, 1-H), 9.17 (s, 1 H, 11-H), 9.67 (s, 1 H, 4-H), 10.37 (s, 1 H, 6-H); ^{13}C-NMR (100 MHz, CD_3OD): δ = 27.1 (CH_2), 27.6 (CH_2), 27.9 (CH_2), 33.7 (CH_2), 40.1 (CH_2), 41.2 (CH_2), 44.8 (CH_2), 111.9 (C_q), 126.3 (CH), 128.2 (CH), 128.5 (CH), 129.5 (CH), 129.6 (CH), 130.6 (C_q), 132.9 (CH), 136.0 (CH), 136.9 (CH), 138.2

(C_q), 138.3 (C_q), 139.3 (C_q), 142.5 (CH), 144.6 (CH), 148.2 (CH), 150.6 (C_q), 153.8 (C_q), 164.6 (CO), 174.4 (CO); elemental analysis calcd (%) for $C_{31}H_{30}F_6N_8O_6$ (724.6): C 51.38, H 4.17, N 15.46; found: C 51.60, H 4.30, N 15.77.

5.3 Single Crystal X-Ray Diffraction Analysis

Single crystals of **42a**, **44** and **38c** were obtained by crystallization from acetontrile–water. The X-ray diffraction measurements with **42a** and **44** were performed with a STOE IPDS,[a] whereas single-crystal measurements with **38c** were performed with a Siemens SMART CCD diffractometer.[b] The program SHELXS-97[172a] was used to perform the structure solutions by direct methods. The structures were refined on F^2 values using the program SHELXL-97.[172b] The hydrogen atoms were geometrically positioned and constrained. The non-hydrogen atoms were refined with anisotropic thermal parameters. For **44**, the hydrogen atoms of water molecules within the lattice could not be refined. Crystal data and structure refinement details are given in Table 5.1.

[a] In cooperation with H. Mikus and Prof. H.-J. Deiseroth, Institut für Anorganische Chemie, Universität Siegen (Siegen, Germany).

[b] In cooperation with Dr. Jan W. Bats, Institut für Organische Chemie und Chemische Biologie, Johann-Wolfgang-Goethe-Universität Frankfurt (Frankfurt am Main, Germany).

Table 5.1. Crystal data and structure refinement details of the compounds **42a**, **44** and **38c**.

Parameter	**42a**	**44**	**38c**
CCDC No.	275724	275725	298121
Molecular Formula	$C_{22}H_{18}B_2F_8N_2$	$C_{22}H_{22}B_2F_8N_2O_2$	$C_{24}H_{16}B_2F_8N_2$
Temperature / K	173(2)	123(2)	159(2)
Wavelength / Å	0.71073	0.71073	0.71073
Space group	$P\bar{1}$ (No. 2)	$P\,2_1/n$ (No. 14, cell choice 2)	$C2/c$ (No. 15)
Unit cell dimensions	a = 10.538(1) Å	a = 11.921(1) Å	a = 18.083(5) Å
	b = 7.4098(7) Å	b = 15.150(1) Å	b = 9.4536(18) Å
	c = 13.373(1) Å	c = 13.503(1) Å	c = 12.1006(19) Å
	α = 93.29(1)°		
	β = 102.77(1)°	β = 112.15(1)°	β = 90.37(2)°
	γ = 86.60(1)°		
Volume / Å^3	1015.5(2)	2258.7(3)	2068.5(7)
Z	2	4	4
Calculated density / g cm^{-3}	1.583	1.529	1.625
Absorption coefficient / mm^{-1}	0.144	0.141	0.145
F(000)	492	1064	1024
Crystal size / mm	0.3 × 0.3 × 0.2	0.3 × 0.3 × 0.2	0.60 × 0.28 × 0.14
Measured θ range	$2.76 \geq \theta \geq 30.44$	$2.11 \geq \theta \geq 27.16$	$2.25 \leq \theta \leq 32.59$
Limiting indices	$-14 \geq h \geq 14$	$-15 \geq h \geq 15$	$-26 \leq h \leq 26$
	$-10 \geq k \geq 10$	$-19 \geq k \geq 19$	$-14 \leq k \leq 13$
	$-18 \geq l \geq 18$	$-17 \geq l \geq 17$	$-18 \leq l \leq 17$
Reflections collected / unique	15232 / 5598	19635 / 4803	14494 / 3519
R_{int}	0.0475	0.0731	0.0580
Data / restraints / parameters	5598 / 0 / 309	4803 / 0 / 349	3519 / 0 / 164
Goodness of fit on F^2	0.943	0.918	1.028
R values [$I^2 \geq 2\sigma(I)$]	R_1 = 0.0440 wR_2 = 0.0746	R_1 = 0.0628 wR_2 = 0.1549	R_1 = 0.0472, wR_2 = 0.1069
R values (all data)	R_1 = 0.0746 wR_2 = 0.1209	R_1 = 0.1212 wR_2 = 0.1759	R_1 = 0.0876 wR_2 = 0.1252
Final Fourier residuals	0.686 and –0.305 e Å^{-3}	0.690 and –0.519 e Å^{-3}	0.385 and –0.294 e Å^{-3}

5.4 Investigations of the Photophysical Properties

5.4.1 UV/Visible Absorption and Fluorescence Spectroscopy

All spectrophotometric measurements were performed in thermostated quartz sample cells (pathlength ℓ = 1 cm) at 20 °C in spectral-grade solvents (Fluka, Riedel–de Haën). Solutions were freshly prepared by dilution of stock solutions (1 mM in acetonitrile or methanol). For the diazoniapolycyclic salts (compounds **7a–c**, **38a–c**, **42a–c**, **44**, **51**), the solution concentrations were 20 µM for absorption spectroscopy and 5 µM for fluorescence spectroscopy; for the other compounds investigated in this study, the concentrations were 50 and 10 µM for absorption and fluorescence spectroscopy, respectively. Spectrophotometer slit widths were 2 nm for absorption spectroscopy and 2.5 nm for emission spectroscopy. Fluorescence emission spectra were smoothed using the moving-average function implemented into the Cary Eclipse software, and corrected by multiplication of the raw spectra by the system response function, $\kappa(\lambda)$, provided by the manufacturer.

The relative fluorescence quantum yields, Φ_F, were determined by the standard method,[18,173] taking into account the refractive indices of the solvents (Eq. 5.1).

$$\Phi_F = \frac{J_x\,(1 - T_s)}{J_s\,(1 - T_x)} \times \frac{n_x^{\,2}}{n_s^{\,2}} \times \Phi_s \qquad \text{(Eq. 5.1)}$$

The subscripts “x” and “s” refer to the substance under investigation and the reference dye, respectively; $J = \int I_F(\lambda)\,\mathrm{d}\lambda$ is the emission integral over the area of interest; $T = 10^{-\varepsilon(\lambda_{ex})c\ell}$ is the optical transmittance of the sample solution at the excitation wavelength, λ_{ex}; and n is the refractive index of the solvent.

Since the compounds investigated in this study exhibit fluoresce emission in various areas of the visible part of the spectrum (410–650 nm), it was necessary to use several reference dyes for the determination of the relative quantum yields. Thus, Coumarin 1 (Aldrich), Coumarin 153 (laser grade, Acros Organics) and Cresyl Violet (Radiant Dyes) were used as references (Table 5.2).

Table 5.2. Fluorescence quantum yield standards used in this work.

Reference dye	λ_{abs} / nm [a]	λ_{em} / nm [b]	Φ_F (solvent) [c]	Ref.
Coumarin 1	340–400	400–520	0.73 (EtOH)	174
Coumarin 153	380–480	480–650	0.38 (EtOH)	174
Cresyl Violet	520–620	580–720	0.54 (MeOH)	175

[a] Absorption range; [b] useful fluorescence emission range; [c] fluorescence quantum yield.

5.4.2 Acid–Base Spectrophotometric Titrations of Compound 27d

[AG-II-42]

The Britton–Robinson buffer solution[95] was prepared from boric acid, phosphoric acid and sodium acetate (0.04 M each) in purified water and neutralized to pH 7.0 by addition of 2 M NaOH solution.

An aliquot (20 mL) of a 50 µM solution of compound **27d** in the buffer solution was placed into a beaker equipped with a magnetic stirrer and a pH sensor. The spectrophotometric titration was performed by adding aliquots of aqueous HCl solution (2 M), measuring the pH of the solution, and recording UV/Vis absorption spectra of a portion (ca. 3 mL) of the solution, using quartz spectrophotometric cells. After recording each spectrum, the sample was quantitatively returned to the titration beaker.

The titrations were performed three times in the pH range between 1 and 7, and the data from UV/Vis spectra were plotted as function of pH of the solution. To obtain the value of the acidity constant, the titration isotherms were numerically fitted to the Henderson–Hasselbach equation in the form of Eq. 5.2.[176]

$$A = \frac{A_{HA}\, 10^{-pH} + A_A\, 10^{-pK_a}}{10^{-pH} + 10^{-pK_a}} \qquad \text{(Eq. 5.2)}$$

Here A is the absorbance at the selected fixed wavelength in the course of titration, A_{HA} is the absorbance at this wavelength of the protonated form, and A_A is the absorbance at this wavelength of the basic form.

5.4.3 Viscosity Dependence of Fluorescence

5.4.3.1 Fluorescence Spectroscopy using Water–Glycerol Mixtures

[AG-III-21]

Glycerol–water mixtures with different viscosity were prepared by mixing the weighted amounts of purified water and anhydrous, spectroscopy-grade glycerol (Fluka), such that the total weight of the mixtures was 40.0 g in each case. The composition of the mixtures was additionally checked by the measurement of their refractive indices and comparison with published data (Table 5.3).[96]

Table 5.3. Preparation of glycerol–water mixtures of varied viscosity.

Weight-% glycerol	n_D^{20} [a]	η_{20} / cP [b]	d_{20} / g mL^{-1} [c]
0	1.3328	1.005	1.0000
20	1.3571	1.769	1.0470
40	1.3849	3.750	1.0995
60	1.4137	10.96	1.1533
70	1.4287	22.94	1.1808
80	1.4431	62.00	1.2079
85	1.4510	112.9	1.2214
90	1.4581	234.6	1.2347
95	1.4663	545.0	1.2482
100	1.4732	1499	1.2609

[a] Measured refractive index; [b] dynamic viscosity at 20 °C, according to Ref. 96; [c] density at 20 °C, according to Ref. 96.

Aliquots (50 µL) of the stock solutions of the dyes were pipetted into glass vials, and the latter were left open until the solvent evaporated. To the residues, weighted amounts of the glycerol–water mixtures were added such that their volume equaled 5.00 mL in each case. The vials were tightly closed and placed into a warm (50–60 °C) ultrasonic bath to dissolve the dyes. Especially in the case of highly viscous samples, prolonged treatment (30–40 min) was necessary for the complete solubilization. The final concentration of the dyes was 10 µM.

After cooling to room temperature, the samples were transferred into disposable fluorimetric cells (polymethylmethacrylate, Carl Roth GmbH, Karlsruhe, Germany) and their fluorescence spectra were measured at 20 °C at the conditions described above.

5.4.3.2 Fluorescence Spectroscopy at Different Temperatures

[AG-III-23]

For the fluorescence measurements at different temperatures, solutions of the dyes in anhydrous glycerol (c = 10 μM) were prepared as described above and placed into quartz fluorimetric cells. The emission spectra were recorded in the range 0–100 °C in 5–10 °C steps, using the thermoelectric temperature controller. Between temperature changes, the samples were left for 10–15 min to reach the thermal equilibrium. Viscosities and the refractive indices of glycerol at different temperatures (the latter were used for the calculations of the quantum yield of fluorescence according to Eq. 5.1)[177] are given in Table 5.4. The changes in the molar concentration of the dyes, caused by the thermal expansion of the solvent, were not taken into account.

Table 5.4. Viscosities and refractive indices of anhydrous glycerol at different temperatures.

T / °C	η / cP [a]	n_D [b]	T / °C	η / cP [a]	n_D [b]
0	12070	1.48027	40	284	1.47145
5	6772	1.47850	50	142	1.47047
10	3900	1.47688	60	81.3	1.46966
15	2322	1.47565	70	50.6	1.46893
20	1412	1.47442	80	31.9	1.46819
25	919	1.47356	90	21.3	1.46741
30	612	1.47272	100	14.8	1.46654

[a] Dynamic viscosity at 20 °C, according to Ref. 96; [b] refractive index, according to Ref. 177.

5.4.4 Photodegradation of Diazoniapolycyclic Salts 38c and 51 in Solution

[AG-II-133]

The solutions of the salts **38c** and **51** at a concentration c = 100 μM were prepared in purified water. For studies at oxygen-free conditions, samples were deoxygenated by passing argon gas for at least 45 min through the solutions; otherwise, solutions were air-equilibrated. The solutions were placed into quartz reduced-path spectrophotometric cells (pathlength ℓ = 2 mm; side area 3.33 cm²) and irradiated in a Rayonet photoreactor (λ_L = 350 nm, irradiance I_L = 7.2 mW cm^{-2}) for 1 h. UV/Vis absorption spectra were determined in 5 to

10 min intervals. The relative decrease of the absorption, $A(t)/A_0$, was plotted as a function of irradiation time, *t*.

5.5 Nucleic Acids Binding Studies

5.5.1 Buffer Solutions

All buffer solutions were prepared from purified water (resistivity 18 MΩ cm^{-1}) and biochemistry-grade chemicals (Fluka BioChemika Ultra). The buffer solutions were stored at 4 °C up to three months and filtered through a membrane filter (pore size 0.45 μm; Carl Roth GmbH, Karlsruhe, Germany) prior to use.

BPE buffer (6.0 mM Na_2HPO_4, 2.0 mM NaH_2PO_4, 1.0 mM Na_2EDTA; total Na^+ concentration 16.0 mM; pH 7.0) was routinely used for DNA titrations and thermal denaturation studies (except for the works with triplex DNA and synthetic oligonucleotides).

BPES buffer (6.0 mM Na_2HPO_4, 2.0 mM NaH_2PO_4, 1.0 mM Na_2EDTA, 185 mM NaCl; total Na^+ concentration 201 mM; pH 7.0) was used for thermal denaturation studies with the triplex DNA and for competition dialysis experiments.

ODN buffer (6.1 mM Na_2HPO_4, 3.9 mM NaH_2PO_4, 1.0 mM Na_2EDTA, 20 mM NaCl; total Na^+ concentration 38.1 mM; pH 7.0) was used for thermal denaturation studies with synthetic oligonucleotides.

ETN buffer (1 mM Na_2EDTA, 10 mM TRIS, 10 mM NaCl; pH 7.0) was used for flow linear dichroism studies of DNA–ligand complexes.

$I_{½}$ buffer (5.0 mM KH_2PO_4, 50 mM NaCl; pH 7.4) was used for works with plasmid DNA.

5.5.2 Nucleic Acids

Calf thymus DNA (type I; highly polymerized sodium salt) was purchased from Sigma (St. Louis, MO, USA) and used without further purification. $[Poly(dAdT)]_2$, $[poly(dGdC)]_2$, poly(dA)–poly(dT) and poly(dT) were purchased from Amersham Biosciences (Piscataway, NJ, USA). Ct DNA was dissolved in an appropriate buffer (*vide supra*) at a concentration of 1–2 mg mL^{-1} and left at 4 °C overnight. After treatment (10 min) in an ultrasonic bath, the

solution was filtered through a PVDF membrane filter (pore size 0.45 µm; Carl Roth GmbH, Karlsruhe, Germany) to remove any insoluble material.

Triplex poly(dA)–[poly(dT)]$_2$ was prepared by mixing equimolar amounts of poly(dT) and poly(dA)–poly(dT), dissolved each in BPES buffer at a concentration of approx. 1 mM (bases or bp, respectively), heating to 90 °C in a water bath, and slow cooling to 4 °C overnight.[81] Concentrations of nucleic acid samples were determined by UV absorbance measurements of diluted (1:20) stock solution, using the extinction coefficients given in the Table 5.5; the quality of nucleic acids was checked by comparing their melting temperatures with the published data.[81,139]

Table 5.5. Properties of nucleic acids used in this work.

Nucleic Acid	Unit [a]	λ_{max} / nm [b]	ε / cm^{-1} M^{-1} [c]	T_m / °C [d]
poly(dT)	base	264	8520	—
ct DNA	bp	260	12824	68.2 ± 0.2
[poly(dAdT)]$_2$	bp	262	13200	44.0 ± 0.2
poly(dA)–poly(dT)	bp	260	12000	74.9 ± 0.4
[poly(dGdC)]$_2$	bp	254	16800	> 100
poly(dA)–[poly(dT)]$_2$	bt	260	17200	42.8 ± 0.2 [e] [f] 74.8 ± 0.1 [g]

[a] Nucleic base, base pair, or base triplet, respectively; [b] absorption maximum; [c] molar extinction coefficient with respect to the unit; [d] melting temperature of the DNA, determined in BPE buffer; [e] determined in BPES buffer; [f] triplex-to-duplex transition; [g] duplex-to-coil transition.

5.5.3 Spectrophotometric and Spectrofluorimetric Titrations

5.5.3.1 Sample Preparation and Experimental Conditions

Spectrophotometric titrations of acridizinium salts with ct DNA, aimed at the determination of the binding constants, were performed in aqueous BPE buffer at a ligand concentration c_L = 50 µM. To avoid dilution of the analyte solutions, the titrant solutions contained ct DNA at a concentration c_{DNA} = 1–2 mM (bp) (approx. 1–2 mg mL^{-1}) as well as the ligand at the same concentration as in the titrated solution.

Preparation of the titrant solutions: aliquots (50 µL) of the stock solution of the ligand (1 mM in acetonitrile or methanol) were pipetted into Eppendorf vials and the latter were left open until all solvent evaporated. To the remaining residue, 1.00 mL of DNA solution of known

concentration (determined by UV absorbance measurements using the extinction coefficients given in Table 5.5) was added, and the samples were sonicated in 5-min intervals until the ligand dissolved completely.

Titrations: aliquots (2.00 mL) of the analyte solutions in BPE buffer were placed into quartz spectrophotometric cells and titrated with the titrant solutions in 0.5–2 equivalent intervals. UV/Vis or fluorescence spectra were measured at the conditions described in Section 5.4.1 (wavelength range 300–600 nm). The titrations were finished after no changes were observed in absorption spectra upon addition of at least three two-equivalent portions of the titrant. All spectrophotometric titrations were performed at least three times to ensure the reproducibility.

Spectrofluorimetric titrations were performed essentially as described for the spectrophotometric titrations. In this case, a ligand concentration c_L = 10 μM was used, and titrant solutions contained only DNA, as the dilution effect was negligible. The excitation wavelength for spectrofluorimetric titrations corresponded to one of the isosbestic points, as determined from the spectrophotometric titrations.

5.5.3.2 Data Evaluation and Determination of Binding Constants

Firstly, the concentration of the ligand bound to the DNA was calculated (Eq. 5.3).

$$c_b = c_L \times \frac{A_f - A}{A_f - A_b} \qquad \text{(Eq. 5.3)}$$

Here c_L is the bulk concentration of the ligand, A_f is the absorbance at a given wavelength (usually absorption maximum of the unbound ligand) in the absence of DNA, A_b is the absorbance of the fully bound ligand, and A is the absorbance at a given ligand-to-DNA ratio. The standard deviation of the c_b values is given by Eq. 5.4.[178]

$$\sigma_{c_b} = c_b \times \sqrt{\frac{\sigma^2_{A_f} + \sigma^2_A}{(A_f - A)^2} + \frac{\sigma^2_{A_f} + \sigma^2_{A_b}}{(A_f - A_b)^2}} \qquad \text{(Eq. 5.4)}$$

Note that the error in the total concentration of the dye is neglected, since usually the same stock solution is used for all spectrophotometric titrations.

Then, the concentration of the unbound dye (c) was calculated (Eq. 5.5).

$$c = c_L - c_b \qquad \text{(Eq. 5.5)}$$

Its error is equal to the one of the bound dye concentration (Eq. 5.6).

$$\sigma_c = \sigma_{c_b} \qquad \text{(Eq. 5.6)}$$

The ratio of bound ligand molecules per DNA base pair (r) and its standard deviation (σ_r) were calculated using Eqs. 5.7 and 5.8.

$$r = \frac{c_b}{c_{DNA}} \qquad \text{(Eq. 5.7)}$$

$$\sigma_r = \frac{\sigma_{c_b}}{c_{DNA}} \qquad \text{(Eq. 5.8)}$$

Again, no error in the DNA concentration is assumed since it is not determined in the course of titration.

Finally, the r/c values and their standard deviations ($\sigma_{r/c}$) were calculated (Eq. 5.9).

$$\sigma_{r/c} = \frac{r}{c} \times \sqrt{\frac{\sigma^2_{c_b}}{r^2 c^2_{DNA}} + \frac{\sigma^2_{c_b}}{c^2}} = \frac{\sigma_{c_b}}{c} \times \sqrt{\left(\frac{1}{c_{DNA}}\right)^2 + \left(\frac{r}{c}\right)^2} \qquad \text{(Eq. 5.9)}$$

The data were presented as Scatchard plots, *i.e.* r/c *vs.* r values, and numerically fitted to the neighbor exclusion model of McGhee and von Hippel (Eq. 5.10),[69] to determine the values of the binding constant (K) and the binding site size (n). The numerical fitting was performed using the Levenberg–Marquardt non-linear curve fitting algorithm implemented into the Origin® software.

$$\frac{r}{c} = K(1 - nr)\left(\frac{1 - nr}{1 - (n-1)r}\right)^{n-1} \qquad \text{(Eq. 5.10)}$$

5.5.4 DNA Thermal Denaturation Studies

5.5.4.1 Sample Preparation

To avoid possible effects from the co-solvents, aliquots of the stock solution of the ligand (1 mM in acetonitrile or methanol) were pipetted into Eppendorf vials and the latter were left

open until all solvent evaporated. The residue was dissolved in an aqueous buffer. Studies with ct DNA and synthetic double-stranded nucleic acids were performed in BPE buffer; experiments with the triplex DNA were performed in BPES buffer (Section 5.5.1). The volume of the buffer solution was calculated taking into account the concentration of the DNA stock solution, to provide a final volume of 1.00 mL. The samples were degassed in an ultrasonic bath for 15 min. Fixed amounts of nucleic acids (final concentration 40 μM bp or bt) were added; the samples were mixed briefly and transferred into the masked, semi-micro quartz cells (pathlength ℓ = 1 cm).

5.5.4.2 Experimental Conditions

DNA melting curves were recorded with a Varian Cary 100 spectrophotometer equipped with a thermoelectric temperature controller. Samples were heated from 20.0 °C to 97.0 °C at a rate of 0.2 deg min^{-1}, while the absorbance was monitored at 260 nm and, in selected cases, additionally at 370 nm, where only ligands absorb.

5.5.4.3 Data Evaluation and Determination of Melting Temperatures

The melting curves were presented as plots of normalized absorbance change, $\hat{A}$ (Eq. 5.11), versus temperature (Figure 5.1, Figure 5.2).

$$\hat{A} = \frac{A_T - A_{40\,°C}}{A_{max}} \qquad \text{(Eq. 5.11)}$$

Here A_T is absorbance at 260 nm at a given temperature, $A_{40\,°C}$ is absorbance at 40 °C, and A_{max} is the maximum absorbance in the range of interest (usually 40–90 °C).

To determine the temperatures of the melting transitions, T_m, numerical derivation of the plots was performed. In the case of sharp peaks, these were taken as maxima in the derivative plots; otherwise, the peak areas were approximated with Gaussian peak functions, which centers were taken as the melting temperatures. In the case of extremely broad (> 15 °C) melting transitions, the melting temperature was defined as the middle point of the corresponding absorbance change.

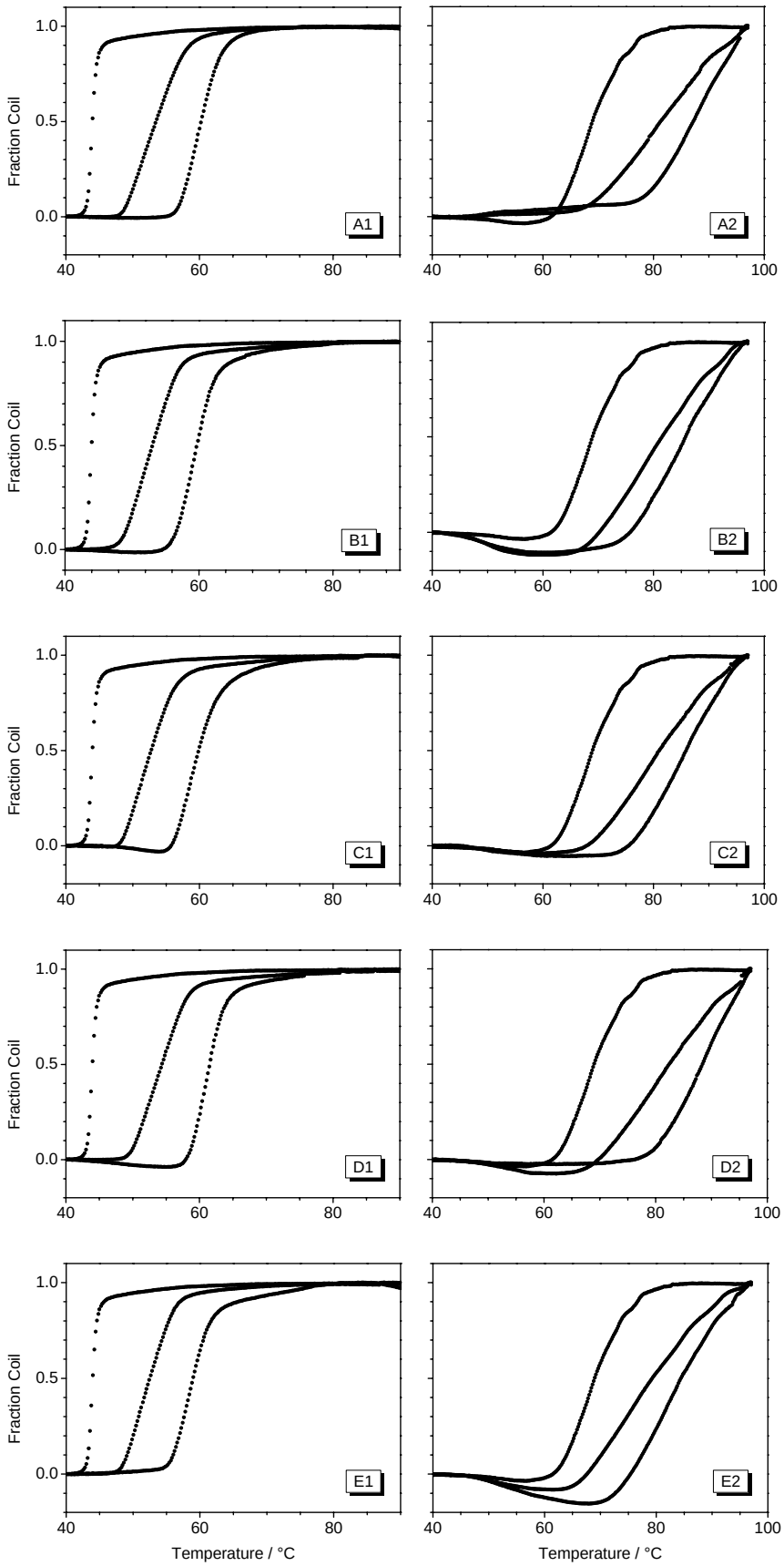

Figure 5.1. Melting profiles of $[poly(dAdT)]_2$ (1) and ct DNA (2) in the presence of **7a** (A), **7b** (B), **7c** (C), **42a** (D) and **42b** (E) at ligand-to-DNA ratios (r) of 0, 0.2, and 0.5; c_{DNA} = 40 μM (bp) in BPE buffer.

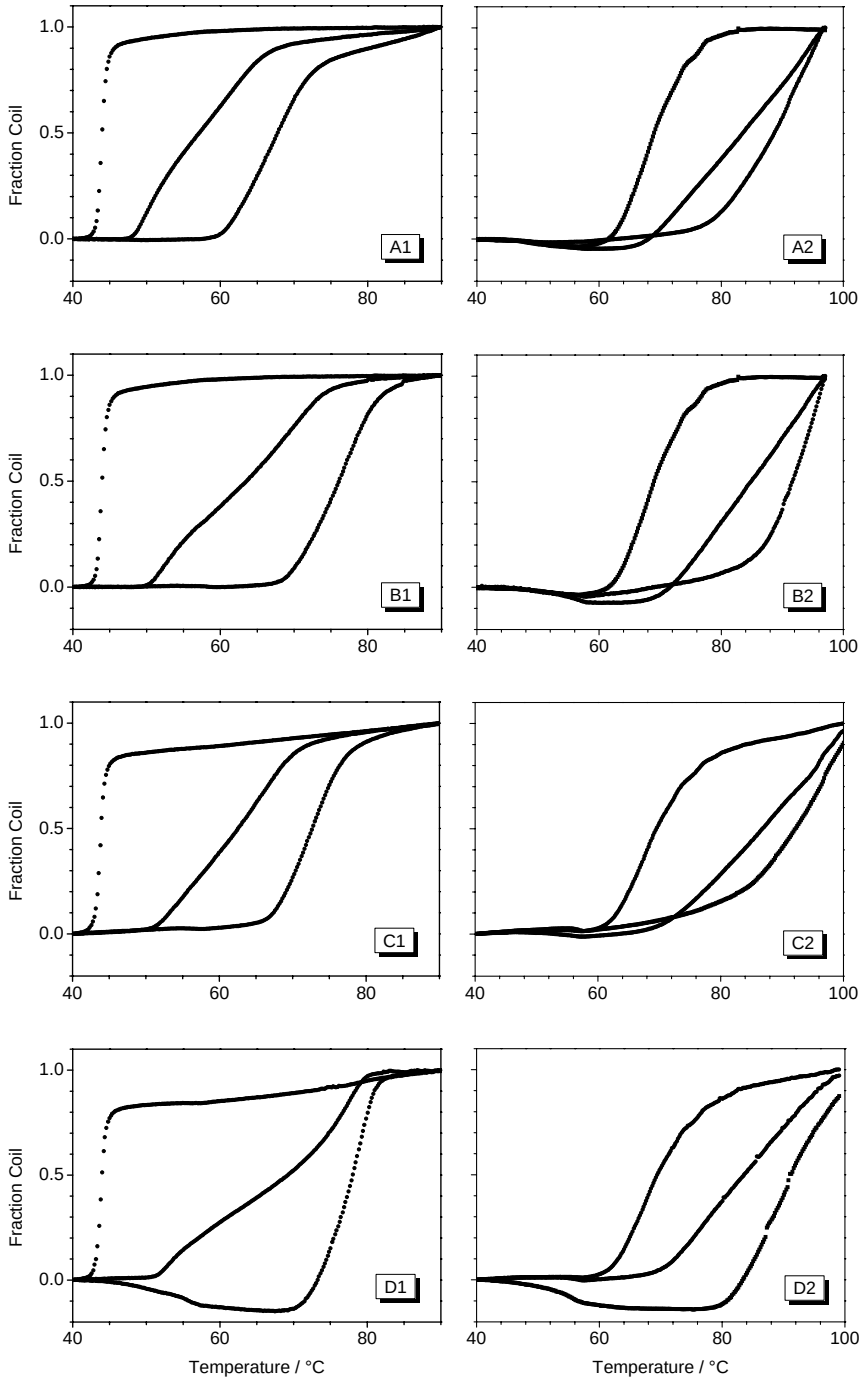

Figure 5.2. Melting profiles of $[poly(dAdT)]_2$ (1) and calf thymus DNA (2) in the presence of **38a** (A), **38b** (B), **38c** (C) and **51** (D) at ligand-to-DNA ratios (r) of 0, 0.2, and 0.5; c_{DNA} = 40 µM (bp) in BPE buffer.

The ligand-induced shifts of DNA melting transitions (ΔT_m) were calculated according to Eq. 5.12 and plotted as a function of ligand-to-DNA ratio, $r = c_L / c_{DNA}$.

$$\Delta T_m = T_m(\text{DNA-Ligand}) - T_m(\text{DNA}) \qquad \text{(Eq. 5.12)}$$

5.5.4.4 Salt Dependence of Melting Temperatures

[AG-II-107]

To determine the melting temperatures of the $[poly(dAdT)]_2$ duplex at various Na^+ concentration, a series of solutions was prepared by mixing the corresponding amounts of BPE and BPES buffers (Table 5.6).

Table 5.6. Sample preparation for determination of T_m values at various ionic-strength conditions

Sample No.	Total $[Na^+]$ / mM	V_{BPE} / µL	V_{BPES} / µL
1	16	960	0
2	25	910	50
3	40	830	130
4	60	722	238
5	100	506	454
6	195	0	960

Aliquots of a stock solution of the polynucleotide (40 µL of the 1.0 mM solution in BPE buffer; final concentration 40 µM bp) were added, and melting temperatures were determined as described in Sections 5.5.4.2–5.5.4.3. The experiment was then repeated in the presence of the ligand **7b** at $r = 0.5$ (ligand concentration $c_L = 20$ µM).

5.5.4.5 Thermal Denaturation of Oligonucleotide–Ligand Complexes

Oligodeoxyribonucleotides (synthesis scale 200 nmol, purified by RP-HPLC) were purchased from Eurogentec S.A. (Seraing, Belgium); their quality was confirmed by mass-spectrometric analysis data provided by the manufacturer. Lyophilized ODNs were dissolved in ODN buffer (Section 5.5.1) to a strand concentration of 500 µM; the required volume of the buffer depends on the amount of the ODN in each particular sample, as indicated by the manufacturer. Solutions of the ODNs were stored at −25 °C.

Working solutions of the ligands were prepared in ODN buffer at concentration of 200 µM, by dilution of the stock solutions (1 mM in methanol or acetonitrile). Samples for thermal denaturation studies were prepared by mixing two oligonucleotide strands (final concentration of each strand 5 µM) with working solutions of the ligands and ODN buffer, as indicated in Table 5.7.

Table 5.7. Sample preparation for thermal denaturation experiments with ODNs.

Sample Nr.	r	c_L / µM	V_L / µL	$V_{ODN\text{-}A}$ / µL	$V_{ODN\text{-}B}$ / µL	V_{Buffer} / µL
1	0	0	0	10	10	980
2	0.2	1.00	5.00	10	10	975
3	0.5	2.50	12.5	10	10	968
4	1.0	5.00	25.0	10	10	955
5	1.5	7.50	37.5	10	10	943
6	2.0	10.0	50.0	10	10	930

After mixing and degassing for 15 min in the ultrasonic bath, the samples were transferred into the masked, semi-micro quartz cells (pathlength $\ell = 1$ cm) and melting curves were recorded. In the case of experiments with ODNs, an additional annealing step was required. Therefore, the instrument was set to perform the following program:

(1) heating from ambient temperature to 80.0 °C in a 2.5 deg min^{-1} ramp;

(2) annealing at 80.0 °C for 5 min;

(3) cooling to 5 °C in a 1.0 deg min^{-1} ramp;

(4) heating from 5 to 90 °C in a 0.2 deg min^{-1} ramp. At this stage, absorbance of samples was monitored at 260 nm.

To determine the temperatures of melting transitions, T_m, numerical derivation of the plots was performed, and the peak areas were approximated with a Gaussian peak function. The ligand-induced shifts of DNA melting transitions (ΔT_m) were calculated according to Eq. 5.11 and plotted as a function of ligand-to-DNA ratio, $r = c_L / c_{DNA}$. In this case, c_{DNA} refers to the concentration of ODN strands.

5.5.5 Competition Dialysis Assay

[AG-I-115/116/120]

5.5.5.1 Sample Preparation and Experimental Conditions

All dialysis experiments were performed in aqueous BPES buffer (Section 5.5.1). For each dialysis assay, 500 mL of the 1 µM ligand solution were placed into a beaker. Five various DNA samples (1.25 mL at the concentration of 75 µM monomeric unit) were placed into separate dialysis tubes (MW cutoff 3500 Da; Carl Roth GmbH, Karlsruhe, Germany). All five

tubes were placed into the beaker containing the ligand solution, and dialysed with continuous stirring for 48 h at room temperature (20–22 °C) under light protection. At the end of this period, aliquots of DNA samples (1.00 mL) were taken from the dialysis tubes and placed into microfuge tubes. Sodium dodecyl sulfate (SDS; 111 µL of 10% w/v aqueous solution; final concentration 1%) was added, and samples were mixed thoroughly. The total ligand concentration within each dialysis tube (c_t) was determined spectrophotometrically, using the calibration curve of the corresponding ligand. The concentration of the free ligand (c_f) was determined with an aliquot of the dialysate solution by the same procedure. The amount of bound ligand was determined by the difference, $c_b = c_t - c_f$, and plotted as a bar graph.

5.5.5.2 Calibration Curves

The addition of SDS, that is employed to dissociate the DNA–ligand complexes, results in bathochromic shifts of the ligand absorption maxima by 5–10 nm, both for the diazoniapolycyclic salts (Figure 5.3, A–B) and for ethidium bromide (reference compound). Therefore, the calibration curves were used to determine the actual ligand concentrations. These curves were derived from samples with known concentrations of the ligand in the presence of 1% SDS, in order to determine the extinction coefficients of the ligands at these conditions.

Two sets of nine samples with different ligand concentrations (0.5, 1.0, 1.5, 2.0, 3.0, 4.0, 6.0, 10.0, 15.0 µM) were prepared by dilution of the ligand stock solution (20 µM in BPES buffer) to the final volume of 1.00 mL. SDS (111 µL of aqueous 10% w/v solution; final concentration 1% w/v) or equal amount of purified water was added, and samples were thoroughly mixed and analyzed by UV/Vis absorption spectroscopy. The calibration curves for ligands in the presence of 1% w/v SDS were constructed using the corresponding values of absorbance at the absorption maxima (Figure 5.3, C). The extinction coefficients of ligands **7b** and **38a** in BPES buffer in the presence of 1% SDS are given in Table 5.8.

Table 5.8. Absorption maxima and extinction coefficients for the ligands in BPES buffer in the presence of 1% (w/v) SDS.

Ligand	λ_{max} / nm	ε_{max} / cm^{-1} M^{-1}
7b	358.5	53800
38a	375.0	28500

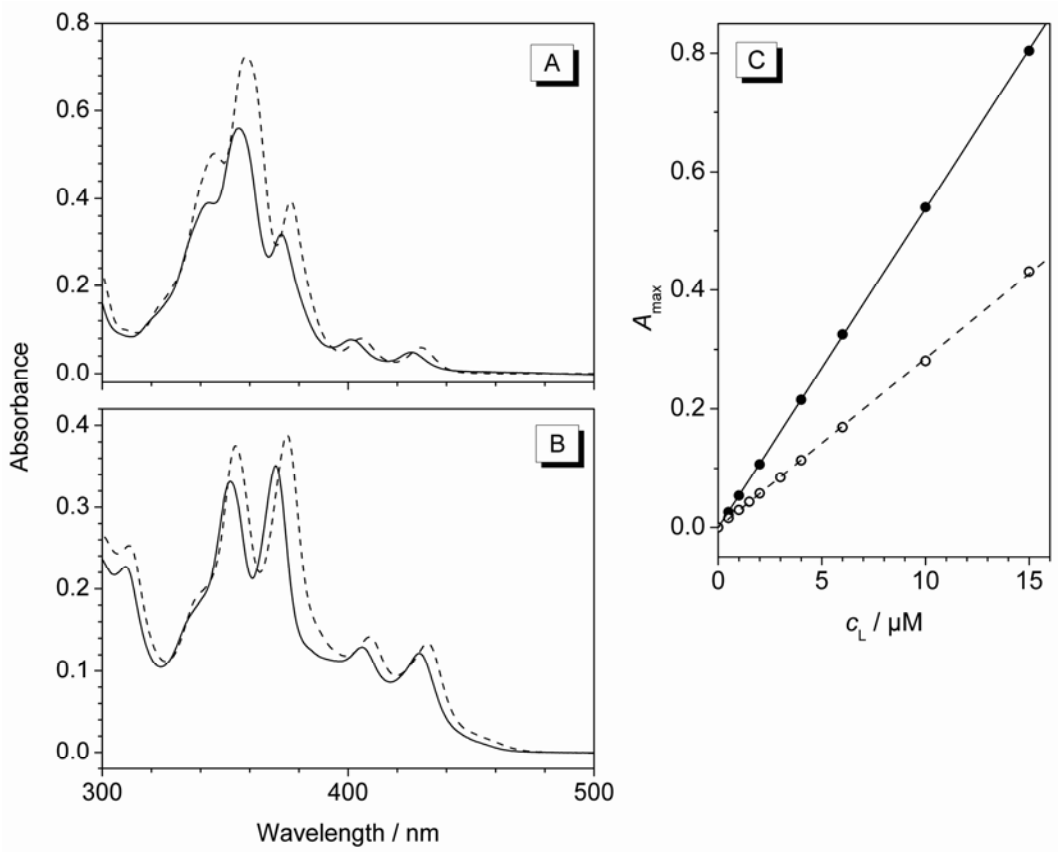

Figure 5.3. Representative absorption spectra of **7b** (A) and **38a** (B) in BPES buffer in the absence (solid lines) and in the presence (dashed lines) of 1% (w/v) SDS. Ligand concentration c_L = 15 µM in all cases. (C) Calibration graphs for determination of extinction coefficients of **7b** (filled circles and solid lines) and **38a** (open circles and dashed lines) in BPES buffer containing 1% (w/v) SDS.

5.5.6 Linear Dichroism Spectroscopy[a]

Linear dichroism spectra of the ligand–nucleic acid complexes were recorded in ETN buffer (Section 5.5.1) in a flow cell on a Jasco J500A spectropolarimeter equipped with an IBM PC and a Jasco J interface. Partial alignment of the DNA was provided by a linear-flow device designed by Wada and Kozawa[179] at a shear gradient of approx. 800 RPM. Concentration of DNA in samples for LD spectroscopy constituted approx. 1 mM (bp), and ligand-to-DNA ratios r = 0, 0.04, 0.08 and 0.2 were used.

Linear dichroism is defined as the differential absorption of orthogonal forms of linearly polarized light (Eq. 5.13).

[a] In cooperation with A. Faccio and Dr. G. Viola, Department of Pharmaceutical Sciences, Universitá di Padova (Padua, Italy).

$$LD = A_{\parallel} - A_{\perp} \qquad \text{(Eq. 5.13)}$$

$A_{\parallel}$ corresponds to the absorbance of the sample when the light is polarized parallel to the orientation of flow, and $A_{\perp}$ is the perpendicular absorbance. The "reduced" linear dichroism, LD_r, reflects the dependence of the LD on the wavelength (Eq. 5.14).

$$LD_r = LD / A_{iso} \qquad \text{(Eq. 5.14)}$$

Here A_{iso} is the absorbance of an isotropic sample, determined by the measurement of absorption spectra of ligand–DNA complexes. The "reduced" linear dichroism may be related to the orientation of DNA (S) and the angle between the respective light-absorbing transition moment and DNA helix axis according to Nordén *et al.*[79b] (Eq. 5.15).

$$LD_r = \frac{3}{2} \times S\,(3\cos^2\alpha - 1) \qquad \text{(Eq. 5.15)}$$

Assuming a value of $\alpha = 90°$ for the DNA bases for a ligand bound to it, α is given by Eq. 5.16.

$$\alpha_L = \arccos\sqrt{\frac{1}{3} \times \left(1 - \frac{(LD_r)_L}{(LD_r)_{DNA}}\right)} \qquad \text{(Eq. 5.16)}$$

Here $(LD_r)_L$ is the reduced linear dichroism for the ligand, $(LD_r)_{DNA}$ is the reduced LD for DNA and α_L defines the ligand-DNA relative orientation. For an intercalated system, $\alpha_L \approx 90°$ and $(LD_r)_L \approx (LD_r)_{DNA}$.

5.6 Protein Binding Studies

5.6.1.1 Proteins

[AG-III-01/02]

Bovine serum albumin (BSA, fraction V, $\geq$ 98.0%) was purchased from Fluka (Buchs, Switzerland); human serum albumin (HSA, 97–99%, lyophilized) and chicken egg white albumin (CEA, grade VI, 99%, crystallized, lyophilized) were purchased from Sigma (St.

Louis, USA). Lyophilized proteins were dissolved in BPE buffer at a concentration of approx. 10 mg mL^{-1}; these stock solutions may be stored at 4 °C for limited periods (up to two weeks).

The actual concentration of the stock protein solutions was determined using the conventional Bradford assay.[180] The Bradford reagent was purchased from Sigma (St. Louis, USA) and used according to the manufacturer's instructions. Standard protein solution (1 mg mL^{-1} BSA, Sigma) was used to construct the calibration curve for the Bradford assay.

5.6.1.2 Fluorimetric Titrations of Proteins

[AG-II-137–AG-II-144]

Samples for fluorimetric titrations were prepared in quartz fluorimetric cells from 2.00 mL of the 10 μM solution of the ligand in BPE buffer and 20 μL of 5% (w/v) solution of SDS in purified water; the final concentration of SDS in a sample was 0.05% (w/v). It proved to be crucial to add the SDS solution immediately before the titration step since, in the absence of proteins, slow SDS-induced aggregation of ligands was observed, which causes irreproducibility of the fluorimetric titrations.

Fluorimetric titrations were performed by adding aliquots of protein solutions (10 mg mL^{-1} in BPE buffer) to the titrated ligand–SDS solution until no further changes in fluorescence spectra were observed; the final concentration of the added protein constituted approx. 0.8–1.0 mg mL^{-1}. For all arylamino-substituted acridizinium salts, the excitation wavelength of λ_{ex} = 397 nm was used, which corresponds to the absorption maximum, and the fluorescence emission signal was recorded in the 450–720 nm range. Emission intensity, taken at the wavelength of the fluorescence maximum of the fully complexed dye (λ_{max}), was plotted as a function of added protein concentration, c_L, to give the graphs of the binding isoterms.

For titrations in the low range of protein concentration (0–60 μg mL^{-1}), stock solutions of the proteins were diluted with BPE buffer to a concentration of 1 mg mL^{-1} and used for the titrations of sample solutions prepared as described above. In this case, however, only the fluorescence intensity at λ_{max} values (found from the titrations in the high concentration range) was measured, using the "Concentration" application of the Cary Eclipse® software package. The values of the fluorescence intensity, $I_F(\lambda_{max})$, were plotted versus the added protein concentration c_L, to give the graphs of the binding isoterms in the range of low protein concentrations.

5.7 Photocleavage of Plasmid DNA

5.7.1 Preparation of Abasic Plasmid DNA

[AG-III-05/06]

Commercially available pBR322 DNA (Fermentas GmbH, St. Leon-Rot, Germany; 100 µg at a concentration of 0.5 mg mL^{-1} in 10 mM Tris-HCl, 1 mM EDTA buffer, pH 7.6) was precipitated by the addition of 3 M sodium acetate solution (pH 5.2; 20 µL) and 96% EtOH (500 µL). After standing at −25 °C overnight, the sample was centrifugated (30 min at 13 000 RPM), and the supernatant was discarded. The residue was washed with 70% EtOH (500 µL), centrifugated as indicated above, and the supernatant was discarded. The residue was dissolved in 25 mM sodium acetate buffer (pH 4.8; 100 µL). At this stage, the concentration of DNA constitutes approx. 1 mg mL^{-1}, as losses of DNA during the precipitation step were not estimated. The solution was divided into two portions of 50 µL.

One of the samples (AP-pBR322) was converted into abasic DNA by incubation in a water bath at 70 °C for 20 min; this treatment is known to introduce approx. 1.8 abasic sites per plasmid molecule. In the case of the second portion (N-pBR322), the heating step was omitted, as this was intended to serve as a reference, intact pBR322 DNA.

The DNA of both portions was immediately precipitated by the addition of 3 M sodium acetate solution (pH 5.2; 5 µL) and 96% EtOH (125 µL). After standing at −25 °C overnight, the samples were centrifugated as indicated above, and the supernatants were discarded. The residues were washed with 70% EtOH (125 µL), centrifugated as indicated above, and the supernatants were discarded. The residues were dissolved in $I_{½}$ buffer (pH 7.4; 500 µL), to give the final DNA concentration of approx. 100 µg mL^{-1}. These stock solutions of intact and abasic DNA may be stored at −25 °C for limited periods of time (2–5 days).

5.7.2 Sample Preparation and Irradiation

[AG-III-07]

Working solutions of regular pBR322 DNA (N-pBR322) and abasic plasmid DNA (AP-pBR322) were prepared by mixing stock solutions of DNA (40 µL) with $I_{½}$ buffer (60 µL) and purified water (100 µL). The concentration of the DNA in the working solutions was approx. 20 µg mL^{-1}.

Two sets of 16 samples were prepared by mixing the corresponding working DNA solutions (5 µL) with aqueous solutions of the corresponding photosensitizer (100 µM; 5 µL). For the preparation of reference samples, the photosensitizer solution was replaced with an equal volume of purified water. The final concentration of the plasmid DNA in samples was about 10 µg mL^{-1} and that of the photosensitizer was 50 µM. The samples were mixed thoroughly, centrifugated (2.5 min at 10 000 RPM), and degassed by blowing argon gas over sample solutions. The samples were then irradiated in a Rayonet photoreactor (λ_L = 350 nm, irradiance I_L = 7.2 mW cm^{-2}) for the periods of time as indicated in Table 5.9.

Table 5.9. Sample preparation for investigation of photocleavage of plasmid DNA

Sample No.	1 [a]	2 [b]	3 [c]	4	5	6	7	8	9	10	11	12	13	14	15 [a]	16 [b]
Sensitizer	–	–	+	+	+	+	+	+	+	+	+	+	+	+	–	–
Exposure time	–	45	–	2	2	5	5	10	10	15	15	30	30	45	–	45

[a] Reference sample non-irradiated; [b] reference sample irradiated; [c] sample with sensitizer non-irradiated.

5.7.3 Gel Electrophoresis and Data Evaluation

Following the irradiation, gel loading buffer (2.5 µL) was added to DNA samples and, after mixing, aliquots (10 µL) of samples were simultaneously run in a 1% agarose gel containing 0.50 mg L^{-1} ethidium bromide (running buffer: TBE, 17.8 mM Tris, 17.8 mM boric acid, 0.4 mM EDTA, pH 8.0) at a voltage of 80 V.[181] After electrophoresis, the DNA bands were visualized with a UV transilluminating table (λ_L = 312 nm) and photographed with a digital camera (Figure 5.4). The strand break percentages (SB) were calculated using Eq. 5.17.

$$SB = \frac{r_2}{1.66\, r_1 + r_2} \times 100 \qquad \text{(Eq. 5.17)}$$

Here r_1 and r_2 are the intensities of the superhelical and nicked DNA bands, respectively, as determined by the integration of the band areas with the Gel-Pro Express™ software (Media Cybernetics, Inc). The data were plotted as a bar graph.

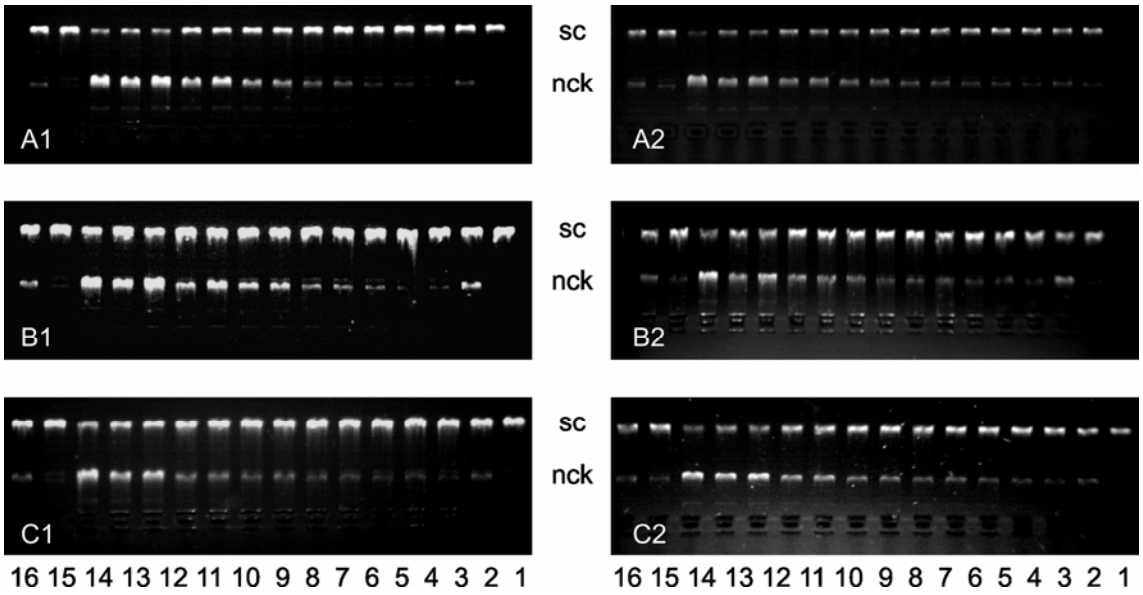

Figure 5.4. Results of the photocleavage of fully-paired pBR322 (1) and AP-pBR322 DNA (2) by compounds **55b** (A), **54a** (B) and **54b** (C). Labels: sc, supercoiled DNA; nck, nicked DNA; numbers indicate the assignment of the bands (Table 5.9).

5.8 Quantum Chemical Calculations

Quantum chemical calculations of 9-(4-chlorophenylamino)acridizinium (**27j**), *N*-isopropylacridizinium-9-carboxamide (**55a**) and the 3-substituted isomer of **55a** were performed using the semiempirical AM1 method implemented into HyperChem software.[182] The counter-ions were excluded from the calculations.

The ground-state geometry was calculated using self-consistent field (SCF) procedure with a convergence limit of 1×10^{-4} J mol^{-1}. The closed-shell Hartree–Fock (RHF) algorithm was used, and the full optimization was performed by the Polak-Ribiere conjugate-gradient method. The molecular orbitals and the electronic spectrum were calculated at the energy-minimized geometry by a configuration interaction method, involving five highest occupied and five lowest unoccupied molecular orbitals and a total of 51 singly-excited configurations.

The ground-state potential energy surface for **27j** was constructed by performing a stepwise rotation about the torsion angle θ(C9–N$_{exo}$–C1′–C2′), using a force constant f = 2000 for this torsion. Additionally, the torsion angle φ(C8–C9–N$_{exo}$–C1′) was frozen at 0° (as found at the equilibrium geometry) using the same value of the force constant, to prevent the umbrella-type turn-out of the system, and all other geometrical parameters were fully optimized. The excited-state potential energy surface was constructed essentially in the same way, requesting the excited singlet-state geometry optimization (keyword “excited-state = yes”).

6 REFERENCES

[1] H. Ihmels, D. Otto, *Top. Curr. Chem.* **2005**, *258*, 161–204.

[2] a) D. E. Thurston, *Br. J. Cancer*, **1999**, *80*, 65–85; b) I. Haq, J. Ladbury, *J. Mol. Recognit.* **2000**, *13*, 188–197.

[3] L. S. Lerman, *J. Mol. Biol.* **1961**, *3*, 18–30.

[4] J.-B. LePecq, C. Paoletti, *J. Mol. Biol.* **1967**, *27*, 87–106.

[5] a) L. G. Lee, C.-H. Chen, L. A. Chui, *Cytometry* **1986**, *7*, 508–517; b) J. Nygren, N. Svanvik, M. Kubista, *Biopolymers* **1998**, *46*, 39–51.

[6] B. A. Armitage, *Top. Curr. Chem.* **2005**, *253*, 55–76.

[7] W. A. Denny in *DNA and RNA Binders: From Small Molecules to Drugs* (Eds.: M. Demeunynck, C. Bailly, W. D. Wilson), Wiley–VCH, Weinheim, **2003**, pp. 482–502.

[8] H. Ihmels, K. Faulhaber, D. Vedaldi, F. Dall'Acqua, G. Viola, *Photochem. Photobiol.* **2005**, *81*, 1107–1115.

[9] W. D. Wilson, A. N. Gough, J. J. Doyle, M. W. Davidson, *J. Med. Chem.* **1976**, *19*, 1261–1263.

[10] H. Ihmels, K. Faulhaber, C. Sturm, G. Bringmann, K. Messer, N. Gabellini, D. Vedaldi, G. Viola, *Photochem. Photobiol.* **2001**, *74*, 505–511.

[11] G. Viola, M. Bressanini, N. Gabellini, D. Vedaldi, F. Dall'Acqua, H. Ihmels, *Photochem. Photobiol. Sci.* **2002**, *1*, 882–889.

[12] G. Viola, H. Ihmels, H. Kraußer, D. Vedaldi, F. Dall'Acqua, *ARKIVOC* **2004**, *(v)*, 219–230.

[13] K. Faulhaber, *Dissertation*, Bayerische Julius-Maximilians-Universität Würzburg (Germany), **2003** (http://opus.bibliothek.uni-wuerzburg.de/opus/frontdoor.php?source_opus=679).

[14] H. Ihmels, B. Engels, K. Faulhaber, C. Lennartz, *Chem. Eur. J.* **2000**, *6*, 2854–2864.

[15] H. Ihmels, A. Salbach, submitted to *Photochem. Photobiol*.

[16] C. Bohne, K. Faulhaber, B. Giese, A. Häfner, A. Hofmann, H. Ihmels, A.-K. Köhler, S. Perä, F. Schneider, M. A. L. Sheepwash, *J. Am. Chem. Soc.* **2005**, *127*, 76–85.

[17] B. Armitage, *Chem. Rev.* **1998**, *98*, 1171–1200.

[18] B. Valeur, *Molecular Fluorescence: Principles and Applications*, Wiley–VCH, Weinheim, **2002**.

[19] M. Wahl, F. Koberling, M. Patting, E. H. Rahn, *Curr. Pharm. Biotechnol.* **2004**, *5*, 299–308.

[20] P. Prentø, *Biotech. Histochem.* **2001**, *76*, 137–161.

[21] L.-T. Jin, J.-K. Choi, *Electrophoresis* **2004**, *25*, 2429–2438.

[22] G. Cosa, K.-S. Focsaneanu, J. R. N. McLean, J. P. McNamee, J. C. Scaniano, *Photochem. Photobiol.* **2001**, *73*, 585–599.

[23] a) H. S. Rye, S. Yue, D. E. Wemmer, M. A. Quesada, R. P. Haugland, R. A. Mathies, A. N. Glazer, *Nucleic Acids Res.* **1992**, *20*, 2803–2812; b) T. L. Netzel, K. Nafisi, M. Zhao, I. Johnson, *J. Phys. Chem.* **1995**, *99*, 17936–17947.

[24] S. Gurrieri, C. Bustamante, C. *Biochem. J.* **1997**, *326*, 131-138.

[25] H. Zipper, H. Brunner, J. Bernhagen, F. Vitzthum, *Nucleic Acids Res.* **2004**, *32*, e103.

[26] N. W. Luedtke, Q. Liu, Y. Tor, *Chem. Eur. J.* **2005**, *11*, 495–508.

[27] L. R. Williams, *Biotech. Histochem.* **2001**, *76*, 127–132.

[28] a) W. W. C. Quigley, N. J. Dovichi, *Anal. Chem.* **2004**, *76*, 4645–4658; b) B. C. Giordano, L. Jin, A. J. Couch, J. P. Ferrance, J. P. Landers, *Anal. Chem.* **2004**, *76*, 4705–4714.

[29] J.-R. Daban, S. Bartolomé, M. Samsó, *Anal. Biochem.* **1991**, *199*, 169–174.

[30] a) B. K. Hartman, S. Udenfriend, *Anal. Biochem.* **1969**, *30*, 391–394; b) P. M. Horowith, S. Bowman, *Anal. Biochem.* **1987**, *165*, 430–434.

[31] a) K. Berggren, E. Chernokalskya, T. H. Steinberg, C. Kemper, M. F. Lopez, Z. Diwu, R. P. Haugland, W. F. Patton, *Electrophoresis* **2000**, *21*, 2509–2521; b) T. H. Steinberg, L. J. Jones, R. P. Haugland, V. L. Singer, *Anal. Biochem.* **1996**, *239*, 223–237.

[32] G. M. Edelman, W. O. McClure, *Acc. Chem. Res.* **1968**, *1*, 65–70.

[33] Y. Suzuki, K. Yokoyama, *J. Am. Chem. Soc.* **2005**, *127*, 17799–17802.

[34] a) P. P. Chan, P. M. Glazer, *J. Mol. Med.* **1997**, *75*, 267–282; b) M. Faria, C. Giovannangeli, *J. Gene Med.* **2001**, *3*, 299–310.

[35] N. Thuong, C. Hélène, *Angew. Chem.* **1993**, *105*, 697–723; *Angew. Chem. Int. Ed.* **1993**, *32*, 666–690.

[36] a) P. B. Dervan, A. T. Poulin-Kerstien, E. J. Fechter, B. S. Edelson, *Top. Curr. Chem.* **2005**, *253*, 1–31; b) P. B. Dervan, *Bioorg. Med. Chem.* **2001**, *9*, 2215–2235.

[37] a) A. Klug, *J. Mol. Biol.* **1999**, *293*, 215–218; b) D. J. Segal, C. F. Barbas III, *Curr. Opin. Biotechnol.* **2001**, *12*, 632–637.

[38] J. L. Asensio, T. Brown, A. N. Lane, *Structure Fold. Des.* **1999**, *7*, 1–11; PDB ID: 1BWG (http://www.pdb.org).

[39] a) H. E. Moser, P. B. Dervan, *Science* **1987**, *238*, 645–650; b) J. C. François, T. Saison-Behmoaras, C. Barbier, M. Chassignol, N. T. Thuong, C. Hélène, *Proc. Natl. Acad. Sci. USA* **1989**, *86*, 9702–9706.

[40] a) M. Grigoriev, D. Praseuth, A. L. Guieysse, P. Robin, N. T. Thuong, C. Hélène, A. Harel-Bellan, *Proc. Natl. Acad. Sci. USA* **1993**, *90*, 3501–3505; b) L. Perrouault, U. Asseline, C. Rivalle, N. T. Thuong, E. Bisagni, C. Giovannangeli, T. Le Doan, C. Hélène, *Nature* **1990**, *344*, 358–360.

[41] P. B. Arimondo, G. S. Laco, C. J. Thomas, L. Halby, D. Pez, P. Schmitt, A. Boutorine, T. Garestier, Y. Pommier, S. M. Hecht, J.-S. Sun, C. Bailly, *Biochemistry* **2005**, *44*, 4171–4180.

[42] a) T. C. Jenkins, *Curr. Med. Chem.* **2000**, *7*, 99–115; b) C. Escudé, T. Garestier, J.-S. Sun, *Methods Enzymol.* **2001**, *340*, 340–357; c) K. R. Fox, R. A. Darby in *DNA and RNA Binders: From Small Molecules to Drugs* (Eds.: M. Demeunynck, C. Bailly, W. D. Wilson), Wiley–VCH, Weinheim, **2003**, pp. 360–383.

[43] a) D. M. Gowers, K. R. Fox, *Nucleic Acids Res.* **1999**, *27*, 1569–1577; b) C. Escudé, J.-S. Sun, *Top. Curr. Chem.* **2005**, *253*, 109–148.

[44] a) J. L. Mergny, G. Duval-Valentin, C. H. Nguyen, L. Perrouault, B. Faucon, M. Rougée, T. Montenay-Garestier, E. Bisagni, C. Hélène, *Science* **1992**, *256*, 1681–1684; b) D. S. Pilch, M. J. Waring, J.-S. Sun, M. Rougée, C.-H. Nguyen, E. Bisagni, T. Garestier, C. Hélène, *J. Mol. Biol.* **1993**, *232*, 926–946.

[45] C. Escudé, C. H. Nguyen, S. Kukureti, Y. Janin, J.-S. Sun, E. Bisagni, T. Garestier, C. Hélène, *Proc. Natl. Acad. Sci. USA* **1998**, *95*, 3591–3596.

[46] a) M.-P. Teulade-Fichou, D. Perrin, A. Boutorine, D. Polverari, J.-P. Vigneron, J.-M. Lehn, J.-S. Sun, T. Garestier, C. Hélène, *J. Am. Chem. Soc.* **2001**, *123*, 9283–9292; b) O. Baudoin, C. Marchand, M.-P. Teulade-Fichou, J.-P. Vigneron, J.-S. Sun, T. Garestier, C. Hélène, J.-M. Lehn, *Chem. Eur. J.* **1998**, *4*, 1504–1508.

[47] a) W. D. Wilson, F. A. Tanious, S. Mizan, S. Yao, A. S. Kiselyov, G. Zon, L. Strekowski, *Biochemistry* **1993**, *32*, 10614–10621; b) L. Strekowski, M. Hojjat, E. Wolinska, A. N. Parker, E. P. Paliakov, T. Gorecki, F. A. Tanious, W. D. Wilson, *Bioorg. Med. Chem. Lett.* **2005**, *15*, 1097–1100.

[48] J. Ren, C. Bailly, J. B. Chaires, *FEBS Lett.* **2000**, *470*, 355–359.

[49] P. M. Murphy, V. A. Phillips, S. A. Jennings, N. C. Garbett, J. B. Chaires, T. C. Jenkins, R. T. Wheelhouse, *Chem. Commun.* **2003**, 1160–1161.

[50] K. R. Fox, P. Polucci, T. C. Jenkins, S. Neidle, *Proc. Natl. Acad. Sci. USA* **1995**, *92*, 1887–1891.

[51] a) I. Haq, J. E. Ladbury, B. Z. Chowdhry, T. C. Jenkins, *J. Am. Chem. Soc.* **1996**, *118*, 10693–10701; b) Y. Kan, B. Armitage, G. B. Schuster, *Biochemistry* **1997**, *36*, 1461–1466.

[52] J. B. Chaires, J. Ren, D. Hamelberg, A. Kumar, V. Pandya, D. W. Boykin, W. D. Wilson, *J. Med. Chem* **2004**, *47*, 5729–5742.

[53] a) L.-K. Wang, B. D. Rogers, S. M. Hecht, *Chem. Res. Toxicol.* **1996**, *9*, 75–83; b) J. S. Lee, L. J. P. Latimer, K. J. Hampel, *Biochemistry* **1993**, *32*, 5591–5597.

[54] L. Guittat, P. Alberti, F. Rosu, S. Van Miert, E. Thetiot, L. Pieters, V. Gabelica, E. De Pauw, A. Ottaviani, J.-F. Riou, J.-L. Mergny, *Biochimie* **2003**, *85*, 535–547.

[55] a) R. Zain, C. Marchand, J. Sun, C. H. Nguyen, E. Bisagni, T. Garestier, C. Hélène, *Chem. Biol.* **1999**, *6*, 771–777; b) C. Marchand, C. H. Nguyen, B. Ward, J.-S. Sun, E. Bisagni, T. Garestier, C. Hélène, *Chem Eur. J.* **2000**, *6*, 1559–1563; c) A. Zaid, J.-S. Sun, C. H. Nguyen, E. Bisagni, T. Garestier, D. S. Grierson, R. Zain, *ChemBioChem* **2004**, *5*, 1550–1557.

[56] E. S. Belousov, I. A. Afonina, I. V. Kutyavin, *Nucleic Acids Res.* **1998**, *26*, 1324–1328.

[57] J. R. Spitzner, I. K. Chung, M. T. Muller, *J. Biol. Chem.* **1995**, *270*, 5932–5943.

[58] a) K. Bonjean, M. C. De Pauw-Gillet, M. P. Defresne, P. Colson, C. Houssier, L. Dassonneville, C. Bailly, R. Greimers, C. Wright, J. Quetin-Leclercq, M. Tits, L. Angenot, *Biochemistry* **1998**, *37*, 5136–5146; b) Y. Urasaki, G. Laco, Y. Takebayashi, C. Bailly, G. Kohlhagen, Y. Pommier, *Cancer Res.* **2001**, *61*, 504–508.

[59] J. Lhomme, J.-F. Constant, M. Demeunynck, *Biopolym. Nucl. Acid Sci.* **1999**, *52*, 65–83.

[60] J.-F. Constant, M. Demeunynck in *DNA and RNA Binders: From Small Molecules to Drugs* (Eds.: M. Demeunynck, C. Bailly, W. D. Wilson), Wiley–VCH, Weinheim, **2003**, pp. 247–277.

[61] a) J. R. Bertrand, J.-J. Vasseur, A. Gouyette, B. Rayner, J. L. Imbach, C. Paoletti, C. Malvy, *J. Biol. Chem.* **1989**, *264*, 14172–14178; b) C. Malvy, H. Safraoui, E. Bloch, J. R. Bertrand, *Anti-Cancer Drug Des.* **1988**, *2*, 361–370.

[62] a) M. Jourdan J. Garcia, J. Lhomme, M.-P. Teulade-Fichou, J.-P. Vigneron, J.-M. Lehn, *Biochemistry* **1999**, *38*, 14205–14213; b) N. Berthet, J. Michon, J. Lhomme, M.-P. Teulade-Fichou, J.-P. Vigneron, J.-M. Lehn, *Chem. Eur. J.* **1999**, *5*, 3625–3630.

[63] a) N. Berthet, J.-F. Constant, M. Demeunynck, P. Michon, J. Lhomme, *J. Med. Chem.* **1997**, *40*, 3346–3352; b) P. Belmont, M. Jordan, M. Demeunynck, J.-F. Constant, J. Garcia, J. Lhomme, *J. Med. Chem.* **1999**, *42*, 5153–5159.

[64] a) J.-F. Constant, T. R. O'Connor, J. Lhomme, J. Laval, *Nucleic Acids Res.* **1988**, *16*, 2691–2703; b) A. Fkyerat, M. Demeunynck, J.-F. Constant, P. Michon, J. Lhomme, *J. Am. Chem. Soc.* **1993**, *115*, 9952–9959.

[65] A. Martelli, J.-F. Constant, M. Demeunynk, J. Lhomme, P. Dumy, *Tetrahedron* **2002**, *58*, 4291–4298.

[66] A. Martelli, M. Jourdan, J.-F. Constant, M. Demeunynck, P. Dumy, *Bioorg. Med. Chem. Lett.* **2006**, *16*, 154–157.

[67] H. Ihmels, K. Faulhaber, G. Viola in *Highlights in Bioorganic Chemistry: Methods and Applications* (Eds.: C. Schmuck, H. Wennemers), Wiley–VCH, Weinheim, **2004**, pp. 172–190.

[68] D. E. Graves in *Methods in Molecular Biology, Vol. 95: DNA Topoisomerase Protocols, Part II: Enzymology and Drugs* (Eds.: N. Osheroff, M. A. Bjornsti), Humana Press, Totowa, NJ, **2001**, pp. 161–169.

[69] J. D. McGhee, P. H. von Hippel, *J. Mol. Biol.* **1974**, *86*, 469–489.

[70] G. Löber, *J. Luminesc.* **1981**, *22*, 221–265.

[71] J.-L. Mergny, L. Lacroix, *Oligonucleotides* **2003**, *13*, 515–537.

[72] R. A. J. Darby, M. Sollogoub, C. McKeen, L. Brown, A. Risitano, N. Brown, C. Barton, T. Brown, K. R. Fox, *Nucleic Acids Res.* **2002**, *30*, e39.

[73] a) M. S. Han, A. K. R. Lytton-Jean, B.-K. Oh, J. Heo, C. A. Mirkin, *Angew. Chem.* **2006**, *118*, 1839–1842; *Angew. Chem. Int. Ed.* **2006**, *45*, 1807–1810; b) M. S. Han, A. K. R. Lytton-Jean, C. A. Mirkin, *J. Am. Chem. Soc.* **2006**, *128*, 4954–4955.

[74] C. H. Nguyen, C. Marchand, S. Delage, J.-S. Sun, T. Garestier, C. Hélène, E. Bisagni, *J. Am. Chem. Soc.* **1998**, *120*, 2501–2507.

[75] D. Murphy, R. Eritja, G. Redmond, *Nucleic Acids Res.* **2004**, *32*, e65.

[76] D. M. Crothers, *Biopolymers* **1971**, *10*, 2147–2160.

[77] a) J. D. McGhee, *Biopolymers* **1976**, *15*, 1345–1375; b) C. H. Spink, S. E. Wellman, *Methods Enzymol.* **2001**, *340*, 193–211.

[78] a) C. H. Spink, J. B. Chaires, *J. Am. Chem. Soc.* **1997**, *119*, 10920–10928; b) F. Leng, J. B. Chaires, M. J. Waring, *Nucleic Acids Res.* **2003**, *31*, 6191–6197; c) T. Cui, S. Wei, K. Brew, F. Leng, *J. Mol. Biol.* **2005**, *325*, 629–645.

[79] a) B. Nordén, M. Kubista, T. Q. Kurucsev, *Quart. Rev. Biophys.* **1992**, *25*, 51–170; b) B. Nordén, T. J. Kurucsev, *J. Mol. Recognit.* **1994**, *7*, 141–156.

[80] a) G. Cohen, H. Eisenberg, *Biopolymers* **1969**, *8*, 45–55; b) S. Satyanarayana, J. C. Dabrowiak, J. B. Chaires, *Biochemistry* **1993**, *32*, 2573–2584.

[81] a) J. Ren, J. B. Chaires, *Biochemistry* **1999**, *38*, 16067–16075; b) J. B. Chaires, *Curr. Med. Chem. – Anti-Cancer Agents*, **2005**, *5*, 339–352; c) J. B. Chaires, *Top. Curr. Chem.* **2005**, *253*, 33–53.

[82] a) F. Rosu, E. De Pauw, L. Guittat, P. Alberti, L. Lacroix, P. Mailliet, J.-F. Riou, J.-L. Mergny, *Biochemistry* **2003**, *42*, 10361–10371; b) R. A. Heald, C. Modi, J. C. Cookson, I. Hutchinson, C. A. Laughton, S. M. Gowan, L. R. Kelland, M. F. G. Stevens, *J. Med. Chem.* **2002**, *45*, 590–597.

[83] E. M. Kosower, *Acc. Chem. Res.* **1982**, *15*, 259–266.

[84] S. Naruto, H. Mizuta, H. Nishimura, *Tetrahedron Lett.* **1976**, *17*, 1597–1600.

[85] O. van den Berg, W. F. Jager, S. J. Picken, *J. Org. Chem.* **2006**, 71, 2666–2676.

[86] a) R. J. Alaimo, *J. Med. Chem.* **1970**, *13*, 554–556; b) R. J. Alaimo, *J. Pharm. Sci.* **1974**, *63*, 1939–1941; c) R. J. Alaimo, M. M. Goldenberg (Morton Norwich Products, Inc.), US 3899479, **1975**; d) R. J. Alaimo (Morton Norwich Products, Inc.), US 3997547, **1976**.

[87] a) G. M. Sanders, M. van Dijk, H. C. van der Plas, *J. Heterocycl. Chem.* **1982**, *19*, 797–800; b) G. M. Sanders, M. van Dijk, H. C. van der Plas, *J. Heterocycl. Chem.* **1983**, *20*, 407–414.

[88] C. K. Bradsher, J. P. Sherer, J. H. Parham, *J. Chem. Eng. Data* **1965**, *10*, 180–183.

[89] H. Ihmels in *Science of Synthesis: Houben-Weyl Methods of Molecular Transformations, Vol. 15* (Ed.: D. StC. Black), Georg Thieme, Stuttgart, **2004**, pp. 907–946.

[90] D. Mörler, F. Kröhnke, *Liebigs Ann. Chem.* **1971**, *744*, 65–80.

[91] S. Arai, M. Hida, in *Advances in Heterocyclic Chemistry, Vol. 55* (Ed. A. R. Katritzky), Academic Press, **1992**, pp. 261–358.

[92] T. Miyadera, R. Tachikawa, *Tetrahedron* **1969**, *25*, 837–845.

[93] a) C. Xue, F.-T. Luo, *J. Org. Chem.* **2003**, *68*, 4417–4421; b) R. Grice, L. N. Owen, *J. Chem. Soc.* **1963**, 1947–1954.

[94] C. Reichardt, *Solvents and Solvent Effects in Organic Chemistry*, 3rd ed., Wiley–VCH, Weinheim, **2003**.

[95] H. T. S. Britton, R. A. Robinson, *J. Chem. Soc.* **1931**, 458–473.

[96] L. Andrussow, B. Schram in *Eigenschaften der Materie in Ihren Aggregatzuständen: Transportphänomene I (Landolt-Börnstein, Bd. 5a)* (Ed. K. Schäfer), Springer, Berlin, **1969**, pp. 371–373.

[97] L. J. Jones, R. P. Haugland, V. L. Singer, *BioTechniques* **2003**, *34*, 850–861.

[98] a) J. Fabian, H. Hartmann, *Light Absorption of Organic Colorants*, Springer, Berlin, **1980**; b) A. A. Ischenko, *Structure and Luminescent Spectral Properties of Polymethine Dyes*, Naukova Dumka, Kiev, **1994** (in Russian).

[99] F. Effenberger, P. Fischer, W. W. Schoeller, W.-D. Stohrer, *Tetrahedron* **1978**, *34*, 2409–2417; b) J. Firl, H. Braun, A. Amann, R. Barnett, *Z. Naturforsch.* **1980**, *35b*, 1406–1414.

[100] a) C. Hansch, C. Leo, R. W. Taft, *Chem. Rev.* **1991**, *91*, 165–195; b) H. Mayr, T. Bug, M. F. Gotta, N. Hering, B. Irrgang, B. Janker, B. Kempf, R. Loos, A. R. Ofial, G. Remennikov, H. Schimmel, *J. Am. Chem. Soc.* **2001**, *123*, 9500–9512.

[101] R. Gawinecki, K. Trzebiatowska, *Dyes Pigm.* **2000**, *45*, 103–107.

[102] R. Bosque, J. Sales, *J. Chem. Inf. Comput. Sci.* **2002**, *42*, 1154–1163.

[103] a) M. L. Horng, K. Dahl, G. Jones II, M. Maroncelli, *Chem. Phys. Lett.* **1999**, *315*, 363–370; b) W. F. Jager, D. Kudasheva, D. C. Neckers, *Macromolecules* **1996**, *29*, 7351–7355.

[104] N. Nijegorodov, R. Mabbs, *Spectrochim. Acta, Part A* **2001**, *57*, 1449–1462.

[105] J. Bendig, S. Helm, D. Kreysig, J. Wilda, *J. prakt. Chemie*, **1982**, *324*, 978–986.

[106] a) E. M. Kosower, H. Dodiuk, K. Tanizawa, M. Ottolenghi, N. Orbach, *J. Am. Chem. Soc.* **1975**, *97*, 2167–2178; b) H. Dodiuk, E. M. Kosower, *J. Phys. Chem.* **1977**, *81*, 50–54; c) E. M. Kosower, H. Dodiuk, *J. Phys. Chem.* **1978**, *82*, 2012–2015.

[107] J. A. Dean (Ed.), *Lange's Handbook of Chemistry, 14th Edition*, McGraw–Hill, New York, **1992**.

[108] M. Maus, K. Rurack, *New J. Chem.* **2000**, *24*, 677–686.

[109] S. A. Jonker, F. Ariese, J. W. Verhoeven, *Recl. Trav. Chim. Pays-Bas*, **1989**, *108*, 109–115.

[110] a) G. Oster, Y. Nishijima, *J. Am. Chem. Soc.* **1956**, *78*, 1581–1584; b) T. Förster, G. Hoffmann, *Z. physik. Chem. NF*, **1971**, *75*, 63–76; c) M. Vogel, W. Rettig, *Ber. Bunsenges. Phys. Chem.* **1985**, *89*, 962–968; c) P. Gautam, A. Harriman, *J. Chem. Soc., Faraday Trans.* **1994**, *90*, 697–701.

[111] M. Belletête, R. S. Sarpal, G. Durocher, *Chem. Phys. Lett.* **1993**, *201*, 145–152.

[112] a) R. O. Loutfy, B. A. Arnold, *J. Phys. Chem.* **1982**, *86*, 4205–4211; b) W. Rettig, *J. Phys. Chem.* **1982**, *86*, 1970–1976; c) B. Wandelt, P. Turkewitch, B. R. Stranix, G. D. Darling,

J. Chem. Soc., Faraday Trans. **1995**, *91*, 4199–4205; d) A. Demeter, T. Bérces, L. Biszók, V. Wintgens, P. Valat, J. Kossanyi, *J. Phys. Chem.* **1996**, *100*, 2001–2011; e) G. H. Bon Hoa, J. Kossanyi, A. Demeter, L. Biszók, T. Bérces, *Photochem. Photobiol. Sci.* **2004**, *3*, 473–482.

[113] D. Otto, personal communication.

[114] a) M. J. S. Dewar, E. G. Zoebisch, E. F. Healy, J. J. P. Stewart, *J. Am. Chem. Soc.* **1985**, *107*, 3902–3909; b) M. J. S. Dewar, K. M. Dieter, *J. Am. Chem. Soc*. **1986**, *108*, 8075–8086; c) J. J. P. Stewart, *J. Comp. Aided Mol. Design* **1990**, *4*, 1–103.

[115] T. Clark in *Recent Experimental and Computational Advances in Molecular Spectroscopy, Vol. 406* (Ed. R. Fausto), Kluwer, Dordrecht, **1993**, pp. 369–380.

[116] a) P. K. McCarthy, G. J. Blanchard, *J. Phys. Chem.* **1993**, *97*, 12205–12209; b) J. Rodríguez, D. Scherlis, D. Estrin, P. F. Aramendía, R. M. Negri, *J. Phys. Chem. A* **1997**, *101*, 6998–7006; c) J. Peszke, W. Śliwa, *Spectrochim. Acta, Part A* **2002**, *58*, 2127–2133.

[117] a) H. Ihmels, D. Leusser, M. Pfeiffer, D. Stalke, *J. Org. Chem.* **1999**, *64*, 5715–5718; b) H. Ihmels, C. J. Mohrschladt, A. Schmitt, M. Bressanini, D. Leusser, D. Stalke, *Eur. J. Org. Chem.*, **2002**, 2624–2632; c) F. Maassarani, M. Pfeffer, G. Le Borgne, *Organometallics* **1990**, *9*, 3003–3005; d) K. Sato, S. Arai, T. Yamagishi, T. Tanase, *Acta Cryst.* **2001**, *C57*, 174–175.

[118] a) R. O. Loutfy, *Pure Appl. Chem.* **1986**, *58*, 1239–1248; b) P. Bosch, F. Catalina, T. Corrales, C. Peinado, *Chem. Eur. J.* **2005**, *11*, 4314–4325.

[119] M. A. Haidekker, T. P. Brady, D. Lichlyter, E. A. Theodorakis, *J. Am. Chem. Soc.* **2006**, *128*, 398–399.

[120] a) M. A. Haidekker, T. Ling, M. Anglo, H. Y. Stevens, J. A. Frangos, E. A. Theodorakis, *Chem. Biol.* **2001**, *8*, 123–131; b) M. A. Haidekker, T. P. Brady, S. H. Chalian, W. Akers, D. Lichlyter, E. A. Theodorakis, *Bioorg. Chem.* **2004**, *32*, 274–289.

[121] a) N. J. Turro, X.-G. Lei, *Langmuir* **1995**, *11*, 2525–2533; b) S. F. Santos, D. Zanette, H. Fischer, R. Itri, *J. Colloid Interface Sci.* **2003**, *262*, 400–408.

[122] S. H. Lee, J. K. Suh, M. Li, *Bull. Korean Chem. Soc.* **2003**, *24*, 45–48.

[123] E. Daniel, G. Weber, *Biochemistry* **1966**, *5*, 1893–1900.

[124] V. S. Jisha, K. T. Arun, M. Hariharan, D. Ramaiah, *J. Am. Chem. Soc.* **2006**, *128*, 6024–6025.

[125] G.-J. Lee, C.-B. Cho, D.-J. Lee, J.-W. Park, S. K. Kim, *Bull. Korean Chem. Soc.* **1999**, *20*, 653–656.

[126] a) C. K. Bradsher, J. C. Parham, *J. Org. Chem.* **1964**, *29*, 856–858; b) A. P. Krapcho, S. A. Cadamuro, *J. Heterocycl. Chem.* **2004**, *41*, 291–294.

[127] a) C. K. Bradsher, J. P. Sherer, *J. Heterocycl. Chem.* **1968**, *5*, 253–257; b) D. L. Fields, T. H. Regan, *J. Heterocycl. Chem.* **1972**, *10*, 195–199.

[128] Y. Takeuchi, N. Dennis, *Org. Magn. Reson.* **1976**, *8*, 21–27.

[129] C. K. Bradsher, L. S. Davies, *J. Org. Chem.* **1973**, *38*, 4167–4170.

[130] H. Takeshita, A. Mori, S. Ohta, *Bull. Chem. Soc. Jpn.* **1974**, *47*, 2437–2439.

[131] a) E. B. Barnett, F. G. Sanders, *J. Chem. Soc.* **1933**, 434–437; b) A. S. Bailey, K. C. Bryant, R. A. Hancock, S. H. Morrell, J. C. Smith, *J. Inst. Petroleum* **1947**, *33*, 503–526.

[132] J. Sepiol, *Synthesis* **1983**, 559–563.

[133] a) J. Wolinska-Mocydlarz, P. Canonne, L. C. Leitch, *Synthesis* **1974**, 566–568; b) A. Terfort, H. Görls, H. Brunner, *Synthesis* **1997**, 79–86.

[134] a) C. K. Bradsher, *Chem. Rev.* **1987**, *87*, 1277–1297; b) C. K. Bradsher in *Comprehensive Heterocyclic Chemistry, Vol. 2* (Eds.: A. R. Katritzky, C. W. Reeds), Pergamon, Oxford, **1984**, 525–579.

[135] I. B. Berlman, *J. Phys. Chem.* **1970**, *74*, 3085–3093.

[136] A. W. Johnson, *J. Org. Chem.* **1959**, *24*, 833–836.

[137] C. Sotiriou-Leventis, A.-M. M. Rawashdeh, W. S. Oh, N. Leventis, *Org. Lett.* **2002**, *4*, 4113–4116.

[138] a) R. G. Harvey, *Polycyclic Aromatic Hydrocarbons*, Wiley–VCH, New York, **1997**; b) W. H. Laarhoven, T. J. Cuppen, R. J. F. Nivard, *Tetrahedron* **1970**, *26*, 4865–4881.

[139] A. W. McConnaughie, T. C. Jenkins, *J. Med. Chem.* **1995**, *38*, 3488–3501.

[140] a) F. I. Zubkov, E. V. Nikitina, V. V. Kouznetsov, L. D. A. Duarte, *Eur. J. Org. Chem.* **2004**, 5064–5074; b) S. Winstein, R. F. Heck, *J. Org. Chem.* **1972**, *37*, 825–836; c) B. Staskun, *Tetrahedron* **1972**, *28*, 5069–5079.

[141] a) C. K. Bradsher, J. D. Turner, *J. Org. Chem.* **1966**, *31*, 565–567; b) D. L. DeHaven-Hudkins, J.-A. Dority (Sterling Winthrop Inc.), US 5554620, **1996**.

[142] J. D. Turner, C. K. Bradsher, *J. Org. Chem.* **1967**, *32*, 1169–1173.

[143] R. B. Moodie, K. Schofield, *Acc. Chem. Res.* **1976**, *9*, 287–292.

[144] S. Mallena, M. P. H. Lee, C. Bailly, S. Neidle, A. Kumar, D. W. Boykin, W. D. Wilson, *J. Am. Chem. Soc.* **2004**, *126*, 13659–13669.

[145] D. S. Pilch, C. Yu, D. Makhey, E. J. LaVoie, A. R. Srinivasan, W. K. Olson, R. R. Sauers, K. J. Breslauer, N. E. Geacintov, L. F. Liu, *Biochemistry* **1997**, *36*, 12542–12553.

[146] R. Owczarzy, Y. You, B. G. Moreira, J. Manthey, L. Huang, M. A. Behlke, J. A. Walder, *Biochemistry* **2004**, *43*, 3537–3554.

[147] C. Schildkraut, S. Lifson, *Biopolymers* **1965**, *3*, 195–208.

[148] a) M. D. Frank-Kamenetskii, S. M. Mirkin, *Annu. Rev. Biochem.* **1995**, *64*, 65–95; b) D. Vlieghe, L. V. Meervelt, A. Dautand, B. Gallois, G. Précigoux, O. Kennard, *Science* **1996**, *273*, 1702–1705.

[149] S. Grimme, S. D. Peyerimhoff, *Chem. Phys.* **1996**, *204*, 411–417.

[150] C. K. Bradsher, J. C. Parham, *J. Heterocycl. Chem.* **1964**, *1*, 30–33.

[151] M. Bodanszky, A. Bodanszky, *The Practice of Peptide Synthesis, 2nd Ed.*, Springer, New York, **1994**.

[152] a) T. Wieland, R. Sehring, *Liebigs Ann. Chem.* **1950**, *569*, 117–121; b) T. Wieland, H. Bernhard, *Liebigs Ann. Chem.* **1951**, *572*, 190–194.

[153] a) N. J. Leonard, K. Ito, *J. Am. Chem. Soc.* **1973**, *95*, 4010–4016; b) M. Hisatome, N. Maruyama, K. Ikeda, T. Furutera, T. Ishikawa, K. Yamakawa, *Chem. Pharm. Bull.* **1996**, *44*, 1801–1811.

[154] a) S. Poritere, R. Paegle, M. Lidaks, *Khim. Geterotsikl. Soedin.* **1985**, 126–130.

[155] C. K. Bradsher, L. E. Beavers, *J. Am. Chem. Soc*. **1955**, *77*, 4812–4813.

[156] J. Bolte, C. Demuynck, M. F. Lhomme, J. Lhomme, J. Barbet, B. P. Roques, *J. Am. Chem. Soc.* **1982**, *104*, 760–765.

[157] W. Müller, F. Albrecht, W. Richter, *Z. physik. Chem.* **1982**, *263*, 721–733.

[158] W. Müller, D. M. Crothers, *Eur. J. Biochem.* **1975**, *54*, 267–277.

[159] A. Zedda, N. Zucca, G. Erriu, *Appl. Phys. Comm.* **1985**, *5*, 45–55.

[160] C. K. Bradsher, J. C. Parham, *J. Org. Chem.* **1963**, *28*, 83–85.

[161] a) J. Brison, C. de Bakker, N. Defay, F. Geerts-Evrard, M.-J. Marchant, R. H. Martin, *Bull. Soc. Chim. Belg.* **1983**, *92*, 901–912; b) R. W. Skeean, O. P. Goel, *Synthesis* **1990**, 628–630.

[162] W. S. Lindsay, P. Stokes, L. Humber, V. Boekelheide, *J. Am. Chem. Soc.* **1961**, *83*, 943–949.

[163] a) M. Newcomb, S. S. Moore, D. J. Cram, *J. Am. Chem. Soc.* **1977**, *99*, 6405–6410; b) P. R. Markies, R. M. Altink, A. Villena, O. S. Akkerman, F. Bickelhaupt, W. J. J. Smeets, A. L. Spek, *J. Organomet. Chem.* **1991**, *402*, 289–312.

[164] M. E. van der Boom, Y. Ben-David, D. Milstein, *J. Am. Chem. Soc.* **1999**, *121*, 6652–6656.

[165] a) W. D. Rohrbach, F. Gerson, R. Möckel, V. Boekelheide, *J. Org. Chem.* **1984**, *49*, 4128–4132; b) T. Kamada, Y. Gama, N. Wasada, *Bull. Chem. Soc. Jpn.* **1989**, *62*, 3024–3025.

[166] W. Ried, H. Bodem, *Chem. Ber.* **1958**, *91*, 1981–1982.

[167] M. R. Dahrouch, P. Jara, L. Mendez, Y. Portilla, D. Abril, G. Alfonso, I. Chavez, J. M. Manriquez, *Organometallics* **2001**, *20*, 5591–5597.

[168] H. Jenkner (Chemische Fabrik Kalk GmbH), US 3833666, **1974**.

[169] R. H. Mitchell, V. Boekelheide, *J. Am. Chem. Soc.* **1974**, *96*, 1547–1557.

[170] N. M. Yoon, C. S. Pak, H. C. Brown, S. Krishnamurthy, T. P. Stocky, *J. Org. Chem.* **1973**, *38*, 2786–2792.

[171] M. Hannon, A. Rodger, N. H. Mann (Univ. Warwick), WO 2005/033119, **2005**.

[172] a) G. M. Sheldrick, *SHELXS-97—Program for the Solution of Crystal Structures*, University of Göttingen, Germany, **1997**; b) G. M. Sheldrick, *SHELXL-97—Program for the Refinement of Crystal Structures*, University of Göttingen, Germany, **1997**.

[173] J. N. Demas, G. A. Crosby, *J. Phys. Chem.* **1971**, *75*, 991–1024.

[174] G. Jones, W. R. Jackson, C. Y. Choi, W. R. Bergmark, *J. Phys. Chem.* **1985**, *89*, 294–300.

[175] D. Magde, J. H. Brannon, T. L. Cremers, J. Olmsted, *J. Phys. Chem.* **1979**, *83*, 696–699.

[176] J. Polster, H. Lachmann, *Spectrometric Titrations: Analysis of Chemical Equilibria*, VCH, Weinheim, **1989**.

[177] M. Chevalier, *Compt. Rend.* **1953**, *236*, 1650–1652.

[178] P. R. Bevington, D. K. Robinson, *Data Reduction and Error Analysis for the Physical Sciences, 3rd Ed.*, McGraw-Hill, Boston, **2003**.

[179] A. Wada, S. Kozawa, *J. Polym. Sci.: Part A* **1964**, *2*, 853–864.

[180] I. M. Rosenberg, *Protein Analysis and Purification, 2nd Ed.*, Birkhäuser, Boston, **2005**.

[181] L. A. Osterman, *Methods of Protein and Nucleic Acids Research*, Springer, Berlin, **1984**.

[182] HyperChem™ 7.51, Hypercube, Inc., 1115 NW 4th Street, Gainesville, FL 32601, USA.

APPENDIX A STRUCTURE CHART

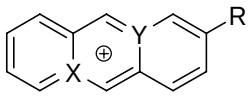

A^-

		X	Y	R	A
5a		N	C	H	Br
5b		N	C	NH_2	BF_4
27a	[AG-I-024] [AG-I-133]	N	C	$N(CH_2)_4$	BF_4
27b	[AG-I-014] [AG-I-016]	N	C	$N(CH_2CH_2)_2O$	BF_4
27c	[AG-I-026] [AG-I-048]	N	C	$N(Me)CH_2CH_2OH$	PF_6
27d	[AG-I-025]	N	C	$NH(4\text{-}C_6H_4NMe_2)$	Br
27e	[AG-I-022] [AG-I-135]	N	C	$NH(4\text{-}C_6H_4OMe)$	Br
27f	[AG-I-106]	N	C	$NH(4\text{-}C_6H_4Me)$	Br
27g	[AG-I-142]	N	C	NHC_6H_5	Br
27h	[AG-I-141]	N	C	$NH(4\text{-}C_6H_4F)$	Br
27i	[AG-I-028]	N	C	$NH(4\text{-}C_6H_4Br)$	Br
27j	[AG-I-104]	N	C	$NH(4\text{-}C_6H_4Cl)$	Br
27k	[AG-I-108]	N	C	$NH(3\text{-}C_6H_4Cl)$	Br
27ℓ	[AG-I-081]	N	C	$N(Me)CH_2CH_2OC(O)Me$	PF_6
28	[AG-I-087] [AG-I-092]	N	C	SMe	BF_4
29	[AG-I-015] [NS-I-005]	N	C	Br	Br
55a	[AG-I-057] [AG-I-061] [AG-I-110]	N	C	$CONHCHMe_2$	BF_4
55b	[AG-I-122]	N	C	$CONH(CH_2)_3CH_3$	BF_4
55c	[AG-I-132]	N	C	$CONH(CH_2)_3NMe_2$	Cl
56a (Br^-)	[AG-I-048] [AG-I-079]	N	C	COOH	Br
56a (BF_4^-)	[AG-I-055]	N	C	COOH	BF_4
56b (Br^-)	[AG-I-139]	C	N	COOH	Br
56b (BF_4^-)	[AG-I-164]	C	N	COOH	BF_4

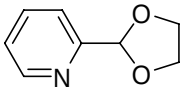

32

[AG-I-001]
[MK-I-001]

dop =

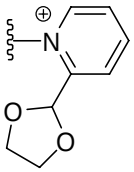

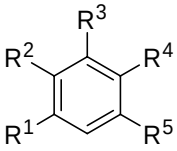

		R^1	R^2	R^3	R^4	R^5
31a		CH_2OH	H	H	SMe	H
31b	[AG-I-082]	CH_2Br	H	H	SMe	H
33	[AG-I-084]	CH_2dop (Br^-)	H	H	SMe	H
40a (2Br^-)	[MK-I-004] [AG-I-114]	CH_2dop (Br^-)	Me	H	CH_2dop (Br^-)	Me
40a (2BF_4^-)	[MK-I-015]	CH_2dop (BF_4^-)	Me	H	CH_2dop (BF_4^-)	Me
40b (2Br^-)	[MK-I-018]	CH_2dop (Br^-)	Me	CH_2dop (Br^-)	H	H
40b (2BF_4^-)	[MK-I-021]	CH_2dop (BF_4^-)	Me	CH_2dop (BF_4^-)	H	H
40c (2Br^-)	[AG-I-091]	CH_2dop (Br^-)	Br	CH_2dop (Br^-)	H	H
40c (2BF_4^-)	[AG-I-093]	CH_2dop (BF_4^-)	Br	CH_2dop (BF_4^-)	H	H
40d (2Br^-)	[AG-I-116]	CH_2dop (Br^-)	CF_3	CH_2dop (Br^-)	H	H
40d (2BF_4^-)	[AG-I-119]	CH_2dop (BF_4^-)	CF_3	CH_2dop (BF_4^-)	H	H
41a (2Br^-)	[AG-I-003]	CH_2dop (Br^-)	CH_2dop (Br^-)	H	H	H
41a (2BF_4^-)	[AG-I-006]	CH_2dop (BF_4^-)	CH_2dop (BF_4^-)	H	H	H
41b (2Br^-)	[MK-I-002]	CH_2dop (Br^-)	H	H	CH_2dop (Br^-)	H
41b (2BF_4^-)	[MK-I-008]	CH_2dop (BF_4^-)	H	H	CH_2dop (BF_4^-)	H
41c (2Br^-)	[JPM-006]	CH_2dop (Br^-)	H	CH_2dop (Br^-)	H	H
41c (2BF_4^-)	[JPM-007]	CH_2dop (BF_4^-)	H	CH_2dop (BF_4^-)	H	H
43	[NS-I-007]	CH_2Br	Me	H	CH_2Br	Me
45a	[AG-I-088]	COOH	Me	COOH	H	H
45b	[MK-I-013]	CH_2OH	Me	CH_2OH	H	H
45c	[MK-I-017]	CH_2Br	Me	CH_2Br	H	H
46	[AG-I-090]	CH_2Br	Br	CH_2Br	H	H
47	[NS-I-012]	CH_2Br	CF_3	CH_2Br	H	H

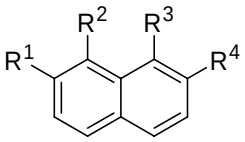

		R^1	R^2	R^3	R^4
48a (2Br^-)	[MK-I-006]	H	CH_2dop (Br^-)	CH_2dop (Br^-)	H
48a (2BF_4^-)	[MK-I-012]	H	CH_2dop (BF_4^-)	CH_2dop (BF_4^-)	H
48b (2Br^-)	[MK-I-011]	CH_2dop (Br^-)	H	H	CH_2dop (Br^-)
48b (2BF_4^-)	[MK-I-020]	CH_2dop (BF_4^-)	H	H	CH_2dop (BF_4^-)
48c (2Br^-)	[AG-I-149a]	CH_2dop (Br^-)	H	CH_2dop (Br^-)	H
48c (2BF_4^-)	[AG-I-149b]	CH_2dop (BF_4^-)	H	CH_2dop (BF_4^-)	H
49	[AG-I-144]	Me	H	Me	H
50	[AG-I-147]	CH_2Br	H	CH_2Br	H

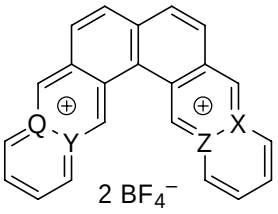

2 BF_4^-

		Q	X	Y	Z
38a	[MK-I-019]	C	C	N	N
38b	[MK-I-024]	N	N	C	C
38c	[AG-I-151]	C	N	N	C

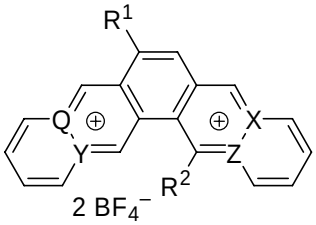

2 BF_4^-

		Q	X	Y	Z	R^1	R^2
7a	[AG-I-007]	C	C	N	N	H	H
7b	[MK-I-010]	N	N	C	C	H	H
7c	[JPM-008]	C	N	N	C	H	H
42a	[MK-I-016] [AG-I-120]	N	N	C	C	Me	Me
42b	[MK-I-023]	C	N	N	C	H	Me
42c	[AG-I-095]	C	N	N	C	N	O^-

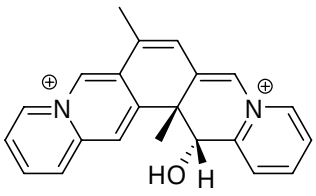

2 BF_4^- **44**

[AG-I-101]

[AG-I-118]

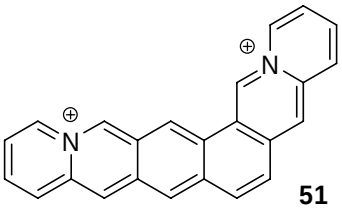

2 BF_4^- **51** [AG-I-150]

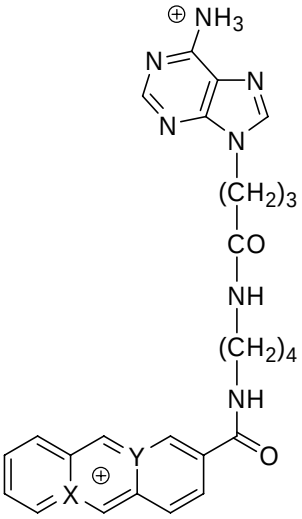

2 $CF_3CO_2^-$

		X	Y
54a	[AG-I-160]	N	C
54b	[AG-I-166]	C	N

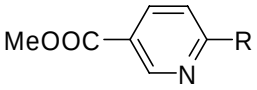

		R
57		Me
58	[AG-I-137]	$CH(OCH_2)_2$

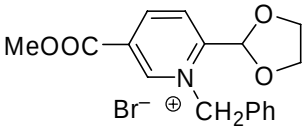

59 [AG-I-138]

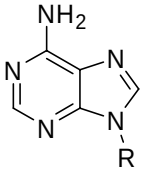

		R
60	[AG-I-032]	$(CH_2)_3COOEt$
61	[AG-I-042]	$(CH_2)_3COOH$
62	[AG-I-115] [AG-I-165]	$(CH_2)_3CONH(CH_2)_4NH_2$

CURRICULUM VITÆ

Personal

Last Name	Granzhan
First Name	Anton
Born	14.10.1979 in Rubishne (Ukraine)
Citizenship	Ukrainian

Education

Lyceum of Rubishne, Ukraine

1994–1996	High-school certificate (chemistry-biology option) with a Gold Medal

National Technical University, Kiev, Ukraine

1996–2000	B.Sc. (Hons), Chemistry and Chemical Technology
2000–2002	Diploma (Hons), Chemical Technology (Biotechnology)

University of Siegen, Germany

2003–2006	Ph.D. student in Organic Chemistry
	Thesis advisor: Prof. Dr. Heiko Ihmels

Research Experience

Institute of Organic Chemistry, NAS of Ukraine, Kiev, Ukraine (Dept. of Color and Structure of Organic Compounds)

1997–2002	Research Assistant (in 2002 Research Engineer). Part-time work within the research group of Dr. Yuri Slominskii.

Department of Physics, University of Regensburg, Germany

2002–2003 Fellow of the Graduate College "Sensory Photoreceptors in Natural and Artificial Systems".

Supervisor: Prof. Dr. A. Penzkofer

Research project: "Photostability of bacteriochlorophyll *c* in solution and in aggregates"

Department of Pharmaceutical Sciences, University of Padua, Italy

September 2005 Visiting scientist in the group of Prof. F. Dall'Acqua.
Supervisor: Dr. Giampietro Viola

Department of Organic Chemistry, University of Siegen, Germany

2003–2006 Research towards a Ph.D. degree.
Supervisor: Prof. Dr. Heiko Ihmels

Teaching Experience

Teaching Assistant, University of Siegen

2003–2006 Taught the lab courses:

- *Introduction to Organic Chemistry* (BSc level; average class size 10 students; taught in German)
- *Advanced Organic Chemistry I & II* (MSc level; average class size 3-5 students; taught in English)
- *Project in Organic Chemistry* (MSc level; individual supervision)

Academic Awards and Honors

- Parliament of Ukraine Scholarship (2000–2001)
- 1st Prize, Ukrainian Student Chemistry Olympiad (1999, 2000)
- International Higher Education Support Program Grants GSU073145 (1997), GSU063158 (1996)
- Silver Medal, The 28th International Chemistry Olympiad (1996)